ISSN 2218-4333 (online)

World Journal of *Clinical Oncology*

World J Clin Oncol 2011 January 10; 2(1): 1-72

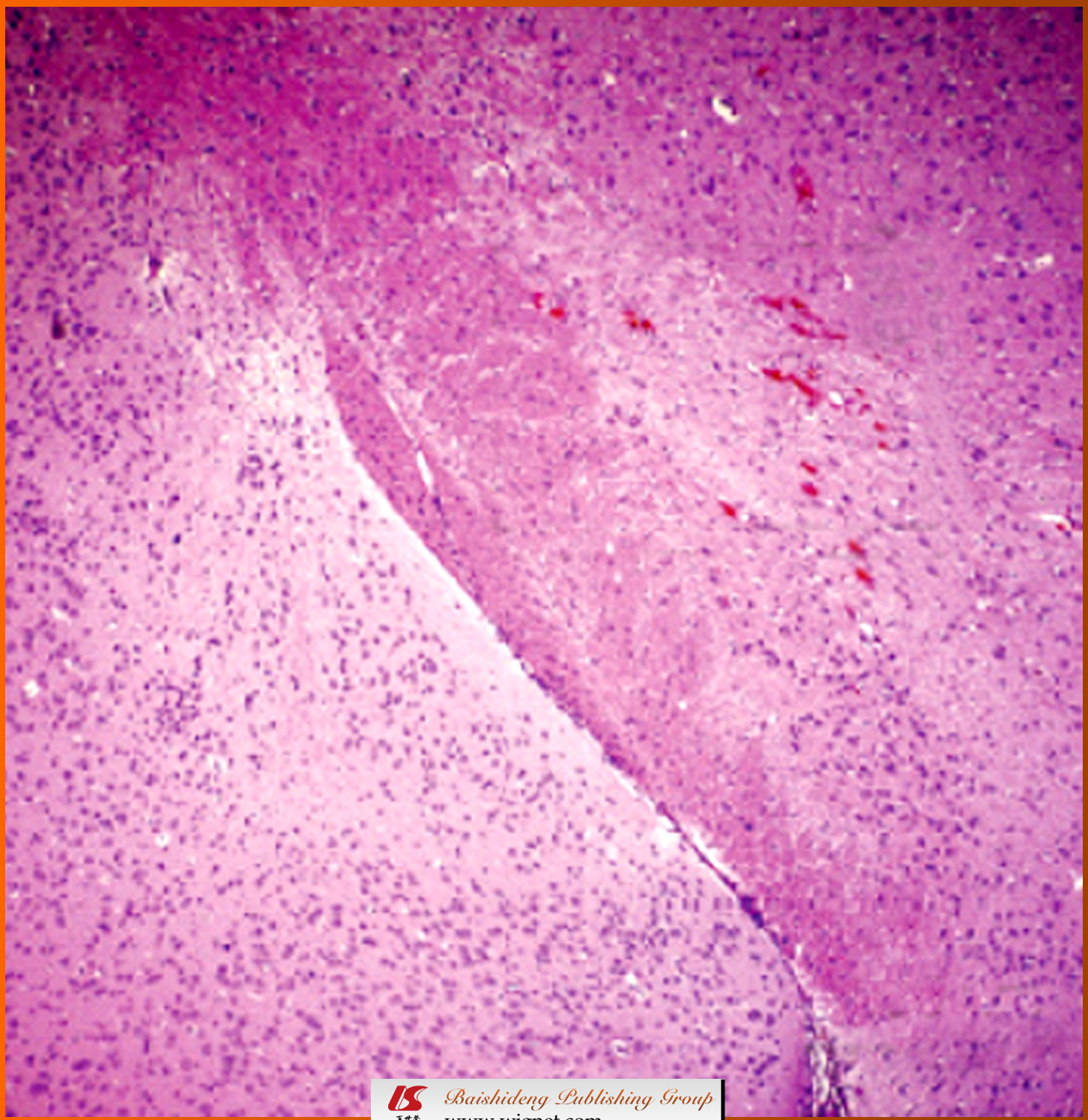

Baishideng Publishing Group
www.wjgnet.com

WJCO World Journal of Clinical Oncology

A peer-reviewed, online, open-access journal of oncology

Editorial Board

2010-2014

The *World Journal of Clinical Oncology* Editorial Board consists of 315 members, representing a team of worldwide experts in oncology. They are from 33 countries, including Australia (6), Belgium (2), Brazil (1), Canada (5), China (34), Egypt (2), Finland (1), France (4), Germany (14), Greece (7), Hungary (1), India (5), Iran (1), Israel (2), Italy (27), Japan (20), Malaysia (1), Mexico (1), Netherlands (6), New Zealand (1), Peru (1), Poland (1), Portugal (4), Saudi Arabia (1), Singapore (9), South Korea (7), Spain (7), Sweden (1), Switzerland (2), Thailand (2), Turkey (6), United Kingdom (11), and United States (122).

Robert Mandic, *Marburg*
Klaus Mross, *Freiburg*
Lars Mueller, *Kiel*
Katharina Pachmann, *Jena*
Matthias Peiper, *Düsseldorf*
Gerd J Ridder, *Freiburg*
Harun M Said, *Wuerzburg*

Greece

Leonidas Duntas, *Athens*
Nicholas Pavlidis, *Ioannina*
Professor A Polyzos, *Athens*
Alexander D Rapidis, *Athens*
Evangelia Razis, *Athens*
Dimitrios Roukos, *Ioannina*
Kostas Syrigos, *Athens*

Hungary

Zsuzsa Schaff, *Budapest*

India

Tanya Das, *Kolkata*
G Arun Maiya, *Manipal*
Ravi Mehrotra, *Allahabad*
Sanjeeb K Sahoo, *Bhubaneswar*
Sarwat Sultana, *New Delhi*

Iran

Ali Kabir, *Tehran*

Israel

Avi Hefetz Khafif, *Tel-Aviv*
Doron Kopelman, *Caesarea*

Italy

Luca Arcaini, *Pavia*
Enrico Benzoni, *Tolmezzo*
Rossana Berardi, *Ancona*
Valentina Bollati, *Milan*
Emilio Bria, *Rome*
Guido Cavaletti, *Monza*
Paolo Chieffi, *Naples*
Marco Ciotti, *Rome*
Giuseppe G Di Lorenzo, *Naples*
Alfio Ferlito, *Udine*
Daris Ferrari, *Abbiategrasso*
Alessandro Franchi, *Florence*
Gennaro Galizia, *Naples*
Roberto Mazzanti, *Firenze*
Michele N Minuto, *Pisa*
Simone Mocellin, *Padova*
Nicola Normanno, *Naples*
Marco G Paggi, *Rome*
Domenico Rubello, *Rovigo*
Antonio Russo, *Palermo*
Daniele Santini, *Rome*
Bruna Scaggiante, Trieste
Riccardo Schiavina, *Bologna*
Enzo Spisni, *Bologna*
Bruno Vincenzi, *Rome*
Giovanni Vitale, *Cusano Milanino*

Japan

Hidefumi Aoyama, *Niigata*
Takaaki Arigami, *Kagoshima*
Narikazu Boku, *Shizuoka*
Kazuaki Chikamatsu, *Chuo*
Toru Hiyama, *Higashihiroshima*
Satoru Kakizaki, *Gunma*
Shuichi Kaneko, *Kanazawa*
Koji Kawakami, *Kyoto*
Hiroki Kuniyasu, *Kashihara*
Eiji Miyoshi, *Suita*
Toru Mukohara, *Kobe*
Atsushi Nakajima, *Tokyo*
Takahide Nakazawa, *Sagamihara*
Seishi Ogawa, *Tokyo*
Youngjin Park, *Chiba prefecture*
Naoya Sakamoto, *Tokyo*
Hidekazu Suzuki, *Tokyo*
Michiko Yamagata, *Shimotsuga-gun*
Hiroki Yamaue, *Wakayama*

Malaysia

Min-Tze Liong, *Penang*

Mexico

Rafael Moreno-Sanchez, *Mexico*

Netherlands

Jurgen J Futterer, *Nijmegen*
Bart M Gadella, *Utrecht*
Johannes A Langendijk, *Groningen*
IM Verdonck-de Leeuw, *Amsterdam*
J Voortman, *Amsterdam*

New Zealand

Joanna Skommer, *Auckland*

Peru

Henry L Gomez, *Lima*

Poland

Lukasz Wicherek, *Bydgoszcz*

Portugal

Antonio Araujo, *Porto*
Rui M Medeiros, *Porto*
Paula Ravasco, *Lisbon*
Rui Manuel Reis, *Braga*

Saudi Arabia

Shahab Uddin, *Riyadh*

Singapore

Wei Ning Chen, *Singapore*
John M Luk, *Singapore*
Shu Wang, *Singapore*
Celestial Yap, *Singapore*
Khay-Guan Yeoh, *Singapore*
George W Yip, *Singapore*
Yong Zhang, *Singapore*
Zhan Zhang, *Singapore*

South Korea

Ho-Seong Han, *Seoul*
Young-Seoub Hong, *Busan*
Ja Hyeon Ku, *Seoul*
Geon Kook Lee, *Goyang-si*
Jae Cheol Lee, *Seoul*
Woo Sung Moon, Jeonju
Hyun Ok Yang, *Gangeung*

Spain

Maurizio Bendandi, *Pamplona*
Joan Carles, *Barcelona*
Javier Cortés Castán, *Barcelona*
Jose M Cuezva, *Madrid*
Jesús Prieto, *Pamplona*

Sweden

Lalle Hammarstedt, *Stockholm*

Switzerland

A Lugli, *Basel*
Jacqueline Schoumans, *Lausanne*

Thailand

Suebwong Chuthapisith, *Bangkok*
Songsak Petmitr, *Bangkok*

Turkey

Nejat Dalay, *Istanbul*
Seher Demirer, *Ankara*
Zafer Özgür Pektaş, *Adana*
Alper Sevinc, *Gaziantep*
Engin Ulukaya, *Gorukle Bursa*
Isik G Yulug, *Ankara*

United Kingdom

Shahriar Behboudi, *London*
Alastair David Burt, *Newcastle*

WJCO World Journal of Clinical Oncology

Contents

Monthly Volume 2 Number 1 January 10, 2011

EDITORIAL

1 Eagles report: Developing cancer biomarkers from genome-wide DNA methylation analyses
Schulz WA, Goering W

TOPIC HIGHLIGHT

8 High intensity focused ultrasound in clinical tumor ablation
Zhou YF

28 Imaging of gastroenteropancreatic neuroendocrine tumors
Tan EH, Tan CH

44 Cancer prognosis using support vector regression in imaging modality
Du X, Dua S

50 Role of optical spectroscopy using endogenous contrasts in clinical cancer diagnosis
Liu Q

64 Optical mammography: Diffuse optical imaging of breast cancer
Lee K

World Journal of Clinical Oncology
Volume 2 Number 1 January 10, 2011

Contents

ACKNOWLEDGMENTS	I	Acknowledgments to reviewers of *World Journal of Clinical Oncology*
APPENDIX	I	Meetings
	I-V	Instructions to authors
ABOUT COVER		Zhou YF. High intensity focused ultrasound in clinical tumor ablation. *World J Clin Oncol* 2011; 2(1): 8-27 http://www.wjgnet.com/2218-4333/full/v2/i1/8.htm
AIM AND SCOPE		*World Journal of Clinical Oncology* (*World J Clin Oncol*, *WJCO*, online ISSN 2218-4333, DOI: 10.5306) is a monthly peer-reviewed, online, open-access, journal supported by an editorial board consisting of 315 experts in oncology from 33 countries. The aim of *WJCO* is to report rapidly new theories, methods and techniques for prevention, diagnosis, treatment, rehabilitation and nursing in the field of oncology. *WJCO* covers etiology, epidemiology, evidence-based medicine, informatics, diagnostic imaging, endoscopy, tumor recurrence and metastasis, tumor stem cells, radiotherapy, chemotherapy, interventional radiology, palliative therapy, clinical chemotherapy, biological therapy, minimally invasive therapy, physiotherapy, psycho-oncology, comprehensive therapy, oncology-related traditional medicine, integrated Chinese and Western medicine, and nursing. *WJCO* covers tumors in various organs/tissues, including the female reproductive system, bone and soft tissue, respiratory system, urinary system, endocrine system, skin, breast, nervous system, head and neck, digestive system, and hematologic and lymphatic system.
FLYLEAF	I-III	Editorial Board

NAME OF JOURNAL
World Journal of Clinical Oncology

LAUNCH DATE
November 10, 2010

SPONSOR
Beijing Baishideng BioMed Scientific Co., Ltd.,
Room 903, Building D, Ocean International Center,
No. 62 Dongsihuan Zhonglu, Chaoyang District,
Beijing 100025, China
Telephone: 0086-10-8538-1892
Fax: 0086-10-8538-1893
E-mail: baishideng@wjgnet.com
http://www.wjgnet.com

EDITING
Editorial Board of *World Journal of Clinical Oncology*,
Room 903, Building D, Ocean International Center,
No. 62 Dongsihuan Zhonglu, Chaoyang District,
Beijing 100025, China
Telephone: 0086-10-5908-0036
Fax: 0086-10-8538-1893
E-mail: wjco@wjgnet.com
http://www.wjgnet.com

PUBLISHING
Baishideng Publishing Group Co., Limited,
Room 1701, 17/F, Henan Building,
No.90 Jaffe Road, Wanchai, Hong Kong, China
Fax: 00852-3115-8812
Telephone: 00852-5804-2046
E-mail: baishideng@wjgnet.com
http://www.wjgnet.com

SUBSCRIPTION
Beijing Baishideng BioMed Scientific Co., Ltd.,
Room 903, Building D, Ocean International Center,
No. 62 Dongsihuan Zhonglu, Chaoyang District,
Beijing 100025, China
Telephone: 0086-10-8538-1892
Fax: 0086-10-8538-1893
E-mail: baishideng@wjgnet.com
http://www.wjgnet.com

ONLINE SUBSCRIPTION
One-Year Price 216.00 USD

PUBLICATION DATE
January 10, 2011

CSSN
ISSN 2218-4333 (online)

EDITORIAL OFFICE
Na Ma, Director
World Journal of Clinical Oncology
Room 903, Building D, Ocean International Center,
No. 62 Dongsihuan Zhonglu, Chaoyang District,
Beijing 100025, China
Telephone: 0086-10-8538-1892
Fax: 0086-10-8538-1893
E-mail: wjco@wjgnet.com
http://www.wjgnet.com

INSTRUCTIONS TO AUTHORS
Full instructions are available online at http://www.wjgnet.com/2218-4333/g_info_20100722172206.htm. If you do not have web access please contact the editorial office.

ONLINE SUBMISSION
http://www.wjgnet.com/2218-4333office

World Journal of Clinical Oncology

Online Submissions: http://www.wjgnet.com/2218-4333office
wjco@wjgnet.com
doi:10.5306/wjco.v2.i1.1

World J Clin Oncol 2011 January 10; 2(1): 1-7
ISSN 2218-4333 (online)

EDITORIAL

Eagles report: Developing cancer biomarkers from genome-wide DNA methylation analyses

Wolfgang A Schulz, Wolfgang Goering

Wolfgang A Schulz, Wolfgang Goering, Department of Urology, Medical Faculty, Heinrich Heine University, 40225 Duesseldorf, Germany
Author contributions: Schulz WA and Goering W researched the literature and wrote the paper.
Supported by The Deutsche Forschungsgemeinschaft and the Deutsche Krebshilfe
Correspondence to: Wolfgang A Schulz, PhD, Professor, Department of Urology, Medical Faculty, Heinrich Heine University, 40225 Duesseldorf,
Germany. wolfgang.schulz@uni-duesseldorf.de
Telephone: +49-211-8118966 Fax: +49-211-8115846
Received: July 28, 2010 Revised: August 26, 2010
Accepted: September 2, 2010
Published online: January 10, 2011

Abstract

Analyses of DNA methylation in human cancers have identified hypermethylation of individual genes and diminished methylation at repeat elements as common alterations, and have thereby provided important mechanistic insights into cancer biology as well as biomarkers for cancer detection, prognosis and prediction of therapy responses. The techniques available in the past were best suited for investigations of individual candidate genes and sequences, whereas recently developed high-throughput techniques promise to generate unbiased and comprehensive surveys of DNA methylation states across entire genomes. In this minireview we give a short overview of established and novel techniques and outline some major questions that can now be addressed to develop further cancer biomarkers and therapies based on DNA methylation.

Key words: Bisulfite; CpG-island; Deep sequencing; DNA hypermethylation; Hypomethylation; Methylcytosine-binding domain

Peer reviewers: Hengmi Cui, PhD, Assistant Professor, Center for Epigenetics and Division of Molecular Medicine, Johns Hopkins University School of Medicine, 855 N Wolfe Street/572 Rangos Building, Baltimore, MD 21205, United States; Sherven Sharma, Gene Medicine Laboratory, VA Greater Los Angeles Health Care System,11301 Wilshire Blvd., Bldg. 114, Rm. 103, Los Angeles, CA 90073-1003, United States

Schulz WA, Goering W. Eagles report: Developing cancer biomarkers from genome-wide DNA methylation analyses. *World J Clin Oncol* 2011; 2(1): 1-7 Available from: URL: http://www.wjgnet.com/2218-4333/full/v2/i1/1.htm DOI: http://dx.doi.org/10.5306/wjco.v2.i1.1

DNA METHYLATION CHANGES IN HUMAN CANCERS

Epigenetic alterations are now firmly established as causative factors in the development and progression of human cancers, especially changes in DNA methylation. In mammalian cells, methylation of DNA bases occurs almost exclusively at the 5'-position of cytosines and in adult somatic cells it is essentially only present at cytosines in the dinucleotide cytosine-guanosine (CpG). Since their discovery in the 1980's, DNA methylation changes in human cancers have mostly been analyzed on a gene-by-gene basis, i.e. metaphorically speaking, from a frog perspective. Now, novel techniques which have developed over the last decade provide the means to survey DNA methylation in a more comprehensive fashion across the genome. This eagle's view of the DNA "methylome" of various normal and cancer cells is expected to generate ample opportunities for the development of diagnostic, prognostic and predictive biomarkers to be used in clinical oncology. In this minireview, we will give a brief overview of DNA methylation changes in human cancers, describe current and emerging techniques for their analysis, with their respective strengths and limitations, and outline possible future developments.

In the human genome, CpG-sites occur at only one

quarter of the expected frequency in general and the remaining CpG-sites are often clustered in CpG-islands. Many of the approximately 30 000 CpG-islands straddle the transcriptional start sites of genes. Most CpG-islands are never methylated under physiological conditions, not even during germ cell or embryonic development. In contrast, isolated CpG-sites within genes or intergenic regions are often methylated. In particular, most of the CpG sites located in repeat sequences within the genome are densely methylated in normal somatic cells. Many repeat sequences originate from ancient retroviruses (human endogenous retroviruses, HERV) or simpler endogenous retroelements (SINEs and LINEs). Methylation of such retroelements helps to constrain their activity. In addition to repeat sequences, selected single copy genes can be methylated in normal cells, among them some important determinators of pluripotency and cell lineage[1]. Here, methylation aids in restricting their expression to certain cell types. Finally, DNA methylation of specific sequences helps in the selection of a single allele for expression, as in imprinted genes, and in choosing one active gene out of a cluster, e.g. in the immune system and presumably in the brain[2,3].

This elaborate pattern of DNA methylation is disturbed in almost every human cancer. There are principally two types of changes, which occur quite independent of each other. In the case of DNA hypermethylation, methylation appears at otherwise unmethylated CpG-islands. CpG-island hypermethylation is usually associated with silencing of the affected gene promoter[4]. In the case of DNA hypomethylation, methylation is lost from retroelements and single-copy genes, permitting transcription of normally repressed sequences[5]. As one might predict, abnormalities in DNA methylation patterns are generally more pronounced in high-stage and high-grade cancers. Nevertheless, research over the last two decades has revealed a high degree of specificity in DNA methylation changes between different cancer types and among cancers of the same type at different stages of progression. These differences can be exploited for cancer detection and classification with respect to subtype and prognosis. For instance, the GSTP1 gene is hypermethylated in approximately 90% of all prostate cancers[6]. Additionally, certain methylation changes are associated with differential response to specific therapies and can be used as predictive biomarkers. A prominent example is hypermethylation of the *MGMT* CpG-island which indicates silencing of the gene. The *MGMT* gene encodes the methyl-O-guanosyl DNA methyltransferase, which reverses and repairs DNA alkylation. Accordingly, gliomas with *MGMT* hypermethylation can be predicted to respond more favorably to the alkylating drug temozolomide[7].

Analyses of DNA methylation changes in cancer diagnostics have unique advantages resulting from the very biochemical properties of this epigenetic mechanism. First, DNA *per se* is a rather stable molecule. Second, methylation at the 5'-position of cytosine is chemically stable, is difficult to establish except by enzymatic transfer and equally difficult to reverse in the absence of specific enzymes. Third, the turnover of methylcytosine at most genomic sites is, under most conditions, slow. As a consequence of these properties, DNA methylation changes can be robustly analyzed in a large variety of biological samples, including biopsies, body fluids, and archival material[8]. With modern techniques, minute amounts of DNA can be analyzed, permitting high sensitivity. In addition, since most CpG-islands are never methylated, hypermethylation in CpG-islands is often highly specific for tumor cells. Importantly, analyses from clinical samples and body fluids especially should always include appropriate quality controls to avoid artefacts resulting from, e.g. limited amounts of DNA or fixation.

In practice, a limitation to the specificity of DNA hypermethylation assays arises from the tendency of some CpG-islands to become hypermethylated in aging, inflamed and preneoplastic tissues, albeit usually not quite as densely as in full-blown malignancies[9]. Another practical limit to the sensitivity of DNA hypermethylation assays is set by the heterogeneity of the changes within one tumor type and within individual tumors. Typically, a particular CpG-island is hypermethylated in a fraction of all cases and not all CpG-sites within the island are affected to the same extent in each individual tumor cell. Cases like *GSTP1* hypermethylation in prostate cancer, where practically all CpGs within a CpG-island are methylated in almost all tumors of one entity constitute fortunate exceptions (Figure 1). In such cases, the sensitivity of a methylation assay will strongly depend on the technique used (as discussed below) and its specificity may suffer, if hypermethylation of the gene is also present in preneoplastic tissue. Finally, tumor tissues comprise a mixture of several different cell types including stromal, endothelial and immune cells, in addition to the actual cancer cells. Although most CpG-islands are completely unmethylated in all cell types, methylation can display considerable specificity at some CpG-islands, in particular at their "shores"[10] and even more so at CpG-dinucleotides outside CpG-islands[11].

ESTABLISHED TECHNIQUES FOR ANALYZING DNA METHYLATION CHANGES IN HUMAN CANCERS

Many currently used assays for DNA methylation are based on bisulfite conversion of DNA[12]. Bisulfite attaches itself to the C-6 of the cytosine ring. Subsequently, under alkaline conditions, the sulfonated cytosine is deaminated and desulfonated to uracil. The methyl group at the C-5 position prevents sulfonation and, therefore, methylcytosine remains the same. When polymerase chain reaction (PCR) is performed on the modified DNA, uracil results in thymine and methylcytosine in cytosine. Sequencing of the PCR products yields a reliable picture of the DNA methylation pattern at each CpG in the amplified sequence and is the current gold standard for DNA methylation analysis. Sequencing can be performed directly on the PCR product or after cloning. Direct sequencing yields an overall picture of the methylation pattern across several hundred bases, but standard Sanger

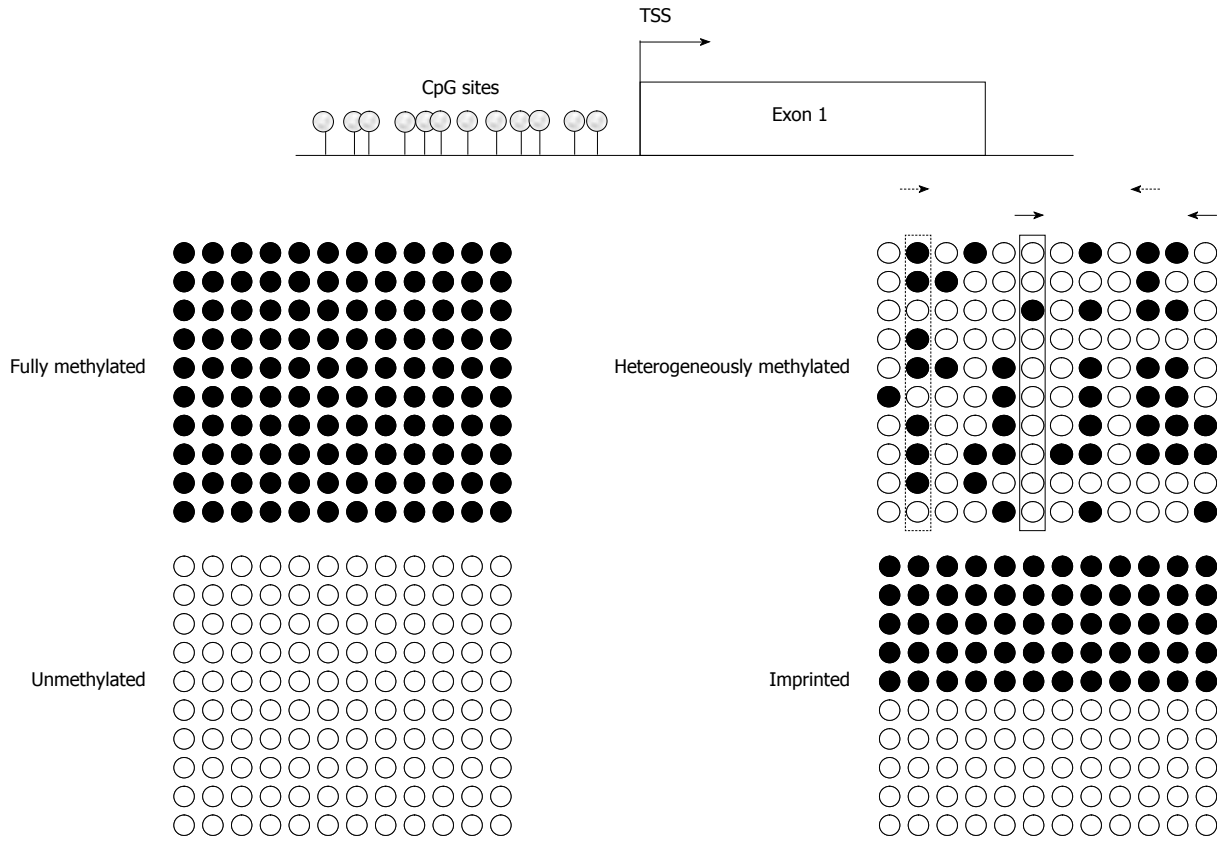

Figure 1 Assaying various methylation states by different techniques. Idealized bisulfite sequencing results of cytosine-guanosine (CpG)-sites in a proximal promoter region (TSS denoting the transcriptional start site), showing fully methylated, unmethylated, heterogeneously methylated and typical imprinted (differentially methylated) states. Each circle corresponds to a single CpG site, each line to one cloned allele. Filled circles represent methylated and empty circles unmethylated cytosines. Bisulfite sequencing gives an excellent indication of methylation state at every single CpG site, but quantification requires an adequate number of investigated clones. Pyrosequencing, methylcytosine-binding domain (MBD)- or methylation-specific polymerase chain reaction (MS-PCR)-based assays will detect 100% methylation at fully methylated and 0% methylation at unmethylated sequences, respectively. Imprinting results in methylation values of 50% at every single CpG site in pyrosequencing. In addition, MS-PCR-assays will detect signals for methylated and unmethylated DNA. For heterogeneously methylated DNA, bisulfite sequencing yields quite clear results, if a sufficient number of clones are used. In contrast, pyrosequencing will identify high methylation values (dotted rectangle) for several CpG sites and low values (solid rectangle) for other sites, whereas MBD-based analyses lead to intermediate overall methylation values. The results of MS-PCR methods depend critically on the chosen CpG-sites and may vary enormously even with small changes in the PCR stringency. For example, MS-PCR assay using primers interrogating CpG sites 2 and 10 (dotted arrow) yields higher methylation values compared to an assay aimed at CpG sites 6 and 12 (solid arrows).

sequencing is not quantitative. Pyrosequencing of PCR products allows a quantitative measure of average methylation at each individual CpG site, but only over relatively short stretches of DNA (up to 100 bases). Sequencing of multiple clones provides the most precise information and can reveal heterogeneous methylation at individual sites or the presence of differentially methylated alleles at imprinted genes. However, this technique is relatively lengthy and expensive.

Many exploratory studies on clinical samples have been performed by the methylation-specific PCR (MS-PCR) technique[13]. Here, PCR primers are chosen to selectively fit either the methylated or unmethylated sequence of interest after bisulfite treatment. Hypermethylation events at CpG-islands result in the appearance of a PCR product with the methylated-specific primers, whereas healthy tissues yield a PCR product only with the unmethylated-specific primers. The PCR products can be visualized on a gel or can be quantitatively determined by real-time PCR using fluorescence probes. In particular, the MethyLight variant of MS-PCR, which employs selective Taqman type probes for detection of the PCR products, is in widespread use[14,15]. The MethyLight method can be designed to avoid the potential problem of bias introduced by using different primer pairs in MS-PCR. MS-PCR or MethyLight are excellent techniques to detect or even quantify methylation that is homogeneously absent or present, but they can result in highly variable results at partially and heterogeneously methylated sequences.

Many problems of applying DNA methylation analysis in clinical practice arise from the heterogeneous character and distribution of methylation changes on the one hand and of partially altered methylation in preneoplastic tissues on the other hand. For cancer detection, assaying multiple methylation markers increases sensitivity and helps to discriminate against changes caused by aging, inflammation and preneoplasia. For prognosis and classification, multiple markers are mandatory to cover biological heterogeneity arising during cancer progression and due to histological subtypes. For therapy prediction, using multiple markers could allow prediction of the response to alternative therapies. The most straightforward way to analyze multiple

CpG sites and sequences is multiplexing of individual assays. The MethyLight technique can be straightforwardly automated and has been employed to measure methylation at dozens of genes across hundreds of samples in a semi-quantitative fashion[16]. More recently, mass spectrometry has been developed for automated analysis of DNA methylation at multiple sites in large sample sets. Typically, the analyses exploit differences in nucleotide molecular mass following bisulfite treatment[17,18]. Conceivably, these or other automatable multiplex techniques may form the basis of DNA methylation assays in clinical routine use in the near future. For instance, some of the difficulties arising from the heterogeneous composition of tumor samples may be solved by digital PCR combined with high resolution melting (HRM) or pyrosequencing methods as discussed by Mikeska *et al*[19]. Obviously, however, multiplex assays interrogate a predefined set of sequences and cannot provide a global and unbiased overview of DNA methylation patterns and their changes in cancers.

Detection of DNA hypomethylation in cancer poses still another set of challenges. Hypomethylation occurs foremost at retroelements and other repetitive sequences in the genome. These repeats are similar, but not identical and methylation at retroelements in particular can be heterogeneous in normal cells and the decrease in cancer cells at various CpG-sites variable. Hypomethylation at single-copy sequences is likewise often partial and heterogeneous. In general, DNA hypomethylation accrues in many cancers with tumor progression[20]. Therefore hypomethylation alterations might be exploited as biomarkers of prognosis, but unfortunately the specificity and sensitivity of assays for hypomethylation in cancer are so far limited. Global and comprehensive surveys of DNA methylation in cancer might help to identify specific hypomethylation changes useful as biomarkers.

NOVEL TECHNIQUES FOR ANALYZING DNA METHYLATION CHANGES IN HUMAN CANCERS

Several techniques have now come close to providing comprehensive surveys of the methylation pattern of normal and cancerous cells and tissues.

Some of these techniques are also based on bisulfite modification of DNA. The most straightforward approach to screening whole genomes for methylation changes would be genome-wide high-throughput sequencing following bisulfite conversion, which has become a realistic prospect with the advent of novel high-throughput ("deep") sequencing techniques[21]. The main obstacles prohibiting - at present - a broad use of this technique are the high fraction of repeat sequences in the genome and the reduced complexity of the DNA after bisulfite treatment due to the conversion of many cytosines to uracils. Both factors complicate the assignment of sequences from the sequencing "reads" to the genome. These same factors have also limited the use of arrays in DNA methylation analysis, although, e.g. bead-based arrays have already provided some promising results[22,23]. It is expected that these technical and bioinformatic obstacles will be overcome in the near future. For the time being, many researchers avoid them by investigating only more easily accessible parts of the genome isolated from the rest, e.g. by digestion with certain restriction enzymes and fractionation. The great advantage of bisulfite sequencing is that it yields information on the methylation of individual CpGs, deep sequencing with sufficient coverage (meaning multiple sequencing of the same segment) can even provide quantitative information at heterogeneously methylated sites.

In the meantime, techniques based on the biological recognition of methylcytosine by enzymes or antibodies - rather than on its chemical properties as in the bisulfite reaction - have made great advances. The oldest technique of this kind is the use of restriction enzymes that cut DNA dependent on its methylation status[24]. Methylation differences result in differentially sized fragments that can be detected by Southern blotting or in the loss of a PCR product spanning the restriction site. Based on this simple principle, a variety of techniques have been developed in the past to explore differential methylation at a larger scale, such as 2D gels or hybridization to arrays after differential amplification of cut and uncut sequences[25,26]. A novel technique for genome-wide methylation analysis, referred to as comprehensive high-throughput array-based relative methylation (CHARM), uses the bacterial enzyme McrBC for cleaving of DNA dependent on its methylation state followed by array hybridization of the fragments[27]. This technique was used to unravel cell lineage and tumor-specific methylation differences at CpG island shores[10,28].

The more recently developed technique of methylation-dependent immunoprecipitation (MeDIP) exploits the affinity of a methylcytosine antibody to enrich methylated sequences from the genome. Differences between tumor cells and their normal counterparts can be identified by comparative hybridization of the selected sequences to arrays or by high-throughput sequencing[18,29].

In the cell nucleus, methylated DNA is recognized by specific proteins such as MBD2 or MeCP2 *via* a specific domain, the methylcytosine-binding domain (MBD). This biological recognition mechanism is exploited by novel techniques. They use recombinant proteins containing an MBD fused to another protein that can be easily captured on beads or columns, such as an antibody F_c domain or a glutathione transferase. As in MeDIP, array hybridization or high-throughput sequencing can follow to characterize the selected DNA[30,31]. A promising variation of this technique has entered research using proteins that recognize specifically unmethylated CpGs[32]. This technique may facilitate the analysis of hypomethylation events.

All present-day capture techniques do not provide methylation information at single CpG resolution, but enrich methylated or unmethylated sequences. Another limitation is the need for a certain CpG density to achieve efficient precipitation or binding of methylated DNA[31]. DNA with lower CpG-density will not be as reliably captured, even if fully methylated. Neither, however, requires

bisulfite treatment of DNA and capture techniques based on MBD proteins even work with native DNA which needs only to be fragmented.

DNA METHYLATION CHANGES IN HUMAN CANCERS: OPEN QUESTIONS

Together, these approaches promise to provide us with a more complete picture of DNA methylation patterns in normal cells from different cell types, tissues and developmental stages. They will reveal how much individuals differ from each other. The results will help to elucidate the physiological functions of DNA methylation, e.g. in the immune system and in the brain, which are intriguing but poorly understood. We hope to learn how DNA methylation changes in autoimmune, neurological, psychiatric and cardiovascular diseases. In the field of oncology, eagle-eye perspectives of DNA methylation patterns are expected to yield important mechanistic insights into cancer pathogenesis and to provide a robust basis for the rational development of methylation-based diagnostic assays and epigenetic targeted drugs.

One of the most burning questions is how many DNA methylation changes cancers may harbor. Extrapolating from current knowledge, it is anticipated that large differences will be detected among cancer types and subtypes. For instance, carcinogenesis in the prostate involves a coordinate change in the methylation of several genes including *GSTP1*, whereas methylation changes in bladder cancer appear to accrue in a rather stochastic fashion with cancer progression, the largest differences existing between papillary and invasive subtypes[33]. In colorectal cancers, the molecularly defined CpG-island methylated phenotype (CIMP)+ cases are already known to contain an unusually large number of methylation changes, which may ultimately turn out to range into the thousands. In comparison, the average number of aberrantly methylated genes (primarily CpG-islands) across all cancers is speculated to figure in the lower hundreds, similar to the average number of point mutations within genes emerging from the first genome-wide sequencing projects[34]. We should also find out which methylation changes occur across many cancers and which are relatively specific. From current knowledge, *RASSF1A* and *GSTP1* hypermethylation, respectively, are representatives of these kinds of changes[35,36]. Moreover, the identification of cell-type specific methylation patterns may provide markers for estimating the cellular heterogeneity of tumors, or identifying specific cell populations, as has been proposed for regulatory T cells[37]. Methylation signatures of tumor stem cells should be particularly interesting, not only for heuristic purposes, but also for prognosis and therapy. Already, DNA methylation profiles have been successfully established for embryonic stem cells[21].

A second important question coming closer to being answered is what causes alterations of DNA methylation in cancer. Are the changes determined by systematic defects in the molecular network of factors directing and maintaining normal patterns or do they occur in a more random manner by accidents, perhaps followed by selection for those changes lending a growth advantage to the tumor cells? The answer to this question is essential for the further development of epigenetic therapies. In the former case, therapies will rather be directed towards restoring normal methylation regulation. In the latter case, therapies should aim at reexpression of individual antitumor genes which have been inactivated by epigenetic accidents. In either case, detailed analysis of the underlying molecular mechanisms will have to follow on the large-scale surveys to accompany and support drug development. This research will also provide biomarkers for prediction and monitoring of therapy responses.

The third result of systematic surveys of genomic methylation will be a broad and robust basis from which candidates can be chosen for further investigation and development for clinical use as biomarkers for detection and classification. Experience from the past suggests that methylation analyses of single genes will only provide reliable biomarkers in exceptional cases. Evidently, only a very small part of cancer genomes has been analyzed for methylation so far and this conclusion could be wrong. However, we think that the development of an optimized set of methylation markers for each cancer or tissue may be the most promising strategy, because of maximum sensitivity and specificity, but also the potential to cover the different scopes of detection, prognosis and prediction. Costs for high-throughput analyses, especially DNA sequencing, are declining fast. It may, therefore, even be possible that appropriately standardized and controlled whole-genome analyses could replace multiplex assays for DNA methylation in the future. In any case, development and validation of an optimal set of methylation biomarkers will certainly be necessary for each cancer type individually.

Finally, large-scale methylation analyses of human cancers will provide an important database for researchers studying molecular mechanisms of pathogenesis. Hypermethylation events are often associated with gene silencing and some of the silenced genes may be functionally important[4]. In this fashion, important pathogenetic processes in particular cancers may be identified and new targets for therapy may be developed. The same expectation applies to DNA hypomethylation which often occurs at genes associated with invasion and metastasis and leads to expression of cancer-testis antigens[38]. It also may permit reactivation of retroelements that promote genomic instability[5]. Therefore, anti-metastatic and immune therapies should benefit from insights into DNA hypomethylation, in particular.

Large-scale approaches have not only offered new possibilities for analysis of DNA methylation in cancer, but also for studying global patterns of gene copy number alterations and mutations as well as changes in expression of mRNAs and other RNA species. More and more, integrative analyses assessing changes at various levels are used to classify cancer subtypes[39] or to identify aberrantly active molecular pathways[40]. Analyses of DNA methylation are

expected to become integrated into these global analyses shortly. In particular, large-scale sequencing has revealed a peculiar landscape of point mutations in cancer[41], in which a relatively small number of genes are frequently mutated in each cancer type and a larger number of others carry point mutations in only a few cases each. Most of the frequently mutated genes, such as *TP53* or *KRAS*, have indeed long been known. Even after integrating copy number alterations with such studies, fewer consistent and obviously functionally important genetic changes have emerged from a large number of recently published studies. Many researchers now suspect that epigenetic changes, termed epimutations, may account, to a large extent, for the elusive "drivers" of tumor development and progression. If so, targeting epigenetic changes may turn out to be even more valuable in cancer therapy than hitherto assumed. Integrating large-scale analyses of DNA methylation with those of other changes will help to address this issue.

Developments in science are often driven by the fruitful interplay between large-scale surveys and detailed analysis of individual factors and mechanisms, the synergism between frog and eagle approaches. In the 1980's, DNA methylation research encompassed both the analysis of single restriction sites at individual genes and global, albeit unspecific measurements of total methylcytosine content. Similarly, the comprehensive surveys of genomic methylation patterns are complemented by detailed molecular analysis of the interaction of multiple epigenetic regulators at individual genes during the establishment of DNA methylation and chromatin patterns. The development of DNA methylation assays for clinical oncology by analysis of candidate genes has clearly reached a limit. Likewise, the further development of epigenetic drugs for cancer treatment requires a broader understanding of the overall changes in DNA methylation. Thus, the reports of the eagles are eagerly awaited.

REFERENCES

1 **Reik W**. Stability and flexibility of epigenetic gene regulation in mammalian development. *Nature* 2007; **447**: 425-432
2 **Dulac C**. Brain function and chromatin plasticity. *Nature* 2010; **465**: 728-735
3 **Wilson CB**, Rowell E, Sekimata M. Epigenetic control of T-helper-cell differentiation. *Nat Rev Immunol* 2009; **9**: 91-105
4 **Jones PA**, Baylin SB. The epigenomics of cancer. *Cell* 2007; **128**: 683-692
5 **Schulz WA**, Steinhoff C, Florl AR. Methylation of endogenous human retroelements in health and disease. *Curr Top Microbiol Immunol* 2006; **310**: 211-250
6 **Nelson WG**, De Marzo AM, Yegnasubramanian S. Epigenetic alterations in human prostate cancers. *Endocrinology* 2009; **150**: 3991-4002
7 **Hegi ME**, Liu L, Herman JG, Stupp R, Wick W, Weller M, Mehta MP, Gilbert MR. Correlation of O6-methylguanine methyltransferase (MGMT) promoter methylation with clinical outcomes in glioblastoma and clinical strategies to modulate MGMT activity. *J Clin Oncol* 2008; **26**: 4189-4199
8 **Laird PW**. The power and the promise of DNA methylation markers. *Nat Rev Cancer* 2003; **3**: 253-266
9 **Teschendorff AE**, Menon U, Gentry-Maharaj A, Ramus SJ, Weisenberger DJ, Shen H, Campan M, Noushmehr H, Bell CG, Maxwell AP, Savage DA, Mueller-Holzner E, Marth C, Kocjan G, Gayther SA, Jones A, Beck S, Wagner W, Laird PW, Jacobs IJ, Widschwendter M. Age-dependent DNA methylation of genes that are suppressed in stem cells is a hallmark of cancer. *Genome Res* 2010; **20**: 440-446
10 **Ji H**, Ehrlich LI, Seita J, Murakami P, Doi A, Lindau P, Lee H, Aryee MJ, Irizarry RA, Kim K, Rossi DJ, Inlay MA, Serwold T, Karsunky H, Ho L, Daley GQ, Weissman IL, Feinberg AP. Comprehensive methylome map of lineage commitment from haematopoietic progenitors. *Nature* 2010; **467**: 338-342
11 **Dokun OY**, Florl AR, Seifert HH, Wolff I, Schulz WA. Relationship of SNCG, S100A4, S100A9 and LCN2 gene expression and DNA methylation in bladder cancer. *Int J Cancer* 2008; **123**: 2798-2807
12 **Clark SJ**, Harrison J, Paul CL, Frommer M. High sensitivity mapping of methylated cytosines. *Nucleic Acids Res* 1994; **22**: 2990-2997
13 **Herman JG**, Graff JR, Myöhänen S, Nelkin BD, Baylin SB. Methylation-specific PCR: a novel PCR assay for methylation status of CpG islands. *Proc Natl Acad Sci USA* 1996; **93**: 9821-9826
14 **Weisenberger DJ**, Siegmund KD, Campan M, Young J, Long TI, Faasse MA, Kang GH, Widschwendter M, Weener D, Buchanan D, Koh H, Simms L, Barker M, Leggett B, Levine J, Kim M, French AJ, Thibodeau SN, Jass J, Haile R, Laird PW. CpG island methylator phenotype underlies sporadic microsatellite instability and is tightly associated with BRAF mutation in colorectal cancer. *Nat Genet* 2006; **38**: 787-793
15 **Anglim PP**, Galler JS, Koss MN, Hagen JA, Turla S, Campan M, Weisenberger DJ, Laird PW, Siegmund KD, Laird-Offringa IA. Identification of a panel of sensitive and specific DNA methylation markers for squamous cell lung cancer. *Mol Cancer* 2008; **7**: 62
16 **Eads CA**, Danenberg KD, Kawakami K, Saltz LB, Blake C, Shibata D, Danenberg PV, Laird PW. MethyLight: a high-throughput assay to measure DNA methylation. *Nucleic Acids Res* 2000; **28**: E32
17 **Vanaja DK**, Ehrich M, Van den Boom D, Cheville JC, Karnes RJ, Tindall DJ, Cantor CR, Young CY. Hypermethylation of genes for diagnosis and risk stratification of prostate cancer. *Cancer Invest* 2009; **27**: 549-560
18 **Flanagan JM**, Cocciardi S, Waddell N, Johnstone CN, Marsh A, Henderson S, Simpson P, da Silva L, Khanna K, Lakhani S, Boshoff C, Chenevix-Trench G. DNA methylome of familial breast cancer identifies distinct profiles defined by mutation status. *Am J Hum Genet* 2010; **86**: 420-433
19 **Mikeska T**, Candiloro ILM, Dobrovic A. The implications of heterogeneous DNA methylation for the accurate quantification of methylation. *Epigenomics* 2010; **2**: 56173
20 **Wilson AS**, Power BE, Molloy PL. DNA hypomethylation and human diseases. *Biochim Biophys Acta* 2007; **1775**: 138-162
21 **Lister R**, Pelizzola M, Dowen RH, Hawkins RD, Hon G, Tonti-Filippini J, Nery JR, Lee L, Ye Z, Ngo QM, Edsall L, Antosiewicz-Bourget J, Stewart R, Ruotti V, Millar AH, Thomson JA, Ren B, Ecker JR. Human DNA methylomes at base resolution show widespread epigenomic differences. *Nature* 2009; **462**: 315-322
22 **Bibikova M**, Lin Z, Zhou L, Chudin E, Garcia EW, Wu B, Doucet D, Thomas NJ, Wang Y, Vollmer E, Goldmann T, Seifart C, Jiang W, Barker DL, Chee MS, Floros J, Fan JB. High-throughput DNA methylation profiling using universal bead arrays. *Genome Res* 2006; **16**: 383-393
23 **Thirlwell C**, Eymard M, Feber A, Teschendorff A, Pearce K, Lechner M, Widschwendter M, Beck S. Genome-wide DNA methylation analysis of archival formalin-fixed paraffin-embedded tissue using the Illumina Infinium HumanMethylation27 BeadChip. *Methods* 2010; Epub ahead of print
24 **Singer-Sam J**, LeBon JM, Tanguay RL, Riggs AD. A quantitative HpaII-PCR assay to measure methylation of DNA

from a small number of cells. *Nucleic Acids Res* 1990; **18**: 687
25 **Costello JF**, Hong C, Plass C, Smiraglia DJ. Restriction landmark genomic scanning: analysis of CpG islands in genomes by 2D gel electrophoresis. *Methods Mol Biol* 2009; **507**: 131-148
26 **Ushijima T**, Yamashita S. Methylation-sensitive representational difference analysis (MS-RDA). *Methods Mol Biol* 2009; **507**: 117-130
27 **Irizarry RA**, Ladd-Acosta C, Carvalho B, Wu H, Brandenburg SA, Jeddeloh JA, Wen B, Feinberg AP. Comprehensive high-throughput arrays for relative methylation (CHARM). *Genome Res* 2008; **18**: 780-790
28 **Irizarry RA**, Ladd-Acosta C, Wen B, Wu Z, Montano C, Onyango P, Cui H, Gabo K, Rongione M, Webster M, Ji H, Potash JB, Sabunciyan S, Feinberg AP. The human colon cancer methylome shows similar hypo- and hypermethylation at conserved tissue-specific CpG island shores. *Nat Genet* 2009; **41**: 178-186
29 **Cheung HH**, Lee TL, Davis AJ, Taft DH, Rennert OM, Chan WY. Genome-wide DNA methylation profiling reveals novel epigenetically regulated genes and non-coding RNAs in human testicular cancer. *Br J Cancer* 2010; **102**: 419-427
30 **Serre D**, Lee BH, Ting AH. MBD-isolated Genome Sequencing provides a high-throughput and comprehensive survey of DNA methylation in the human genome. *Nucleic Acids Res* 2010; **38**: 391-399
31 **Li N**, Ye M, Li Y, Yan Z, Butcher LM, Sun J, Han X, Chen Q, Zhang X, Wang J. Whole genome DNA methylation analysis based on high throughput sequencing technology. *Methods* 2010; Epub ahead of print
32 **Jørgensen HF**, Ben-Porath I, Bird AP. Mbd1 is recruited to both methylated and nonmethylated CpGs via distinct DNA binding domains. *Mol Cell Biol* 2004; **24**: 3387-3395
33 **Neuhausen A**, Florl AR, Grimm MO, Schulz WA. DNA methylation alterations in urothelial carcinoma. *Cancer Biol Ther* 2006; **5**: 993-1001
34 **Stratton MR**, Campbell PJ, Futreal PA. The cancer genome. *Nature* 2009; **458**: 719-724
35 **Perry AS**, Foley R, Woodson K, Lawler M. The emerging roles of DNA methylation in the clinical management of prostate cancer. *Endocr Relat Cancer* 2006; **13**: 357-377
36 **Richter AM**, Pfeifer GP, Dammann RH. The RASSF proteins in cancer; from epigenetic silencing to functional characterization. *Biochim Biophys Acta* 2009; **1796**: 114-128
37 **Wieczorek G**, Asemissen A, Model F, Turbachova I, Floess S, Liebenberg V, Baron U, Stauch D, Kotsch K, Pratschke J, Hamann A, Loddenkemper C, Stein H, Volk HD, Hoffmüller U, Grützkau A, Mustea A, Huehn J, Scheibenbogen C, Olek S. Quantitative DNA methylation analysis of FOXP3 as a new method for counting regulatory T cells in peripheral blood and solid tissue. *Cancer Res* 2009; **69**: 599-608
38 **De Smet C**, Lurquin C, Lethé B, Martelange V, Boon T. DNA methylation is the primary silencing mechanism for a set of germ line- and tumor-specific genes with a CpG-rich promoter. *Mol Cell Biol* 1999; **19**: 7327-7335
39 **Lindgren D**, Frigyesi A, Gudjonsson S, Sjödahl G, Hallden C, Chebil G, Veerla S, Ryden T, Månsson W, Liedberg F, Höglund M. Combined gene expression and genomic profiling define two intrinsic molecular subtypes of urothelial carcinoma and gene signatures for molecular grading and outcome. *Cancer Res* 2010; **70**: 3463-3472
40 **Taylor BS**, Schultz N, Hieronymus H, Gopalan A, Xiao Y, Carver BS, Arora VK, Kaushik P, Cerami E, Reva B, Antipin Y, Mitsiades N, Landers T, Dolgalev I, Major JE, Wilson M, Socci ND, Lash AE, Heguy A, Eastham JA, Scher HI, Reuter VE, Scardino PT, Sander C, Sawyers CL, Gerald WL. Integrative genomic profiling of human prostate cancer. *Cancer Cell* 2010; **18**: 11-22
41 **Bell DW**. Our changing view of the genomic landscape of cancer. *J Pathol* 2010; **220**: 231-243

S- Editor Cheng JX **L- Editor** Webster JR **E- Editor** Ma WH

World Journal of Clinical Oncology

Online Submissions: http://www.wjgnet.com/2218-4333office
wjco@wjgnet.com
doi:10.5306/wjco.v2.i1.8

World J Clin Oncol 2011 January 10; 2(1): 8-27
ISSN 2218-4333 (online)

TOPIC HIGHLIGHT

E YK Ng, PhD, PGDTHE, Associate Professor, *Series Editor*

High intensity focused ultrasound in clinical tumor ablation

Yu-Feng Zhou

Yu-Feng Zhou, Division of Engineering Mechanics, School of Mechanical and Aerospace Engineering, Nanyang Technological University, 50 Nanyang Avenue, Singapore 639798, Singapore
Author contributions: Zhou YF solely contributed to this paper.
Correspondence to: Yu-Feng Zhou, PhD, Division of Engineering Mechanics, School of Mechanical and Aerospace Engineering, Nanyang Technological University, 50 Nanyang Avenue, Singapore 639798, Singapore. yfzhou@ntu.edu.sg
Telephone: +65-67904482 Fax: +65-67924062
Received: June 24, 2010 Revised: July 26, 2010
Accepted: August 2, 2010
Published online: January 10, 2011

Abstract

Recent advances in high intensity focused ultrasound (HIFU), which was developed in the 1940s as a viable thermal tissue ablation approach, have increased its popularity. In clinics, HIFU has been applied to treat a variety of solid malignant tumors in a well-defined volume, including the pancreas, liver, prostate, breast, uterine fibroids, and soft-tissue sarcomas. In comparison to conventional tumor/cancer treatment modalities, such as open surgery, radio- and chemo-therapy, HIFU has the advantages of non-invasion, non-ionization, and fewer complications after treatment. Over 100 000 cases have been treated throughout the world with great success. The fundamental principles of HIFU ablation are coagulative thermal necrosis due to the absorption of ultrasound energy during transmission in tissue and the induced cavitation damage. This paper reviews the clinical outcomes of HIFU ablation for applicable cancers, and then summarizes the recommendations for a satisfactory HIFU treatment according to clinical experience. In addition, the current challenges in HIFU for engineers and physicians are also included. More recent horizons have broadened the application of HIFU in tumor treatment, such as HIFU-mediated drug delivery, vessel occlusion, and soft tissue erosion ("histotripsy"). In summary, HIFU is likely to play a significant role in the future oncology practice.

Key words: High intensity focused ultrasound; Thermal ablation; Image-guided therapy; Cancer; Bubble cavitation; Bioeffects

Peer reviewer: Nathalie Lassau, MD, PhD, Imaging Department, Institut Gustave Roussy, 39 Rue Camille Desmoulins, 94800 Villejuif, France; Ali Syed Arbab, MD, PhD, Associate Scientist and Director, Cellular and Molecular Imaging Laboratory, Department of Radiology, Henry Ford Hospital, 1 Ford Place, 2F, Box 82, Detroit, MI 48202, United States; Ravi Murthy, MD, Interventional Radiology, UT MD Anderson Cancer Center, 1400 Pressler Street, Unit 1471, Houston, TX 77042, United States; Ronald Xiaorong Xu, PhD, Assistant Professor, Biomedical Engineering Department, The Ohio State University, 270 Bevis Hall, 1080 Carmack Rd., Columbus, OH 43210, United States

Zhou YF. High intensity focused ultrasound in clinical tumor ablation. *World J Clin Oncol* 2011; 2(1): 8-27 Available from: URL: http://www.wjgnet.com/2218-4333/full/v2/i1/8.htm DOI: http://dx.doi.org/10.5306/wjco.v2.i1.8

INTRODUCTION

Cancer is a major public health problem for human beings in both developed and developing countries. Currently, one in four deaths in the United States is due to cancer[1]. Cancer therapy demand in the United States will grow annually by 10% through 2009. Increases will be driven by more incidence and detection of cancer coupled with a range of highly effective, but expensive, new treatment modalities. $16.8 billion are spent each year for cancer therapies in the United States[2]. This represents historical demand data from 1994, 1999 and 2004 and forecasts to 2009 and 2014 by cancer type (e.g. breast, digestive system, genital system, leukemia, lymphoma), by product/procedure (e.g. chemotherapy drugs, surgery, radiation therapy, biotechnology-based drugs, hormonal therapy, vaccines, nanotechnology, stem cells), and by institution/provider

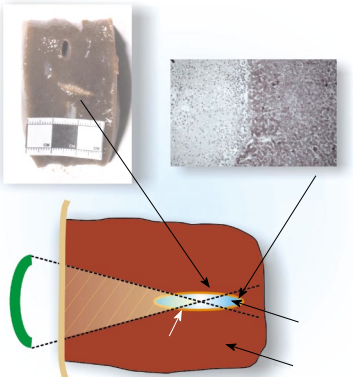

Figure 1 The high intensity focused ultrasound beam passes through overlying skin and other tissues without harming them and is focused to necrose a localized tumor region, which may lie deep within the body. There is a very sharp boundary between dead and live cells at this contour.

(e.g. hospitals, outpatient facilities, physicians' offices, home health care). The conventional therapy modalities are open surgery, chemo- and radio-therapy, which carry significant morbidity and mortality, and may be associated with long in-patient stays and recovery periods. A major goal of technological and medical research in fighting cancer is to significantly reduce local, regional, and systemic side effects, as compared with conventional therapies and to provide additional therapeutic options in cases where conventional therapies fail. New modalities have been introduced in recent years, such as radiofrequency, laser, microwaves, and cryoablation therapies.

The application of ultrasound in clinics is no longer limited to diagnosis. High intensity focused ultrasound (HIFU) is being promoted as the only completely noninvasive and extracorporeal method to treat primary solid tumors and metastatic disease. The key of HIFU treatment is to deliver the energy required to raise the tissue temperature to a cytotoxic level sufficiently fast such that the tissue vasculature does not have a significant effect on the extent of cell killing (Figure 1). Coagulative necrosis caused by heat differs in microscopic appearance and host response from the classical ischemic-type coagulative necrosis: heat coagulation favors giant cell reaction with chronic inflammation whereas ischemic-type necrosis causes healing mainly with granulation tissue. In addition, with heat coagulation, the surrounding normal fatty tissue frequently shows histological signs of fat necrosis. The boundary between apparently totally disrupted cells and normal tissue is no more than 50 μm in width[3]. However, lethal complications may develop if some vital blood vessels adjacent to the tumors are severely damaged. This indicates that large blood vessels are probably less vulnerable to HIFU damage than solid tissues (such as tumor tissue), presumably due to the blood flow dissipating the thermal energy from the vessel wall. Therefore, HIFU is a relatively safe method to ablate tumors in close proximity to major blood vessels, where surgical resection is often contraindicated and may be hazardous. The clinical applications for HIFU have been widely explored in neurosurgery, ophthalmology, urology, gynecology, and oncology[3-5] for about 100 000 patients to date, mainly in Asia and Europe. Preliminary reports suggest that there is reduced toxicity with HIFU ablation compared with other ablation techniques, such as cryotherapy, percutaneous alcohol ablation, and either percutaneous or laparoscopic radiofrequency because of the noninvasive nature of the procedure[6]. In addition, there is an upper size limit for tumors that can be treated, approximately 3-4 cm in diameter, with minimally invasive methods.

HIFU technology has the following advantages that justify research efforts: pain is minimized (the procedure is minimally- or non-invasive); the procedure cost is low as compared with traditional surgery; there are no remaining scars; recovery is faster than with traditional surgical methods; if any hemorrhage occurs, ultrasound (US) has the potential to stop the bleeding; the therapy can be repeated, theoretically, an infinite number of times because there is no dose limit; there is no ionizing radiation from magnetic resonance imaging (MRI) and diagnostic US, as opposed to other systems that are guided by X-rays; and maintenance of the system is low. Unpleasant side effects of current cancer therapies are often the limiting factor for treatment. For example, neurotoxic effects may limit the dose of a cytotoxic agent in chemotherapy. Similarly, in radiotherapy some critical surrounding normal tissues may receive an irradiation dose causing irreversible damage. Clinical trials, in which 68 patients have been treated at the Royal Marsden Hospital in London, have demonstrated that HIFU treatment for liver cancer is well tolerated by fully conscious patients who are treated on an outpatient basis and have not needed local anesthesia or sedation[7]. Altogether, HIFU has been becoming a viable thermal tissue ablation modality for solid tumors and an interesting topic for ultrasound researchers and engineers.

This article initially introduces the principles of HIFU, its history and development from a technical viewpoint. Secondly, clinical outcomes of current HIFU applications in the treatment of prostate, breast, liver, renal tumors, and uterine fibroids are reviewed. It is noted that, with the development and wide acceptance of HIFU ablation, its application is not limited to the diseases mentioned above. Finally, the practical experiences of successful tumor ablation and technical challenges met in clinical applications are summarized from numerous trials. Furthermore, other HIFU-related technologies, which may play an important role in future cancer treatment, are also introduced.

HIFU BACKGROUND

History

The first therapeutic trial of high intensity ultrasound beams was carried out in 1942[8]. The Fry brothers are credited with the first application of HIFU for neurologic disorders in humans[9]. Early attempts to generate HIFU lesions in the brain through the intact skull bone were unsuccessful[8,10]. Small lesions were found in the brain, but there was profound damage to the scalp. Although

it was claimed that the symptoms of Parkinsonism were eliminated, this treatment was not taken further, probably because of the concurrent development of the drug L-dopa. The requirement to remove a section of the skull bone and the lack of imaging sophistication limited the progress of this neurosurgical research in its earlier days. In 1970s, US was used to induce hyperthermia (elevation of tissue temperature to about 43℃) in the entire tumor volume for an extended time (about 1 h)[11]. A rediscovery of HIFU for the treatment of tumors occurred in the 1990s with the refinement of modern technologies in transducer design, modes of energy delivery, and real time imaging. Precise targeting and good treatment follow-up techniques (with anatomical and functional imaging) were available with diagnostic US scanning and MRI techniques, which paved the way to realizing the full potential of HIFU treatment. The ability of HIFU to target subcutaneous tissue volumes and produce almost instantaneous cell death by coagulation necrosis in the selected regions of deep-seated soft tissue tumors has made it a candidate for direct and rapid treatment of tumors[3-5].

HIFU principles

HIFU relies on the same principles as conventional US. The time-averaged intensities of typical diagnostic US (B-mode, pulsed or continuous Doppler) can be up to 720 mW/cm^2 according to United States Food and Drug Administration (USFDA) regulations. In contrast, the intensity of HIFU in the focal region is about several orders higher, 100-10 000 W/cm^2, with peak compression pressures of up to 70 MPa and peak rarefaction pressures up to 20 MPa.

Two main mechanisms are involved in the HIFU ablation: a thermal effect and a mechanical effect. The thermal effect of HIFU is heat generation due to absorption of the acoustic energy with a rapid elevation of temperature in the local tissue. Tissue temperature elevated to more than 60℃ for 1 s will generally lead to instantaneous and irreversible cell death *via* coagulation necrosis in most tissues, which is the primary mechanism for tumor cell destruction in HIFU therapy. Ultrasound beam focusing results in high intensities only at a specific location within a small volume (e.g. about 1 mm in diameter and about 10 mm in length), which minimizes the potential for thermal damage to tissue outside the focal region. Since the thermal mechanism is better understood and its effect is easier to control, it is preferred in tissue ablation.

Tissue thermal damage at high-temperature exposures can be predicted by using an Arrhenius analysis or the Sapareto-Dewey iso-effect thermal dose relationship, which demonstrate that tissue thermal damage is approximately linearly dependent on exposure time and exponentially on the temperature elevation[12]. For convenience, a thermal dose, which is expressed in equivalent minutes at 43℃ (EM43℃ or t_{43}), is usually applied in hyperthermia or high-temperature hyperthermia. Thermal doses of 120-240 min at 43℃ irreversibly damage and coagulate critical cellular protein, tissue structural components and the vasculature leading to immediate tissue destruction, however, the threshold varies with tissue type[13]. At the borders of the thermal coagulated lesion, the tissue will die within 2-3 d.

Mechanical effects induced by HIFU are associated with acoustic pulses only at high intensities, including cavitation, micro-streaming, and radiation force. Cavitation is defined as the creation or motion of a gas cavity in an acoustic field due to alternating compression and expansion of tissue as an ultrasound burst propagates through it. There are two forms of cavitation: stable and inertial cavitation[14]. Stable cavitation is the stable oscillation of the size of the bubble when exposed to a low-pressure acoustic field. Inertial cavitation is violent oscillations of the bubble and rapid growth of the bubble during the rarefaction phase when they reach their size of resonance, eventually leading to the violent collapse and destruction of the bubble. The violent collapse will produce shock waves of very high pressure (20-30 000 bars) and high temperature (2000-5000 K) in the microenvironment[14]. The oscillating motion of stable cavitation causes the rapid movement of fluid near the bubble due to its oscillating motion, which is called the "micro-streaming" effect. Micro-streaming can produce high shear forces that can cause transient damage to cell membranes and may play a role in US-enhanced drug or gene delivery[15]. Meanwhile, radiation force is developed when an acoustic wave is either absorbed or reflected. If the medium is liquid and can move freely, the liquid motion will lead to the generation of microscopic streaming, which can also induce cell apoptosis[16]. In apoptotic cells, the nucleus of the cell self-destructs with rapid degradation of DNA by endonucleases. Apoptosis may be an important delayed bioeffect in tissue exposed to HIFU, especially in cell types that regenerate poorly, such as neurons.

HIFU system

HIFU devices for clinical use fall into three main categories: extracorporeal, transrectal, and interstitial. Extracorporeal transducers are used for targeting organs that are readily accessible through an acoustic window on the skin, whereas transrectal devices are used for the treatment of the prostate and interstitial probes are being developed for the treatment of biliary duct and esophageal tumors.

Focusing a high-intensity US beam can be achieved by a concave self-focusing transducer (e.g. Sonablate-500, Focus Surgery, USA), or arranging multiple piston transducers on the truncated surface of a spherical bowl (e.g. FEP-BY02, Beijing Yuande Biomedical Engineering, China), or fronting a flat transducer with a suitably designed acoustic lens (e.g. Model-JC, Chongqing HAIFU™, China). The -6 dB beam size of HIFU system in its focal region is usually 1-3 mm in width and about 10 mm in length, depending on the geometrical size and acoustic parameters of the HIFU transducer applied. However, the detectable and treatable tumor/cancer in HIFU is at least 1 cm in size. In order to treat the target, HIFU focus should be scanned throughout the entire volume. Moving and/or rotating the HIFU transducer with a fixed focus in a mechanical way

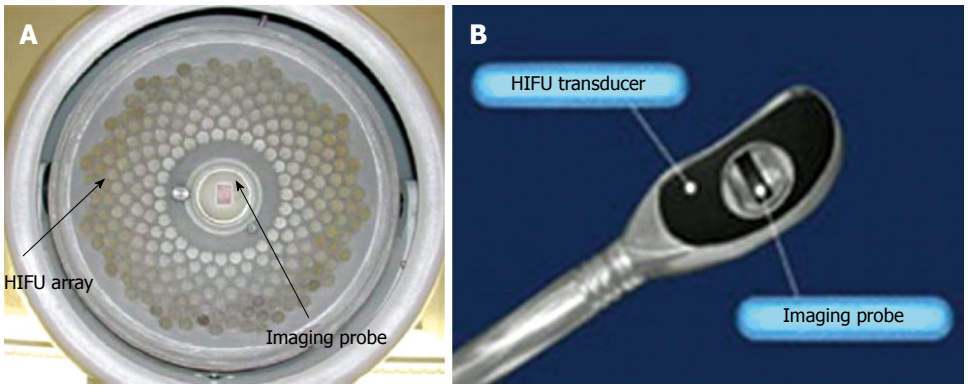

Figure 2 The structure of (A) an extracorporeal (FEP-BY02) and (B) a transrectal (Ablatherm) high intensity focused ultrasound transducer. HIFU: High intensity focused ultrasound.

was the common method used in the first generation of HIFU systems because of the simplicity in control regardless of the system type. Thanks to developments in electrical control and US transducer fabrication, another focusing and scanning approach became available in the second generation by utilizing phased array technology and adjusting the amplitude and phase of each element individually. Phased array allows more rapid and electrical steering of the HIFU focus through tissue, and greater flexibility in focal geometry. Tissue inhomogeneity in abdominal-pelvic (e.g. uterine fibroids and renal tumors) or transcranial applications might cause focal beam distortion and might largely decrease the focusing ability in deep-seated tissues. Focal beam patterns can be virtually restored by using the phase correction procedure as in US imaging. Subsequently, significant improvement on the shape of temperature profiles and the accuracy of temperature control are expected.

The acoustic energy may be delivered in two ways in HIFU ablation. A single exposure may be made with the transducer held stationary. When larger volumes are to be ablated, the transducer may be moved in discrete steps either mechanically or electronically, and fired at each position, where the distance between "shots" will determine whether lesions are overlapped or separated, depending on the necessity to achieve confluent regions of cell killing (e.g. FEP-BY02 and Sonablate-500 systems). An alternative exposure strategy is to move the active therapy transducer in pre-determined trajectories (e.g. linear tracks or spirals) to conform to the required treatment volume. If the correct combination of transducer velocity and US energy is used, these result in confluent volumes of cell damage (e.g. Model-JC system).

The optimal choice of therapeutic US frequency is application-specific, and represents a compromise between treatment depth and the desired rate of heating. Frequencies near 1 MHz have been found to be most useful for heat deposition, with frequencies as low as 0.5 MHz being used for deep treatments or with large absorption portion in the propagation path (e.g. transcranial application) and as high as 8 MHz for superficial treatments (e.g. prostatic application)[17]. Usually an extracorporeal device has a wide aperture and a long focal length and is driven at high power. Wide aperture sources have the advantage of distributing the incident energy over a large skin area, thus reducing the acoustic intensity at the wave entry site and the consequent possibility of skin burn. Transrectal and interstitial sources operate at lower powers and higher frequencies as they can be placed closer to the target volume. Typical HIFU systems are shown in Figure 2.

An extracorporeal HIFU device is usually used for targets lying within the breast, abdomen, brain or limbs. Transcutaneous treatments require an appropriate acoustic window on the entry site that provides a propagation path for the focused US beam that is uninterrupted by intervening gas. In addition, it must be possible to couple the US energy to the skin surface using coupling gel, a water balloon, or other suitable liquid path. Extracorporeal HIFU treatments are guided using either US (e.g. FEP-BY02 of Beijing Yuande Biomedical Engineering and Model-JC of Chongqing HAIFU™ Co.) or a MRI modality (ExAblate 2000 of InSightec, Israel).

MRI has excellent anatomical resolution and high sensitivity for tumor detection, thereby offering accurate planning of the tissue to be targeted. In order to be used in the high magnetic fields of MRI, HIFU transducers must be specially designed for compatibility. The lead zirconate titanate (PZT) ceramic material, commonly used for US transducers, contains nickel, which is necessary for the high levels of electrical excitation and mechanical stress induced. However, nickel causes magnetic field distortion. Therefore, the new piezo-composite materials are usually used to develop MRI-compatible transducers. Using MR thermometry, it enables calculation of thermal dose and superimposes a representation of the regions in which the thermal dose has achieved cytotoxic levels on the anatomical MR image. The phase-shift image used to visualize the temperature-dependent changes in proton-resonance frequency using a fast spoiled gradient-recalled echo sequence (SPGR)[18] is more reliable than T1-weighted imaging[19]. MR proton resonance frequency thermometry at 1.5 T with segmented gradient-echo echo planar imaging (GRE-EPI) sequences has been evaluated during liver tumor radiofrequency (RF) ablation. It was found that MR proton resonance frequency thermometry at 1.5 T yields precise

and accurate measurements of temperature increments (1.3 ± 0.4℃ with frame rate of 0.6 s/image). Rapid GRE-EPI sequences minimize intra-scan motion effects and can be used for MR thermometry during RF ablation in moving organs[20]. In addition, T1 or T2 weighted fast spin-echo (FSE) were proven successful to image thermal lesions created by HIFU in rabbit liver *in vivo*. The contrast to noise ratio (CNR) with T1-weighted FSE was significantly higher than T2-weighted FSE (25 *vs* 14). With T1-weighted FSE, the range of repetition time (TR) under which CNR is high ranges from 400 to 900 ms[21]. Therefore, during the HIFU procedure, the temperature-sensitive MRI provides the ability of closed-loop control of energy deposition, with temperature accuracy of 1℃, spatial resolution of 1 mm, and temporal resolution of 1 s. Immediate post-treatment assessment of the therapy is also available.

Although MRI has the advantage of providing temperature data within seconds after HIFU exposure and it is superior to sonography in obese patients[22], MRI guidance is expensive, labor-intensive, and of lower spatial resolution in some cases. The temporal and spatial averaging effect of the MRI thermometry cannot be ignored and leads to the underestimation of temperature. The temperature measured in a single MRI voxel by water proton resonance frequency shift attained a maximum value of only 73℃ after 7 s of continuous HIFU exposure when boiling started, which was detected by visual observation and appearance on the MR images. Theoretical simulation predicted 100℃ after 7 s of exposure and the averaged temperature field over the volume of the MRI voxel 0.3 mm × 0.5 mm × 2 mm yielded a maximum of 73℃, which agreed with the MR thermometry measurement[23]. In comparison, US imaging modality is generally more convenient and mechanically compatible. US guidance provides the benefit of imaging using the same form of energy that is being used for therapy. The most significant is that the condition of the acoustic window can be verified with sonography in real-time (usually 30 Hz frame rate depending on the imaging depth and configuration). Therefore, if the target cannot be well visualized with sonography before or during the HIFU ablation, it is unlikely that HIFU therapy will be effective in the target region, and it may potentially cause thermal injury to unintended tissue (e.g. skin on the acoustic wave entry site). An US diagnostic transducer is usually incorporated into the treatment head (Figure 2), which allows real time imaging of the ablation process. However, the thermally ablated region is not visible on standard B-mode images unless gas bubbles have been induced as hyperechoic spots. In addition, the US image quality may be less than optimal.

HIFU with MRI and US guidance have their advantages and shortcomings. US guidance is good for preprocedural tumor localization, but not good for intraprocedural assessment of therapeutic boundaries because the non-specific acoustic contrast generated by heat-induced tissue bubbles. MRI is good for transient tissue temperature measurement, but cannot effectively measure the "lethal thermal dose" and is not sensitive to fat tissue[24]. In recent years, magnetic resonance-guided focused US surgery (MRgFUS) has been developed as an integrated system for HIFU therapy. Heat sensitive microbubbles have also been explored for enhanced US imaging of lethal thermal doses[25].

The transrectal devices that have been developed for the treatment of benign and malignant prostate disease can be inserted per rectum. The two commercially available devices, the Ablatherm© (Edap Technomed, France) and the Sonablate™ (Focus Surgery, USA), incorporate therapy and imaging transducers into a treatment head mounted at the end of a transrectal probe. Prostate ablation is achieved by placing touching lesions side by side. In the Ablatherm device, lesion length is varied by adjustment of the US power. However, thicker prostates are ablated using two layers of lesions in the Sonablate system, the deeper layer being created using a longer focal length than the more superficial layer. The different focal lengths are achieved by rotating the transducer since the two sides have different geometries. Usually coupling water is circulated and cooled during the HIFU therapy to avoid thermal damage to the interface tissue due to the temperature increase on the surface of the HIFU transducer and to maintain working stability of the HIFU transducer. In contrast, because of the large size of the water balloon in the extracorporeal HIFU system, water cooling in real-time is not required and the degassed water is suggested to be changed every 1-2 h.

There has been increasing interest in the development of high intensity US probes for interstitial use, and volume destruction is obtained by rotating the probe[26]. Usually plane transducers, rather than focusing elements, are used. Once 360° of rotation has been achieved the probe can be repositioned under fluoroscopic or MRI guidance to create other adjacent rings. The interstitial devices can be used for biliary and esophageal tumors, or bloodless partial nephrectomy. It can also be developed into a MR compatible device, or percutaneous and laparoscopic devices. Commercial products are expected to enter the market in the near future.

Popular HIFU systems that have been reported in clinical use are listed in Table 1. With development of the HIFU market, more devices are being developed or are in different stages of clinical trials. Therefore their performance and specifications have not been offered to the public.

System characterization

Conventionally, US exposures are characterized in terms of the acoustic field determined in the free field. The parameters necessary for describing HIFU exposures are frequency, exposure time, transducer characteristics (geometry and configuration), total power delivered, acoustic pressure and intensity, and energy delivery mode. The total acoustic output power is usually determined using a radiation force balance method[27]. The acoustic exposure power is proportional to the discrepancy of force applied to an absorbing target between HIFU on and off, and depends on the beam convergence angle, the shape and properties of the absorbing target, and the HIFU transducer configuration. Other important factors

Table 1 Summary of most popular high-intensity focused ultrasound system for clinical use

Model	Manufacturer	Size (mm)	Focal length (mm)	Frequency (MHz)	Focusing method	Imaging guidance	Clinical applications
FEP-BY02	Beijing Yuande Biomedical Engineering Inc, China	OD = 370 ID = 120	255	1	251 elements driven in phase	GE Logiq series ultrasound system	Liver, kidney, breast, pancreatic, bone tumor and uterine fibroid
Model-JC	Chongqing Haifu Tech Ltd, China	D = 120 or 150	90, 130, 160	0.8, 1.6, 3.2	Flat ceramics with acoustic lens	AU3 ultrasound imaging system	Liver, kidney, breast, pancreatic, bone tumor and uterine fibroid
ExAblate 2000	InSightec Ltd, Israel	120	150	0.9, 1.3	Phased array 208 hexagonal elements, 3 cavitation detector	GE Signa 1.5/3.0T MR imaging system	Uterine fibroids, breast tumor, liver cancer, bone metastases, neurosurgery, prostate cancer
Sonalleve	Philips, USA	N/A	N/A	1.2, 1.4	Phased array	Philips Achieva 1.5/3.0T MR imaging system	Uterine fibroids
Sonablate 500	Focus Surgery Inc., USA	30 × 22	30 and 40 or 45/50	4	2 elements mounted back-to-back	Element for both therapy and imaging	Prostate cancer
Ablatherm	Edap-Technomed, France	40 × 22 ID = 8	45	3	Single concave element	7.5 MHz integrated ultrasound imaging	Prostate cancer
TH-One	Theraclion, France	56	38	3	Single concave element	B-K Medical ultrasound imaging system	Hyperparathyroidism

N/A: Not available; GE: General electronics; MR: Magnetic resonance.

affecting the measurement are the distance of the target from the source, absorption of energy in the water bath between the transducer and the target, and acoustic streaming effects. The radiation force balance method is particularly useful when very strongly focused transducers and phased arrays are being characterized.

Acoustic pressure is measured using a hydrophone. Both needle and polyvinylidene fluoride (PVDF) membrane hydrophones have been used widely in the calibration acoustic field at low (e.g. US diagnostic system) and intermediate (e.g. physiological US devices) power level. PVDF hydrophones have the advantage of only minimally disturbing the field and high sensitivity, but may be prone to cavitation damage at their surface in a high intensity field. Once damaged, the PVDF and needle hydrophone will not be usable until recalibration. Beam profiles are usually measured at much lower output levels than are used for clinical HIFU treatment and it is assumed that a linear extrapolation to high levels is valid[28]. This method introduces errors since it ignores the effects of nonlinear propagation occurring at high pressures, which increases the amplitude of peak positive pressure significantly, reduces the wave front rise time (formation of shock wave), and introduces harmonic components. Recently, a fiber optic probe hydrophone (FOPH) was used in the HIFU acoustic field measurement[29]. FOPH is robust to the cavitation damage to sensor and has a broad bandwidth (up to 100 MHz after deconvolution) to guarantee the accurate measurement of all harmonics. A new tip can be prepared easily with self-calibration even after damage (optical fiber included in the FOPH is supposed to be used for a life time). With use, the acoustic pressure at high power can be measured directly and operation is rather straight-forward. Once the position of the focal peak has been established, the peak acoustic pressure amplitude can be measured, from which intensity will be calculated. The hydrophone is scanned in the focal region under the automatic control of the three-dimensional translational stage, and measured waveforms are transferred to a computer for further off-line processing. The beam size (usually -6 dB/half of maximum pressure in the lateral and axial directions) can be determined from the pressure distribution. Hill *et al*[28] defined a parameter, I_{SAL}, which is the acoustic intensity spatially averaged over the area enclosed by the half pressure maximum contour. It was demonstrated that there was a correlation between lesion diameter and I_{SAL}[30].

CLINICAL APPLICATION

Prostate tumor

Transrectal HIFU treatment of prostate tumors is one of the pilot investigations. Both benign prostate hyperplasia (BPH) and prostate carcinoma have been targeted at a few medical centers in Europe and Japan in the past decade. Initial clinical trials for BPH treatment were encouraging[31,32], with increases in flow rate and decreases in post-void residual volume. However, the long-term results were disappointing[33], with 43.8% of patients requiring a salvage trans-urethral resection of the prostate (TURP) within 4 years. Therefore, HIFU has not been proved significantly better than the "gold standard" treatment (TURP), and is not recommended for treatment of this condition[34].

In contrast, treatment of prostate cancer presents different problems from those associated with BPH treatment[35]. Prostate cancer is a multi-focal disease, with the foci difficult to detect with diagnostic US. The most successful HIFU treatments have been those that have ab-

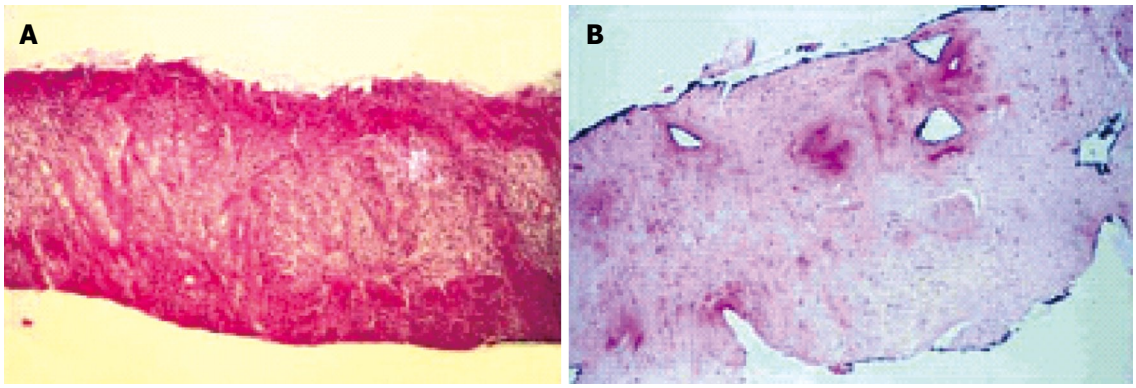

Figure 3 Complete destruction of the glandular tissue due to coagulation necrosis lesion which reaches the capsula and the periprostatic fat 48 h after high intensity focused ultrasound treatment (A) and the necrotic prostatic tissue is replaced by a fibrotic tissue, including the capsula, 3 mo after high intensity focused ultrasound therapy (B).

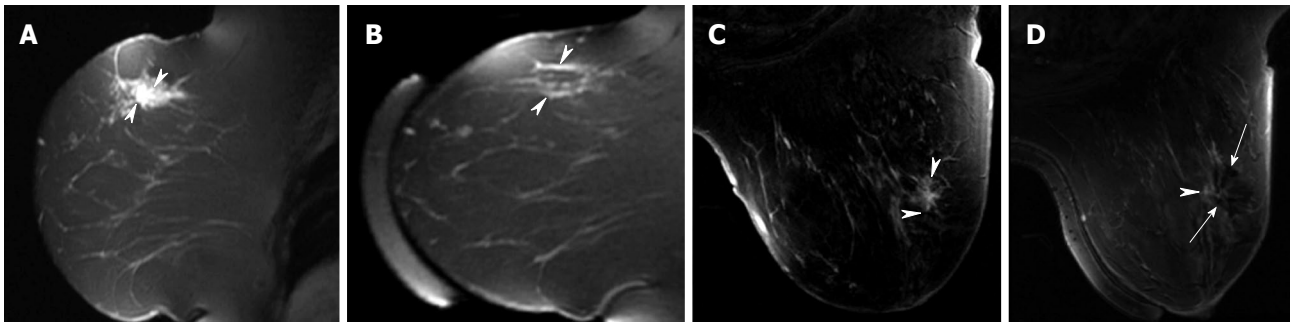

Figure 4 Sagittal contrast-enhanced T1-weighted fat-saturated magnetic resonance sagittal (A) and axial (C) images of a 1.8-cm poorly differentiated invasive ductal carcinoma in a 44-year-old woman before MRgFUS. An irregular enhancing mass is seen in the upper outer quadrant of the right breast (arrow heads). Three days after magnetic resonance-guided focused US surgery (MRgFUS), minimal strikes of enhancement are seen without mass like enhancement in the sagittal image (arrow heads in B), which may represent hyperemia due to reactive inflammation or residual tumor. On the axial image (D), dark signal void area is seen at the site of the prior enhancing mass (long arrows). At histopathology, about 50% of the carcinoma and adjacent normal tissue showed thermal effects and the remaining portion of the carcinoma appeared viable.

lated the whole gland[31,32]. With experience, control rates for the treated tumor have risen from 50% at 8 mo in the early days to 90% more recently[36,37]. Mid-term follow-up (2-5 years) has shown that the prostate specific antigen (PSA) levels remain low and that the negative biopsy rate remains around 90%[36,38,39]. Success rates for the treatment of prostate cancer range from 60%[4] to 80%[40] of patients being disease-free at repeat biopsy and show a reduction of serum PSA values to less than 4 ng/mL[41]. Whole-gland versus focal treatment resulted in a reduced incidence of recurrent tumor of 35% to 17% in one series; in patients not found to be disease-free, reductions in tumor volume greater than 90% have been reported[40]. A representative complete destruction of the glandular tissue due to coagulation necrosis lesion is shown in Figure 3.

Complications reported from prostate HIFU include urinary retention, incontinence, urinary infection, impotence, chronic pain, rectal anal fistulas, and incomplete treatment of disease[42]. Repeat treatment with HIFU is associated with much higher complication rates than single treatments[43,44]. To mitigate urinary retention associated with prostate HIFU, transurethral resection was performed before treatment[45,46]; and in these patients, the length of time with indwelling catheters remaining in the bladder has been reduced from 40 to 7 d[36]. Prostate HIFU seems most appropriate in men older than 65 years, those who are not candidates for surgery, and those who are obese[47,48].

Breast tumor

The standard treatment for women with breast cancer desiring breast conservation is lumpectomy followed by external radiation therapy. There is increasing interest in recent years to use nonsurgical ablation as part of a breast-conservation therapy in patients with early breast cancer. The cosmetic results and side effects after conventional breast-conservation treatment are acceptable to most patients; however, the nonsurgical ablation methods are thought to be psychologically and cosmetically more satisfactory. HIFU is one of the noninvasive and effective techniques to induce local tumor necrosis, and is also suitable for treating patients who are at high risk for surgery with less anesthesia, reduced in-hospital recovery time and cost, less risk of infections, and no scar formation[49] (Figure 4).

The HIFU can precisely deliver energy to a given point in soft tissue without interrupting skin integrity. Very few severe (3rd-degree skin burn) and a few minor adverse events were reported. Proximity to the skin should be avoided, and it is important to keep safety margins during

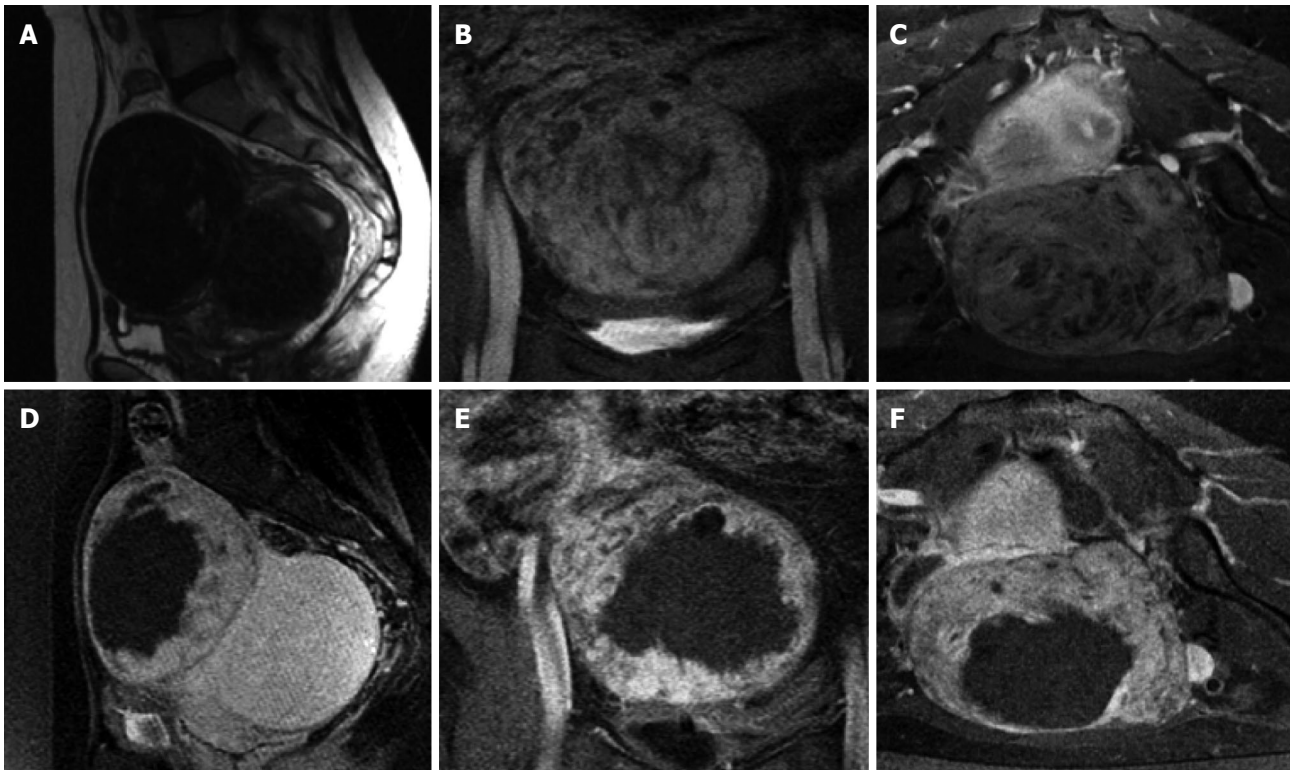

Figure 5 Images of a uterine fibroid pretreatment and posttreatment with MRgFUS. Top, Sagittal T2 fast spin-echo (A), coronal spoiled gradient-recalled echo sequence (SPGR) postgadolinium (B), and axial SPGR postgadolinium (C) are obtained pretreatment. The low SI homogenous fibroid depicted in Figure 3A demonstrates slight heterogenous enhancement pretreatment (Figure 3B, C). Bottom, Sagittal SPGR post-gadolinium (D), coronal SPGR post-gadolinium (E), and axial SPGR post-gadolinium (F) are obtained immediately post-treatment. A new large nonperfused area is identified, consistent with treatment-induced necrosis.

the HIFU treatment of breast carcinomas. In total, 19 of 24 patients were considered to have undergone successful treatment (breast biopsy free of neoplasia after 1 or 2 sessions of HIFU). All patients remained free of metastasis on routine follow-up (mean follow-up, 20.2 mo)[50]. The main argument against noninvasive treatments of breast cancer, including HIFU, is that the margin status cannot be assessed due to lack of pathological specimen. Radiological assessment, mainly post-procedure contrast-enhanced MRI, must replace histopathology.

Uterine fibroids

Uterine leiomyomas (fibroids) are gonadal steroid-dependent benign smooth-muscle tumors and are one of the most common female pelvic tumors, occurring in approximately 25% of women[51]. Whereas many patients remain asymptomatic, others experience symptoms such as pelvic pain, menorrhagia, dysmenorrhea, dyspareunia, urinary frequency, and infertility. The most common organ of origin is the uterus, although fibroids can also arise from the fallopian tubes, broad ligament, or cervix. Women are, however, increasingly seeking less invasive treatment options, perhaps motivated toward fertility preservation and a reduction in procedure recovery time. MRI is an optimal modality for further characterizing fibroids because of its good inherent tissue contrast. The addition of post-intravenous gadolinium imaging further characterizes these benign tumors, detecting homogenous enhancement or areas of internal necrosis, which may affect treatment decisions. Gadolinium helps differentiate cellular from degenerating fibroids; cellular lesions usually demonstrate diffused early homogenous enhancement with dynamic imaging, whereas degenerating fibroids demonstrate irregular, delayed, or no enhancement (Figure 5).

MRgFUS was approved by the USFDA in October 2004, with more than 2000 patients treated to date worldwide. Clinical trials were carried out at 5 medical centers across the United States[52,53], in addition to centers in Japan[54], the United Kingdom, Germany, and Israel. Enrollment of phase Ⅰ/Ⅱ began in 1999. The purpose of this study was to assess the safety and feasibility of MRgFUS in the treatment of fibroids. Suitable symptomatic candidates were chosen using an 8-item symptom severity score (SSS) of the Uterine Fibroid Quality of Life Questionnaire[55]. An SSS of 21 of a possible 40 points were required for entry into the clinical trial, as a reflection of the significant fibroid-related symptom burden. Premenopausal women with symptomatic uterine fibroids who have no desire for future pregnancy were included. This treatment is not indicated for pregnant women, postmenopausal women, or those with contrast-enhanced MRI contraindications. The MRgFUS did indeed result in hemorrhagic necrosis in the area of non-perfusion on the post-treatment MR. Only 10% of patients reported taking pain medication within 72 h of treatment. The phase Ⅲ clinical trial involved treatment of larger volumes in the fibroids of women with

symptomatic uterine fibroids. Seventy-nine percent of treated patients reported a 10-point reduction in their SSS, at 6 mo post-treatment, with a 13.5% mean reduction in treated fibroid volume. Most of the improvement in SSS occurs within the first 3 mo of treatment. However, at 12 mo post-treatment, only 51% of those evaluable reported a 10-point reduction in SSS and 28% of patients underwent an alternative treatment by 12 mo[56]. These results should be interpreted in view of the fact that on average only 10% of the fibroid volume was treated, as this FDA-approved study design sought to maximize safety. Gonadotrophin-releasing hormone agonists (GnRHa) are well known to cause a reduction in fibroid size when administered in a continuous fashion. It has recently been demonstrated that the pretreatment of patients who have fibroids measuring 10 cm or greater with GnRHa, before MRgFUS, has a beneficial effect, enhancing the tissue response to HIFU[57].

Although the clinical outcome is best assessed using a disease-specific questionnaire, symptom relief and fibroid volume reduction cannot be assessed until some period later. Immediately post-treatment with MRgFUS, it was found that apparent diffuse coefficient (ADC) values were significantly lower within the area of treatment, which may suggest cell necrosis and loss of membrane integrity due to this treatment. Long-term changes in ADC values on follow-up studies, and the reason for these changes, remain to be determined. In 109 patients studied, leg and buttock pain were reported after treatment. Although the MR neurography and electromyography studies failed to show any intrinsic damage, the sciatic nerve was revealed in the far field of the sonication region.

Liver tumor

Hepatocellular carcinoma (HCC) is rapidly becoming the most common malignancy worldwide. Surgery, particularly liver transplantation, offers the only real hope for cure; but survival rates are only 25%-30% at 5 years. Despite considerable advances in diagnostic modalities, the overall prognosis of primary and metastatic liver cancer remains dismal. The poor outcome is attributed mainly to the characteristic biological behavior of hepatic cancer: multiple foci of origin, resulting in low rates of respectability and a high risk of postoperative recurrence. For such a multi-focal and frequently recurrent malignancy, a logical and attractive method of treatment would be using a noninvasive therapeutic modality that can selectively destroy multiple tumor nodules scattered throughout the liver without impairing liver function. A noninvasive therapeutic system would also allow repeated application when necessary. Tumors can be destroyed by producing a contiguous lesion lattice encompassing the tumor and appropriate margins of surrounding tissue determined by computer coordination.

Small animal models have established that HIFU can ablate areas of normal liver[58], and energy thresholds for liver tissue destruction have been published[59]. A maximum lesion size was observed on the third day after treatment, and its replacement by a thin fibrous scar after several months[58]. When intensity was kept constant and exposure time increased, the lesion size increased to a maximum, after which longer exposure times did not cause larger lesions. An optimal result was reached when the necrosis area in the liver had the same dimensions as the desired volume at the desired location. After treatment of normal rabbit livers, hyperechogenic patterns at the target location were rarely observed, even when a homogenous lesion was observed at autopsy. When this hyperechogenic pattern was present immediately, it disappeared 3 wk later. In contrast, the hyperechogenic pattern was always present after successful treatment of rabbits bearing a liver tumor. However, there was no correlation between the size of the hyperechogenic area and the volume of the coagulation necrosis at autopsy[58].

Studies of the treatment of HCC and secondary liver metastasis in human clinical trials have also been published[60,61]. Destruction rates as estimated by quantitative microscopy on millimetric tissue slices ranged from 42.5% to 100%. Histology showed a homogenous dwell-delineated coagulation necrosis corresponding to the target volume in the depth of the liver. No viable tumor tissue remained in the treated area[62]. A model-JC HIFU device has been used to treat 68 patients with liver malignancies in China. In 30 cases in which surgical excision followed HIFU ablation, the tumor was totally ablated[63]. Subsequently, 474 patients with HCC were treated using the same device[64]. HIFU has also been used for palliation in patients with advanced-stage liver cancer[65]. After treatment, 87% of patients reported symptomatic improvement. Patients were also randomized between transarterial chemoembolization (TACE) and HIFU[66]. The median patient survival times were 11.3 mo in the combined HIFU-TACE group and 4 mo in the TACE-only group ($P = 0.0042$). Overall, HIFU has been shown significant promise in the treatment of hepatic malignancies. Tumor growth inhibition rates from 65%-93% were seen in the HIFU-treated group. They also showed a longer median survival in groups treated with HIFU or HIFU combined with doxorubicin[67].

Renal tumor

Surgery remains as the mainstay of treatment for renal tumors, with 5-year survival rates greater than 80% after resection[68]. Because most renal tumors are small, a noninvasive approach for their treatment would be attractive. Currently HIFU ablation of renal tumors in humans remains in the early stages of clinical trials. A clinical feasibility study has been performed on 8 patients who showed histological evidence of ablation in the treated areas after excision[69]. Wu *et al*[70] reported a series of 13 patients with renal cell carcinoma. Nine of 10 patients treated for palliation reported a reduction in pain. No side effects occurred after ablation using an experimental handheld device. Further investigations continue to study the efficacy of HIFU treatment of renal cell carcinoma for both cure and palliation[70].

Pancreatic cancer

More than 32000 people are diagnosed with pancreatic

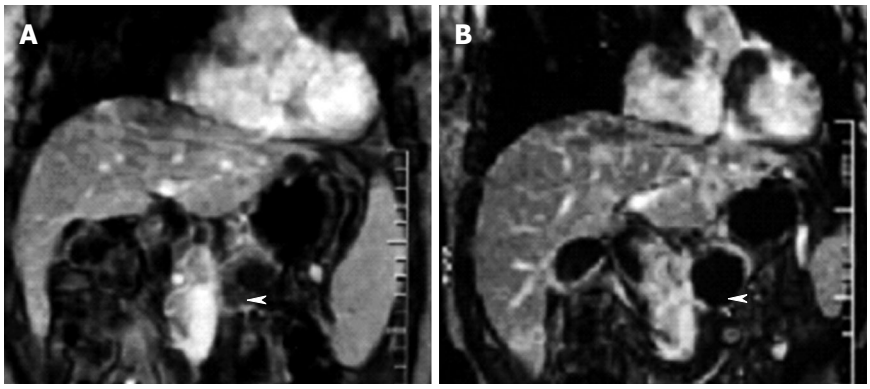

Figure 6 Dynamic contrast-enhanced gradient-echo T1-weighted magnetic resonance images (180/6.0, 90° flip angle, 128 × 256 matrix, 10-mm-thick sections, 2-mm intersection gap, one signal acquired, and 18-s acquisition time) obtained with breath holding in 48-year-old man who underwent high-intensity focused ultrasound ablation for advanced pancreatic cancer. The tumor was 4.5 cm × 4.5 cm in diameter and located in the body of the pancreas. A: Image obtained before high-intensity focused ultrasound shows the blood supply in the pancreatic lesion (arrowhead); B: Image obtained 2 wk after high-intensity focused ultrasound shows no evidence of contrast enhancement in the treated lesion (arrowhead), which is indicative of complete coagulation necrosis in the pancreatic cancer.

cancer annually in the United States and as many as 200 000 patients annually worldwide; the 5-year survival rate is less than 5%[1,71]. Pancreatic adenocarcinoma accounts for 5% of cancer deaths in the United States and is the fourth leading cause of cancer mortality. However, only less than 20% of pancreatic cancer patients can undergo open surgery. Two hundred and twenty-three patients with advanced pancreatic cancer (Tumor Node Metastasis stages Ⅱ-Ⅳ) have been treated in China, and the results from this open-label study suggested that HIFU can reduce the size of pancreatic tumors without causing pancreatitis and thus prolong survival[72]. Before HIFU treatment, all patients had obvious visceral pain that necessitated management with oral analgesic drugs. The pain associated with unresectable pancreatic cancer in 84% of patients, however, had resolved significantly within 24-48 h after a single session of HIFU treatment and the pain relief persisted during the follow-up period. 223 patients were followed up from 8 to 36 mo. The average survival time was 12.5 mo and 6 patients survived more than 3 years. No skin burns caused directly by HIFU were observed in this group, and no deaths had occurred 1 mo after HIFU therapy (Figure 6). During the hospital stay, no signs of tumor hemorrhage, large blood vessel rupture, or gastrointestinal perforation were detected in any patient. No dilatation of the common bile duct or pancreatic duct was visible at follow-up imaging. There was no evidence of postinterventional pancreatitis, peritonitis, or jaundice in any patient during the follow-up period[72,73]. Other initial nonrandomized open-label human studies have provided additional evidence that HIFU treatment of pancreatic tumors indeed relieves pancreatic adenocarcinoma-related pain and focally ablates malignant tissue[66].

Bone tumor

Surgical removal and radiation therapy are commonly used strategies to treat bone tumors. The former is often used for primary bone tumors, whereas the latter is more often than not adopted for bone metastases. Initially HIFU was not considered as a suitable modality for bone diseases because of the great difference of acoustic impedance of bone from that of the surrounding soft tissue. However, Smith *et al*[74] found that focused US beams can target bone tissues and induce necrosis of osteocytes in normal rabbits. In fact, after the bone was destroyed by a lesion, such as an aneurismal bone cyst, the lesion inside the marrow cavity could be verified by diagnostic US imaging[75]. In the targeted region, the destruction of endothelium cells of microvessels and thrombosis was readily detected, suggesting that HIFU could potentially prevent hematogenous dissemination of the tumor cells[76]. The treatable diameters of bone tumor increased with the absorption ratio of bone marrow to tumor, acoustic window of surface skin, and diameter of bone, but decreased with muscle depth and specific absorption rate ratio (SARR) of the bone tumor to the surface skin, bone marrow, and bone[77]. The optimal driving frequency was dependent on tumor depth, US absorption of bone marrow, and bone diameter, but was independent of the acoustic window area and SARR ratio under the three SARR criteria[77].

Ninety-six cases of bone tumors have been successfully treated using HIFU technology as of 2002 in China[78]. 4 patients with primary stage Ⅱ malignant bone tumors, including 3 chondrosarcoma and 1 malignant giant cell tumor of bone, and 4 patients with breast cancer bone metastases were treated with HIFU ablation alone[79]. All treated regions after HIFU had no intensification and there was an even, thin intensification rim around the region (Figure 7). In ^{99m}Tc-MDP bone scan, disappearance of radioactive uptake was found and a radioactive cold region was produced, suggesting complete inactivation of the tumor foci. After an average follow-up of 23.1 mo, no local recurrence was found in any of the cases, which shows HIFU can be an effective stand-alone therapy to manage malignant bone tumors. However, when diagnostic US was used for guidance of HIFU treatment, nerves might not always be clearly detected. In clinics, there were no significant changes in ECG, renal function, and blood electrolytes of patients before and after HIFU. Although ALP activity (a measure of liver function) increased 3 d after HIFU, it returned to the same or lower pre-HIFU

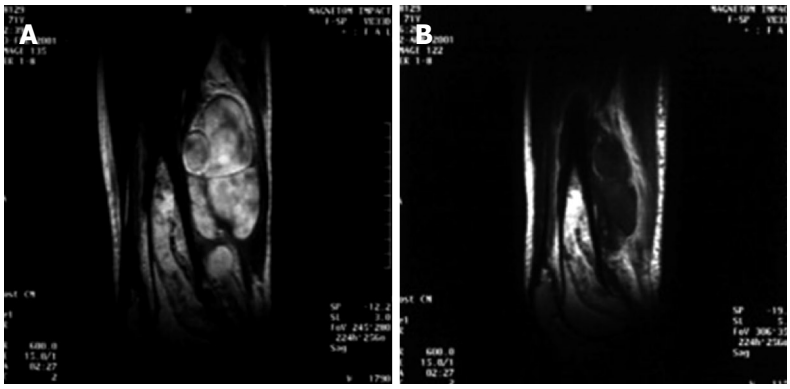

Figure 7 Contrast-enhanced magnetic resonance images (A) before and (B) 14-d after high intensity focused ultrasound ablation in a 45-year-old patient with osteosarcoma at the upper right tibia.

level 1 wk later. Those findings indicated that HIFU ablation had no significant influence on the vital organs.

Further studies were also done using the combination of HIFU and chemotherapy for managing malignant bone tumors in a total of 44 patients[80]. After a mean follow-up time of 17.6 mo, the overall survival rate was 84.1%. For the 34 cases of stage Ⅱb, 30 cases continued to survive disease-free, 2 died of lung and brain metastases, and the other 2 had local recurrence. Among 10 of the stage Ⅲb cases, 5 survived with tumor, 1 had local recurrence, and 5 died of lung metastases. It is conceivable that a limb salvage procedure can be carried out to treat malignant bone tumors of limbs using HIFU and chemotherapy because the preliminary results demonstrated that HIFU is effective and well tolerated. HIFU ablation results in fewer complications and well-preserved limb function because there were no surgical traumas and blood vessels > 2 mm in diameter were retained, which could be beneficial to revascularization and the repair of inactivated tumor bones. In addition, because surgical trauma and repair of the trauma are not involved with HIFU treatment, there would be no delay of postoperative chemotherapy, which is beneficial to ensure the efficacy of chemotherapy and to improve the prognosis[81].

Overall, representative HIFU clinical trials are summarized in Table 2. Although the summation is not complete because of unfinished publication collection, current results show HIFU as a safe and effective modality in multiple cancer treatment.

CLINICAL EXPERIENCE

Among the most important factors that determine the success of HIFU is patient selection. General exclusion criteria are: women who are pregnant or nursing, clinical evidence of brain metastases, subjects with tumors lying < 5 mm from vital structures or either adjacent to the skin or the chest wall, concurrent antiarrhythmic, disease with good prognostic factors, anticoagulant or immunosuppressive medication, ductal carcinoma *in situ* (DCIS) and cancers with an extensive intraductal component or lymphovascular invasion, tumors with very irregular margins, too large size, scattered multiple foci, or in proximity to the nipple, more than one focal breast lesion per quadrant, previous radiation or local thermal therapy, significant background illness or underlying medical condition (e.g. congestive heart failure, chronic obstructive pulmonary disease), metallic implants or other incompatibility with MRI (e.g. permanent implanted pacemakers), an inability to lie still for up to 150 min, and those who had previously documented severe intra-abdominal adhesions.

Critical to the performance of HIFU is the ability to obtain an adequate and optimal acoustic window and ultrasonic beam conformation, including, if possible, algorithms for correcting beam distortion in the presence of interfaces. There are a limited number of such acoustic windows because bone, air, and gas interfere with the propagation of US beams into the body, thus obscuring targets beyond these interfaces. In addition, unavoidable microscopic bubbles in the coupling media and local anesthesia caused scattering of the US beam and thus limited the power delivered to the target. It is therefore recommended that, if local anesthesia is used, it should be placed not in front rather beyond the lesion. The effect of interfaces requires particular attention because it is known that an interface is a potential site of cavitation. The skin of the HIFU entry site must be hair-free, the patient having been instructed to shave all hair the night before the procedure. Although patients with extensive skin scarring in the beam path are excluded, it may, however, be possible to treat patients with non-extensive abdominal wall scarring by angling the beam path, ensuring that the scar is not traversed. Placement of a gel spacing device may allow the bowel loops to be "pushed" out of the treatment field, thereby enlarging the acoustic window and allowing for greater treatment volume. Care should be taken to ensure that the pathway of the treatment beam does not traverse any critical structures (such as bowel loops anterior to the selected outlined sub-volume).

Definition of the target volume by the radiologist or/and operator is of the highest importance because tumor margins must be correctly identified and included in the target volume. During any cancer surgery or abla-

Table 2 Summary of high-intensity focused ultrasound clinical outcomes

Cases	Authors	HIFU system	Patients	Outcomes
BPH	Sullivan *et al*[32]	Sonablate	25 patients (mean age 67 years, range 47-84)	5 patients with large glands were withdrawn; the remaining 20 patients had improvements in the AUA symptom score (20.25 to 9.56), Qmax (9.2 to 13.7 mL/s) and QOL score (4.75 to 2.50)
	Uchida *et al*[34]	Sonablate Sonablate 200	35 patients mean age 68.5 ± 7.7 (52-84) treated by Sonablate; 22 patients mean age 68 ± 6.8 (57-81) treated by Sonablate 200	IPSS and QOL scores showed significant improvement at 3, 6, and 12 mo follow-up (P < 0.001-0.01); maximum flow rate (8.9-15.5 mL/s, P < 0.001) and prostatic volume (32.2-22.8 mL, P < 0.01) were significantly improved at 12 moths follow-up treated by Sonablate 200
Prostate cancer	Chaussy *et al*[36]	Ablatherm	271 patients were selected: 96 in the HIFU group and 175 in the TURP + HIFU group	A significant impact was observed on catheter time (40.0 d *vs* 7.0 d), incontinence (15.4% *vs* 6.9%), urinary infection (47.9% *vs* 11.4%), and the evolution of the post-treatment IPSS (8.91 *vs* 3.37) in favor of TURP + HIFU group; no significant changes were observed regarding efficacy during short-term follow-up, 25% and 4% retreatment rate in the HIFU and TURP + HIFU group, respectively
	Gelet *et al*[37]	Ablatherm	14 patients (mean age 72.5 years) with clinical stage T1 (3) and T2 (11) prostatic cancers	Early complications occurred in 6 (rectal burns 3, urinary retention 2, transient incontinence 1) and late complications in 5 (incontinence 2, bladder neck stenosis 3) patients; the PSA nadir value (1.79 ± 2.35 ng/mL) was achieved at 6 mo and the final PSA value was 2.94 ± 3.27 ng/mL (mean follow-up 380 d); No residual cancer was observed in 7 patients; Residual cancer was found in 7 patients: 4 required complementary treatment (orchidectomy 2, external beam radiation therapy 2)
	Gelet *et al*[40]	Ablatherm	82 patients (mean age 71 ± 5.7 years) with biopsy-proven localized (stage T1-T2) cancer	62% of patients exhibited no disease progression at 60 mo follow-up; the disease-free rate was 68% for the moderate-risk group of 50 patients (PSA < 15.0 ng/mL, Gleason sum < 8, prostate volume < 40 cm^3, and number of positive biopsies < 5); for the low-risk group of 32 patients (PSA < 10 ng/mL and Gleason sum < 7), the disease-free survival rate was 83%
	Chaussy *et al*[41]	Ablatherm	184 patients (mean age of 72 years, range 59-81)	Cancer free in 80% of patients and the tumor mass was reduced more than 90% in the residual cancer; the nadir value of PSA was < 4 ng/mL in 97%, including 61% who had values < 0.5 ng/mL; no severe side effects (fistula, grade 2 or 3 incontinence, rectal mucosal burn) were seen
	Uchida *et al*[41]	Sonablate-500	181 patients (median age of 70 years, range 44-88) and pretreatment PSA was 9.76 ng/mL (range 3.39-89.60)	The disease-free survival rates at 1, 3 and 5 years in all patients were 84%, 80% and 78%, respectively; the disease-free survival rates at 3 years for patients with pretreatment PSA less than 10 ng/mL, 10.01-20.0 ng/mL and more than 20.0 ng/mL were 94%, 75% and 35%, respectively (P < 0.0001)
	Blana *et al*[42]	Ablatherm	223 patients with age of 68.2 ± 6.8 years, PSA 11.3 ± 10 ng/mL (range 0.5-81.2), Gleason score 5.3 ± 1.5 and a prostate volume of 23.5 ± 10.7 cm^3 (range 3-62.5)	The complications rates were: urinary tract infection 0.4%, chronic pelvic pain 0.9%, infravesical obstruction 19.7%, stressincontinence 7.6%, impotence 49.8%; among the 49 patients who received a second HIFU therapy, the cumulative incontinence rate (12.2%, P = 0.024) and cumulative impotence rate (55%, P < 0.001) were significantly increased
	Blana *et al*[43]	Ablatherm	146 patients with a mean age of 66.9 ± 6.7 years, mean PSA of 7.6 ± 3.4 ng/mL, mean Gleason score of 5 ± 1.2, and prostate volume of 23 ± 7.7 cm^3	The median PSA nadir 3 mo after treatment was 0.07 ng/mL (0-5.67); The median PSA at 22 mo follow-up was 0.15 ng/mL (0-12.11), and 87% of patients had constant PSA < 1 ng/mL; 93.4% of patients had negative control biopsies; Of all the patients, 12% underwent transurethral resection because of obstruction with no severe stress incontinence (grade 2-3)
	Vallancien *et al*[45]	Ablatherm	30 patients with a mean age of 72 years, a median prostate volume of 30 cc, a median Gleason score of 6, a median PSA of 7 ng/mL	At a mean of 20 mo of follow-up 86% of patients had negative biopsies after HIFU; Median PSA was 0.9 ng/mL; At 1 year of follow-up the mean International Prostate Symptom Score was 8; Regarding sexual function, 73% of previously potent patients reported preserved sexual activity
	Lee *et al*[45]	Ablatherm	62 patients with clinical stage T1-2, PSA value < 30 ng/mL	After HIFU treatment, 78% of patients had a decreased PSA level to < 0.5 ng/mL within 3 mo; the median value of the last PSA was 0.6 ng/mL and the median nadir PSA was 0.2 ng/mL; The success rates of HIFU were 85, 77 and 47% in low-, intermediate- and high-risk groups, respectively
	Thüroff *et al*[39]	Ablatherm	402 patients with localized (stage T1-2N0-xM0) prostate cancer at 6 sites, mean age of 69.3 ± 7.1 years, mean prostate volume 28.0 ± 13.8 cc, mean PSA 10.9 ± 8.7 ng/mL	Negative biopsy rate in T1-2 primary cancer population was 87.2%, 92.1% in low-risk patients
Breast cancer	Wu *et al*[50]	JC	22 patients (4 in TNM stage Ⅰ, 9 in stage ⅡA, 8 in stage ⅡB, and 1 in stage); Tumor size ranged from 2 to 4.8 cm in diameter (mean 3.4 cm)	After a median follow-up of 54.8 mo, 1 patient died, 1 was lost, and 20 were still alive; 2 of 22 patients developed local recurrence; 5-year disease-free survival and recurrence-free survival were 95% and 89%, respectively; cosmetic result was judged as good to excellent in 94% of patients
	Furusawa *et a*[49]	ExAblate 2000	21 cases median age is 54 years (range 34-72), median diameter of tumor is 15 mm (range 5-50)	1 case of recurrence of pure mucinous carcinoma; 2 cases of skin burns

Uterine fibroids	LeBlang *et al*[52]	ExAblate 2000	147 symptomatic leiomyomas in 80 women (average age: 46, range: 34-55) with average fibroids volume of 175 ± 201 cm^3	The average nonperfused volume ratio was 55% ± 25% immediately after treatment; 6 mo after treatment, the average volume of treated fibroids had decreased to 112 ± 141 cm^3 (n = 81) (P < 0.0001) with an average volume reduction of 31% ± 28%
	Funaki *et al*[54]	ExAblate 2000	91 Japanese women (45 of Type 1-2 and 46 of Type 3)	The mean volume change ratios of Type 1-2 myomas were -36.5% and -39.5% at 6 and 24 mo follow-up, respectively; SSS value for patients with Type 1-2 myomas before MRgFUS was 35.1 ± 21.0, and the values diminished significantly during the 24-mo follow-up period to a mean value of ~15.0; Type 3 myomas did not decrease in size 6 mo after MRgFUS; The reintervention rates were 14.0% for Type 1-2 patients and 21.6% for Type 3 patients at 24 mo follow-up, respectively
Liver cancer	Li *et al*[65]	JC	100 patients (80 male, 20 female, mean age of 56, ranging 30-74 years) including 62 primary and 38 metastatic liver cancers	Clinical symptoms were relieved in 86.6% (71/82) of patients; the ascites disappeared in 6 patients; ALT (95 ± 44) U/L and AST (114 ± 58) U/L were reduced to normal in 83.3% (30/36) and 72.9% (35/48) patients after HIFU, respectively; AFP was lowered by more than 50% in 65.3% (32/49) patients
	Wu *et al*[66]	JC	50 patients with stage IVA HCC (T4N0-1M0) The tumors were 4-14 cm in diameter (mean, 10.5 cm)	The 6-mo and 1-year survival rate was 80.4%-85.4%, and 42.9%, respectively; median reductions in tumor volume at 1, 3, 6, and 12 mo after treatment were 28.6%, 35.0%, 50.0%, and 50.0%, respectively
Renal cancer	Wu *et al*[70]	JC	12 patients with advanced stage renal cell carcinoma and 1 patient with colon cancer metastasized to kidney	After HIFU hematuria disappeared in 7 of 8 patients and flank pain of presumed malignant origin disappeared in 9 of 10 patients; it showed decrease in or absence of tumor blood supply and significant shrinkage of the ablated tumor; 7 patients died (median survival 14.1 mo, range 2-27) and 6 were alive with median follow-up of 18.5 mo (range 10-27)
Pancreatic cancer	Wu *et al*[73]	JC	8 patients mean of 62 years range 48 to 86 years	No complications were observed, and preexisting severe back pain disappeared after intervention; Follow-up images revealed an absence of tumor blood supply and shrinkage of the ablated tumor; a median survival time was 11.25 mo
	He *et al*[72]	FEP-BY02	251 (147 men and 104 women) patients in 25 hospitals with mean age of 59, range 39-82, 3-12 cm tumor diameter; TNM grade Ⅱ 7%, Ⅲ 34%, Ⅳ 59%; Concurrent jaundice 18.7% and pain 68%; Head 183, body 53, 14 trail	21.5% cases exhibited a remarkable effect, 64% exhibited a general effect; survival time is 12.5 mo; 6 patients survived more than 3 years; no complications, such as skin burn, gastrointestinal perforation and pancreatic fistula were observed
Bone metastases	Liberman *et al*[81]	ExAblate 2000	31 patients in 3 medical centers	25 patients underwent the planned treatment and were available at 3 mo follow-up; 72% of the patients reported significant pain improvement; average VAS score was reduced from 5.9 to 1.8 at 3 mo follow-up; 67% of patients reported a reduction in their opioid usage

HIFU: High intensity focused ultrasound; BPH: Benign prostate hyperplasia; AUA: American Urology Association; QOL: Quality of life; PSA: Prostate specific antigen; AFP: α-fetoprotein; MRgFUS: Magnetic resonance-guided focused US surgery.

tion, tumors are excised or ablated along with a surrounding margin of normal tissue, usually no less than 1 cm. The radiological analysis of HIFU-treated liver tumors shows that the median area of ablation seen on MRI is 45% smaller than that predicted at the time of treatment, which is greater than the difference between histological ablation and intended area, 6%[61]. If a target tour is situated at a depth greater than 10 cm from the skin, the attenuation of the normal tissues in the beam-path reduces the likelihood of successful ablation with current devices. Additional factors, such as obstruction of the incident ultrasound energy by the ribs or reflection by tissue interfaces, can also lead to under-treatment. Computation of the optimal planning for dosimetry must be performed as fast as possible (in minutes) and *in situ* (patient installed in the final setup for treatment), to deliver a uniform lethal dose over the entire target volume and to spare as many as possible thermal lesions in healthy tissue. The HIFU planning should include, if possible, physiological information (perfusion) and border conditions.

Performing the HIFU ablation should be under active feedback control of the temperature evolution. On-line adjustment of the acoustical power level and/or of the spatial distribution of heat deposition is therefore necessary. Thermal safety in those regions where the delivered thermal dose is close to the lethal threshold and the stability of the temperature controllers for thermal dose feedback require both very accurate thermometry. The MR thermometry measurements have been used in real time to control the power of a stationary, focused US transducer to achieve the desired treatment outcome in minimum time without violating the imposed safety constraints.

Mis-registration, due to respiratory or bulk patient movement, may be problematic. Detection and compensation of physiological or accidental motion of the patient during the treatment provides significant advantage for accurate control of the delivered thermal dose. Therefore, the tumor location should be monitored throughout therapy. Before the start of an HIFU procedure, an anxiolytic can be given to reduce movement, and an analgesic can be administered to counter the associated discomfort. Patients should be under sedation and local anesthesia

during HIFU ablation, but avoiding general anesthesia (because the procedure is to stay minimally invasive as much as possible). In addition, digestive peristaltic motion was reversibly blocked during the HIFU ablation using a common antispasmodic administrated intramuscularly (tiemonium methylsulfate, Visceralgine).

When addressing cancer applications, the accurate spatial control of the delivered thermal dose is mandatory. Geometrical information from diagnostic imaging and from the positioning system of the HIFU probe must be co-registered to provide referencing of the HIFU probe orientation. The HIFU probe is moved using the freedom degrees of the positioning system (translation and rotation) with the focus of the transducer coinciding with the center of the target volume. A checkup for the correct location of the focal point is preferred, with one or several low-power sonications prior to the high-power ablation.

Immediate post-treatment assessment of the therapy is typically performed with contrast-agent uptake, to assess for local perfusion within the tumor and the neighboring tissues. The best time for follow-up MRI may be approximately 1 wk after HIFU. It was found that more than 90% of the identified tumor volume was treated and the residual cancer was predominantly identified at the periphery of the tumor mass. This shortcoming indicated the need to increase the total targeted area at the periphery. Microbubble contrast-enhanced sonography is also being used to evaluate the treatment effect of HIFU[82]. Another method currently being examined in oncologic applications is the use of PET to assess changes in metabolic activity after HIFU treatment.

The HIFU ablation was well tolerated by patients, with the exception of minor skin burns, and no complications occurred. However, high rate of overall side effects on the diaphragm, abdominal wall or skin at relatively low intensities may be explained by the fact that the skin is close to the focus area (e.g. the target HCC is close to the proximal surface of the liver). Autopsy revealed a perforation of the diaphragm in 50% of the cases and a gastric perforation in 25%[67]. Such complications seem to be related to the size of the target volume: with a large target area, some of the volume may be more frequently located outside of the liver so damaging adjacent organs. Although the majority of patients experienced some discomfort, this was generally transient. Skin toxicity was treated with cool-packs and aloe gel. All adverse events were local to the treatment site and self-limiting. Solution is establishing artificial ascites by injecting normal saline solution or 0.2% hyaluronan water solution into the abdominal cavity or under skin. The method of artificial ascites increases the distance between the skin surface and target and serves as a heat sink to cool overlying structures. It has been illustrated that this method not only reduces the probability and extent of thermal damage to intervening structures but also has no adverse affect on the efficacy of HIFU ablation[83].

LIMITATIONS AND CHALLENGES

Despite its promising noninvasive and nonionizing effects in the therapy of malignancies, particularly those that are widespread or inoperable, the application of HIFU has certain limitations. Continuing research is still in great need in the area of focusing the HIFU pulses, the technique of gradual pulsed exposures to achieve a cumulative therapy result, improving imaging quality for accurate tumor determination and post-treatment evaluation, and developing a real-time monitoring modality for lesion generation and temperature elevation.

Since HIFU is essentially US, any artifacts related to US, such as in US imaging, would apply to HIFU as well, such as acoustic shadowing, reverberation, and refraction. Hence, bones and lungs oppose the penetration of US and some areas of the liver parenchyma adjacent to a rib may be difficult to reach with the focused beam. Gas in the bowel cannot be penetrated by HIFU, and sound waves are reflected back toward the transducer, which have high energy and may produce burns in the intervening tissue. Even small amounts of gas in the gastrointestinal tract can produce burns in the wall of the bowel anterior to the gas and in the abdominal wall musculature overlying the gas. Refraction artifacts can result in energy deposition in the soft tissues adjacent to the target area, and energy deposition can occur superficially to the target.

Non-invasive transcranial HIFU therapy remains very limited due to the strong phase aberrations and absorption induced by the skull. To compensate this distortion, the idea of phased array corrections was introduced to US diagnostic imaging through the skull. Thomas and Fink proposed to use a time reversal mirror in therapeutic US. However, a hydrophone has to be inserted in the neighborhood of the tumor in order to record the signals relating this hydrophone to each element of the therapeutic array[84]. Recently, adaptive corrections of the distortions induced by the skull bone have been performed using a previously acquired 3D computational tomography (CT) scan of the skull bone structure. These CT scan data are used as entry parameters in a finite differences time domain (FDTD) simulation of the full wave propagation equation. A numerical computation is used to deduce the impulse response relating the targeted location and the ultrasound therapeutic array, thus providing a virtual time-reversal mirror[84,85]. Research on a fast algorithm of aberration correction (for both trans-abdominal and cranial applications) on site is still ongoing.

A treatment session lasting for 2 h for a superficial 2-3 cm tumor may be acceptable when compared to the alternative of surgical resection, but is less favorably in comparison to other minimally invasive techniques. The longer treatment time may be justified on the grounds of a lower morbidity and mortality than conventional surgery. Treatment time will be reduced with development of HIFU technology, experience, and in combination with methods to reduce tumor perfusion, such as trans-arterial embolization[66].

Nonsurgical ablation relies on imaging quality for an accurate determination of tumor extent, which is why MRI guidance for HIFU has initially become more rapidly accepted clinically than sonographically guided HIFU[22].

Although MRI is shown to be more accurate than mammography or US in size assessment, even MRI currently cannot exclude small amounts of residual invasive cancer. 3D sonography is likely to better delineate a volume of tissue to be treated than just a single plane or orthogonal planes, which provide valuable information to the performance of HIFU, and most commercially available HIFU systems display with 2D sonography systems. Therefore, the application of 3D sonography techniques is an exciting area of future opportunity, especially for HIFU treatment planning, monitoring, and post-treatment evaluation.

Currently the most important problem of US-guided HIFU ablation is the lack of reliable thermometry and lesion production monitoring. There have been several methods under investigation. A sonographic thermometry is being actively investigated and incorporated in FEP-BY02 system[86]. Elastographic techniques will measure the variation of tissue stiffness during the ablation process in real time[59], especially in some cases in which tissue contrast is not sufficient to visualize a tumor in the background of normal tissue. The speed of sound is temperature dependent, which causes the apparent change in position of echoes in the images of heated tissues in comparison to the unheated ones[87]. However, none of these techniques have achieved wide-spread clinical use yet, although some promising results have been provided with a smaller range of temperature elevation in *ex vivo* experiments.

A controversial question is the possibility of increased risk of metastases after the tumor has been disrupted by HIFU. In a report by Fry *et al*[88], a higher rate (17%-44%) of metastases was observed after HIFU treatment than in the control group. However, that feature was not found in other studies. Yang *et al*[67] described a lower rate of lung metastases in the HIFU-treated group. In a model of prostatic cancer, metastases in 16% of the treated rats was found as compared to 28% in the control group[62]. It was found that one of the most important biological consequences of HIFU treatment is the creation of a large amount of tumor antigens in the form of necrotic cells and the local release of a diverse array of endogenous danger signals from HIFU damaged tumor cells. This biological response has the potential to stimulate an anti-tumor immune response[89,90]. However, little is known about how such significant HIFU-induced changes in the tumor microenvironment may influence the host's anti-tumor immune response.

Clinical thermal ablation methods also include the application of radiofrequency (RF), laser, microwave, and their combination[91]. Currently RF is the front-runner and the most widely practiced and preferred technique. Laser has the advantage of being more MR compatible permitting direct MR monitoring. MR compatible RF electrodes are now available but the application of RF current and image acquisition are incompatible and have to be alternated. Microwave has been used particularly in China to treat small HCC. Current microwave applicators are large and several are usually required for open surgery; one of the focuses of development is to produce a smaller percutaneous probe. Most of these technologies are minimally invasive with almost the same effectiveness in small tumors as with a surgical approach (i.e. complications of 2%-10.6% and mortality of 0.1%-1.4%). In comparison, HIFU requires longer treatment times, limited depth of penetration, and an excellent acoustic window, and excludes the applications with overlying ribs or lung.

HIFU-RELATED TUMOR THERAPY METHODS

Thermal ablation HIFU technology can also be used in treating cancers in the following ways.

Immune response

Adjunctive thermal ablation with carmustine, cyclophosphamide and doxorubicin was found to be beneficial in improving the results of HIFU treatment. It has been postulated that sono-modification of the tumor tissue may enhance tumor immunogenicity and subsequently augment the host immune response against the tumor, although the mechanisms behind this phenomenon remain unknown. Animal experiments show that while there were a few HSP70 positive cells in rabbit VX2 bone tumors before HIFU ablation, HSP70 positive cells significantly increased up to 3 wk after HIFU treatment[92]. Furthermore, HIFU ablation also increased CD25 positive cells in the same rabbit bone tumor model. The increase of HSP70 and CD25 positivity in malignant bone tumors may facilitate tumor-specific antigen presentation to T lymphocytes, which stimulate the proliferation of T lymphocytes and enhance the anti-tumor immune response. In a clinical trial, 16 patients with solid malignancies, including 6 with osteosarcoma, were treated with HIFU. There were significant increases in the population of CD4 (+) lymphocytes ($P < 0.01$) and in the ratio of CD4 (+)/CD8 (+) ($P < 0.05$) after HIFU ablation[90]. Their findings suggest that HIFU ablation may eliminate or significantly reduce potential circulating tumor cells in patients with solid malignancies. While the long-term therapeutic benefits and molecular mechanisms of HIFU-treatment-elicited host immune responses in cancer patients require further investigation, it is conceivable that HIFU ablation may induce massive tumor cell death and/or necrosis, which could lead to the release of tumor antigens to stimulate a host anti-tumor immune response. These changes may ultimately enhance the immune function of tumor-bearing patients and improve their prognosis.

Drug delivery

Drug delivery across the blood-brain barrier (BBB) is one of the most important key factors in the treatment of diseases of the central nervous system (CNS). The BBB is a barrier system of the vessels in the brain that hampers various substances from leaking into the brain. Although this barrier system is important for the maintenance of homeostasis of the brain, it prohibits the delivery of therapeutic agents into the brain and complicates the treat-

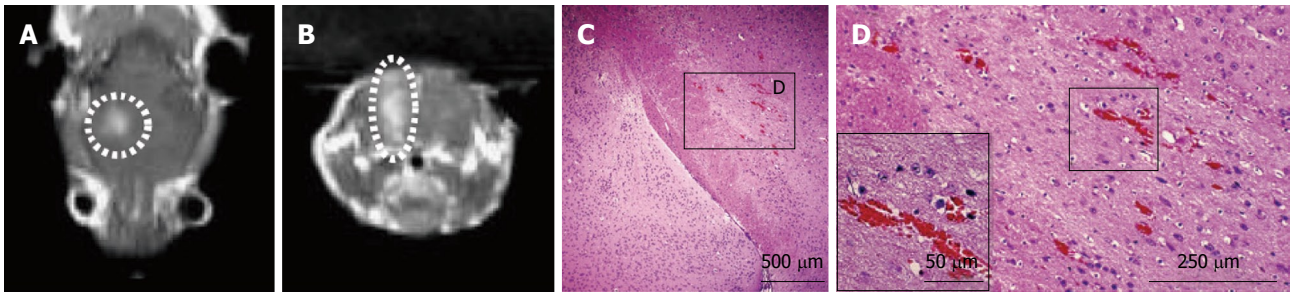

Figure 8 The axial (A) and the coronal magnetic resonance images (B) are presented with a tissue block showing the blood-brain barrier disruption from the mice, overview of the half hemisphere of a mouse with focused ultrasound-induced blood-brain barrier disruption (C) and high magnification of the lesions with severe damage (D).

ment of CNS disorders[93]. The intracellular space in the BBB is so tight that even one of the smallest molecules, such as ions, cannot easily cross the barrier. Current trans-BBB delivery methods include modifying drug formats or attaching with carriers, or focusing on delivery methods such as intracarotid injection and direct catheter insertion into the brain. The major disadvantage of drug modification is its lack of site specificity and not all drugs can be modified. The invasive techniques also limit the candidates for treatment[93].

Although the possibility of using US for BBB disruption has been previously documented, reproducible and reliable opening of the BBB remains difficult[94]. Creating BBB opening without or with only an acceptable magnitude of tissue damage is one of the most challenging issues. When BBB disruption was attempted by means of US with the combined use of microbubble US contrast agent (Optison, Amersham Health Inc., Princeton, NJ), a more reliable and reproducible BBB opening was achieved compared with that when US alone was used. The BBB disruption was achieved at both 1.0- and 3.3-MPa sonication with a burst length of 100 milliseconds[95]. When temperature elevation was measured using MR thermometry, temperature elevation was only 4.8℃ even at the highest amplitude tested. In addition, when the same procedure was performed without the injection of Optison, nearly no BBB opening was achieved (Figure 8). These results indicate that local temperature elevation is not the key mechanism for BBB disruption, and the presence of microbubbles is necessary for the reliable opening of the BBB. The time course study showed that the disrupted BBB repairs itself within approximately 6 h and that the BBB disruption is a transient and reversible event[96]. Long-term follow-up of the sonicated rabbit brain showed nearly no damage, suggesting that the long-term adverse effect of US-induced BBB disruption is minimal[97]. Altogether, it seems reasonable to assume that the parameters for BBB disruption in humans are similar to those used in animal studies. Electron microscopic study suggests that the transcellular pathway is enhanced with US treatment. Drugs were taken up by the endothelial cells by means of vesicle transportation through the endothelial cells and on the loosening or destruction of the tight junctions[96]. From an acoustic point of view, the BBB disruption occurred only with stable cavitation and without the presence of inertial cavitation[98]. US-induced BBB disruption technique can also deliver antibodies to the brain in a localized fashion and the delivered antibodies do not lose their innate function. Herceptin is an antibody against HER-2, which is a receptor for a growth factor and has been shown to be a powerful chemotherapeutic agent against breast tumor. When herceptin was injected into mice using ultrasound-induced BBB disruption technique, the agent was successfully delivered into the brain. Because brain metastases following breast tumors is a very common problem in the clinical field, these results seem promising in providing alternative options for curing patients with brain metastases following breast cancer.

Focusing the US through the intact skull is probably the most exciting and challenging application of the HIFU. CT-derived preliminary information must be coregistered with MR images to correct for wave distortion in bone, in particular, to determine the driving signal (amplitude and phase) for each transducer element to achieve a well-focused beam through the skull. However, until now, no clinical trials have been performed using US-induced BBB disruption techniques. In humans, the cranium is much thicker than that of mice or rats, which means that a more careful and delicate control of US is necessary to form a target inside the brain.

Beside the trans-BBB drug delivery, the cytotoxic potential of the anti-cancer drugs, such as bleomycin and adriamycin, may be restricted by its low membrane permeability. Morphological evaluation of US irradiated cells with scanning electron microscopy showed minor disruption of the cell surface and disappearance of microvilli. It suggests that low intensity US altered the cell membrane thus resulting in anticancer drug uptake into carcinoma cells[82]. Application of low-intensity US to growing tumors is found to enhance intracellular delivery after intraperitoneal or intratumoral administration, thereby potentiating its cytotoxicity. Cell death after treatment was shown to occur by an apoptotic mechanism[99,100]. HIFU was also delivered to a mouse model prior to doxorubicin hydrochloride liposomes. Mean doxorubicin concentration in tumors treated with HIFU pulses was significantly higher (124%) than in the control group. Extravasation of dextran-fluorescein isothiocyanate was observed in the vasculature of HIFU-

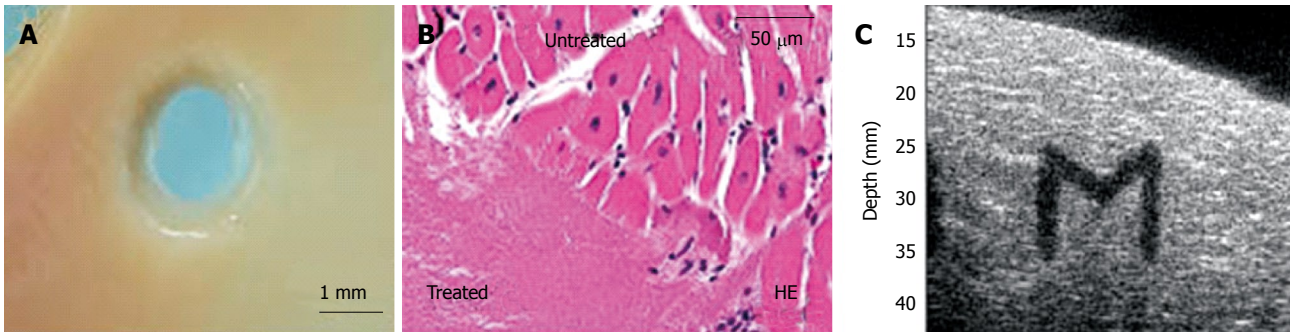

Figure 9 Representative (A) image and (B) histology of tissue erosion after histotripsy, and (C) "M" shape lesion generated by histotripsy shown in ultrasound imaging.

treated tumors but not in that of untreated tumors[101]. Meanwhile, addition of microbubbles in the ultrasound-mediated drug delivery can lower the threshold of bubble cavitation and transiently increase capillary permeability in tumor cells[102]. Although no clinical trials have been performed, this technique could be developed into a localized and effective anticancer treatment with little or no systemic toxicity with enhanced efficiency of thermal ablation.

Vessel occlusion

Blood vessel occlusion is useful for treating arteriovenous malformations (AVM) in different parts of the body for controlling abdominal, peritoneal and pelvic hemorrhage and also for treating some tumors with an identifiable blood supply. HIFU has recently been used to interrupt blood flow in experimental animals[92]. The renal artery branches of rabbits (diameter about 0.6 mm) were occluded by HIFU. Complete cessation of blood flow was observed by color Doppler imaging and MRI, and lack of perfusion was also observed in the renal cortex in the contrast-enhanced image. Postmortem histological evaluation showed an infracted tissue volume corresponding to the wedge shape seen in the ultrasound and MRI images. No damage to the surrounding soft tissue was noted[103]. These results demonstrated that HIFU can be used to induce arterial occlusion, thus producing infarction and necrosis of the perfusion tissue. HIFU may offer a non-invasive, non-surgical technique that effectively obliterates blood flow. However, before clinical applications can be considered, additional studies are needed to obtain data concerning the relationship between the intensity of HIFU required for flow occlusion, blood vessel diameter, and flow velocity, and to investigate possible long-term adverse effects. Blood vessel occlusion may be useful in cancer therapy, where interruption of flow to a tumor may lead to its shrinkage.

Histotripsy

A new technique, "histotripsy", has also been developed to achieve mechanical fractionation of tissue structure using a number of short, high intensity US pulses (20 μs duration, 1 kHz pulse repetition rate, 18 MPa rarefactional pressure)[104]. The transducer has similar geometry and acoustic intensity as the HIFU type, but its center frequency is around 750 kHz. At a fluid-tissue interface, histotripsy results in localized tissue removal with sharp boundaries, which is used to remove cardiac tissue in the treatment of congenital heart disease[105]. In bulk tissue, histotripsy produces mechanical fragmentation of tissue resulting in a liquefied core with very sharply demarcated boundaries. Histology demonstrates treated tissue within the lesion is fragmented to a subcellular level surrounded by an almost imperceptibly narrow margin of cellular injury. As shown in Figure 9B, at the lesion boundary, half of the cell is cut off, and the other half is still intact. The mechanism of histotripsy is acoustic cavitation and energetic microbubble activities fragment and subdivide tissue resulting in cellular destruction[106]. Histotripsy has vast clinical applications where precise tissue ablation and removal are needed (e.g. tumor treatment). Compared to non-invasive thermal therapy, histotripsy has some important advantages: (1) microbubbles produced at the US focus, shown as bright spots on US imaging; (2) energetic microbubble activities can be seen on imaging and provide real-time feedback; (3) the lesions appear darker on US imaging post-treatment; and (4) the lesions can be produced in a very controlled and precise manner. It suggests that in the near future, imaging guided histotripsy can be a potential non-invasive surgery tool. Current clinical targets are: kidney, breast cancer, prostate cancer, several cardiac applications (perforation of the arterial septum for congenital heart disease), BPH, and breast fibroadenoma[107,108].

CONCLUSION

The drive in modern medicine is towards the development of treatments and techniques that minimize intervention to the patient and length of hospital stay. Thermal ablation therapies provide a minimally invasive approach to cancer therapy that is gaining rapid clinical acceptance. Of the available ablative techniques, HIFU is the least invasive and, in many ways, the most attractive. HIFU is being increasingly used for limited applications in Asia and Europe; however, these studies have all been preliminary, and clinical trial results to date have demonstrated HIFU to be safe and clinically effective. Further studies will be necessary before the widespread use of HIFU can be rec-

ommended. Long-term medical benefit and perhaps the beneficial economic impact of this therapy for oncology are of clinical and social importance and will be an area of continuing interest. However, HIFU is still in its infancy, and there remain outstanding technical and treatment delivery questions to be addressed. With improving imaging, advances in transducer technology and energy delivery techniques, and better understanding of HIFU-induced bioeffects, it is probable that the versatility of HIFU will increase and its range of applicability will expand.

REFERENCES

1 **Jemal A**, Siegel R, Ward E, Hao Y, Xu J, Thun MJ. Cancer statistics, 2009. *CA Cancer J Clin* 2009; **59**: 225-249
2 **The Freedonia Group**. Cancer therapies to 2009 - Market research, market share, market size, sales, demand forecast, market leaders, company profiles, industry trends, 2009
3 **ter Haar G**, Rivens I, Chen L, Riddler S. High intensity focused ultrasound for the treatment of rat tumours. *Phys Med Biol* 1991; **36**: 1495-1501
4 **Gelet A**, Chapelon JY, Bouvier R, Rouvière O, Lasne Y, Lyonnet D, Dubernard JM. Transrectal high-intensity focused ultrasound: minimally invasive therapy of localized prostate cancer. *J Endourol* 2000; **14**: 519-528
5 **Visioli AG**, Rivens IH, ter Haar GR, Horwich A, Huddart RA, Moskovic E, Padhani A, Glees J. Preliminary results of a phase I dose escalation clinical trial using focused ultrasound in the treatment of localised tumours. *Eur J Ultrasound* 1999; **9**: 11-18
6 **Dubinsky TJ**, Cuevas C, Dighe MK, Kolokythas O, Hwang JH. High-intensity focused ultrasound: current potential and oncologic applications. *AJR Am J Roentgenol* 2008; **190**: 191-199
7 **ter Haar G**. Acoustic surgery. *Phsics Today* 2001; **54**: 29-34
8 **Lynn JG**, Zwemer RL, Chick AJ, Miller AE. A new method for the generation and use of focused ultrasound in experimental biology. *J Gen Physiol* 1942; **26**: 179-193
9 **Fry WJ**, Barnard JW, Fry EJ, Krumins RF, Brennan JF. Ultrasonic lesions in the mammalian central nervous system. *Science* 1955; **122**: 517-518
10 **Lynn JG**, Putnam TJ. Histology of Cerebral Lesions Produced by Focused Ultrasound. *Am J Pathol* 1944; **20**: 637-649
11 **Hynynen K**, Lulu BA. Hyperthermia in cancer treatment. *Invest Radiol* 1990; **25**: 824-834
12 **Dewey WC**. Arrhenius relationships from the molecule and cell to the clinic. *Int J Hyperthermia* 1994; **10**: 457-483
13 **Diederich CJ**. Thermal ablation and high-temperature thermal therapy: overview of technology and clinical implementation. *Int J Hyperthermia* 2005; **21**: 745-753
14 **Mason TJ**. A sound investment. *Chem Ind* 1998; **21**: 878-882
15 **Pitt WG**, Husseini GA, Staples BJ. Ultrasonic drug delivery--a general review. *Expert Opin Drug Deliv* 2004; **1**: 37-56
16 **Lagneaux L**, de Meulenaer EC, Delforge A, Dejeneffe M, Massy M, Moerman C, Hannecart B, Canivet Y, Lepeltier MF, Bron D. Ultrasonic low-energy treatment: a novel approach to induce apoptosis in human leukemic cells. *Exp Hematol* 2002; **30**: 1293-1301
17 **Haar GT**, Coussios C. High intensity focused ultrasound: physical principles and devices. *Int J Hyperthermia* 2007; **23**: 89-104
18 **Chung AH**, Hynynen K, Colucci V, Oshio K, Cline HE, Jolesz FA. Optimization of spoiled gradient-echo phase imaging for in vivo localization of a focused ultrasound beam. *Magn Reson Med* 1996; **36**: 745-752
19 **Hynynen K**, Freund WR, Cline HE, Chung AH, Watkins RD, Vetro JP, Jolesz FA. A clinical, noninvasive, MR imaging-monitored ultrasound surgery method. *Radiographics* 1996; **16**: 185-195
20 **Cernicanu A**, Lepetit-Coiffe M, Roland J, Becker CD, Terraz S. Validation of fast MR thermometry at 1.5 T with gradient-echo echo planar imaging sequences: phantom and clinical feasibility studies. *NMR Biomed* 2008; **21**: 849-858
21 **Mylonas N**, Ioannides K, Hadjisavvas V, Iosif D, Kyriacou PA, Damianou C. Evaluation of fast spin echo MRI sequence for an MRI guided high intensity focused ultrasound system for in vivo rabbit liver ablation. *J Biol Sci Eng* 2010; **3**: 241-246
22 **Yagel S**. High-intensity focused ultrasound: a revolution in non-invasive ultrasound treatment? *Ultrasound Obstet Gynecol* 2004; **23**: 216-217
23 **Khokhlova TD**, Canney MS, Lee D, Marro KI, Crum LA, Khokhlova VA, Bailey MR. Magnetic resonance imaging of boiling induced by high intensity focused ultrasound. *J Acoust Soc Am* 2009; **125**: 2420-2431
24 **Jolesz FA**, McDannold N. Current status and future potential of MRI-guided focused ultrasound surgery. *J Magn Reson Imaging* 2008; **27**: 391-399
25 **Xu RX**, Povoski SP, Martin EW Jr. Targeted delivery of microbubbles and nanobubbles for image-guided thermal ablation therapy of tumors. *Expert Rev Med Devices* 2010; **7**: 303-306
26 **Makin IR**, Mast TD, Faidi W, Runk MM, Barthe PG, Slayton MH. Miniaturized ultrasound arrays for interstitial ablation and imaging. *Ultrasound Med Biol* 2005; **31**: 1539-1550
27 **Maruvada S**, Harris GR, Herman BA, King RL. Acoustic power calibration of high-intensity focused ultrasound transducers using a radiation force technique. *J Acoust Soc Am* 2007; **121**: 1434-1439
28 **Hill CR**, Rivens I, Vaughan MG, ter Haar GR. Lesion development in focused ultrasound surgery: a general model. *Ultrasound Med Biol* 1994; **20**: 259-269
29 **Zhou Y**, Zhai L, Simmons R, Zhong P. Measurement of high intensity focused ultrasound fields by a fiber optic probe hydrophone. *J Acoust Soc Am* 2006; **120**: 676-685
30 **Hill CR**. Optimum acoustic frequency for focused ultrasound surgery. *Ultrasound Med Biol* 1994; **20**: 271-277
31 **Gelet A**, Chapelon JY, Margonari J, Theillère Y, Gorry F, Souchon R, Bouvier R. High-intensity focused ultrasound experimentation on human benign prostatic hypertrophy. *Eur Urol* 1993; **23** Suppl 1: 44-47
32 **Sullivan LD**, McLoughlin MG, Goldenberg LG, Gleave ME, Marich KW. Early experience with high-intensity focused ultrasound for the treatment of begin prostatic hypertrophy. *British J Urol* 1997; **79**: 172-176
33 **Madersbacher S**, Schatzl G, Djavan B, Stulnig T, Marberger M. Long-term outcome of transrectal high- intensity focused ultrasound therapy for benign prostatic hyperplasia. *Eur Urol* 2000; **37**: 687-694
34 **Uchida T**, Muramoto M, Kyunou H, Iwamura M, Egawa S, Koshiba K. Clinical outcome of high-intensity focused ultrasound for treating benign prostatic hyperplasia: preliminary report. *Urology* 1998; **52**: 66-71
35 **Madersbacher S**, Pedevilla M, Vingers L, Susani M, Marberger M. Effect of high-intensity focused ultrasound on human prostate cancer in vivo. *Cancer Res* 1995; **55**: 3346-3351
36 **Chaussy C**, Thüroff S. The status of high-intensity focused ultrasound in the treatment of localized prostate cancer and the impact of a combined resection. *Curr Urol Rep* 2003; **4**: 248-252
37 **Gelet A**, Chapelon JY, Bouvier R, Souchon R, Pangaud C, Abdelrahim AF, Cathignol D, Dubernard JM. Treatment of prostate cancer with transrectal focused ultrasound: early clinical experience. *Eur Urol* 1996; **29**: 174-183
38 **Beerlage HP**, Thüroff S, Debruyne FM, Chaussy C, de la Rosette JJ. Transrectal high-intensity focused ultrasound using the Ablatherm device in the treatment of localized prostate carcinoma. *Urology* 1999; **54**: 273-277
39 **Thüroff S**, Chaussy C, Vallancien G, Wieland W, Kiel HJ, Le Duc A, Desgrandchamps F, De La Rosette JJ, Gelet A. High-intensity focused ultrasound and localized prostate cancer:

efficacy results from the European multicentric study. *J Endourol* 2003; **17**: 673-677
40 **Chaussy C**, Thüroff S. High-intensity focused ultrasound in prostate cancer: results after 3 years. *Mol Urol* 2000; **4**: 179-182
41 **Uchida T**, Ohkusa H, Yamashita H, Shoji S, Nagata Y, Hyodo T, Satoh T. Five years experience of transrectal high-intensity focused ultrasound using the Sonablate device in the treatment of localized prostate cancer. *Int J Urol* 2006; **13**: 228-233
42 **Blana A**, Rogenhofer S, Ganzer R, Wild PJ, Wieland WF, Walter B. Morbidity associated with repeated transrectal high-intensity focused ultrasound treatment of localized prostate cancer. *World J Urol* 2006; **24**: 585-590
43 **Blana A**, Walter B, Rogenhofer S, Wieland WF. High-intensity focused ultrasound for the treatment of localized prostate cancer: 5-year experience. *Urology* 2004; **63**: 297-300
44 **Chaussy C**, Thüroff S, Rebillard X, Gelet A. Technology insight: High-intensity focused ultrasound for urologic cancers. *Nat Clin Pract Urol* 2005; **2**: 191-198
45 **Vallancien G**, Prapotnich D, Cathelineau X, Baumert H, Rozet F. Transrectal focused ultrasound combined with transurethral resection of the prostate for the treatment of localized prostate cancer: feasibility study. *J Urol* 2004; **171**: 2265-2267
46 **Lee HM**, Hong JH, Choi HY. High-intensity focused ultrasound therapy for clinically localized prostate cancer. *Prostate Cancer Prostatic Dis* 2006; **9**: 439-443
47 **Rebillard X**, Gelet A, Davin JL, Soulie M, Prapotnich D, Cathelineau X, Rozet F, Vallancien G. Transrectal high-intensity focused ultrasound in the treatment of localized prostate cancer. *J Endourol* 2005; **19**: 693-701
48 **Vallancien G**, Prapotnich D, Cathelineau X, Baumert H, Rozet F. Transrectal focused ultrasound combined with transurethral resection of the prostate for the treatment of localized prostate cancer: feasibility study. *J Urol* 2004; **171**: 2265-2267
49 **Furusawa H**, Namba K, Nakahara H, Tanaka C, Yasuda Y, Hirabara E, Imahariyama M, Komaki K. The evolving non-surgical ablation of breast cancer: MR guided focused ultrasound (MRgFUS). *Breast Cancer* 2007; **14**: 55-58
50 **Wu F**, Wang ZB, Zhu H, Chen WZ, Zou JZ, Bai J, Li KQ, Jin CB, Xie FL, Su HB. Extracorporeal high intensity focused ultrasound treatment for patients with breast cancer. *Breast Cancer Res Treat* 2005; **92**: 51-60
51 **Stewart EA**. Uterine fibroids. *Lancet* 2001; **357**: 293-298
52 **LeBlang SD**, Hoctor K, Steinberg FL. Leiomyoma shrinkage after MRI-guided focused ultrasound treatment: report of 80 patients. *AJR Am J Roentgenol* 2010; **194**: 274-280
53 **Fennessy FM**, Tempany CM. A review of magnetic resonance imaging-guided focused ultrasound surgery of uterine fibroids. *Top Magn Reson Imaging* 2006; **17**: 173-179
54 **Funaki K**, Fukunishi H, Sawada K. Clinical outcomes of magnetic resonance-guided focused ultrasound surgery for uterine myomas: 24-month follow-up. *Ultrasound Obstet Gynecol* 2009; **34**: 584-589
55 **Spies JB**, Coyne K, Guaou Guaou N, Boyle D, Skyrnarz-Murphy K, Gonzalves SM. The UFS-QOL, a new disease-specific symptom and health-related quality of life questionnaire for leiomyomata. *Obstet Gynecol* 2002; **99**: 290-300
56 **Stewart EA**, Rabinovici J, Tempany CM, Inbar Y, Regan L, Gostout B, Hesley G, Kim HS, Hengst S, Gedroyc WM. Clinical outcomes of focused ultrasound surgery for the treatment of uterine fibroids. *Fertil Steril* 2006; **85**: 22-29
57 **Smart OC**, Hindley JT, Regan L, Gedroyc WM. Magnetic resonance guided focused ultrasound surgery of uterine fibroids--the tissue effects of GnRH agonist pre-treatment. *Eur J Radiol* 2006; **59**: 163-167
58 **Linke CA**, Carstensen EL, Frizzell LA, Elbadawi A, Fridd CW. Localized tissue destruction by high-intensity focused ultrasound. *Arch Surg* 1973; **107**: 887-891
59 **Frizzell LA**. Threshold dosages for damage to mammalian liver by high intensity focused ultrasound. *IEEE Trans Ultrason Ferroelectr Freq Control* 1988; **35**: 578-581
60 **Vallancien G**, Harouni M, Veillon B, Mombet A, Prapotnich D, Brisset JM, Bougaran J. Focused extracorporeal pyrotherapy: feasibility study in man. *J Endourol* 1992; **6**: 173-181
61 **Wu F**, Wang ZB, Chen WZ, Zou JZ, Bai J, Zhu H, Li KQ, Jin CB, Xie FL, Su HB. Advanced hepatocellular carcinoma: treatment with high-intensity focused ultrasound ablation combined with transcatheter arterial embolization. *Radiology* 2005; **235**: 659-667
62 **Chapelon JY**, Prat F, Sibille A, About El Fadil F, Henry L, Theilliere Y, Cathignol D. Extracorporeal selective focused destruction of hepatic tumours by high intensity ultrasound in rabbits bearing VX-2 carcinoma. *Min Inv Ther* 1992; **1**: 287-293
63 **Wu F**, Chen W, Bai J. Effect of high-intensity focused ultrasound on patients with hepatocellular cancer: preliminary report [in Chinese]. *Chin J Ultrasonog* 1999; **8**: 213-216
64 **Wu F**, Wang Z, Chen W, Zou JZ, Bai J, Zhu H, Li KQ, Xie FL, Jin CB, Su HB, Gao GW. Extracorporeal high-intensity focused ultrasound for treatment of solid carcinomas: four-year Chinese clinical experience. 2nd International Symposium on Therapeutic Ultrasound, Seattle, University of Washington, 2003
65 **Li CX**, Xu GL, Jiang ZY, Li JJ, Luo GY, Shan HB, Zhang R, Li Y. Analysis of clinical effect of high-intensity focused ultrasound on liver cancer. *World J Gastroenterol* 2004; **10**: 2201-2204
66 **Wu F**, Wang ZB, Zhu H, Chen WZ, Zou JZ, Bai J, Li KQ, Jin CB, Xie FL, Su HB. Feasibility of US-guided high-intensity focused ultrasound treatment in patients with advanced pancreatic cancer: initial experience. *Radiology* 2005; **236**: 1034-1040
67 **Yang R**, Reilly CR, Rescorla FJ, Faught PR, Sanghvi NT, Fry FJ, Franklin TD Jr, Lumeng L, Grosfeld JL. High-intensity focused ultrasound in the treatment of experimental liver cancer. *Arch Surg* 1991; **126**: 1002-1009; discussion 1009-1010
68 **Reddan DN**, Raj GV, Polascik TJ. Management of small renal tumors: an overview. *Am J Med* 2001; **110**: 558-562
69 **Vallancien G**, Chartier-Kastler E, Harouni M, Chopin D, Bougaran J. Focused extracorporeal pyrotherapy: experimental study and feasibility in man. *Semin Urol* 1993; **11**: 7-9
70 **Wu F**, Wang ZB, Chen WZ, Bai J, Zhu H, Qiao TY. Preliminary experience using high intensity focused ultrasound for the treatment of patients with advanced stage renal malignancy. *J Urol* 2003; **170**: 2237-2240
71 **Parkin DM**, Pisani P, Ferlay J. Estimates of the worldwide incidence of eighteen major cancers in 1985. *Int J Cancer* 1993; **54**: 594-606
72 **He SX**, Wang GM, Niu SG, Yao B, Wang XJ. The noninvasive treatment of 251 cases of advanced pancreatic cancer with focused ultrasound surgery. 2nd International Symposium on Therapeutic Ultrasound, Seattle, 2002
73 **Wu F**, Wang ZB, Zhu H, Chen WZ, Zou JZ, Bai J, Li KQ, Jin CB, Xie FL, Su HB. Feasibility of US-guided high-intensity focused ultrasound treatment in patients with advanced pancreatic cancer: initial experience. *Radiology* 2005; **236**: 1034-1040
74 **Smith NB**, Temkin JM, Shapiro F, Hynynen K. Thermal effects of focused ultrasound energy on bone tissue. *Ultrasound Med Biol* 2001; **27**: 1427-1433
75 **Gómez J**, Pinar A, Vallcanera A, Moreno A, Cortina H. Sonographic findings in aneurysmal bone cyst in children: correlation with computed tomography findings. *J Clin Ultrasound* 1998; **26**: 59-64
76 **Wu F**, Chen WZ, Bai J, Zou JZ, Wang ZL, Zhu H, Wang ZB. Pathological changes in human malignant carcinoma treated with high-intensity focused ultrasound. *Ultrasound Med Biol* 2001; **27**: 1099-1106
77 **Lu BY**, Yang RS, Lin WL, Cheng KS, Wang CY, Kuo TS.

Theoretical study of convergent ultrasound hyperthermia for treating bone tumors. *Med Eng Phys* 2000; **22**: 253-263
78 **Chen W**, Zhou K. High-intensity focused ultrasound ablation: a new strategy to manage primary bone tumors. *Curr Opin Orthop* 2005; **16**: 494-500
79 **Chen W**, Wang Z, Wu F, Bai J, Zhu H, Zou J, Li K, Xie F, Wang Z. [High intensity focused ultrasound alone for malignant solid tumors] *Zhonghua Zhongliu Zazhi* 2002; **24**: 278-281
80 **Chen W**, Wang Z, Wu F, Zhu H, Zou J, Bai J, Li K, Xie F. [High intensity focused ultrasound in the treatment of primary malignant bone tumor] *Zhonghua Zhongliu Zazhi* 2002; **24**: 612-615
81 **Liberman B**, Gianfelice D, Inbar Y, Beck A, Rabin T, Shabshin N, Chander G, Hengst S, Pfeffer R, Chechick A, Hanannel A, Dogadkin O, Catane R. Pain palliation in patients with bone metastases using MR-guided focused ultrasound surgery: a multicenter study. *Ann Surg Oncol* 2009; **16**: 140-146
82 **Kennedy JE**. High-intensity focused ultrasound in the treatment of solid tumours. *Nat Rev Cancer* 2005; **5**: 321-327
83 **Wu CC**, Chen WS, Ho MC, Huang KW, Chen CN, Yen JY, Lee PH. Minimizing abdominal wall damage during high-intensity focused ultrasound ablation by inducing artificial ascites. *J Acoust Soc Am* 2008; **124**: 674-679
84 **Thomas JL**, Fink MA. Ultrasonic beam focusing through tissue inhomogeneities with a time reversal mirror: application to transskull therapy. *IEEE Trans Ultrason Ferroelectr Freq Control* 1996; **43**: 1122-1129
85 **Marquet F**, Pernot M, Aubry JF, Montaldo G, Marsac L, Tanter M, Fink M. Non-invasive transcranial ultrasound therapy based on a 3D CT scan: protocol validation and in vitro results. *Phys Med Biol* 2009; **54**: 2597-2613
86 **Qian ZW**, Xiong L, Yu J, Shao D, Zhu H, Wu X. Noninvasive thermometer for HIFU and its scaling. *Ultrasonics* 2006; **44** Suppl 1: e31-e35
87 **Annand A**, Kaczkowski PJ. Monitoring formation of high intensity focused ultrasound (HIFU) induced lesions using backscattered ultrasound. *Acoustical Research Letters Online* 2004; **5**: 88-94
88 **Fry FJ**, Johnson LK. Tumor irradiation with intense ultrasound. *Ultrasound Med Biol* 1978; **4**: 337-341
89 **Hu Z**, Yang XY, Liu Y, Sankin GN, Pua EC, Morse MA, Lyerly HK, Clay TM, Zhong P. Investigation of HIFU-induced anti-tumor immunity in a murine tumor model. *J Transl Med* 2007; **5**: 34
90 **Wu F**, Wang ZB, Lu P, Xu ZL, Chen WZ, Zhu H, Jin CB. Activated anti-tumor immunity in cancer patients after high intensity focused ultrasound ablation. *Ultrasound Med Biol* 2004; **30**: 1217-1222
91 **Gillams AR**. Liver ablation therapy. *Br J Radiol* 2004; **77**: 713-723
92 **Si HP**, Xiang LK, Wang Z, Li YY, Wang ZB. Immune changes in bone neoplasm rabbits transplanted with VX2 before and after high intensity focused ultrasound therapy. *Chin J Exp Surg* 2003; **20**: 823-824
93 **Kinoshita M**. Targeted drug delivery to the brain using focused ultrasound. *Top Magn Reson Imaging* 2006; **17**: 209-215
94 **Patrick JT**, Nolting MN, Goss SA, Dines KA, Clendenon JL, Rea MA, Heimburger RF. Ultrasound and the blood-brain barrier. *Adv Exp Med Biol* 1990; **267**: 369-381
95 **Hynynen K**, McDannold N, Vykhodtseva N, Jolesz FA. Noninvasive MR imaging-guided focal opening of the blood-brain barrier in rabbits. *Radiology* 2001; **220**: 640-646
96 **Hynynen K**, McDannold N, Sheikov NA, Jolesz FA, Vykhodtseva N. Local and reversible blood-brain barrier disruption by noninvasive focused ultrasound at frequencies suitable for trans-skull sonications. *Neuroimage* 2005; **24**: 12-20
97 **McDannold N**, Vykhodtseva N, Raymond S, Jolesz FA, Hynynen K. MRI-guided targeted blood-brain barrier disruption with focused ultrasound: histological findings in rabbits. *Ultrasound Med Biol* 2005; **31**: 1527-1537
98 **McDannold N**, Vykhodtseva N, Hynynen K. Targeted disruption of the blood-brain barrier with focused ultrasound: association with cavitation activity. *Phys Med Biol* 2006; **51**: 793-807
99 **Larkin JO**, Casey GD, Tangney M, Cashman J, Collins CG, Soden DM, O'Sullivan GC. Effective tumor treatment using optimized ultrasound-mediated delivery of bleomycin. *Ultrasound Med Biol* 2008; **34**: 406-413
100 **Yu T**, Wang Z, Jiang S. Potentiation of cytotoxicity of adriamycin on human ovarian carcinoma cell line 3AO by low-level ultrasound. *Ultrasonics* 2001; **39**: 307-309
101 **Yuh EL**, Shulman SG, Mehta SA, Xie J, Chen L, Frenkel V, Bednarski MD, Li KC. Delivery of systemic chemotherapeutic agent to tumors by using focused ultrasound: study in a murine model. *Radiology* 2005; **234**: 431-437
102 **Bekeredjian R**, Kroll RD, Fein E, Tinkov S, Coester C, Winter G, Katus HA, Kulaksiz H. Ultrasound targeted microbubble destruction increases capillary permeability in hepatomas. *Ultrasound Med Biol* 2007; **33**: 1592-1598
103 **Delon-Martin C**, Vogt C, Chignier E, Guers C, Chapelon JY, Cathignol D. Venous thrombosis generation by means of high-intensity focused ultrasound. *Ultrasound Med Biol* 1995; **21**: 113-119
104 **Parsons JE**, Cain CA, Abrams GD, Fowlkes JB. Pulsed cavitational ultrasound therapy for controlled tissue homogenization. *Ultrasound Med Biol* 2006; **32**: 115-129
105 **Xu Z**, Fowlkes JB, Rothman ED, Levin AM, Cain CA. Controlled ultrasound tissue erosion: the role of dynamic interaction between insonation and microbubble activity. *J Acoust Soc Am* 2005; **117**: 424-435
106 **Xu Z**, Hall TL, Fowlkes JB, Cain CA. Optical and acoustic monitoring of bubble cloud dynamics at a tissue-fluid interface in ultrasound tissue erosion. *J Acoust Soc Am* 2007; **121**: 2421-2430
107 **Roberts WW**, Hall TL, Ives K, Wolf JS Jr, Fowlkes JB, Cain CA. Pulsed cavitational ultrasound: a noninvasive technology for controlled tissue ablation (histotripsy) in the rabbit kidney. *J Urol* 2006; **175**: 734-738
108 **Xu Z**, Fowlkes JB, Cain CA. A new strategy to enhance cavitational tissue erosion using a high-intensity, Initiating sequence. *IEEE Trans Ultrason Ferroelectr Freq Control* 2006; **53**: 1412-1424

S- Editor Cheng JX **L- Editor** Lutze M **E- Editor** Ma WH

World Journal of Clinical Oncology

Online Submissions: http://www.wjgnet.com/2218-4333office
wjco@wjgnet.com
doi:10.5306/wjco.v2.i1.28

World J Clin Oncol 2011 January 10; 2(1): 28-43
ISSN 2218-4333 (online)

TOPIC HIGHLIGHT

E YK Ng, PhD, PGDTHE, Associate Professor, *Series Editor*

Imaging of gastroenteropancreatic neuroendocrine tumors

Eik Hock Tan, Cher Heng Tan

Eik Hock Tan, Department of Nuclear Medicine and PET, Singapore General Hospital, Outram Road, Singapore 169608, Singapore
Cher Heng Tan, Department of Diagnostic Radiology, Tan Tock Seng Hospital, 11 Jalan Tan Tock Seng, Singapore 308433, Singapore
Author contributions: Tan EH contributes to functional imaging sections; Tan CH contributes to anatomic imaging sections.
Correspondence to: Dr. Eik Hock Tan, Department of Nuclear Medicine and PET, Singapore General Hospital, Outram Road, Singapore 169608, Singapore. andrew.tan@singhealth.com.sg
Telephone: +65-63265767 Fax: +65-62240938
Received: July 19, 2010 Revised: October 20, 2010
Accepted: October 27, 2010
Published online: January 10, 2011

Abstract

Imaging of gastroenteropancreatic neuroendocrine tumors can be broadly divided into anatomic and functional techniques. Anatomic imaging determines the local extent of the primary lesion, providing crucial information required for surgical planning. Functional imaging, not only determines the extent of metastatic disease spread, but also provides important information with regard to the biologic behavior of the tumor, allowing clinicians to decide on the most appropriate forms of treatment. We review the current literature on this subject, with emphasis on the strengths of each imaging modality.

Key words: Magnetic resonance imaging; Neuroendocrine tumor; Positron emission tomography; Somatostatin receptor scintigraphy

Peer reviewers: Tzu-Chen Yen, MD, PhD, Professor and Chairperson, Department of Nuclear Medicine and Molecular Imaging Center, Chang Gung Memorial Hospital and University, Taoyuan, Taiwan, China; Domenico Rubello, MD, Professor, Director of the Department of Nuclear Medicine, PET/CT Centre, Radiology, Medical Physics, Santa Maria della Misericordia Hospital; Via Tre Martiri 140, ZIP 45100, Rovigo, Italy; Ravi Murthy, MD, Interventional Radiology, UT MD Anderson Cancer Center, 1400 Pressler Street, Unit 1471, Houston, TX 77042, United States

Tan EH, Tan CH. Imaging of gastroenteropancreatic neuroendocrine tumors. *World J Clin Oncol* 2011; 2(1): 28-43 Available from: URL: http://www.wjgnet.com/2218-4333/full/v2/i1/28.htm DOI: http://dx.doi.org/10.5306/wjco.v2.i1.28

INTRODUCTION

Neuroendocrine tumors (NETs) are a rare and heterogeneous group of neoplasms, which as the name suggests, are derived from cells of the neuroendocrine system. It was Lubarsch *et al*[1] in 1888, a German pathologist at the University of Munich, who is generally credited with the first report of a carcinoid tumor. He gave the classical microscopic description of multiple ileal carcinoids in two patients, termed "little carcinomata", which he thought originated in the intestinal crypts of Lieberkuhn.

Later in 1907, Ciacco M C coined the term "enterochromaffin" to describe the cells that were thought to give rise to the tumor, and this was further expanded by Feyrter *et al*[2], who proposed the concept of the diffuse neuroendocrine system in an attempt to unify tumors in diverse sites that had similar histological features.

The term neuroendocrine is derived from the similarity of such cells to neural cells in the expression of certain proteins, such as synaptophysin, neuron-specific enolase and chromogranin A. Currently, the following criteria proposed by Langley[3] are generally accepted as defining neuroendocrine cells: (1) The production of a neurotransmitter, neuromodulator or neuropeptide hormone; (2) The presence of dense-core secretory granules from which the hormones are released by exocytosis in response to an external stimulus; and (3) The absence of axons and synapses.

DIAGNOSIS OF NEUROENDOCRINE TUMORS

The morphologic appearance of well-differentiated NETs

Table 1 Guide to World Health Organization classification of neuroendocrine tumors

Behaviour	Metastasis	Muscularis propria invasion	Differentiation	Size (cm)	Angioinvasion	Ki-67 (%)	Hormonal index
WHO criteria (gastrointestinal)							
Benign	-	-	Well-differentiated	≤ 1	-	< 2	-
Benign/Low-grade malignant	-	-	Well-differentiated	1-2	-/+	< 2	-
Low-grade malignant	+	+	Well-differentiated	> 2	+	2-20	+
High-grade malignant	+	+	Poorly-differentiated	Any	+	> 20	-
WHO criteria (pancreas)							
Benign	-	-	Well-differentiated	≤ 1	-	< 2	-/+
Benign/Low-grade malignant	-	-	Well-differentiated	> 2	-/+	< 2	-/+
Low-grade malignant	+	+	Well-differentiated	> 4	+	2-20	+
High-grade malignant	+	+	Poorly-differentiated	Any	+	> 20	-

Exceptions: Malignant duodenal gastrinomas are usually < 1 cm and confined to submucosa. Benign neuroendocrine tumors of the appendix usually invade the muscularis propria. WHO: World Health Organization.

is fairly typical, demonstrating an organoid-type pattern under light microscopy, and diagnosis can be fairly confidently made on the basis of such morphology. In cases of poorly differentiated tumors or neuroendocrine origin or variant morphology, electron microscopy or immunohistochemical assessments might be necessary[4,5].

Several commonly used immunohistochemical markers include synaptophysin, chromogranin, vasoactive monoamine transporter 2, serotonin and substance P[6]. Chromogranin appears to be the most consistent general marker, and has been found to have high sensitivity and specificity in diagnosing NETs[7]. In addition, circulating levels of chromogranin A have been found to correlate with tumor volume and are related to disease extent, and could potentially play a role in disease monitoring and prognostication[8,9].

CLASSIFICATION AND STAGING OF NEUROENDOCRINE TUMORS

Historically, the diverse and widespread nature of disease presentation meant that a large number of descriptions have been used for NETs in different body regions. Also, certain descriptive terms have been used loosely with different connotations between physicians, surgeons and pathologists, leading to further confusion and miscommunication. In response, attempts have been made to organize and categorize the tumors that comprise the neuroendocrine disease spectrum. In 2000, the World Health Organization (WHO) published a classification for NETs of the gastroenteropancreatic system that categorized tumors into 3 broad categories[10]: (1) Well-differentiated neuroendocrine tumor (benign or uncertain malignant potential); (2) Well-differentiated neuroendocrine carcinoma (low grade malignancy); and (3) Poorly differentiated neuroendocrine carcinoma (high grade malignancy). The criteria used for differentiating the various grades include tumor size, angioinvasion, proliferative activity, histological differentiation, presence of metastasis/local invasion, association with certain syndromes, and hormonal/functional activity.

In an attempt to clarify terminology, the term "carcinoid" was reserved to describe well-differentiated NETs, and the term "malignant carcinoid" was used to describe well-differentiated neuroendocrine carcinomas.

Several publications have supported the clinical effectiveness of the WHO criteria in management decision support (Table 1)[11-14], but there was a need for improved prognostication assessment of NETs.

In response, the European Neuroendocrine Tumor Society has attempted to address the staging of NETs. Their staging system addressed 2 issues; the cell characteristics/proliferation capacity of the tumor, and an adapted tumor node metastasis (TNM) staging system[15-17].

The TNM staging system was sub-divided into specific areas such as the stomach, duodenum/proximal jejunum, lower jejunum/ileum, and pancreas, and follows conventional grading criteria assessing for tumor size/invasion, nodal and distant spread.

With regard to cellular grading, three tumor grade categories were identified. Grade I tumors show a low proliferative index (Ki67 </= 2% or < 2 mitoses per HPF), Grade II tumors show a moderate proliferative index (Ki67 3%-20% or 2-20 mitoses per HPF), and Grade III tumors show a high proliferative index (Ki67 > 20% or > 20 mitoses per HPF). In general, Grade 1 and 2 tumors should refer to well-differentiated NETs while Grade 3 tumors indicate poorly differentiated neuroendocrine carcinomas.

Publications have supported the utility of this TNM classification system for prognostication stratification (Table 2)[18], but further validation is required.

ANATOMIC IMAGING OF NEUROENDOCRINE TUMORS

Anatomic imaging of NETs still plays a crucial role in the diagnosis and management of this condition, largely due to its ability to provide anatomical information for surgical planning. The widespread availability of ultrasound (US) and computed tomography (CT), and in most large centers, magnetic resonance imaging (MRI), has led to a number of publications on the imaging detection of NET. Due to the relative paucity of this condition, most of the published data describing the efficacy of each

Table 2a Tumor node metastasis staging (gastric, duodenum, ampulla, jejunum, ileum, pancreas)

TNM staging	Gastric	Duodenum/ampulla/proximal jejunum	Pancreas	Lower jejunum/Ileum
Tx	Primary tumor cannot be assessed	Primary tumor cannot be assessed	Primary tumor cannot be assessed	Primary tumor cannot be assessed
T0	No evidence of primary tumor	No evidence of primary tumor	No evidence of primary tumor	No evidence of primary tumor
Tis	*In situ* tumor/dysplasia (> 0.5 mm)	-	-	-
T1	Tumor invades lamina propria or submucosa and </= 1 cm	Tumor invades lamina propria or submucosa and </= 1 cm	Tumor limited to pancreas and size < 2 cm	Tumor invades mucosa or submucosa and size </= 1 cm
T2	Tumor invades muscularis propria or subserosa or > 1 cm	Tumor invades muscularis propria or > 1 cm	Tumor limited to pancreas and size 2-4 cm	Tumor invades muscularis propria or size > 1 cm
T3	Tumor penetrates serosa	Tumor invades pancreas or retroperitoneum	Tumor limited to pancreas and size > 4 cm or invading duodenum or bile duct	Tumor invades subserosa
T4	Tumors invade adjacent structures (for any T, add M for multiple tumors)	Tumor invades peritoneum or other structures (for any T, add m for multiple tumors)	Tumor invading adjacent organs (stomach, spleen, colon, adrenal gland) or the wall or large vessels (celiac or superior mesenteric artery)	Tumor invades peritoneum/ other organs (for any T, add m for multiple tumors)
Nx	Regional lymph nodes cannot be assessed	Regional lymph nodes cannot be assessed	Regional lymph nodes cannot be assessed	Regional lymph nodes cannot be assessed
N0	No regional lymph node metastasis	No regional lymph node metastasis	No regional lymph node metastasis	No regional lymph node metastasis
N1	Regional lymph node metastasis	Regional lymph node metastasis	Regional lymph node metastasis	Regional lymph node metastasis
Mx	Distant metastasis cannot be assessed	Distant metastasis cannot be assessed	Distant metastasis cannot be assessed	Distant metastasis cannot be assessed
M0	No distant metastasis	No distant metastasis	No distant metastasis	No distant metastasis
M1	Distant metastasis	Distant metastasis	Distant metastasis	Distant metastasis

Table 2b Tumor node metastasis Staging (appendix, colon, rectum)

	Appendix	Colon/rectum
Tx	Primary Tumor cannot be assessed	Primary Tumor cannot be assessed
T0	No evidence of primary tumor	No evidence of primary tumor
T1	Tumor invades lamina propria or submucosa and </= 1 cm	Tumor invades mucosa or submucosa, T1a < 1 cm, T1b 1-2 cm
T2	Tumor invades submucosa, muscularis propria and/or minimally (up to 3 mm) invading subserosa/mesoappendix and </= 2 cm	Tumor invades muscularis propria or > 2 cm
T3	Tumor > 2 cm and/or invasion (more than 3 mm) of the serosa/ mesoappendix	Tumor invades subserosa/pericolic/perirectal fat
T4	Tumors invade peritoneum/other organs	Tumor directly invades other organs and/or perforates visceral peritoneum
Nx	Regional lymph nodes cannot be assessed	Regional lymph nodes cannot be assessed
N0	No regional lymph node metastasis	No regional lymph node metastasis
N1	Regional lymph node metastasis	Regional lymph node metastasis
Mx	Distant metastasis cannot be assessed	Distant metastasis cannot be assessed
M0	No distant metastasis	No distant metastasis
M1	Distant metastasis	Distant metastasis

modality, and consequently studies directly comparing between modalities, suffer from small sample sizes with wide variability in results. Nevertheless, for gastroenteropancreatic (GEP) NETs, it is generally agreed upon that CT and MRI are superior to US, both in terms of lesion detection, and characterization.

Ultrasound

The use of transabdominal ultrasound (TAUS) in GEP NETs is largely confined to the solid viscera. This is due to the fact that sound waves are heavily attenuated by air, and US is therefore not usually suitable for assessment of lesions within the gastrointestinal tract or mesentery. The use of US in tumor diagnosis and staging is further limited by inter-operator variability. Nevertheless, newer techniques, such as contrast enhanced US (CEUS) and endoscopic US (EUS), have found a greater role for US in the management of GEP NETs.

The use of TAUS for assessment of pancreatic lesions is limited, especially in the body and tail region, which are commonly obscured by air and ingested material in the overlying stomach. Therefore, the patient should ideally have fasted for several hours prior to scanning. Using the stomach and proximal duodenum as an acoustic win-

Table 2c ESMO tumor node metastasis clinical classification of neuroendocrine tumors

Disease stage	T	N	M
Gastric, duodenum, ampulla, jejunum, ileum, pancreas			
Stage Ⅰ	T1	N0	M0
Stage Ⅱa	T2	N0	M0
Stage Ⅱb	T3	N0	M0
Stage Ⅲa	T4	N0	M0
Stage Ⅲb	Any T	N1	M0
Stage Ⅳ	Any T	Any N	M1
Appendix			
Stage Ⅰ	T1	N0	M0
Stage Ⅱa	T2	N0	M0
Stage Ⅱb	T3	N0	M0
Stage Ⅲa	T4	N0	M0
Stage Ⅲb	Any T	N1	M0
Stage Ⅳ	Any T	Any N	M1
Colon/rectum			
Stage Ⅰa	T1a	N0	M0
Stage Ⅰb	T1b	N0	M0
Stage Ⅱa	T2	N0	M0
Stage Ⅱb	T3	N0	M0
Stage Ⅲa	T4	N0	M0
Stage Ⅲb	Any T	N1	M0
Stage Ⅳ	Any T	Any N	M1

dow by drinking water is recommended[19]. Characteristic features of pancreatic NETs on US would be a homogenously hypoechoic mass that may sometimes have a hyperechoic halo. Use of CEUS shows promise but requires validation. Detection rate of US for pancreatic NET varies widely and ranges from 0%-66%[20].

EUS is a more invasive method of imaging assessment. Its advantage over TAUS lies in the fact that the US probe is positioned much closer to the organ of interest. This allows the use of higher frequency probes 7.5-12 MHz which provide better spatial resolution in the order of millimeters. Rösch *et al*[21] reported a sensitivity of 82% and a specificity of 95% for EUS in localizing pancreatic NET lesions. In a similar study by McAuley *et al*[20] on insulinomas, for lesions smaller than 2 cm in diameter, EUS carried a sensitivity of 80%-90%, leading the authors to recommend EUS as a screening tool for patients with a known diagnosis of multiple endocrine neoplasia (MEN) type 1.

While previously considered to represent the gold standard of assessment of NETs, preoperative imaging by CT and MRI has largely superseded intraoperative US (IOUS). This is partly because IOUS entails a longer operating time, and carries with it the potential risk of iatrogenic injury (e.g. to the splenic vein) during the course of examination.

CT

Significant improvements in the spatial and temporal resolution of CT have been made over the past decade, with the advent of multidetector row CT (MDCT). This has allowed for multiphasic contrast enhanced CT (CECT) while achieving spatial resolutions in the order of millimeters. The use of biphasic or triphasic CECT is generally considered a prerequisite for detection and characterization of NETs, both for primary disease involving the pancreas, as well as for liver metastases (Figure 1). The reason for this is that the majority of NET lesions show avid early enhancement. CT is regarded as a first-line imaging modality for detection and staging of NETs.

A recommended protocol for imaging of pancreatic NETs would require the patient to be adequately fasted. Ingestion of water just before the CT scan would act as a negative contrast for visualization of periampullary tumors. An unenhanced scan can initially be performed to look for calcifications, which occur in around 20% of cases, and differentiate this from pancreatic adenocarcinomas, which calcify in only approximately 2% of cases[22]. Thin collimation allows for depiction of submillimeter lesions, and this is usually performed at 1.25 to 2.0 mm section thickness[23]. Multiplanar reconstructions may also help improve lesion assessment.

Typically, intravenous administration of iodinated contrast at a rate of 3-5 mL/s is required to provide an adequate bolus. Most MDCT scanners are equipped with automated bolus tracking capabilities, hence allowing for patient-specific adjustments of scan delay times following bolus injection of contrast. On average, arterial phase imaging is performed at 20-25 s following initiation of contrast injection, while the portal venous phase is timed at approximately 50 s. The pancreatic parenchymal phase, which is the time at which the pancreas enhances maximally, is usually at 35-40 s.

The typical pancreatic NET lesion is isodense on the non-contrast scan but shows homogeneous avid arterial enhancement. Vascular encasement and biliary obstruction are considered rare. Atypical lesions include those that are hypovascular (or hypoenhancing), hyperdense on non-contrast scan, cystic (Figure 2) or calcified[24,25]. Non-functioning lesions tend to be larger, and present with mass effect such as biliary dilatation. They may, therefore, appear as heterogeneous lesions with central necrosis or cystic degeneration. Functioning tumors are usually small, with around 50% of lesions measuring less than 1.3 cm in diameter, and therefore, do not cause deformation of the contour of the gland. The main differential for pancreatic NETs would be metastases from clear cell type renal cell carcinoma, both of which may be present in patients with von Hippel Lindau's disease.

CT has the advantage of a wider field of view than US. It is, therefore, suited for detection of nodal and metastatic disease. In the presence of a NET originating from the bowel, the high contrast to noise ratio between the primary lesion and mesenteric fat allows for excellent depiction of the extent of mesenteric retraction (Figure 3). The secondary lesions, most notably liver metastases, tend to show a similar imaging pattern as the primary lesion itself. Esophageal hyperenhancement and small bowel mural thickening are concomitant findings associated with gastrinomas and best depicted on CT.

In terms of lesion detection, sensitivity of detection with CT increases proportionately with lesion size. In gastric NETs, Binstock *et al*[26] showed that those lesions that were larger than 1 cm in diameter and presented with focal wall thickening were detected with increased fre-

Figure 1 Axial contrast enhanced computed tomography image. A: The primary lesion arising from a loop of the ileum, with extension along the mesenteric border. Typical central stipple calcification is evident; B: In the arterial phase showing multiple hypoenhancing bilobar lesions in a non-cirrhotic liver consistent with neuroendocrine tumor metastases; C: In the equilibrium phase showing the typical washout pattern of the lesions corresponding to that in (B).

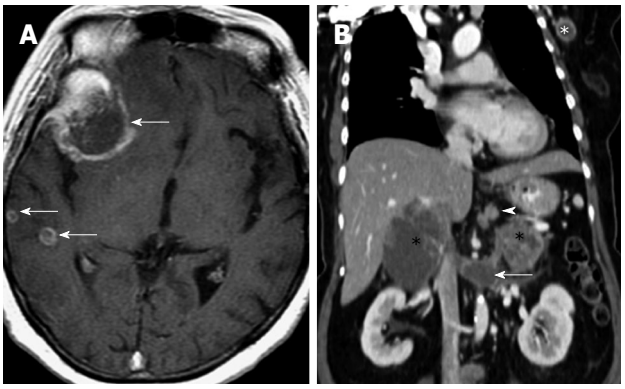

Figure 2 Computed tomography images of a patient with metastatic neuroendocrine carcinoma. A: Axial T1 weighted fat-suppressed image of the brain in a patient with metastatic neuroendocrine carcinoma. Multiple ring enhancing lesions (arrows) are present in the right cerebral hemisphere, consistent with metastases. The dominant lesion in the right frontal lobe was hemorrhagic; B: Reconstructed contrast enhanced computed tomography image of the same patient in the coronal plane shows multiple sites of metastases: perigastric nodes (arrowhead), bilateral adrenal glands (black *), extension into the left renal vein (arrow) and a left axillary lymph node (white *). The primary lesion is believed to have originated from the stomach, which presented as an ulcerated mass on endoscopy (not shown).

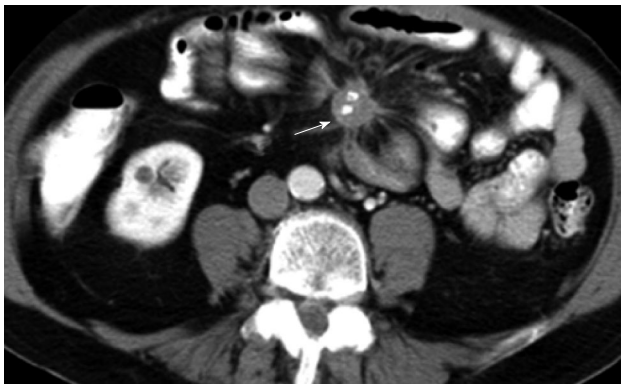

Figure 3 Axial computed tomography image of a patient following gastrointestinal and intravenous administration of iodinated contrast. Spiculated mass with central stippled calcifications and tethering of the mesentery which is characteristic of neuroendocrine tumor. The primary lesion (not shown) is usually small and most commonly found in the ileum. Vascular occlusion is a known complication and may present with features of small bowel ischemia.

quency. Similarly, for the small bowel lesions, CT was able to detect around half of the lesions when the size of the mesenteric masses exceeded 1.5 cm[27]. Interestingly, it is not uncommon to find that the sizes of the metastatic lesions far exceed the size of the primary tumor (Figure 4).

Improvements in CT technology over time, probably also due to the use of multiphasic CECT, have led to a concomitant increase in lesion detection of pancreatic NETs. For example, a retrospective study of cases over 13 years by Gouya *et al*[28] in 2003, showed lesion sensitivity of 94.4% with the use of dual phase thin section CT compared to 28.6% with the use of single slice section CT technology.

Similarly, for metastatic disease to the liver, which can be the most common imaging finding in GI NETs, multiphasic imaging is recommended, with the hepatic arterial phase being best for lesion detection[29]. On standard radiography and CT, bone metastases frequently demonstrate either an osteosclerotic or a mixed osteolytic-osteosclerotic pattern[30].

Magnetic resonance imaging

MRI is considered superior to CT for lesion assessment in the solid visceral organs. In a comparison study between MRI and CT as well as angiography for detection of metastatic lesions, MRI was shown to be superior[31].

As with CT, multiphasic CE MRI is recommended, with fat-suppressed CE T1-weighted (T1W) imaging providing the best accuracy, with an area under the receiver-operating curve (AUROC) of 0.98[32]. This has been corroborated by a more recent study by Herwick *et al*[33].

The advantages of MRI over CT are the lack of ionizing radiation and the use of gadolinium chelate contrast agents, which have a better safety profile in terms of allergic reactions and nephrotoxicity, although the latter point is slightly mitigated by the concerns of nephrogenic systemic fibrosis. Nonetheless, MRI provides added information about the lesions, such as T1 relaxivity and T2 dephasing.

Typically, NET lesions show T2 hyperintensity and T1 hypointensity (Figure 5). In the study by Owen *et al*[34], 14 out of 29 (48.3%) lesions demonstrated this finding, while only one out of 29 (3.4%) showed a reversal of signal, that is, T1 hyperintensity and T2 hypointensity. The study by Semelka *et al*[35] showed a positive predictive value of 96%

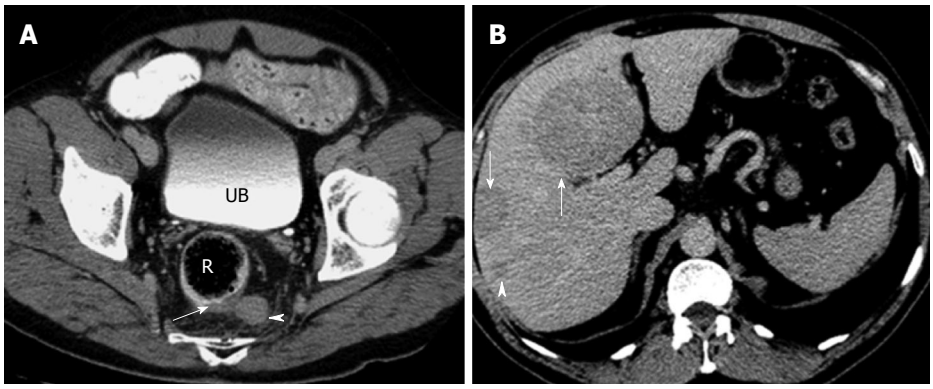

Figure 4 Axial computed tomography images of a patient with histologically proven metastatic neuroendocrine carcinoma. A: Axial contrast enhanced computed tomography (CT) image of the rectum (R) showing focal eccentric thickening of the left posterolateral wall (arrow) with associated enlarged perirectal lymph node (arrowhead). Biopsy confirmed neuroendocrine carcinoma. Note the iodinated contrast in the urinary bladder (UB) indicating the delayed phase of imaging; B: Axial CT image of the same patient in the delayed phase showing multiple hypodense masses (arrows) and nodules (arrowhead) in the liver. These are consistent with metastatic disease. Note that the metastatic disease burden is considerable larger than the primary tumor itself, a not uncommon finding in neuroendocrine tumor.

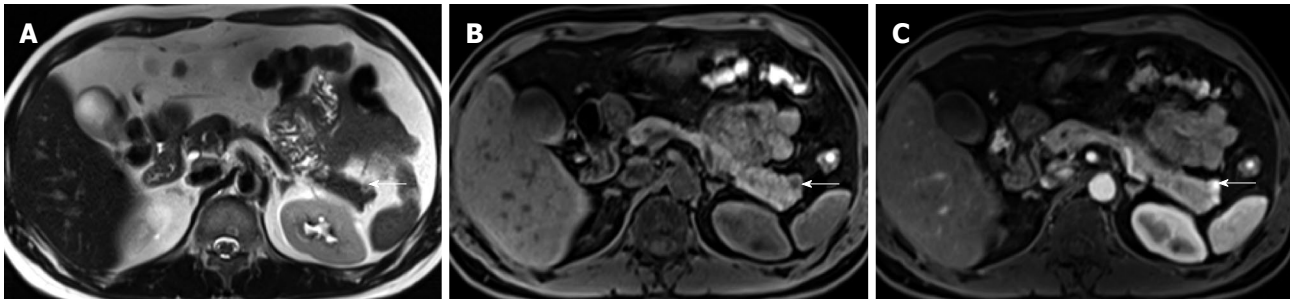

Figure 5 Axial magnetic resonance imaging images of a patient with Zollinger Ellison's syndrome. A: Axial non-contrast T2 weighted image of a patient with known Zollinger Ellison's syndrome secondary to a hyperfunctioning islet cell tumor (arrow) in the pancreatic tail. A T2 hyperintense nodule is present in the pancreatic tail. This corresponded to the site of increased tracer uptake on the octreotide scan (not shown). Note the relatively small size of the lesion, a finding that is typical for functioning islet cell tumors; B: Axial pre-contrast T1 weighted fat-suppressed image showing the lesion (arrow) to be hypointense. This contrasts well with the normal high signal of the pancreatic parenchyma; C: Axial post-contrast T1 weighted fat-suppressed image in the hepatic arterial phase showing avid enhancement within the lesion (arrow). This is the typical enhancement pattern of a neuroendocrine tumor.

for MRI in pancreatic NETs. Gastrinomas tend to show ring or peripheral enhancement while most other subtypes of NETs demonstrated a diffuse pattern of enhancement.

For GI NETs, MRI is able to detect around two-thirds of lesions[36], with fat-suppressed T1W imaging yielding maximal results. Similarly, hepatic metastases are well depicted on MRI, and MRI is often used to further characterize lesions that are equivocal on CT. Like the primary lesions, hepatic metastases appear as T1 hypointense and T2 hyperintense. Bader *et al*[36] showed this finding in 75% of cases. Interestingly, 15% of cases showed increased enhancement only in the arterial phase. Furthermore, some of the metastases may display T2 hyperintensity approaching that of hemangiomas[37]. Nevertheless, T2WI and hepatic arterial phase T1WI fat-suppressed imaging have been shown to be most sensitive[38].

Advances in diffusion weighted imaging (DWI) have led to its widespread clinical use in abdominal imaging. Vossen *et al*[39] showed that there was a statistically significant difference in apparent diffusion coefficient (ADC) values between hemangiomas and NET metastases (as well as other hypervascular liver lesions), with an AUROC of 0.91. An added advantage of using DWI is its ability to reflect lesion changes in treatment response. In the study by Liapi *et al*[40], ADC values rose concomitantly with response to transarterial chemoembolization (TACE), in tandem with decreased enhancement of the treated lesions. For the primary lesions, DWI may allow for preoperative localization of tumors in the pancreas, especially those which do not demonstrate the typical hypervascular pattern[41,42].

FUNCTIONAL IMAGING OF NEUROENDOCRINE TUMORS

The basis of functional imaging lies with the targeted detection of specific cell targets or receptors, allowing precise localization of lesions. In the context of diagnostic imaging, the concentration of receptor molecules in target tissues may be hard to differentiate from background non-specific binding[43]. As such, molecular imaging techniques have often been confined to nuclear-based modalities such as positron emission tomography (PET) or single photon emission CT (SPECT), which are able to generate images with micromolar to picomolar concentrations of imaging probes[44].

The Delphi consensus with regard to the diagnostic imaging of NETs, has acknowledged that functional imaging in the form of somatostatin receptor scintigraphy (SRS) plays a central role in the diagnosis of NETs[45], and we will explore this and various other functional imaging modalities and techniques in relation to their clinical utility in the diagnosis of NETs. Our discussion will focus largely on the gastroenteropancreatic system, but general principles are likely applicable to NETs in other parts of the body.

Somatostatin receptor scintigraphy

Somatostatin receptors are widely distributed in the human nervous system and tissues in the body, including the adrenals, kidneys, pancreas and prostate[46]. Currently, 5 subtypes of somatostatin receptors have been identified in humans (SSRT1, SSRT2, SSRT3, SSRT4, SSRT5), with SSRT2 further classified into subtypes 2A and 2B[47].

Of particular interest, somatostatin receptor expression has been found in a large number of tumors, of which NETs are the archetypical class, and this forms the basis for the molecular imaging of NETs.

The half-life of somatostatin itself is too short (< 2 min) for use in either diagnosis or therapy. As a result, synthetic somatostatin analogues with sufficiently long half-lives have been developed for use in diagnostic imaging or therapeutics.

The first commercially available somatostatin analogue was Octreotide (Sandostatin, Novartis Pharmaceutical Corp), with an approximate half-life of 2 h, and a radiolabeled analogue of octreotide, Octreoscan® (^{111}In-DTPA-Octreotide, D-Phe-Cys-Phe-D-Trp-Lys-Thr-Cys-Thr[ol]), was successfully used to visualize somatostatin receptor positive tumors by gamma camera scintigraphy in the early 1990s[48-50].

Normal physiological uptake is seen in the thyroid, spleen, liver and pituitary due to receptor binding of the peptides, while tracer uptake in the kidneys is predominantly secondary to reabsorption of filtered peptides, and bowel uptake is presumably secondary to hepatobiliary clearance (Figures 6 and 7).

Gamma-based SRS (Octreoscan®) has proved to be a safe, sensitive imaging agent in the detection of GEP NETs, with an overall sensitivity of approximately 80%-90% in patients with gastrointestinal neuroendocrine neoplasms[51-54]. However, limitations include false negative results in organs with significant physiological uptake (e.g. liver) where background uptake may mask lesions, and small volume diseases that may be below the intrinsic spatial resolution of gamma imaging. Additionally, false positives can occur with a variety of lesions, such as the thyroid gland, accessory spleens, granulomatous or inflammatory tissue, and benign or malignant breast lesions[55]. Other types of neoplasms that demonstrate somatostatin receptor expression include meningiomas and lymphomas.

Nonetheless, SRS is considered the "gold standard" in the diagnosis, staging and follow-up of patients with NETs (Figure 8).

Newer generation somatostatin analogues have since been developed, allowing radiolabeling with positron emitting tracers. Together with the development and adoption of hybrid PET/CT modalities, this potentially addresses several limitations faced with first generation SRS, largely related to the poorer spatial resolution of gamma-based probes and the issue of precise anatomical localization (Figures 9 and 10).

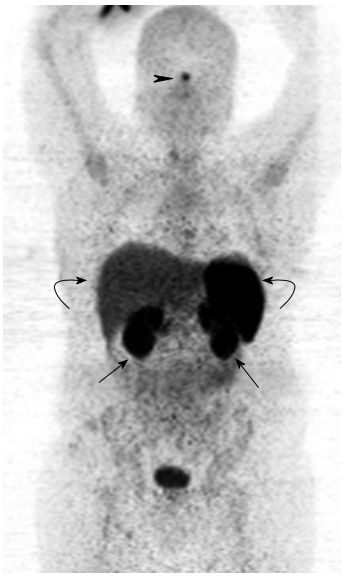

Figure 6 Gallium 68 DOTATATE positron emission tomography from the skull vertex to mid-thigh. The coronal maximum intensity projection image demonstrates physiological areas of tracer uptake in the pituitary (black arrowhead), kidneys (black arrows), liver and spleen (curved arrows).

PET-based SRS has shown high sensitivities, specificities and accuracies in the evaluation of NETs. Initial evaluations using PET-based SRS were encouraging. Hofmann *et al*[56] found higher tumor to non-tumor contrast ratios with significantly higher detection ratios for PET-based SRS, and Kowalski *et al*[57] also concluded that PET-based SRS was able to detect more lesions and was superior in detecting smaller lesions.

A larger prospective study by Gabriel *et al*[58] evaluating the diagnostic value of ^{68}Ga-DOTATOC PET in 84 patients with known or suspected NETs demonstrated a sensitivity of 97%, specificity of 92% and an overall accuracy of 96%, showing significantly higher diagnostic efficacy as compared with SPECT imaging using gamma-based SRS and normal diagnostic CT. In addition, PET-based SRS detected more tumor sites in the liver, nodes and bone as compared with the other modalities, and provided further clinically relevant information in 14% of patients compared with gamma-based scintigraphy and 21% as compared with CT.

This was substantiated by Putzer *et al*[59], who evaluated 51 patients with histologically proven NETs with 68Ga-DOTATOC PET/CT. Reported sensitivity and specificity were 97% and 92%, respectively, higher than CT or bone scan, and detected bone metastasis in patients at a significantly higher rate. This is particularly important as osseous metastasis has a negative prognostic implication on clinical outcomes.

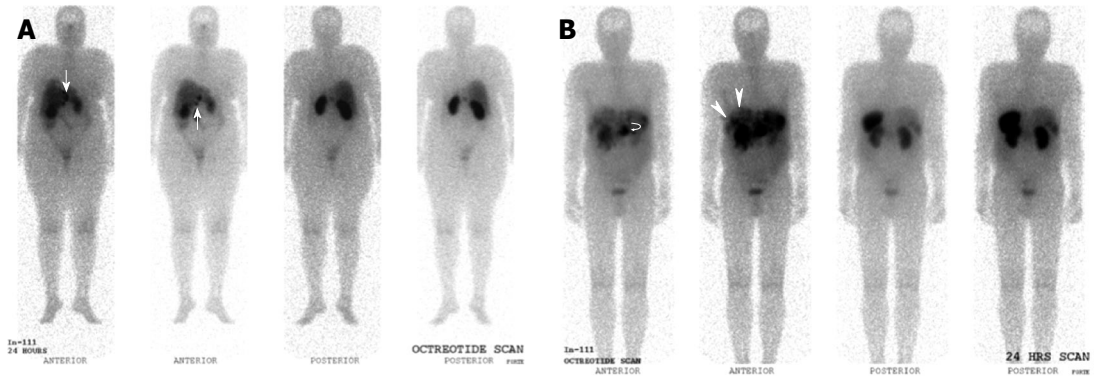

Figure 7 Indium 111 Octreotide Planar whole-body images. A: Indium 111 Octreotide 24-h delayed anterior and posterior planar whole body images in a patient with prior resected pancreatic neuroendocrine carcinoma. Several abnormal tracer foci (white arrows) are seen in the peri-hepatic region, suspicious for somatostatin receptor expressing lesions. These were later confirmed as neuroendocrine nodal metastasis in the peri-hepatic and peri-gastric nodes; B: Indium 111 Octreotide 24-h delayed anterior and posterior planar whole body images in a patient with histologically confirmed neuroendocrine carcinoma of the pancreatic body. Increased tracer focus in the region of the pancreas (curved white arrow) corresponds to the primary pancreatic lesion, while multiple abnormal foci of uptake in the liver (white arrows) are in keeping with hepatic metastasis.

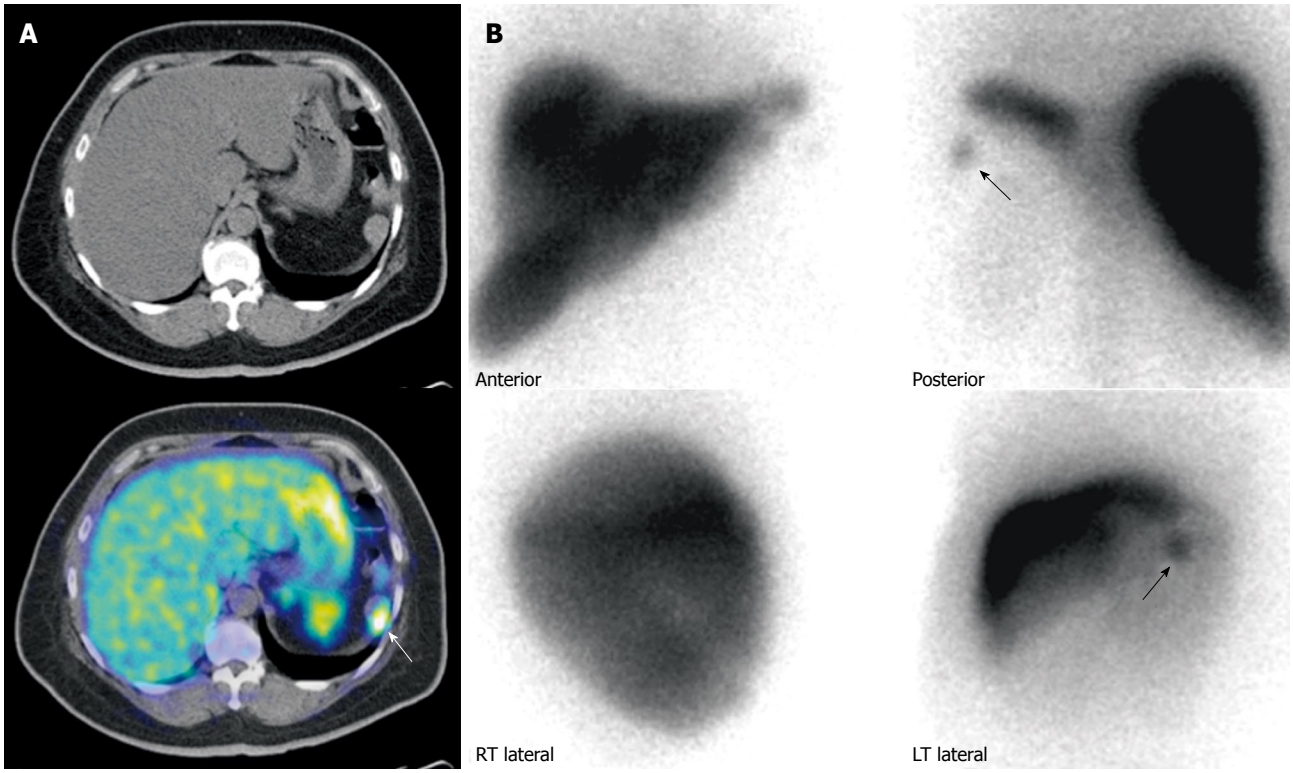

Figure 8 Patient with prior history of neuroendocrine carcinoma in the pancreatic tail, status post partial pancreatectomy and splenectomy. A: Gallium 68 DOTATATE positron emission tomography/computed tomography (PET/CT). Axial CT and fused PET/CT images of the abdomen shows a mass in the left upper abdomen demonstrating significant DOTATATE tracer avidity (white arrow). Considerations included tumor recurrence or splenunculus; B: Technetium 99m Sulfur Colloid scintigraphy. Anterior and posterior planar spot views of the upper abdomen demonstrates a focus of uptake (black arrows) in the left upper abdomen, corresponding to the area of uptake seen on the previous Gallium 68 DOTATATE scan, confirming the mass to be a splenunculus.

Furthermore, the increased diagnostic accuracy of PET-based SRS has been shown in publications to impact on actual clinical management. Ambrosini *et al*[60] evaluated the clinical impact of 68Ga-DOTANOC PET/CT imaging in 90 patients with histologically proven NETs. In the subgroup of patients with concordant PET and CT findings (n = 47), PET resulted in a modification of therapeutic management in 36.2% of patients. In the subgroup of patients with discordant PET and CT findings (n = 42), PET resulted in stage modification in 28.6% of patients and a change in management in 76.2% of patients. Overall, PET imaging affected either staging or therapy in 55.5% of patients imaged, with the most frequent management impact being initiation or continuance of peptide receptor radionuclide therapy, initiation or continuance of somatostatin analogue treatment, or referral for surgery. The author also reported

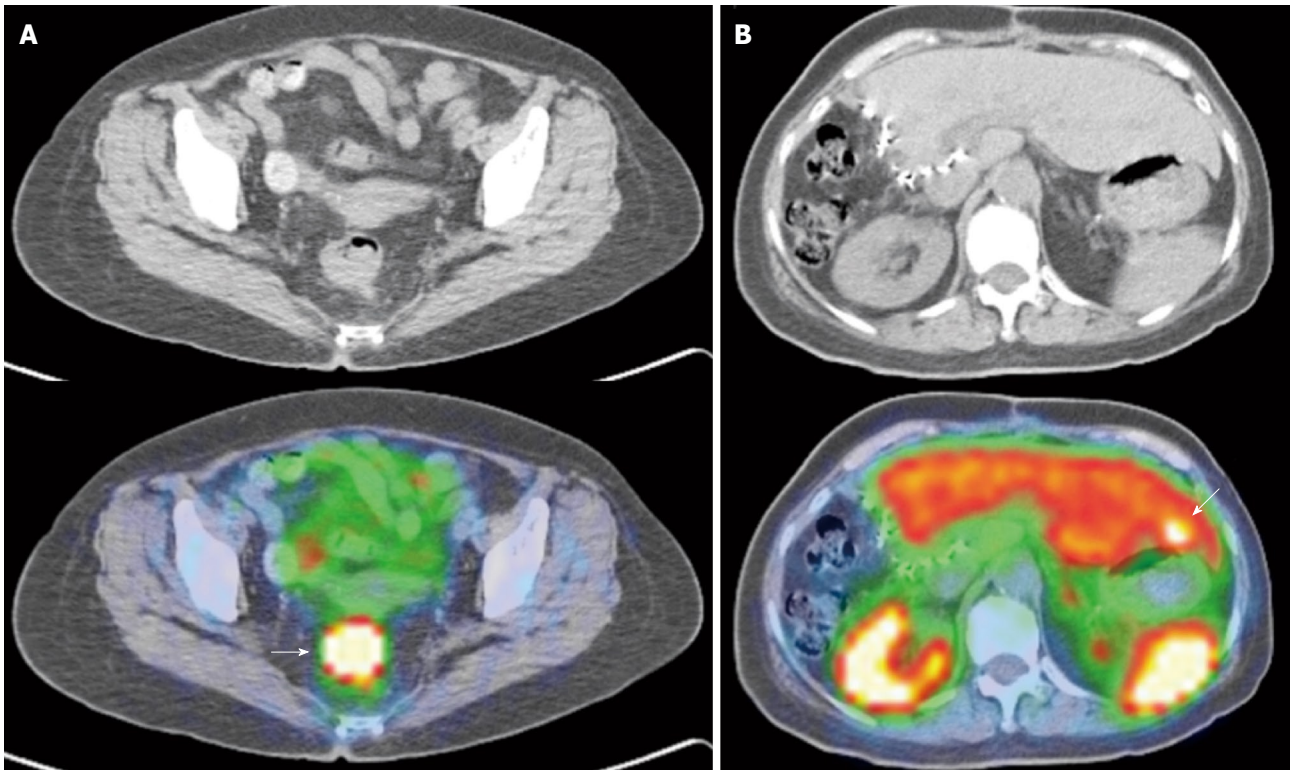

Figure 9 Gallium 68 DOTATATE positron emission tomography/computed tomography of a patient with right hepatic lobe neuroendocrine tumor metastasis, status post resection, but of unknown primary. A: Axial computed tomography (CT) and fused positron emission tomography/CT (PET/CT) image of the pelvis shows an intensely DOTATATE tracer avid eccentric thickening of the rectum (white arrow), suspicious for a rectal primary. This was histologically confirmed as a neuroendocrine carcinoma; B: Axial CT and fused PET/CT image of the abdomen. Surgical clips are seen along the right liver margin, in keeping with previous surgery. There is an intensely tracer avid focus seen in segment 3 (white arrow). Although there were no obvious findings on the correlative non-contrast CT, this is suspicious for an additional liver metastasis. Note the normal physiological uptake in the kidneys, spleen and liver.

that PET prevented unnecessary surgery in 6 patients, and excluded 2 patients with peptide receptor radionuclide treatment who did not show significant somatostatin analogue avidity.

With regard to post-therapy response assessment of NETs following peptide receptor radionuclide therapy, findings are controversial.

Gabriel *et al*[61] evaluated 46 patients with advanced NETs who underwent peptide receptor radionuclide therapy. 68Ga-DOTATOC PET (dedicated PET) and conventional CT was performed pre- and post-therapy for all patients. RECIST criteria were used to evaluate therapy response, with a reported 30% response rate, 48% stable disease and 22% progressive disease. Concordant findings were noted in 70% of cases. In the 30% discrepant group (n = 14), PET-based SRS outperformed CT in 10 patients, was able to detect lesions not seen on CT in 5 patients and accurately determined disease response in 5 patients. In contrast, CT was able to detect small pulmonary lesions in 1 patient not seen on PET, and in the remaining 3 patients, PET-based SRS showed decreased tracer uptake in the lesions, but these were due to tumor dedifferentiation rather than therapy response, while CT clearly showed tumor size and extent of progression.

The author concluded that PET-based SRS showed no advantages over conventional imaging in response assessment, but several limitations in the study have to be noted. Firstly, the study utilized a dedicated PET scanner, while the majority of newer installations are hybrid PET/CT scanners, and the intrinsic limitations of dedicated PET imaging is accounted. Indeed, based on the 4 discrepant findings reported in the study, if a hybrid PET/CT scanner was utilized, it is expected that such discrepancies would not exist. Secondly, the emergence of non-somatostatin analogue avid lesions on post -therapy assessment scans is of clinical use, as it indicates dedifferentiation of tumor, suggesting the need for alternative treatment from peptide receptor radionuclide therapy or somatostatin analogues (Figures 9 and 10).

Overall, PET-based SRS has been routinely found to demonstrate high diagnostic sensitivity, specificity and accuracy[62], with positive clinical impact during pre-therapy staging. The use of SRS for post-therapy assessment is more indeterminate, and further evaluation needs to be carried out.

F18-fluorodeoxyglucose PET/CT

Fluorodeoxyglucose (FDG) PET imaging is a molecular imaging technique that addresses the glucose metabolism of tissue. As a rule of thumb, malignant tumors tend to demonstrate significantly higher levels of glucose metabolism as compared with normal physiological tissue, and this has proven true across a wide range of tumor types[63].

The molecular basis of increased glucose metabolism

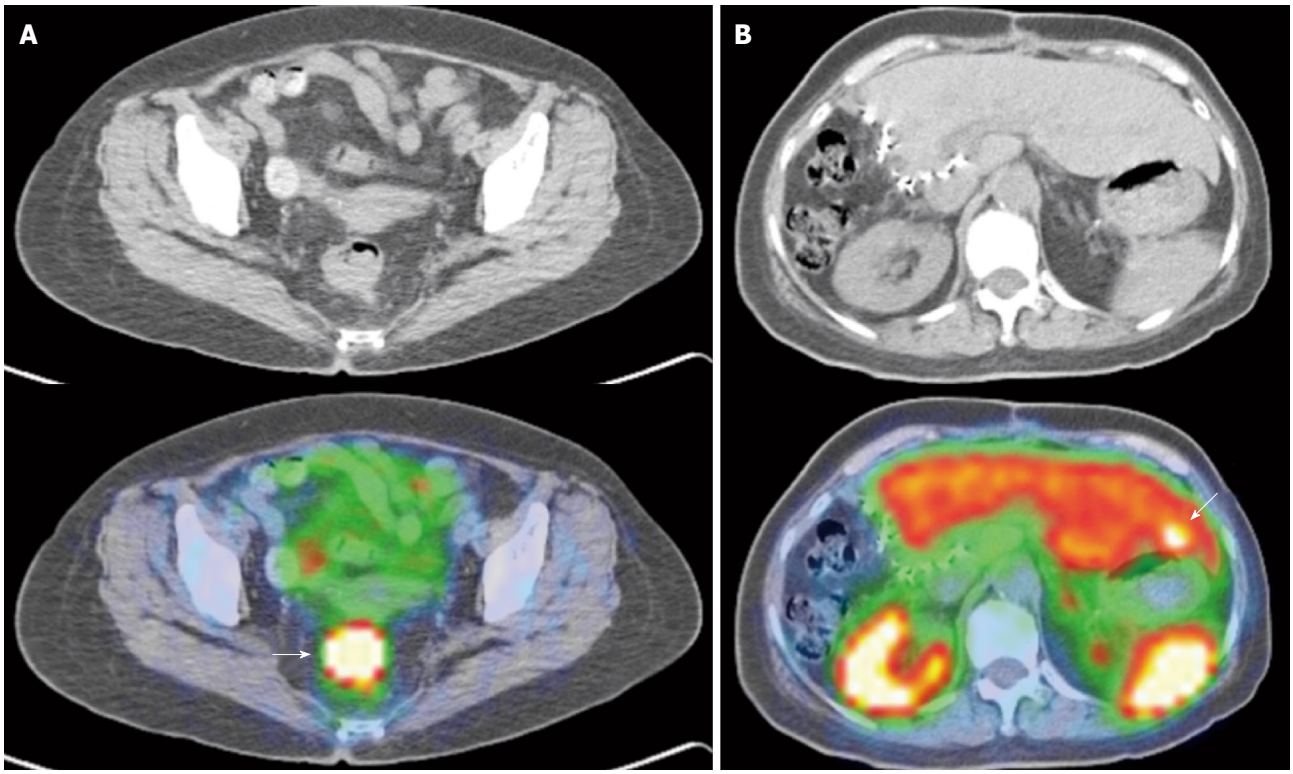

Figure 10 Gallium 68 DOTATATE positron emission tomography/computed tomography of a patient with histologically proven abdominal paraganglioma. For pre-therapy staging. A: Axial computed tomography (CT) and fused positron emission tomography/CT (PET/CT) image of the abdomen demonstrates an intensely DOTATATE avid mass in the inter aorto-caval region (white arrow), correlating with the primary tumor; B: Axial CT and fused PET/CT image of the abdomen shows a peritoneal mass adjacent to the spleen that shows avid tracer uptake (white arrow). This is compatible with a peritoneal deposit.

in tumor cells is complex, and there appears a multitude of factors controlling aerobic glycolysis in tumors[64]. However, 2 major factors have been implicated with increased FDG tumor uptake. Firstly, the overexpression of glucose transporters and activity in tumor cells (predominantly GLUT-1, 3 and 5) which actively drive glucose into the cells, and secondly, the overexpression of hexokinase enzymes (predominantly hexokinase-2) that increase glucose metabolism[65,66].

The use of FDG PET in NETs is currently controversial. There are limited sensitivities overall, but there is emerging evidence that the presence of increased glucose metabolism in tumors highlights an increased propensity for invasion and metastasis, and overall poorer prognosis. This correlates with mathematically-based telogenic models and empiric data reviewed by Gillies *et al*[67], where such increased glucose metabolism confers an "evolutionary advantage" in cancer cells over normal parenchymal tissue.

An early study performed by Adams *et al*[68] found that FDG PET only demonstrated increased glucose uptake in less differentiated tumors with high proliferative activity. Another small study performed by Pasquali *et al*[69] evaluated the clinical use of FDG PET against conventional gamma-based SRS and CT, and again found that FDG PET was able to detect NETs characterized by rapid growth or aggressive behavior. Garin *et al*[70] performed a prospective study evaluating the clinical outcomes of 38 patients with metastatic NETs. FDG PET, SRS and conventional CT were performed for these patients, and patients were tracked to determine progression-free survival and overall survival. Overall 2 year survival and progression-free survival was 73% and 45%, respectively, and it was found that most patients with FDG PET positive lesions had early progressive disease (14/15 for FDG PET positive as compared with 2/23 for FDG PET negative). Furthermore, when only patients with low-grade tumors were considered, FDG PET was able to predict those with early progression. Progression-free survival was 87% ± 7% and 75% ± 10% at 1 and 2 years, respectively, for FDG PET negative lesions, as compared with 7% ± 6% and 0% at 1 and 2 years, respectively, for FDG PET positive patients. Overall, the relative risk of early progression with FDG PET positive lesions was 10.7 (95% CI: 2.8-40.6).

In terms of survival, FDG PET negative patients fared better than patients with FDG avid lesions. Overall survival was 95% ± 5% at both 1 and 2 years, respectively, for FDG PET negative patients, *vs* 72% ± 12% and 42% ± 13% at 1 and 2 years, respectively, for 18F-FDG PET positive patients.

Overall, the use of FDG PET appears promising in disease prognostication, possibly influencing aggressiveness of management. In addition, dual tracer imaging using both FDG and SRS PET might possibly be used in post-therapy assessment following peptide receptor radionuclide therapy to evaluate for tumor dedifferentiation or the "flip-flop" phenomenon[71] (Figure 11).

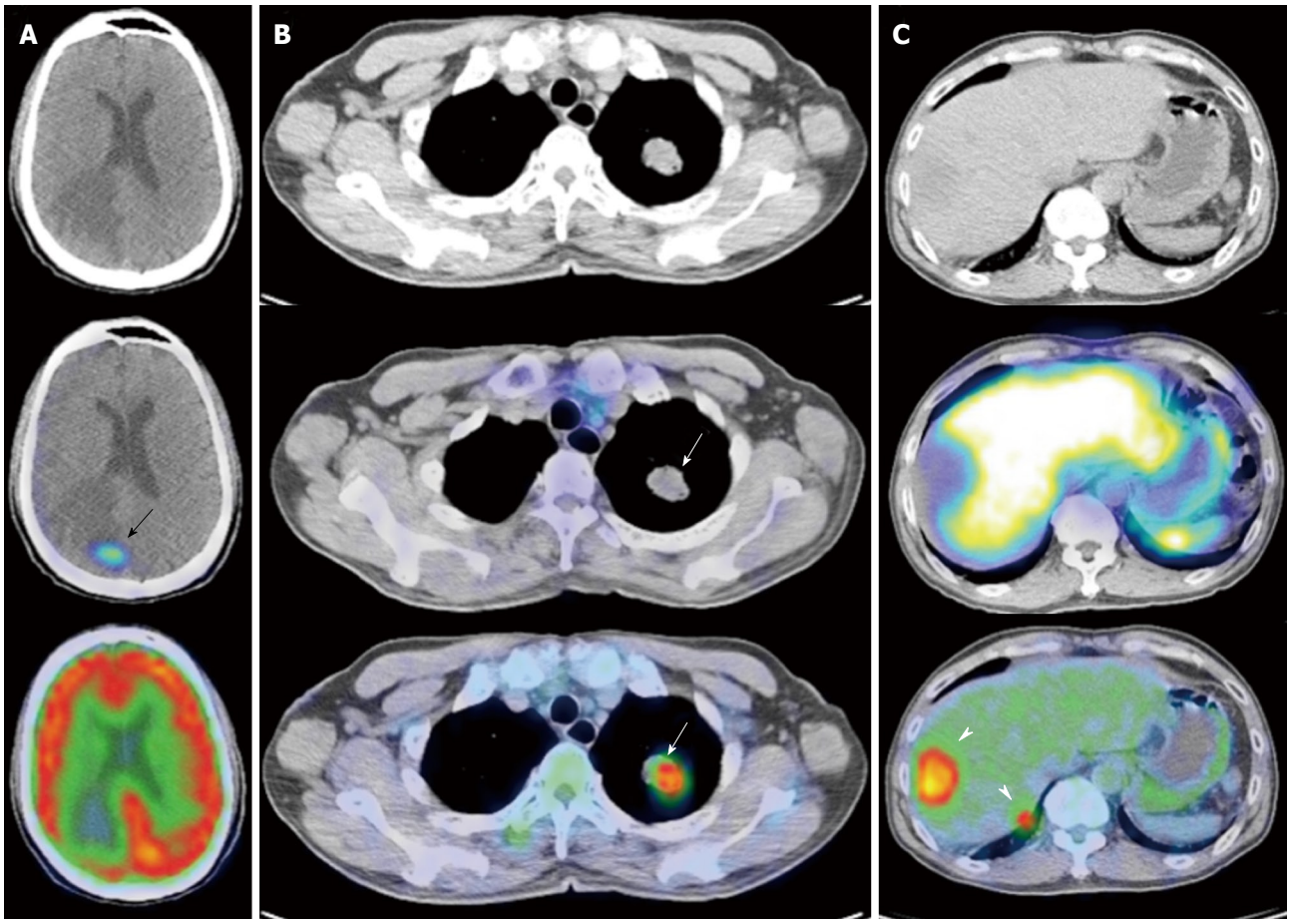

Figure 11 Gallium 68 DOTATATE and Fluorine 18 fluorodeoxyglucose positron emission tomography/computed tomography of a patient with metastatic neuroendocrine carcinoma. A: Axial computed tomography (CT), fused DOTATATE positron emission tomography//CT (PET/CT) and fused fluorodeoxyglucose (FDG) PET/CT images of the brain. There is a focus of moderately increased DOTATATE uptake seen in the right occipital lobe (black arrow) associated with adjacent vasogenic edema, but no definite corresponding FDG uptake is seen; B: Axial CT, fused DOTATATE PET/CT and fused FDG PET/CT images of the thorax. There is an intensely FDG avid mass in the left upper lobe, but no corresponding DOTATATE tracer avidity is seen (white arrows), demonstrating an example of the "flip-flop" phenomenon secondary to tumor dedifferentiation; C: Axial CT, fused DOTATATE PET/CT and fused FDG PET/CT images of the abdomen. Again, there are intensely FDG avid lesions in the right liver lobe (white arrowheads) that do not demonstrate significant DOTATATE uptake, indicative of neuroendocrine tumor dedifferentiation.

F18-Dihydroxyphenylalanine PET/CT

The APUD Concept by Everson Pearse[72] describes the ability of neuroendocrine type cells to take up and decarboxylate amino acid precursors, and there have been various efforts to evaluate the utility of radiolabeled amine precursors to image NETs. Examples of such precursors include hydroxytryptophan, hydroxyephedrine, dopamine and dihydroxyphenylalanine (DOPA). The radiolabeled DOPA analogues are transported into NETs *via* the sodium independent system L, and the activity of amino acid decarboxylase in the cells is important for intracellular retention of the metabolized radiolabeled DOPA analogue. Becherer *et al*[73] in the evaluation of 23 patients with histologically proven NETs concluded that 18F-DOPA PET performed better that gamma-based SRS in visualizing lesions, with the highest sensitivity in visualizing skeletal and mediastinal lesions. Reported sensitivities were 81.3% for the liver, 90.9% for the skeleton and 100% for the mediastinum and lymph nodes.

Koopmans *et al*[74] evaluated 53 patients in a prospective single-center diagnostic accuracy study using 18F-DOPA PET, conventional CT and SRS without any CT correlation, and reported that 18F-DOPA PET detected more lesions, more positive regions and more lesions per region as compared with the other modalities. Reported sensitivities at the patient, region and lesion levels were 100%, 95% and 96%, respectively.

Kauhanen *et al*[75] evaluated 82 patients with suspected/known NETs using 18F-DOPA PET, comparing the diagnostic accuracy with histological findings and clinical follow-up. 32 patients were for primary diagnosis and staging, while 61 patients were for restaging. Overall accuracy for gastrointestinal NETs was approximately 89%.

Overall, based on a meta-analysis by Jager *et al*[76], the radiolabeled DOPA analogues have reported sensitivities in the range of 65%-96% for the detection of individual lesions, with most of the values in the upper half of this range.

The advantages of DOPA PET over conventional anatomic imaging or gamma-based SRS are fairly conclusive, but the role in comparison with PET-based SRS techniques is still uncertain. Accuracies for PET-based

Table 3 Summary comparison of the various imaging modalities

	Advantages	Disadvantages	Utility
Ultrasound	Widely available modality, dynamic visualization of lesions, no ionizing radiation	Limited to solid organ systems, inter-operator variability	Possible use as a screening tool for assessing the liver and pancreatic head
CT	Widely available modality, wide field of view, allowing evaluation of nodal disease and metastasis, good sensitivity	Ionizing radiation, non specific modality, low negative predictive value for small volume nodes	First line imaging modality
MRI	Superior to CT for assessment in solid organs, no ionizing radiation, gadolinium contrast agent safety profile better than CT agents in terms of allergic reaction and nephrotoxicity, ability to further characterize lesions using different sequencing	Not as widely available as compared with CT or ultrasound, more specialized diagnostic imaging expertise in interpretation, lower specificity in characterizing neuroendocrine lesions as compared with functional imaging modalities	Local staging of disease, including vascular involvement, use in pediatric age group in which ionizing radiation is of greater concern
SRS	Good sensitivity and specificity, able to accurately characterize lesions; single modality staging; allows for dosimetric evaluation of suitability for peptide receptor radionuclide therapy; proven impact on clinical management	Ionizing radiation; not as widely available as CT or ultrasound, requiring nuclear imaging capabilities; more specialized diagnostic imaging expertise in interpretation	Gold standard in the evaluation of neuroendocrine tumors
Flurodeoxyglucose PET	Possible use in disease prognostication and management stratification, possible use in post treatment assessment to evaluate for tumor dedifferentiation	Generally poor sensitivity for neuroendocrine tumors, ionizing radiation	Not routinely performed for neuroendocrine tumor assessment, possible utility in prognostication and post therapy assessment
Dihydroxyphenylalanine PET	Good sensitivities in the evaluation of neuroendocrine tumors, shows promise especially in assessments of insulinomas	Requires more specialized nuclear facilities (e.g. gaseous F18) for synthesis of the radioisotope, PET based SRS has generally similar or better accuracies in the detection and staging of neuroendocrine tumors, ionizing radiation	Possible clinical utility in the evaluation of insulinomas

CT: Computed tomography; MRI: Magnetic resonance imaging; PET: Positron emission tomography; SRS: Somatostatin receptor scintigraphy.

SRS as discussed earlier appear to be comparable or better than DOPA PET. In a head to head comparison between 68Ga-DOTATATE and 18F-DOPA PET in the diagnosis of differentiated metastatic NETs, patient-based sensitivities were 96% for 68Ga-DOTATATE compared with 56% for 18F-DOPA, with 68Ga-DOTATATE PET proving clearly superior for detection and staging of NETs[77].

In addition, the clinical impact of PET-based SRS has been established in several publications, and the added advantage of SRS is that it allows the suitability assessment for peptide receptor radionuclide therapy, something that DOPA PET does not allow.

FUNCTIONAL IMAGING OF PANCREATIC NEUROENDOCRINE TUMORS

Pancreatic endocrine tumors comprise approximately 2%-10% of all pancreatic tumors[78,79], and are named after the predominant hormone that they secrete.

Insulinomas are the most common, accounting for approximately 60% of pancreatic NETs. They are tumors arising from pancreatic B-cells and are frequently solitary and largely benign. Typically, only 10% of insulinomas are multiple, 10% malignant, and 10% are associated with the Multiple Endocrine Neoplasm (MEN) type 1 syndrome[80]. Gastrinomas are the second most common tumors, accounting for approximately 20% of such tumors. Other rarer types include glucagonomas, somatostatinomas, vasoactive intestinal peptide secreting tumors (VIPomas), adrenocorticotropic secreting tumors (ACTHoma), GRFomas, calcitonin-producing tumors and parathyroid hormone-related peptide tumors.

Such tumors can be broadly classified as functional or non-functional, and although earlier studies estimated non-functional tumors to account for 18%-66% of tumors[81], later large studies have classified 60%-80% of pancreatic NETs as non-functional[82,83].

In approaching functional or molecular imaging of pancreatic neuroendocrine or islet-cell tumors, it is prudent to do so based on 2 separate groups: Insulinomas and non-insulinoma pancreatic NETs.

With regard to insulinomas, the role of SRS is uncertain, as there is generally poor sensitivity in the detection of such tumors. The reasons for this are multifactorial. Firstly, a significant percentage of insulinomas do not express significant densities of somatostatin receptors, especially subtypes 2 and 5. In addition, somatostatin receptors are not significantly expressed in non-malignant insulinomas further limiting SRS sensitivity[84]. However, malignant insulinomas are known to overexpress somatostatin receptors, and SRS has potential imaging roles in such tumors for prognostication and staging[85].

In contrast, gamma-based SRS has reported sensitivity and specificity for non-insulinoma pancreatic NETs of approximately 80%-90%[86,87], and is indicated for use in pre-therapy localization and staging, especially when demonstration of extra-hepatic metastatic lesions is required.

Several reports have established the promising utility of PET-based SRS for imaging non-insulinoma pancreatic NETs[88-90]. The use of PET-based SRS is expected to have improved resolutive capabilities as compared with conventional gamma-based SRS, in keeping with findings from gastrointestinal carcinoid imaging, but further validation is needed.

The utility of FDG PET in the evaluation of pancreatic NETs is indeterminate. FDG PET has generally poor sensitivities in the detection of such tumors (approximately 50%)[91], but may have a role in prognostication as it allows the identification of NETs characterized by aggressive growth or behavior[92-93].

DOPA PET appears to show promise in the evaluation of pancreatic NETs. Koopmans *et al*[94] in the evaluation of 23 patients with pancreatic islet cell tumors reported a sensitivity of 89% using 18F-DOPA PET, as compared with 78% and 87% for gamma-based SRS and conventional CT, respectively.

In the same study, 5-hydroxytryptophan (5-HTP) was also used as a delivery ligand in the targeted imaging of NETs. 5-HTP is the direct precursor for the serotonin pathway, and thus, is potentially of use in all neuroendocrine type tumors[95]. In relation to pancreatic islet cell tumors, the study reported sensitivities of 100% for 11C-5-HTP in the detection of pancreatic NETs (Table 3).

CONCLUSION

The discussions on the various imaging modalities used in the diagnostic imaging of NETs highlight several of the modalities and various key points, but this is not a comprehensive review. This is partly due to the extensive and complex nature or NETs, and partly due to the explosive growth and developments in medical imaging. In summary, an understanding of the historical and molecular underpinnings of NETs, and the intrinsic uses and limitations of each diagnostic imaging modality, are essential for the physician involved in the management of this complex disease.

REFERENCES

1 **Lubarsch O**. Ueber den primären krebs des ileum nebst bemerkungen über das gleichzeitige vorkommen von krebs und tuberculose. *Virchows Arch Pathol Anat* 1888; **111**: 280-317
2 **Feyrter F**. Über diffuse endokrine epitheliale Organe. *Zentralblatt Innere Medizin* 1938; **59**: 546-556
3 **Langley K**. The neuroendocrine concept today. *Ann N Y Acad Sci* 1994; **733**: 1-17
4 **Said JW**, Vimadalal S, Nash G, Shintaku IP, Heusser RC, Sassoon AF, Lloyd RV. Immunoreactive neuron-specific enolase, bombesin, and chromogranin as markers for neuroendocrine lung tumors. *Hum Pathol* 1985; **16**: 236-240
5 **Hainsworth JD**, Wright EP, Johnson DH, Davis BW, Greco FA. Poorly differentiated carcinoma of unknown primary site: clinical usefulness of immunoperoxidase staining. *J Clin Oncol* 1991; **9**: 1931-1938
6 **Chetty R**. An overview of practical issues in the diagnosis of gastroenteropancreatic neuroendocrine pathology. *Arch Pathol Lab Med* 2008; **132**: 1285-1289
7 **Campana D**, Nori F, Piscitelli L, Morselli-Labate AM, Pezzilli R, Corinaldesi R, Tomassetti P. Chromogranin A: is it a useful marker of neuroendocrine tumors? *J Clin Oncol* 2007; **25**: 1967-1973
8 **Zatelli MC**, Torta M, Leon A, Ambrosio MR, Gion M, Tomassetti P, De Braud F, Delle Fave G, Dogliotti L, degli Uberti EC. Chromogranin A as a marker of neuroendocrine neoplasia: an Italian Multicenter Study. *Endocr Relat Cancer* 2007; **14**: 473-482
9 **Nobels FR**, Kwekkeboom DJ, Coopmans W, Schoenmakers CH, Lindemans J, De Herder WW, Krenning EP, Bouillon R, Lamberts SW. Chromogranin A as serum marker for neuroendocrine neoplasia: comparison with neuron-specific enolase and the alpha-subunit of glycoprotein hormones. *J Clin Endocrinol Metab* 1997; **82**: 2622-2628
10 **Solcia E**, Kloppel G, Sobin LH. Histological typing of endocrine tumours. World Health Organization International Histological Classification of Tumours. 2nd ed. Berlin, Germany: Springer, 2000
11 **Artale S**, Giannetta L, Cerea G, Maggioni D, Pedrazzoli P, Schiavetto I, Napolitano M, Veronese S, Bramerio E, Gambacorta M, Vanzulli A, Pisconti S, Pugliese R, Siena S. Treatment of metastatic neuroendocrine carcinomas based on WHO classification. *Anticancer Res* 2005; **25**: 4463-4469
12 **Bajetta E**, Catena L, Procopio G, Bichisao E, Ferrari L, Della Torre S, De Dosso S, Iacobelli S, Buzzoni R, Mariani L, Rosai J. Is the new WHO classification of neuroendocrine tumours useful for selecting an appropriate treatment? *Ann Oncol* 2005; **16**: 1374-1380
13 **Panzuto F**, Nasoni S, Falconi M, Corleto VD, Capurso G, Cassetta S, Di Fonzo M, Tornatore V, Milione M, Angeletti S, Cattaruzza MS, Ziparo V, Bordi C, Pederzoli P, Delle Fave G. Prognostic factors and survival in endocrine tumor patients: comparison between gastrointestinal and pancreatic localization. *Endocr Relat Cancer* 2005; **12**: 1083-1092
14 **Mezzetti M**, Raveglia F, Panigalli T, Giuliani L, Lo Giudice F, Meda S, Conforti S. Assessment of outcomes in typical and atypical carcinoids according to latest WHO classification. *Ann Thorac Surg* 2003; **76**: 1838-1842
15 **Oberg K**, Jelic S. Neuroendocrine gastroenteropancreatic tumors: ESMO clinical recommendation for diagnosis, treatment and follow-up. *Ann Oncol* 2009; **20** Suppl 4: 150-153
16 **Rindi G**, Klöppel G, Alhman H, Caplin M, Couvelard A, de Herder WW, Erikssson B, Falchetti A, Falconi M, Komminoth P, Körner M, Lopes JM, McNicol AM, Nilsson O, Perren A, Scarpa A, Scoazec JY, Wiedenmann B. TNM staging of foregut (neuro)endocrine tumors: a consensus proposal including a grading system. *Virchows Arch* 2006; **449**: 395-401
17 **Rindi G**, Klöppel G, Couvelard A, Komminoth P, Körner M, Lopes JM, McNicol AM, Nilsson O, Perren A, Scarpa A, Scoazec JY, Wiedenmann B. TNM staging of midgut and hindgut (neuro) endocrine tumors: a consensus proposal including a grading system. *Virchows Arch* 2007; **451**: 757-762
18 **Pape UF**, Jann H, Müller-Nordhorn J, Bockelbrink A, Berndt U, Willich SN, Koch M, Röcken C, Rindi G, Wiedenmann B. Prognostic relevance of a novel TNM classification system for upper gastroenteropancreatic neuroendocrine tumors. *Cancer* 2008; **113**: 256-265
19 **Rockall AG**, Reznek RH. Imaging of neuroendocrine tumours (CT/MR/US). *Best Pract Res Clin Endocrinol Metab* 2007; **21**: 43-68
20 **McAuley G**, Delaney H, Colville J, Lyburn I, Worsley D, Govender P, Torreggiani WC. Multimodality preoperative imaging of pancreatic insulinomas. *Clin Radiol* 2005; **60**: 1039-1050
21 **Rösch T**, Lightdale CJ, Botet JF, Boyce GA, Sivak MV Jr, Yasuda K, Heyder N, Palazzo L, Dancygier H, Schusdziarra V. Localization of pancreatic endocrine tumors by endoscopic ultrasonography. *N Engl J Med* 1992; **326**: 1721-1726
22 **Noone TC**, Hosey J, Firat Z, Semelka RC. Imaging and localization of islet-cell tumours of the pancreas on CT and

MRI. *Best Pract Res Clin Endocrinol Metab* 2005; **19**: 195-211
23 **Sheth S**, Hruban RK, Fishman EK. Helical CT of islet cell tumors of the pancreas: typical and atypical manifestations. *AJR Am J Roentgenol* 2002; **179**: 725-730
24 **Power N**, Reznek RH. Imaging pancreatic islet cell tumours. *Imaging* 2002; **14**: 147-159
25 **Balci NC**, Semelka RC. Radiologic features of cystic, endocrine and other pancreatic neoplasms. *Eur J Radiol* 2001; **38**: 113-119
26 **Binstock AJ**, Johnson CD, Stephens DH, Lloyd RV, Fletcher JG. Carcinoid tumors of the stomach: a clinical and radiographic study. *AJR Am J Roentgenol* 2001; **176**: 947-951
27 **Woodard PK**, Feldman JM, Paine SS, Baker ME. Midgut carcinoid tumors: CT findings and biochemical profiles. *J Comput Assist Tomogr* 1995; **19**: 400-405
28 **Gouya H**, Vignaux O, Augui J, Dousset B, Palazzo L, Louvel A, Chaussade S, Legmann P. CT, endoscopic sonography, and a combined protocol for preoperative evaluation of pancreatic insulinomas. *AJR Am J Roentgenol* 2003; **181**: 987-992
29 **Paulson EK**, McDermott VG, Keogan MT, DeLong DM, Frederick MG, Nelson RC. Carcinoid metastases to the liver: role of triple-phase helical CT. *Radiology* 1998; **206**: 143-150
30 **Gibril F**, Doppman JL, Reynolds JC, Chen CC, Sutliff VE, Yu F, Serrano J, Venzon DJ, Jensen RT. Bone metastases in patients with gastrinomas: a prospective study of bone scanning, somatostatin receptor scanning, and magnetic resonance image in their detection, frequency, location, and effect of their detection on management. *J Clin Oncol* 1998; **16**: 1040-1053
31 **Pisegna JR**, Doppman JL, Norton JA, Metz DC, Jensen RT. Prospective comparative study of ability of MR imaging and other imaging modalities to localize tumors in patients with Zollinger-Ellison syndrome. *Dig Dis Sci* 1993; **38**: 1318-1328
32 **Ichikawa T**, Peterson MS, Federle MP, Baron RL, Haradome H, Kawamori Y, Nawano S, Araki T. Islet cell tumor of the pancreas: biphasic CT versus MR imaging in tumor detection. *Radiology* 2000; **216**: 163-171
33 **Herwick S**, Miller FH, Keppke AL. MRI of islet cell tumors of the pancreas. *AJR Am J Roentgenol* 2006; **187**: W472-W480
34 **Owen NJ**, Sohaib SA, Peppercorn PD, Monson JP, Grossman AB, Besser GM, Reznek RH. MRI of pancreatic neuroendocrine tumours. *Br J Radiol* 2001; **74**: 968-973
35 **Semelka RC**, Custodio CM, Cem Balci N, Woosley JT. Neuroendocrine tumors of the pancreas: spectrum of appearances on MRI. *J Magn Reson Imaging* 2000; **11**: 141-148
36 **Bader TR**, Semelka RC, Chiu VC, Armao DM, Woosley JT. MRI of carcinoid tumors: spectrum of appearances in the gastrointestinal tract and liver. *J Magn Reson Imaging* 2001; **14**: 261-269
37 **Debray MP**, Geoffroy O, Laissy JP, Lebtahi R, Silbermann-Hoffman O, Henry-Feugeas MC, Cadiot G, Mignon M, Schouman-Claeys E. Imaging appearances of metastases from neuroendocrine tumours of the pancreas. *Br J Radiol* 2001; **74**: 1065-1070
38 **Dromain C**, de Baere T, Baudin E, Galline J, Ducreux M, Boige V, Duvillard P, Laplanche A, Caillet H, Lasser P, Schlumberger M, Sigal R. MR imaging of hepatic metastases caused by neuroendocrine tumors: comparing four techniques. *AJR Am J Roentgenol* 2003; **180**: 121-128
39 **Vossen JA**, Buijs M, Liapi E, Eng J, Bluemke DA, Kamel IR. Receiver operating characteristic analysis of diffusion-weighted magnetic resonance imaging in differentiating hepatic hemangioma from other hypervascular liver lesions. *J Comput Assist Tomogr* 2008; **32**: 750-756
40 **Liapi E**, Geschwind JF, Vossen JA, Buijs M, Georgiades CS, Bluemke DA, Kamel IR. Functional MRI evaluation of tumor response in patients with neuroendocrine hepatic metastasis treated with transcatheter arterial chemoembolization. *AJR Am J Roentgenol* 2008; **190**: 67-73
41 **Lee SS**, Byun JH, Park BJ, Park SH, Kim N, Park B, Kim JK, Lee MG. Quantitative analysis of diffusion-weighted magnetic resonance imaging of the pancreas: usefulness in characterizing solid pancreatic masses. *J Magn Reson Imaging* 2008; **28**: 928-936
42 **Anaye A**, Mathieu A, Closset J, Bali MA, Metens T, Matos C. Successful preoperative localization of a small pancreatic insulinoma by diffusion-weighted MRI. *JOP* 2009; **10**: 528-531
43 **Katzenellenbogen BS**, Fang H, Ince BA, Pakdel F, Reese JC, Wooge CH, Wrenn CK. William L. McGuire Memorial Symposium. Estrogen receptors: ligand discrimination and antiestrogen action. *Breast Cancer Res Treat* 1993; **27**: 17-26
44 **Mankoff DA**, Link JM, Linden HM, Sundararajan L, Krohn KA. Tumor receptor imaging. *J Nucl Med* 2008; **49** Suppl 2: 149S-163S
45 **Ricke J**, Klose KJ, Mignon M, Oberg K, Wiedenmann B. Standardisation of imaging in neuroendocrine tumours: results of a European delphi process. *Eur J Radiol* 2001; **37**: 8-17
46 **Mundschenk J**, Unger N, Schulz S, Höllt V, Schulz S, Steinke R, Lehnert H. Somatostatin receptor subtypes in human pheochromocytoma: subcellular expression pattern and functional relevance for octreotide scintigraphy. *J Clin Endocrinol Metab* 2003; **88**: 5150-5157
47 **Taniyama Y**, Suzuki T, Mikami Y, Moriya T, Satomi S, Sasano H. Systemic distribution of somatostatin receptor subtypes in human: an immunohistochemical study. *Endocr J* 2005; **52**: 605-611
48 **Bakker WH**, Krenning EP, Reubi JC, Breeman WA, Setyono-Han B, de Jong M, Kooij PP, Bruns C, van Hagen PM, Marbach P. In vivo application of [111In-DTPA-D-Phe1]-octreotide for detection of somatostatin receptor-positive tumors in rats. *Life Sci* 1991; **49**: 1593-601
49 **Bakker WH**, Albert R, Bruns C, Breeman WA, Hofland LJ, Marbach P, Pless J, Pralet D, Stolz B, Koper JW. [111In-DTPA-D-Phe1]-octreotide, a potential radiopharmaceutical for imaging of somatostatin receptor-positive tumors: synthesis, radiolabeling and in vitro validation. *Life Sci* 1991; **49**: 1583-1591
50 **Krenning EP**, Bakker WH, Kooij PP, Breeman WA, Oei HY, de Jong M, Reubi JC, Visser TJ, Bruns C, Kwekkeboom DJ. Somatostatin receptor scintigraphy with indium-111-DTPA-D-Phe-1-octreotide in man: metabolism, dosimetry and comparison with iodine-123-Tyr-3-octreotide. *J Nucl Med* 1992; **33**: 652-658
51 Carcinoid tumors, carcinoid syndrome, and related disorders. Williams textbook of endocrinology. 10th ed. Philadelphia, Pa: Saunders, 2003: 661-690
52 **Kälkner KM**, Janson ET, Nilsson S, Carlsson S, Oberg K, Westlin JE. Somatostatin receptor scintigraphy in patients with carcinoid tumors: comparison between radioligand uptake and tumor markers. *Cancer Res* 1995; **55**: 5801s-5804s
53 **Kwekkeboom DJ,** Krenning EP, Bakker WH, Oei HY, Kooij PP, Lamberts SW. Somatostatin analogue scintigraphy in carcinoid tumours. *Eur J Nucl Med* 1993; **20**: 283-292
54 **Westlin JE**, Janson ET, Arnberg H, Ahlström H, Oberg K, Nilsson S. Somatostatin receptor scintigraphy of carcinoid tumours using the [111In-DTPA-D-Phe1]-octreotide. *Acta Oncol* 1993; **32**: 783-786
55 **Gibril F**, Reynolds JC, Chen CC, Yu F, Goebel SU, Serrano J, Doppman JL, Jensen RT. Specificity of somatostatin receptor scintigraphy: a prospective study and effects of false-positive localizations on management in patients with gastrinomas. *J Nucl Med* 1999; **40**: 539-553
56 **Hofmann M**, Maecke H, Börner R, Weckesser E, Schöffski P, Oei L, Schumacher J, Henze M, Heppeler A, Meyer J, Knapp H. Biokinetics and imaging with the somatostatin receptor PET radioligand (68)Ga-DOTATOC: preliminary data. *Eur J Nucl Med* 2001; **28**: 1751-1757
57 **Kowalski J**, Henze M, Schuhmacher J, Mäcke HR, Hofmann M, Haberkorn U. Evaluation of Positron Emission Tomography Imaging Using [68Ga]-DOTA-D Phe1-Tyr3-Octreotide in Comparison to [111In]-DTPAOC SPECT. First Results in

Patients with Neuroendocrine Tumors. *Mol Imaging Biol* 2003; **5**: 42-48
58 **Gabriel M**, Decristoforo C, Kendler D, Dobrozemsky G, Heute D, Uprimny C, Kovacs P, Von Guggenberg E, Bale R, Virgolini IJ. 68Ga-DOTA-Tyr3-octreotide PET in neuroendocrine tumors: comparison with somatostatin receptor scintigraphy and CT. *J Nucl Med* 2007; **48**: 508-518
59 **Putzer D**, Gabriel M, Henninger B, Kendler D, Uprimny C, Dobrozemsky G, Decristoforo C, Bale RJ, Jaschke W, Virgolini IJ. Bone metastases in patients with neuroendocrine tumor: 68Ga-DOTA-Tyr3-octreotide PET in comparison to CT and bone scintigraphy. *J Nucl Med* 2009; **50**: 1214-1221
60 **Ambrosini V**, Campana D, Bodei L, Nanni C, Castellucci P, Allegri V, Montini GC, Tomassetti P, Paganelli G, Fanti S. 68Ga-DOTANOC PET/CT clinical impact in patients with neuroendocrine tumors. *J Nucl Med* 2010; **51**: 669-673
61 **Gabriel M**, Oberauer A, Dobrozemsky G, Decristoforo C, Putzer D, Kendler D, Uprimny C, Kovacs P, Bale R, Virgolini IJ. 68Ga-DOTA-Tyr3-octreotide PET for assessing response to somatostatin-receptor-mediated radionuclide therapy. *J Nucl Med* 2009; **50**: 1427-1434
62 **Modlin IM**, Oberg K, Chung DC, Jensen RT, de Herder WW, Thakker RV, Caplin M, Delle Fave G, Kaltsas GA, Krenning EP, Moss SF, Nilsson O, Rindi G, Salazar R, Ruszniewski P, Sundin A. Gastroenteropancreatic neuroendocrine tumours. *Lancet Oncol* 2008; **9**: 61-72
63 **Gambhir SS**, Czernin J, Schwimmer J, Silverman DH, Coleman RE, Phelps ME. A tabulated summary of the FDG PET literature. *J Nucl Med* 2001; **42**: 1S-93S
64 **Pauwels EK**, Sturm EJ, Bombardieri E, Cleton FJ, Stokkel MP. Positron-emission tomography with [18F]fluorodeoxyglucose. Part I. Biochemical uptake mechanism and its implication for clinical studies. *J Cancer Res Clin Oncol* 2000; **126**: 549-559
65 **Zhao S**, Kuge Y, Mochizuki T, Takahashi T, Nakada K, Sato M, Takei T, Tamaki N. Biologic correlates of intratumoral heterogeneity in 18F-FDG distribution with regional expression of glucose transporters and hexokinase-II in experimental tumor. *J Nucl Med* 2005; **46**: 675-682
66 **Bos R**, van Der Hoeven JJ, van Der Wall E, van Der Groep P, van Diest PJ, Comans EF, Joshi U, Semenza GL, Hoekstra OS, Lammertsma AA, Molthoff CF. Biologic correlates of (18)fluorodeoxyglucose uptake in human breast cancer measured by positron emission tomography. *J Clin Oncol* 2002; **20**: 379-387
67 **Gillies RJ**, Robey I, Gatenby RA. Causes and consequences of increased glucose metabolism of cancers. *J Nucl Med* 2008; **49** Suppl 2: 24S-42S
68 **Adams S**, Baum R, Rink T, Schumm-Dräger PM, Usadel KH, Hör G. Limited value of fluorine-18 fluorodeoxyglucose positron emission tomography for the imaging of neuroendocrine tumours. *Eur J Nucl Med* 1998; **25**: 79-83
69 **Pasquali C**, Rubello D, Sperti C, Gasparoni P, Liessi G, Chierichetti F, Ferlin G, Pedrazzoli S. Neuroendocrine tumor imaging: can 18F-fluorodeoxyglucose positron emission tomography detect tumors with poor prognosis and aggressive behavior? *World J Surg* 1998; **22**: 588-592
70 **Garin E**, Le Jeune F, Devillers A, Cuggia M, de Lajarte-Thirouard AS, Bouriel C, Boucher E, Raoul JL. Predictive value of 18F-FDG PET and somatostatin receptor scintigraphy in patients with metastatic endocrine tumors. *J Nucl Med* 2009; **50**: 858-864
71 **Krenning EP**, Valkema R, Kwekkeboom DJ, de Herder WW, van Eijck CH, de Jong M, Pauwels S, Reubi JC. Molecular imaging as in vivo molecular pathology for gastroenteropancreatic neuroendocrine tumors: implications for follow-up after therapy. *J Nucl Med* 2005; **46** Suppl 1: 76S-82S
72 **Pearse AG**. The cytochemistry and ultrastructural of polypeptide hormone producing cells of the APUD series and the embryogenic, physiologic and pathologic implications of the concept. *J Histochem Cytochem* 1969; **17**: 303-313
73 **Becherer A**, Szabó M, Karanikas G, Wunderbaldinger P, Angelberger P, Raderer M, Kurtaran A, Dudczak R, Kletter K. Imaging of advanced neuroendocrine tumors with (18)F-FDOPA PET. *J Nucl Med* 2004; **45**: 1161-1167
74 **Koopmans KP**, de Vries EG, Kema IP, Elsinga PH, Neels OC, Sluiter WJ, van der Horst-Schrivers AN, Jager PL. Staging of carcinoid tumours with 18F-DOPA PET: a prospective, diagnostic accuracy study. *Lancet Oncol* 2006; **7**: 728-734
75 **Kauhanen S**, Seppänen M, Ovaska J, Minn H, Bergman J, Korsoff P, Salmela P, Saltevo J, Sane T, Välimäki M, Nuutila P. The clinical value of [18F]fluoro-dihydroxyphenylalanine positron emission tomography in primary diagnosis, staging, and restaging of neuroendocrine tumors. *Endocr Relat Cancer* 2009; **16**: 255-265
76 **Jager PL**, Chirakal R, Marriott CJ, Brouwers AH, Koopmans KP, Gulenchyn KY. 6-L-18F-fluorodihydroxyphenylalanine PET in neuroendocrine tumors: basic aspects and emerging clinical applications. *J Nucl Med* 2008; **49**: 573-586
77 **Haug A**, Auernhammer CJ, Wängler B, Tiling R, Schmidt G, Göke B, Bartenstein P, Pöpperl G. Intraindividual comparison of 68Ga-DOTA-TATE and 18F-DOPA PET in patients with well-differentiated metastatic neuroendocrine tumours. *Eur J Nucl Med Mol Imaging* 2009; **36**: 765-770
78 **Barakat MT**, Meeran K, Bloom SR. Neuroendocrine tumours. *Endocr Relat Cancer* 2004; **11**: 1-18
79 **Mignon M**. Natural history of neuroendocrine enteropancreatic tumors. *Digestion* 2000; **62** Suppl 1: 51-58
80 **de Herder WW**, Niederle B, Scoazec JY, Pauwels S, Kloppel G, Falconi M, Kwekkeboom DJ, Oberg K, Eriksson B, Wiedenmann B, Rindi G, O'Toole D, Ferone D. Well-differentiated pancreatic tumor/carcinoma: insulinoma. *Neuroendocrinology* 2006; **84**: 183-188
81 **Falconi M**, Plockinger U, Kwekkeboom DJ, Manfredi R, Korner M, Kvols L, Pape UF, Ricke J, Goretzki PE, Wildi S, Steinmuller T, Oberg K, Scoazec JY. Well-differentiated pancreatic nonfunctioning tumors/carcinoma. *Neuroendocrinology* 2006; **84**: 196-211
82 **Pape UF**, Böhmig M, Berndt U, Tiling N, Wiedenmann B, Plöckinger U. Survival and clinical outcome of patients with neuroendocrine tumors of the gastroenteropancreatic tract in a german referral center. *Ann N Y Acad Sci* 2004; **1014**: 222-233
83 **Corleto VD**, Panzuto F, Falconi M, Cannizzaro R, Angeletti S, Moretti A, Delle Fave G, Farinati F. Digestive neuroendocrine tumours: diagnosis and treatment in Italy. A survey by the Oncology Study Section of the Italian Society of Gastroenterology (SIGE). *Dig Liver Dis* 2001; **33**: 217-221
84 **Virgolini I**, Traub-Weidinger T, Decristoforo C. Nuclear medicine in the detection and management of pancreatic islet-cell tumours. *Best Pract Res Clin Endocrinol Metab* 2005; **19**: 213-227
85 **Proye C**, Malvaux P, Pattou F, Filoche B, Godchaux JM, Maunoury V, Palazzo L, Huglo D, Lefebvre J, Paris JC. Noninvasive imaging of insulinomas and gastrinomas with endoscopic ultrasonography and somatostatin receptor scintigraphy. *Surgery* 1998; **124**: 1134-1143; discussion 1143-1144
86 **Lebtahi R**, Cadiot G, Sarda L, Daou D, Faraggi M, Petegnief Y, Mignon M, le Guludec D. Clinical impact of somatostatin receptor scintigraphy in the management of patients with neuroendocrine gastroenteropancreatic tumors. *J Nucl Med* 1997; **38**: 853-858
87 **Krenning EP**, Kwekkeboom DJ, Bakker WH, Breeman WA, Kooij PP, Oei HY, van Hagen M, Postema PT, de Jong M, Reubi JC. Somatostatin receptor scintigraphy with [111In-DTPA-D-Phe1]- and [123I-Tyr3]-octreotide: the Rotterdam experience with more than 1000 patients. *Eur J Nucl Med* 1993; **20**: 716-731
88 **Henze M**, Schuhmacher J, Dimitrakopoulou-Strauss A, Strauss LG, Mäcke HR, Eisenhut M, Haberkorn U. Exceptional increase in somatostatin receptor expression in pancreatic neuroendocrine tumour, visualised with (68)Ga-

DOTATOC PET. *Eur J Nucl Med Mol Imaging* 2004; **31**: 466
89 **Froidevaux S**, Eberle AN, Christe M, Sumanovski L, Heppeler A, Schmitt JS, Eisenwiener K, Beglinger C, Mäcke HR. Neuroendocrine tumor targeting: study of novel gallium-labeled somatostatin radiopeptides in a rat pancreatic tumor model. *Int J Cancer* 2002; **98**: 930-937
90 **Gabriel M**, Decristoforo C, Kendler D, Dobrozemsky G, Heute D, Uprimny C, Kovacs P, Von Guggenberg E, Bale R, Virgolini IJ. 68Ga-DOTA-Tyr3-octreotide PET in neuroendocrine tumors: comparison with somatostatin receptor scintigraphy and CT. *J Nucl Med* 2007; **48**: 508-518
91 **Nakamoto Y**, Higashi T, Sakahara H, Tamaki N, Itoh K, Imamura M, Konishi J. Evaluation of pancreatic islet cell tumors by fluorine-18 fluorodeoxyglucose positron emission tomography: comparison with other modalities. *Clin Nucl Med* 2000; **25**: 115-119
92 **Pasquali C**, Rubello D, Sperti C, Gasparoni P, Liessi G, Chierichetti F, Ferlin G, Pedrazzoli S. Neuroendocrine tumor imaging: can 18F-fluorodeoxyglucose positron emission tomography detect tumors with poor prognosis and aggressive behavior? *World J Surg* 1998; **22**: 588-592
93 **Eriksson B**, Orlefors H, Oberg K, Sundin A, Bergström M, Långström B. Developments in PET for the detection of endocrine tumours. *Best Pract Res Clin Endocrinol Metab* 2005; **19**: 311-324
94 **Koopmans KP**, Neels OC, Kema IP, Elsinga PH, Sluiter WJ, Vanghillewe K, Brouwers AH, Jager PL, de Vries EG. Improved staging of patients with carcinoid and islet cell tumors with 18F-dihydroxy-phenyl-alanine and 11C-5-hydroxy-tryptophan positron emission tomography. *J Clin Oncol* 2008; **26**: 1489-1495
95 **Orlefors H**, Sundin A, Garske U, Juhlin C, Oberg K, Skogseid B, Langstrom B, Bergstrom M, Eriksson B. Whole-body (11)C-5-hydroxytryptophan positron emission tomography as a universal imaging technique for neuroendocrine tumors: comparison with somatostatin receptor scintigraphy and computed tomography. *J Clin Endocrinol Metab* 2005; **90**: 3392-400

S- Editor Cheng JX **L- Editor** Webster JR **E- Editor** Ma WH

World Journal of Clinical Oncology

Online Submissions: http://www.wjgnet.com/2218-4333office
wjco@wjgnet.com
doi:10.5306/wjco.v2.i1.44

World J Clin Oncol 2011 January 10; 2(1): 44-49
ISSN 2218-4333 (online)

TOPIC HIGHLIGHT

E YK Ng, PhD, PGDTHE, Associate Professor, *Series Editor*

Cancer prognosis using support vector regression in imaging modality

Xian Du, Sumeet Dua

Xian Du, Sumeet Dua, Department of Computer Science, Louisiana Tech University, Ruston, LA 71272, United States
Author contributions: Both authors contributed equally to this work.
Correspondence to: Dr. Sumeet Dua, Department of Computer Science, Louisiana Tech University, Nethken-235, Ruston, LA 71272, United States. sdua@coes.latech.edu
Telephone: +1-318-2572830 Fax: +1-318-2574922
Received: August 3, 2010 Revised: August 24, 2010
Accepted: August 31, 2010
Published online: January 10, 2011

Abstract

The proposed techniques investigate the strength of support vector regression (SVR) in cancer prognosis using imaging features. Cancer image features were extracted from patients and recorded into censored data. To employ censored data for prognosis, SVR methods are needed to be adapted to uncertain targets. The effectiveness of two principle breast features, tumor size and lymph node status, was demonstrated by the combination of sampling and feature selection methods. In sampling, breast data were stratified according to tumor size and lymph node status. Three types of feature selection methods comprised of no selection, individual feature selection, and feature subset forward selection, were employed. The prognosis results were evaluated by comparative study using the following performance metrics: concordance index (CI) and Brier score (BS). Cox regression was employed to compare the results. The support vector regression method (SVCR) performs similarly to Cox regression in three feature selection methods and better than Cox regression in non-feature selection methods measured by CI and BS. Feature selection methods can improve the performance of Cox regression measured by CI. Among all cross validation results, stratified sampling of tumor size achieves the best regression results for both feature selection and non-feature selection methods. The SVCR regression results, perform better than Cox regression when the techniques are used with either CI or BS. The best CI value in the validation results is 0.6845. The best CI value corresponds to the best BS value 0.2065, which were obtained in the combination of SVCR, individual feature selection, and stratified sampling of the number of positive lymph nodes. In addition, we also observe that SVCR performs more consistently than Cox regression in all prognosis studies. The feature selection method does not have a significant impact on the metric values, especially on CI. We conclude that the combinational methods of SVCR, feature selection, and sampling can improve cancer prognosis, but more significant features may further enhance cancer prognosis accuracy.

Key words: Breast cancer imaging; Cancer prognosis; Sampling; Support vector regression

Peer reviewer: Harun M Said, Assistant Professor, Department of Radiation Oncology, University of Wuerzburg, Josef Schneider Str.11, D-97080 Wuerzburg, Germany

Du X, Dua S. Cancer prognosis using support vector regression in imaging modality. *World J Clin Oncol* 2011; 2(1): 44-49 Available from: URL: http://www.wjgnet.com/2218-4333/full/v2/i1/44.htm DOI: http://dx.doi.org/10.5306/wjco.v2.i1.44

INTRODUCTION

Cancer causes millions of deaths every year worldwide, and the number of these deaths is constantly on the rise[1]. The World Health Organization (WHO) estimates that in 2030, 12 million people worldwide will die from cancer or cancer-related complications. This number represents a

possible 4.6 million increase from the recorded 7.4 million cancer-related deaths that occurred in 2004. Extensive research into cancer and cancer-related problems helps average people understand behavioral and environmental causes of cancer. The discovery and understanding of cancer pathology, in turn, can help people prevent, detect, and control and treat cancer. This discovery is important, as it has been shown that one-third of cancer cases can be controlled in cases where early detection, diagnosis, prognosis, and treatment occur.

Cancer prognosis is the long-term prediction of cancer susceptibility, recurrence, and survivability[2]. Early prognosis of cancer can improve the survival rate for cancer patients. Using imaging modalities, such as functional magnetic resonance imaging (fMRI), positron emission tomography (PET), and computed tomography (CT), histological information about patients can be integrated for cancer diagnosis and prognosis[3]. High throughput imaging technologies lead to a large number of features and parameters in molecular, cellular, and organic images, which can support the clinical prognosis of cancer. However, large amounts of imagery data overwhelm clinicians involved in oncological decision making. The need to analyze and understand these large amounts of data have led to the development of computational statistical machine learning and data mining methods for oncological imagery.

Breast cancer is the most frequent type of cancer, and is the leading cause of death among women (ranking first in the world and second in the USA as a cause of cancer-related deaths among women)[1,4]. Breast imaging techniques, including ultrasound, mammography, MRI, and PET, provide mechanisms to screen and diagnose breast tumors based on the geometry level (e.g. tumor and/or tissue shape) and the cell level (e.g. tumor cells)[5]. The use of *in vivo* molecular and cellular imaging of breast cancer has increased because it is advantageous for bridging breast and cellular macrofeatures. The screening and measurement of breast cancer at the molecular and cellular levels also derives from our knowledge that cancer begins in a single cell, transforming that cell from a normal state to a tumor and cloning the tumor to multiple cells, also called metastasizing. Thus, a cancer prognosis based on the processing and analysis of cell imaging is highly efficient and effective[3,6].

Imaging techniques that are entirely non-invasive cannot provide a perfect diagnosis and/or prognosis for a breast cancer case. A traditional biopsy can help clinicians examine the pathology of a breast mass perfectly, but this process causes pain for patients. For example, clinically, tumor size, lymph node status, and metastasis (TNM) are mostly employed in breast staging systems as predicative factors[7,8]. To acquire the TNM information from patients, clinicians need to measure the excised tumor and examine the presence and status of lymph nodes obtained from patients' axilla. The above invasive operations cause pain in patients' arms and can further cause infections. Hence, researchers use fine needle aspirations (FNAs) to minimize the invasiveness and enhance the imaging techniques (e.g. mammography) in breast cancer examination and prognosis. To obtain FNAs, clinicians insert a gauge needle into a breast lump and remove a small number of cell samples. Using microscopes, we can capture cell images and examine the features of cells for cancer prognosis. Thus, the prognosis procedure includes three steps: acquisition of cell images using FNAs and imaging techniques, image processing and feature extraction from cellular images, and pattern recognition and prediction using machine learning techniques. The first two steps result in a set of features for breast cancer diagnosis and prognosis. In breast cancer diagnosis, pattern recognition methods provide labels for breast features: benign or malignant. In cases where breast images are labeled malignant, machine-learning methods will be applied to predict the long-term effects of the cancer. Cancer prognosis is difficult because the censored medical data are uncertain information. Censored data are the observations recorded without the precisely known event time during follow-ups in cancer patients, e.g. the survival time of a cancer patient after the tumor was removed by surgery. Censored data include left-censored data and right-censored data. Left censored data are observations of cancer after cancer recurs. This data only include the upper bound of the cancer recurring time (the time at which the clinicians observed the recurrence). Right-censored data are observations of cancer before cancer recurs, e.g. patient dies disease-free. This data only includes the lower bound of cancer recurring time (the time at which the patient dies). Both types of censored data are incomplete and lack specificity required for clinical research. As conventional regression methods were designed to predict certain target values, new algorithms are needed to predict the censored data.

In this paper, we present a novel computational framework for cancer prognosis that uses support vector regression (SVR) and sampling algorithms. We use the publicly available dataset: Wisconsin prognostic breast cancer (WPBC)[9] to evaluate the strength of SVR for cancer prognosis. In the next section, we briefly describe the WPBC dataset. Then, we describe how the SVR method is applied for cancer prognosis. Next, we demonstrate the experimental prognosis results using various sampling methods. Finally, we conclude the strength and limitations of using the SVR method in cancer prognosis.

BREAST IMAGING AND CELL FEATURES

The WPBC dataset was collected from several breast cancer cases, and image features were extracted by the researchers in the University of Wisconsin[6]. The dataset largely comprises of 155 patients monitored for recurrence within 24 mo. The data comprises of 30 cytological features and 2 histological features: number of metastasized lymph nodes and tumor size. The records only included the patients who had invasive breast cancer. The images of FNA samples were acquired from the breast masses of the patients. For each image, 30 cell features were extracted to describe the cell nuclei in the image. The imaging cell features include radius, texture, perimeter, area, smoothness, compactness, concavity, concave points, symmetry, and fractal dimension (see the details in[6]).

Three descriptors of each feature were recorded for each image in the WPBC dataset: mean, standard deviation, and largest value of the feature. As tumor size, lymph node status, and metastasis (TNM) are clinically employed in breast staging systems as predicative factors[8], tumor size and lymph node status were also collected in measurements of centimeters and number of positive axillary lymph nodes, respectively. There are 198 instances: 151 censored (nonrecurring) instances and 47 recurring instances. For the recurring cases, the recurrence time (left-censored data) was recorded, and for the censored instances, the disease-free time (right-censored data) was recorded. The censored data make the prognosis challenging because of its uncertainty.

In the next section, we review support vector machines (SVM) and SVR methods, and explain the above challenge in depth.

SVM AND SVR

SVM is a machine-learning method that uses support vectors, instead of modeling structures, (e.g. multilayer preceptor), to map inputs to outputs. SVM was introduced by Vapnik[10] as a classification and prediction method. SVM can be applied for both regression and classification. Given a dataset (x_i,y_i), where x_i represents data points using vectors and y_i denotes label of the vector x_i(e.g. $y_i \varepsilon \{-1, +1\}$), SVM algorithms can be applied to classify the data points with the hyperplane that has the maximum distance to the nearest data points on each side.

SVR incorporates the concepts of ε-threshold area and loss function into support vector machines to approximate the state value of a given system using feature vectors. In SVR[11], y_i denotes the obtained target value of vector x_i, and $f(x_i)$ denotes the predicted target value of vector x_i. The central motivation for using SVR is to seek the small or flat ε-neighborhood that describes most data points and to panelize the data points that fall outside of ε-neighborhood. As shown in Figure 1A, the data points that fall into ε-insensitive area will have zero-loss and the data points outside of ε neighborhood will have a loss defined by slack variables ξ or ξ*. The slack variables can be defined as a loss function. For example, the ε-insensitive linear loss function is most employed as follows (as shown in Figure 1A):

$$|\zeta| = \begin{cases} 0 & when\ |\zeta| \le \varepsilon \\ |\zeta| & otherwise \end{cases}$$

Thus, a linear SVR can be formulated formally in the following:

$$\min \ \frac{1}{2}\|w\|^2 + C\sum_{i=1}^{l}(\zeta_i + \zeta_i^*)$$

$$s.t. \begin{cases} y_i - \boldsymbol{w}^T \boldsymbol{x}_i - b \le \varepsilon + \zeta_i \\ \boldsymbol{w}^T \boldsymbol{x}_i + b - y_i \le \varepsilon + \zeta_i^* \\ \zeta_i, \zeta_i^* \ge 0 \end{cases} \quad (1)$$

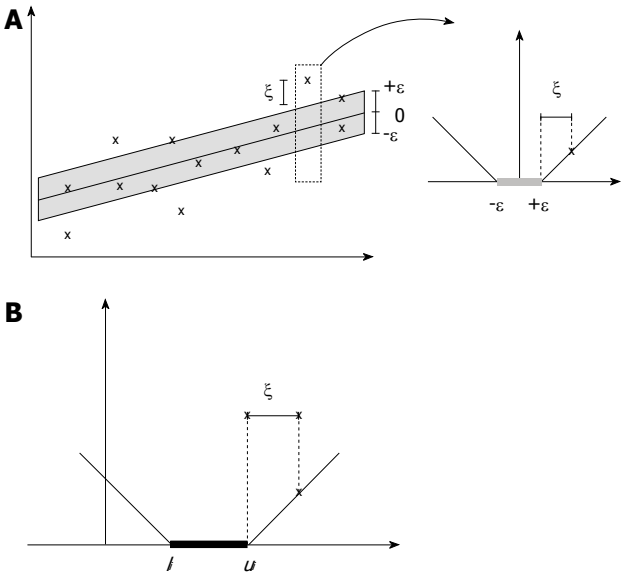

Figure 1 ε-insensitive linear loss function (A) and the linear loss function in support vector regression method (B).

Where, C is a positive constant that determines the trade-off between the flatness of function and the amount up to which deviations larger than the threshold ε are tolerated.

Using Lagrangian multipliers $a_i \geqslant 0$ and $a_i^* \geqslant 0$ for the constraints in Equation, and taking derivatives with respect to primal variables, the optimal solution to the above regression formulation is:

$$f(\boldsymbol{x}) = \sum_{i=1}^{l}(\alpha_i - \alpha_i^*)\langle \boldsymbol{x}, \boldsymbol{x}_i \rangle + b \quad (2)$$

$$\boldsymbol{w} = \sum_{i=1}^{l}(\alpha_i - \alpha_i^*)\boldsymbol{x}_i \quad (3)$$

The traditional SVR method has been employed successfully for event prediction because of its robustness and accuracy. However, we can only find few applications using SVR for medical and cancer prognosis, because traditional SVR methods require that the training data have certain target values, while clinicians can only provide uncertain censored target values, e.g. interval target values. Shivaswamy *et al*[12] proposed a SVR method, called SVCR, to approximate the target values for censored data[12]. We apply the SVCR method in the project. We summarize the SVCR algorithm in the next section.

SVR FOR CENSORED DATA

The SVCR algorithm solves the censored data problem by adapting the loss function to interval values in censored data. Given the interval bounds: lower bound l_i, $_i = 1,\ldots n$, and upper bound u_i for each censored data (x_i,l_i,u_i), the loss function is defined as:

$$c(f(x_i), l_i, u_i) = \max(l_i - f(x_i), f(x_i) - u_i) \quad (4)$$

As illustrated in Figure 1B, the modified loss function in SVCR follows the theory that when the predicted value $f(x_i)$ falls into the interval (l_i,u_i), no penalization is applied in the loss function. Then, the SVR for censored data is formulated as follows:

$$\min \ \frac{1}{2}\|w\|^2 + C\left(\sum_{i\in U}\zeta_i + \sum_{i\in L}\zeta_i^*\right)$$
$$s.t. \begin{cases} \boldsymbol{w}^T\boldsymbol{x}_i + b \geq l_i + \zeta_i, \forall i \in L; \\ \boldsymbol{w}^T\boldsymbol{x}_i + b \leq u_i + \zeta_i^*, \forall i \in U; \\ \zeta_i, \zeta_i^* \geq 0. \end{cases} \quad (5)$$

In the above, U includes the indices of the data points that have a finite right upper bound, and L includes the indices of the data points that have finite left lower bound. Using Lagrangian multipliers and optimization methods, the above problem can be solved by Equation.

COMPARATIVE EVALUATION

To evaluate the strength of SVRC in cancer prognosis using imaging features, we compare the regression results by combining feature selection and sampling methods. We also compare the results of SVRC with those of the conventional prognosis method: Cox regression, using the concordance index (CI) and Brier score (BS) as performance metrics. We review these methods below.

Cox regression[13] is an approach used to measure the effect of a set of features on the event outcomes, e.g. the recurrence of cancer. The Cox regression model uses a hazard function to measure the decline of survival time. Using the hazard function, we can estimate the non-survival (or event) probability at a time point. Given a set of feature values $\{f_i\}$, $i = 1,\ldots,d$, and their associated decline parameters s_i for an individual, the hazard function for that individual is formulated as follows:

$$h(t) = h_0(t)\exp\left(\sum_i (s_i f_i)\right) \quad (6)$$

In the above, decline parameters s_i can be approximated using maximum likelihood estimation. We use the above function in Cox regression.

To accurately measure the performance of regression models, we need to investigate the combination of feature subsets which can generate the optimal regression result. Feature selection can be programmed in two directions: by removing the most insignificant individual features one-by-one from the feature set after ranking features according to their significance of prediction results, or by adding the most significant features one-by-one into a feature subset pool after evaluating prediction accuracy of various feature subsets. The ranking of individual features or feature subsets both require metrics, e.g. redundancy and independency. We used the algorithms and metrics proposed in[14] for the above removing or adding feature procedures: individual features are scored by *P*-value according to their pair-wise association with the events (see details in[14]).

Feature selection methods cannot guarantee a fair validation of regression models because samples may present stratified effects on the model. For example, in clinical research, breast cancer can be graded by tumor size[15]. This stratification indicates that the normal cross-validation method may not be able to generalize the breast cancer prognosis model. One solution to this problem is to randomly select the same number of instances in each grading level of the known grading features for each training dataset. This solution, in turn, evaluates the strength of a regression model at different levels of grading features.

The combination of the above feature selection, sampling, and regression methods results in a set of prognostic values for performance evaluation. Given certain target values, we can calculate prediction errors to measure the accuracy of regression algorithms. However, for cancer data, prediction errors cannot be accessed because most of the data are censored. Predication accuracy can be evaluated by measuring whether the predicted time is ahead of the target value. Researchers have proposed a variety of evaluation metrics to measure the prediction accuracy of methods that use censored data, e.g. CI[16] and BS[17].

The CI is a generalization of the area under the ROC curve. The CI measures the concordance between predicted and observed events. When the predicted probability of events p_t is bigger than the actual occurrence of the events q_t at time t, we say that the prediction result is concordant with the actual event. Hence, the paired comparison between all samples in the given dataset results in the percentage of correct predicted concordances among all sample pairs. In particular, $CI = 1$, $CI = 0.5$ and $CI = 0$ denote the perfect prediction, random prediction, and all-fail prediction, respectively.

BS is a metric function that measures the difference between the predicted probability of events p_t and the occurrence of events q_t at time t. Using the notions above, the BS is formulated as follows for T predicted results:

$$BS = \frac{1}{T}\sum_{t=1}^{T}(p_t - q_t)^2 \quad (7)$$

EXPERIMENTAL RESULTS

In the experiment, we aim to evaluate the power of the SVCR method for cancer prognosis using CI and BS. We evaluate cancer prognosis using the following sampling methods: cross validation of all data, stratified sampling of data for tumor size, and lymph node status. We choose 4-fold cross validation for all experiments and sort the data by their increasing tumor size (noted in centimeters), divide them in bins, and then select the same number of random samples from each bin. It is generally accepted that bigger tumors indicate more cancer complexity. We divide the data into three groups according to tumor size: $\leqslant$ 2 cm; 2 cm < but $\leqslant$ 5 cm; 5 cm <.

As inflammation and number of lymph nodes are related to breast cancer complexity[15,18], we perform stratified sampling, as above, for the lymph node status

Table 1 Cross validation results for three feature selection methods using 32 features and 194 instances

	SVCR			Cox regression		
	IS	FFS	NS	IS	FFS	NS
CI	0.6316	0.6333	0.6321	0.6623	0.6333	0.5677
BS	0.2770	0.3609	0.2675	0.2487	0.3319	0.2294

IS: Individual feature selection; FFS: Forward feature selection; NS: Non-feature selection; SVCR: Support vector regression method.

Table 2 Cross validation results for three feature selection methods and without lymph nodes status (32 features) and 198 instances

	SVCR			Cox regression		
	IS	FFS	NS	IS	FFS	NS
CI	0.6532	0.6733	0.6579	0.6465	0.6733	0.5981
BS	0.1969	0.3468	0.2109	0.2504	0.4975	0.3321

IS: Individual feature selection; FFS: Forward feature selection; NS: Non-feature selection; SVCR: Support vector regression method.

as well. We divide the data into three groups according to the number of positive lymph nodes observed in surgery: ⩽ 2 cm; 2 cm < but ⩽ 5 cm; 5 cm <.

As shown in Tables 1-4 we demonstrate the performance of various combinational methods. The results shown in Table 1 are obtained after we delete the four instances that have unknown feature values and use all 32 imaging features for feature selection. We find that SVCR performs consistently in three feature selection methods and performs better than Cox regression in the non-feature selection method by measuring the CI values. This result follows those of Khan *et al*[19], who obtained test results for the same dataset using Cox and their proposed SVRC algorithm respectively: 0.6031 and 0.6963. They did not describe the feature selection or sampling algorithms in the report[19]. The results shown in Table 1 demonstrate that feature selection methods can improve the performance of Cox regression measured by CI and BS. As shown in Tables 1-4, seven of eight Cox regression results using feature selection perform better than the reported Cox regression result[19]. These results demonstrate that stratified sampling of the number of positive lymph nodes can achieve the best regression results using feature selection methods. This phenomenon corresponds to the conclusion that lymph node status can improve the accuracy of breast cancer prognosis using imaging features, especially when used in correlation with the SVCR method. As shown in Tables 2-4, SVCR regression performs better than Cox regression measured by CI and BS. The best CI value in all validation results is 0.6845, which is almost the same as the 0.6963 using the patented method, SVRC, which was reported in[19]. The above best CI value corresponds to the best BS value 0.2065. In addition, we also observe that SVCR performs more robustly than Cox regression in all prognosis studies.

Table 3 Cross validation results for three feature selection methods and stratified sampling with respect to tumor size and 194 instances

	SVCR			Cox regression		
	IS	FFS	NS	IS	FFS	NS
CI	0.6390	0.6021	0.6246	0.6244	0.6021	0.5867
BS	0.2904	0.3149	0.3377	0.2588	0.4424	0.3390

IS: Individual feature selection; FFS: Forward feature selection; NS: Non-feature selection; SVCR: Support vector regression method.

Table 4 Cross validation results for three feature selection methods and stratified sampling with respect to lymph nodes status and 194 instances

	SVCR			Cox regression		
	IS	FFS	NS	IS	FFS	NS
CI	0.6845	0.6769	0.6572	0.6341	0.6769	0.6145
BS	0.2065	0.3311	0.2643	0.2147	0.3400	0.3273

IS: Individual feature selection; FFS: Forward feature selection; NS: Non-feature selection; SVCR: Support vector regression method.

The metric values, especially CI, remain consistent regardless of the feature selection method used in the three sampling data sets.

CONCLUSION

We conclude that the combinational methods of SVCR, feature selection, and sampling can improve cancer prognosis for the following reasons: First, SVCR performs better than Cox regression for cancer prognosis, measured by CI and BS, particularly when accompanied by feature selection and stratified sampling. Second, feature selection and stratified sampling can improve the accuracy of the SVCR regression results by introducing expert knowledge, such as tumor size and lymph node status. Third, SVCR performs more robustly when used in conjunction with feature selection for cancer prognosis than sampling algorithms do. This conclusion indicates that SVCR inherits the robustness of SVR algorithms. Fourth, we discover that using the current regression model and cancer cell image features, even accompanied by the FNA features and expert knowledge, the prognosis accuracy is lower than the accuracy of traditional biopsies. The discovery of more significant cancer cell image features may improve prognosis accuracy. Lastly, more accurate regression methods are needed for considering the censored data in cancer prognosis.

REFERENCES

1 **WHO Cancer Fact Sheet**. World Health Organization (WHO), 2009: 297
2 **Cruz JA**, Wishart DS. Applications of machine learning in cancer prediction and prognosis. *Cancer Inform* 2007; **2**: 59-77
3 **Fass L**. Imaging and cancer: a review. *Mol Oncol* 2008; **2**:

115-152
4 Cancer Facts & Figures 2010. American Cancer Society 2010. Available from: URL: http://www.cancer.org/
5 **Mankoff D**. Imaging in breast cancer - breast cancer imaging revisited. *Breast Cancer Res* 2005; **7**: 276-278
6 **Street WN**, Wolberg WH, Mangasarian OL. Nuclear feature extraction for breast tumor diagnosis. IS&t/SPIE International Symposium on Electronic Imaging. *Sci Technol* 1995; **1995**: 861-870
7 **Black MM**, Opler SR, Speer FD. Survival in breast cancer cases in relation to the structure of the primary tumor and regional lymph nodes. *Surg Gynecol Obstet* 1955; **100**: 543-551
8 **Basilion JP**. Current and future technologies for breast cancer imaging. *Breast Cancer Res* 2001; **3**: 14-16
9 **Mangasarian OL**, Street WN, Wolberg WH. Breast Cancer Diagnosis and Prognosis Via Linear Programming. *Operat Res* 1995; **43**: 570-577
10 **Vapnik V**. Estimation of dependences based on empirical data. New York: Springer Verlag, 1982
11 **Smola AJ**, Schölkopf B. A tutorial on support vector regression. *Stat Comput* 2004; **3**: 199-222
12 **Shivaswamy PK**, Chu W, Jansche M. A support vector approach to censored targets. The 7th IEEE International Conference on Data Mining, 2007: 655-660
13 **Cox DR**. Regression models and life-tables. *J R Stat Soc* 1972; **34**: 187-220
14 **Bøvelstad HM**, Nygård S, Størvold HL, Aldrin M, Borgan Ø, Frigessi A, Lingjaerde OC. Predicting survival from microarray data--a comparative study. *Bioinformatics* 2007; **23**: 2080-2087
15 **Singletary SE**, Allred C, Ashley P, Bassett LW, Berry D, Bland KI, Borgen PI, Clark G, Edge SB, Hayes DF, Hughes LL, Hutter RV, Morrow M, Page DL, Recht A, Theriault RL, Thor A, Weaver DL, Wieand HS, Greene FL. Revision of the American Joint Committee on Cancer staging system for breast cancer. *J Clin Oncol* 2002; **20**: 3628-3636
16 **Harrel FE**. Regression modeling strategies, with applications to linear models, logistic regression, and survival analysis. New York, NY: Springer, 2001
17 **Graf E**, Schmoor C, Sauerbrei W, Schumacher M. Assessment and comparison of prognostic classification schemes for survival data. *Stat Med* 1999; **18**: 2529-2545
18 **Crump M**, Goss PE, Prince M, Girouard C. Outcome of extensive evaluation before adjuvant therapy in women with breast cancer and 10 or more positive axillary lymph nodes. *J Clin Oncol* 1996; **14**: 66-69
19 **Khan FM**, Zubek VB. Support vector regression for censored data (svrc): a novel tool for survival analysis. Data Mining, 2008. ICDM '08. Eighth IEEE International Conference on, 2008: 863-868

S- Editor Cheng JX **L- Editor** Webster JR **E- Editor** Ma WH

World Journal of Clinical Oncology

Online Submissions: http://www.wjgnet.com/2218-4333office
wjco@wjgnet.com
doi:10.5306/wjco.v2.i1.50

World J Clin Oncol 2011 January 10; 2(1): 50-63
ISSN 2218-4333 (online)

TOPIC HIGHLIGHT

E YK Ng, PhD, PGDTHE, Associate Professor, *Series Editor*

Role of optical spectroscopy using endogenous contrasts in clinical cancer diagnosis

Quan Liu

Quan Liu, Division of Bioengineering, School of Chemical and Biomedical Engineering, Nanyang Technological University, N1.3-B2-06, 70 Nanyang Drive, Singapore 637457, Singapore
Author contributions: Liu Q wrote this review alone.
Correspondence to: Quan Liu, PhD, Division of Bioengineering, School of Chemical and Biomedical Engineering, Nanyang Technological University, N1.3-B2-06, 70 Nanyang Drive, Singapore 637457, Singapore. quanliu@ntu.edu.sg
Telephone: +65-65138298 Fax: +65-67911761
Received: August 6, 2010 Revised: October 17, 2010
Accepted: October 24, 2010
Published online: January 10, 2011

Abstract

Optical spectroscopy has been intensively studied for cancer management in the past two decades. This review paper first introduces the background of optical spectroscopy for cancer management, which includes the advantages of optical techniques compared to other established techniques, the principle of optical spectroscopy and the typical setup of instrumentation. Then the recent progress in optical spectroscopy for cancer diagnosis in the following organs is reviewed: the brain, breast, cervix, lung, stomach, colon, prostate and the skin. Reviewed papers were selected from the PubMed database with keywords combining the terms of individual optical spectroscopy techniques and cancers. The primary focus is on the *in vivo* applications of optical spectroscopy in clinical studies. *Ex vivo* studies are also included for some organs to highlight special applications or when there are few *in vivo* results in the literature. Practical considerations of applying optical spectroscopy in clinical settings such as the speed, cost, complexity of operation, accuracy and clinical value are discussed. A few commercially available clinical instruments that are based on optical spectroscopy techniques are presented. Finally several technical challenges and standard issues are discussed and firm conclusions are made.

Key words: Cancer diagnosis; Clinical oncology; Endogenous contrasts; Optical spectroscopy

Peer reviewers: William Andrew Yeudall, BDS, PhD, Associate Professor, VCU Philips Institute of Oral and Craniofacial Molecular Biology, Virginia Commonwealth University School of Dentistry, 521 N 11th St, Richmond, VA 23298-0566, United States; Murielle Mimeault, PhD, Department of Biochemistry and Molecular Biology, College of Medicine, Eppley Cancer Institute, 7052 DRC, University of Nebraska Medical Center, 985870 Nebraska Medical Center, Omaha, NE 68198-5870, United States

Liu Q. Role of optical spectroscopy using endogenous contrasts in clinical cancer diagnosis. *World J Clin Oncol* 2011; 2(1): 50-63 Available from: URL: http://www.wjgnet.com/2218-4333/full/v2/i1/50.htm DOI: http://dx.doi.org/10.5306/wjco.v2.i1.50

INTRODUCTION

Optical spectroscopy for cancer diagnosis has been a hot research area over the past two decades. This paper will review several popular optical spectroscopy techniques including diffuse reflectance spectroscopy, fluorescence spectroscopy and Raman spectroscopy, which are based on interrogating endogenous optical contrasts in tissues. Several other promising optical spectroscopy techniques such as light scattering spectroscopy[1], coherent backscattering spectroscopy[2], and low coherence spectroscopy[3], are not included because they are relatively less studied in clinical applications. Reviewed papers were selected from the PubMed database with keywords combining the terms of individual optical spectroscopy techniques and cancers.

This paper first introduces the background of optical spectroscopy for cancer management, which includes the advantages of optical spectroscopy techniques compared to other established techniques, the principle of optical spectroscopy and the typical setup of instrumentation.

The recent progress of optical spectroscopy for cancer diagnosis in the following organs is then reviewed, which includes the brain, breast, cervix, lung, stomach, colon, prostate and the skin. The practical considerations of applying optical spectroscopy in clinical settings such as the speed, cost, complexity of operation, accuracy and clinical value are discussed, in which several commercially available clinical instruments based on optical spectroscopy techniques are also presented. Finally several technical challenges and standard issues are discussed, and the conclusions are made.

BACKGROUND IN OPTICAL SPECTROSCOPY FOR TISSUE CHARACTERIZATION

Advantages of optical techniques in clinical oncology compared to other established modalities

Optical spectroscopy and imaging techniques have emerged as promising alternative or adjunct tools to other established imaging modalities in clinical oncology such as ultrasonography, X-ray computed tomography (CT) and magnetic resonance imaging (MRI) in recent years. Tremendous growth has been achieved in the past three decades. Compared to these established imaging modalities, optical techniques possess several unique advantages that make them particularly attractive in clinical cancer management.

First, optical irradiation is non-ionizing, thus, does not present a health hazard even for a relatively long exposure time. Thus, optical measurements can be repeated as necessary. Second, optical measurements are sensitive to biochemical and morphological changes associated with carcinogenesis through the interaction between light and endogenous molecules in tissues. Third, technical advances in light sources and detectors have made it practical to achieve real time, or close to real time, optical measurements in many situations. Although the penetration depth of light is in general considered to be small as compared to X-ray or ultrasound, the sensing depth of optical measurements can actually be varied from a few hundred micrometers to several centimeters by tuning light wavelengths and manipulating source-detector configuration[4]. The tunable sensing depth adds extra flexibility and sensitivity for those special clinical scenarios. Last but not least, the development of fiber-optic probes and miniaturized detectors has made it feasible to incorporate optical spectroscopy into commercial endoscopy systems to reach internal organs.

Principles of optical spectroscopy for cancer diagnosis

The basis of optical spectroscopy for tissue characterization is built upon various light-tissue interactions including absorption, scattering and fluorescence. In the following paragraphs, how the three basic light-tissue interactions contribute to detected optical signals and how the optical signal can be used for cancer diagnosis will be described.

Absorption refers to the phenomenon in which a molecule absorbs excitation light photons without emitting new photons. The major light absorber in tissues is hemoglobin in the whole optical spectrum[5]. Total hemoglobin concentration reflects the degree of vascularization, which can be useful in examining angiogenesis during cancer development. The absorption spectrum of hemoglobin can change with its degree of oxygenation. Therefore, hemoglobin oxygenation is another important parameter that can affect tissue absorption in addition to total hemoglobin concentration. As hemoglobin is the oxygen carrier present in human blood, the variation in hemoglobin oxygenation could indicate the change in the balance between oxygen demand and oxygen supply in tissues. Water and lipid can absorb near-infra-red light. Previous studies have demonstrated that water and lipid contents are significantly different between normal breast tissue and breast cancer[6].

Scattering refers to the phenomenon in which a photon is deflected from the incident direction after interacting with a molecule in the tissue. There are two types of scattering in general, i.e. elastic scattering and inelastic scattering. Elastic scattering is a type of scattering that occurs without a frequency change from the incident photon to the scattered photon, which is also called Raleigh scattering. Major tissue elastic scatterers include nuclei, mitochondria and collagen fibers[7]. Elastic scattering has been shown to be effective in detecting epithelial pre-cancers[8,9] because of the changes in nuclei size, nucleus-to-cytoplasm ratio and the density of collagen fibers in cancer cells. Inelastic scattering refers to the scattering type in which a frequency change occurs. Depending on whether the frequency of scattered photons decreases or increases, inelastic scattering is called Stokes Raman scattering (frequently just Raman scattering) or anti-Stokes Raman scattering[10]. Raman scattering will be covered in this paper as the fundamental phenomenon behind Raman spectroscopy. However, anti-Stokes Raman scattering will not be touched because it is much less explored in clinical settings. Raman scatterers in tissues include cell cytoplasm, cell nucleus, fat, collagen, cholesterol-like lipid deposits and water[11].

Fluorescence refers to the emission of light that results from the return of a molecule from a singlet excited state to the ground state. Due to energy loss in the process, the emission wavelength is always longer than the excitation wavelength. The fluorophore refers to those molecules exhibiting fluorescence when illuminated by light at certain wavelengths. Fluorescence light emitted from fluorophore molecules is subject to absorption and scattering when propagating in tissues, which could induce difficulty in the interpretation of fluorescence spectra. The most extensively studied fluorophore molecules are reduced nicotinamide adenine dinucleotide (NADH) and flavin adenine dinucleotide (FAD). These two molecules are metabolic coenzymes involved in the reduction-oxidation process to produced energy for cellular activities. The fluorescence contributed by these two fluorophores has been explored to estimate redox ratios to reflect the variation in the metabolic rate of tissues[12].

Table 1 lists primary absorbers and scatterers; while Table 2[13] tabulates endogenous fluorophores and their peak excitation and emission wavelengths.

Diffuse reflectance spectroscopy measures light inten-

Table 1 Primary absorbers and scatterers present in tissues

Light-tissue interaction	Source
Absorption	Hemoglobin, β-carotene, water, lipid
(Raleigh) scattering	Nuclei, mitochondria, collagen fibers
Raman scattering	Cell cytoplasm, cell nucleus, fat, collagen, cholesterol-like lipid deposits and water

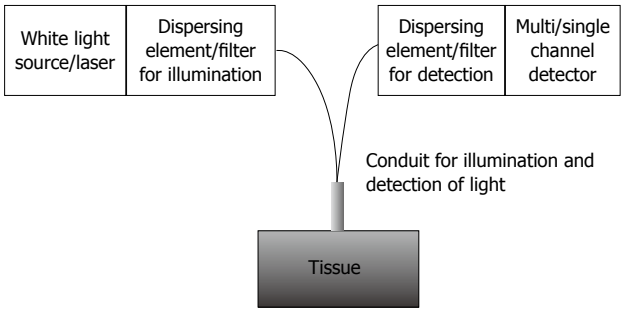

Figure 1 A general schematic of a fiber-optic system for optical spectroscopy.

sity at the excitation wavelengths. Measured diffuse reflectance spectra are sensitive to the absorption and scattering properties of tissues. Fluorescence spectroscopy measures fluorescence light intensity at the emission wavelengths that are longer than the excitation wavelength. Measured fluorescence light is subject to the effect of light absorption and scattering especially when the sensing volume is large. Raman spectroscopy measures Raman light intensity at the wavelengths longer than the excitation wavelength, but the wavelength range of detected Raman light is typically smaller than that in fluorescence spectroscopy. Detected Raman spectra are also subject to the effect of light absorption and scattering.

Instrumentation

A general schematic of a fiber-optic optical spectroscopy system for point measurements[14] is shown in Figure 1. This system consists of a light source (a white light source or laser), a dispersing element or band-pass filter for selection of illumination wavelengths, a conduit for delivery of illumination light and collection of emitted light, a dispersing element or band pass filter for selection of emission wavelengths, and a single-channel or multi-channel detector for measurement of signal intensities at the wavelengths of interest.

The fiber-optic probe is often used as the conduit for delivery of illuminating light and collection of emitted light[15]. A fiber-optic probe is usually a metal cylindrical tube with one or multiple optical fibers assembled in it. Some fibers are used for delivering light onto the tissue surface; the same fibers or other fibers depending on the probe design are used for collecting light emanating from the tissue surface.

In diffuse reflectance spectroscopy and fluorescence spectroscopy, a white light source such as xenon lamp is frequently used to provide a large range of wavelengths.

Table 2 Primary endogenous fluorophores, their peak excitation-emission wavelength pairs and location in human epithelial tissues[13]

Category of fluorophores	Endogenous fluorophores	Peak excitation-emission wavelength pair (nm)	Primary tissue location
Structural protein	Collagen	325-400	Stroma
Electron carrier	FAD	450-535	Cells
	NADH	351-460	Cells
Amino acid	Tryptophan	280-350	Proteins

FAD: Flavin adenine dinucleotide; NADH: Reduced nicotinamide adenine dinucleotide.

Various lasers can also be used when the excitation light with high power is needed. The dispersing element for illumination is typically a monochromator and sometimes there is no dispersing element which is called broadband illumination. The dispersing element for detection can be a monochromator, which is often followed by a single-channel detector such as a photomultiplier tube (PMT). Alternatively, the dispersing element can be a spectrograph, which is followed by a multi-channel detector such as a charge coupled device (CCD). This configuration enables rapid measurements of optical spectra, but frequently at the cost of lower sensitivity to light at certain wavelengths as compared to the configuration of single-channel detectors.

In Raman spectroscopy, the excitation light is typically provided by a high power laser because of weak Raman signals. A laser line filter, which transmits laser light while suppressing ambient light, is frequently used to clean excitation light. In the detection module, a long pass filter is used to remove excitation light. Then a spectrograph disperses Raman light of various wavelengths at different spatial locations, which are then mapped onto a CCD to achieve rapid measurements. The laser line filter and the long pass filter could be mounted at the tip of the illumination fibers and the detector fibers in the probe to reduce the background Raman signal from fibers.

OPTICAL SPECTROSCOPY TECHNIQUES IN CLINICAL CANCER DIAGNOSIS

While optical spectroscopy may play an important role in many aspects of clinical cancer management such as cancer screening in the breast[16,17], cervix[18,19], oral cavity[20], and treatment planning and monitoring in the brain[21], breast[22] and the prostate[23,24], emphasis will be placed on cancer diagnosis due to the following reasons: First, cancer diagnosis appears to be the most frequently cited goal in relevant publications. Second, the optical techniques developed for cancer diagnosis are in general also applicable to cancer screening and treatment planning as well as outcome evaluation.

In this literature review, the preference will be given to *in vivo* clinical studies. *Ex vivo* or *in vitro* studies are sometimes mentioned to highlight specific applications. No preclinical studies will be included. The review will be organized in terms of organ sites, which cover the brain,

breast, cervix, lung, stomach, colon, prostate and the skin. For each organ site, a brief description of the state of the art is presented, followed by representative studies.

Brain

Diffuse reflectance spectroscopy in the near infra-red (NIR) spectrum, sometimes named NIR spectroscopy, has attracted much attention in brain imaging since the 1990s, because of the relatively large penetration depth of NIR light. It was found feasible to detect brain activities through intact skulls[25] especially in children. The major physiological parameters extracted from NIR spectroscopy include total hemoglobin concentration and tissue oxygenation. Because of weak scattering in this range, light transport in this region can be described by an analytical expression, i.e. diffuse theory, which greatly facilitates data analysis. This technique is frequently used in an imaging modality, i.e. diffuse optical tomography (DOT). Multiple detectors are used to reconstruct three-dimensional images of cerebral hemodynamics. For a review of DOT imaging in the brain, please refer to Jacobs *et al*[26], Gibson *et al*[27], and Huppert *et al*[28]. However, because most brain cancers in an intact skull are not within the reach of light, this technique is less studied in clinical oncology.

Diffuse reflectance spectroscopy in the visible spectrum and fluorescence spectroscopy have been studied in tumor margin assessment or tissue characterization during neurosurgery procedures. Compared to NIR spectroscopy, diffuse reflectance spectroscopy in the visible spectrum and fluorescence spectroscopy possess higher chemical sensitivity. The problem of small penetration depth associated with ultraviolet and visible light is no longer an issue during surgery, which opens a new venue to apply optical spectroscopy in brain cancer management. For a review on the neuro-oncological applications of optical spectroscopy, please refer to Toms *et al*[29]. A few representative studies were briefly reviewed below.

Lin *et al*[30] investigated the applicability of combined autofluorescence and diffuse-reflectance spectroscopy for intraoperative detection of infiltrating tumor margins (ITM) in a pilot *in vivo* clinical trial consisting of 26 brain tumor patients. A two-step empirical discrimination algorithm yielded a sensitivity and specificity of 100% and 76%, respectively, in differentiating ITM from normal brain tissues.

Antonsson *et al*[31] investigated the use of diffuse reflectance spectroscopy for differentiating tissue types to improve intracerebral guidance during deep brain stimulation. Diffuse reflectance spectroscopy measurements in 10 patients were recorded for three different functional targets including the subthalamic nucleus (STN), internal globus pallidus (GPi) and zona incerta (Zi). Significant intensity differences between white and gray matter were found to be at least 14% ($P < 0.05$) and 20% ($P < 0.0001$) for MRI and spectral-sorted data, respectively.

Lin *et al*[32] further investigated the feasibility of using diffuse reflectance and fluorescence spectroscopy to differentiate pediatric neoplastic and epileptogenic brain from normal brain in an *in vitro* study. Statistically significant differences ($P < 0.01$) were found between (1) neoplastic brain and normal gray matter; (2) epileptogenic brain and normal gray matter; and (3) neoplastic brain and normal white matter.

Krafft *et al*[33] explored the use of Raman spectroscopic mapping for distinguishing between normal brain tissue and gliomas and meningiomas. *Ex vivo* tissues were examined by a Raman spectrometer with 785 nm excitation coupled to a microscope. Normal brain tissue was found to contain higher levels of lipids, intracranial tumors have more hemoglobin and lower lipid to protein ratios, meningiomas contain more collagen with maximum collagen content in normal meninges.

Breast

Breast cancer is perhaps the most extensively studied cancer in the community of biomedical optics. Optical spectroscopy techniques have been explored in a variety of forms in breast cancer diagnosis, including non-invasive breast cancer imaging, tumor characterization for margin assessment during breast surgery and "optical biopsy" measurements in needle biopsy or fine needle aspiration procedures.

Non-invasive breast cancer imaging can be performed in diffuse optical tomography[34,35] or diffuse reflectance spectroscopy often in the frequency domain[6,36]. Multiple wavelengths are used to achieve spectroscopic measurements and provide functional images of the breast, which include hemoglobin concentration, oxygen saturation, water and lipid content as well as scattering properties. Although this approach sounds attractive, it suffers from low spatial resolution due to multiple light scattering. To tackle this problem, other imaging modalities such as CT and MRI were proposed to provide anatomical images at a high spatial resolution[35,37,38], which is incorporated into the DOT reconstruction algorithm to combine with the functional images obtained in DOT. Because of the advantage in the signal to noise ratio, optical equipment in the frequency domain is preferred in many cases. For a more detailed review of this technique, please refer to publications[35,39,40]. Shah *et al*[36] and Tromberg *et al*[16] have provided excellent discussion on the potential roles of optical spectroscopy in the clinical management of breast cancer.

Tumor margin assessment during open surgery using optical spectroscopy has been reported by several groups[41-44] as summarized in Table 3. It is worth noting that the accuracy changes with the classification algorithm[41] which suggests the importance of selecting appropriate data analysis methods. There is a special case[42] in which Raman spectroscopy detected a grossly invisible cancer that was confirmed by pathologic review. This finding gave the patient a chance for a second surgical procedure to prevent the recurrence of cancer.

All these previous studies demonstrated that optical spectroscopy could be used in a real-time fashion to guide tissue excision during breast surgery, potentially to reduce the need for repeated surgery resulting from positive margins, and thereby reducing the recurrence rate of breast cancer following mastectomy surgery.

Needle biopsy has become another popular carrier of fiber-optic probes for performing optical spectros-

Table 3 Summary of techniques, patient population and accuracy in previous optical spectroscopy studies for intraoperative breast margin assessment

Author	Techniques	Patient population	Accuracy
Bigio *et al*[41]	Elastic-scattering spectroscopy (a special diffuse reflectance spectroscopy)	31 women, a total of 72 histology sites in breast tissue	Sensitivities of 69% and specificities of 85% for breast tissue
Haka *et al*[42]	Raman spectroscopy	9 patients undergoing partial mastectomy procedures	Accuracy of 100% for carcinoma; accuracy of 93.3% for distinguishing cancerous from normal and benign tissues
Ramanujam *et al*[43]	Diffuse reflectance spectroscopy in spectral imaging	55 margins in 48 patients.	Sensitivity of 79% and specificity of 67% for detection of residual tumor, with an 89% sensitivity for ductal carcinoma *in situ* alone
Keller *et al*[44]	Autofluorescence and diffuse reflectance spectroscopy and spectral imaging	145 normal spectra were obtained from 28 patients, and 34 tumor spectra were obtained from 12 patients	Differentiate normal tissue or tumor with 85% sensitivity and 96% specificity

copy, which is technically called "optical biopsy". The advantages of "optical biopsy" compared to physical biopsy are not only non-invasiveness and high accuracy but also an increased sensing tissue volume, which could greatly reduce the chance of missing hidden cancer sites. Manoharan *et al*[45] performed an early study to picture the possibility of incorporating Raman spectroscopy into a biopsy needle for breast cancer examination. Bigio *et al*[41] performed transdermal-needle measurement using elastic scattering spectroscopy for instant diagnosis with minimal invasiveness for breast tissue examination. The accuracy of transdermal-needle measurements combined with spectral measurements in open surgery is reported in Table 3.

van Veen *et al*[46] performed differential path-length spectroscopy (DPS), which is essentially a type of diffuse reflectance spectroscopy, on healthy and malignant breast tissue using a fiber-optic needle probe. A special tissue model was used to yield information on the local tissue blood content, the local blood oxygenation, the average micro-vessel diameter, the beta-carotene concentration and the scatter slope. The histological outcome of core-needle biopsies taken from the same location was used as the gold standard. Malignant breast tissue has a smaller tissue oxygenation and a higher blood content compared to normal breast tissue.

Yu *et al*[47] developed a side-firing fiber-optic sensor based on near-infrared spectroscopy for guiding core needle biopsy diagnosis of breast cancer. The sensor is inserted into a core biopsy needle to measure diffuse reflectance spectra in the NIR spectrum at the biopsy site through an aperture on the needle before the tissue is removed for histology. Preliminary *in vivo* measurements were performed on 10 normal or benign breast tissues from 5 women undergoing stereo- or ultrasound-guided core needle biopsy and showed good correlation with histopathology.

Zhu *et al*[48] explored the use of fluorescence spectroscopy for guiding breast biopsies. A total of 121 biopsy samples with accompanying histological diagnosis were obtained clinically. The statistical data analysis provided a cross-validated sensitivity and specificity of up to 81% and 87%, respectively, for discrimination between malignant and fibrous/benign samples, and up to 81% and 81%, respectively, for discriminating between malignant and adipose samples. The corresponding receiver operator curves (ROC) yielded an area under the curve (AUC) of 0.87 and 0.84 in two cases. It is noted that ROC is a graph of sensitivity against (1-specificity) and the AUC is an indicator of the diagnostic performance.

In these applications, quantitative methods have been developed in all optical spectroscopy techniques, which provide extra information to elucidate the biochemical basis of carcinogenesis in the breast in addition to its use for diagnosis. For instance, diffuse reflectance spectroscopy has been used to derive vascular oxygenation and total hemoglobin content in breast cancer[5]. Raman spectroscopy was used to derive information on cholesterol-like lipid deposits, fat, collagen, and cell nucleus/cytoplasm[42].

Cervix

Because of relatively easy access to the cervix, numerous studies[14,49-51] have been reported on the *in vivo* diagnostics of cervical neoplasia. Cardenas-Turanzas *et al*[52] presented an excellent review on the clinical effectiveness of diffuse reflectance and fluorescence spectroscopy for the *in vivo* diagnosis of cervical intraepithelial neoplasia. According to this review, optical spectroscopy showed a similar performance to colposcopy and can be an effective adjunct to colposcopy to help localize lesions. It also has potential use in cervical screening or to triage patients on Pap smear.

The following review papers may also be helpful. Murali Krishna *et al*[51] provided a brief overview on the optical spectroscopic approach to cervical cancer diagnosis as well as on radiation therapy and radiation resistance. Bazant-Hegemark *et al*[53] reviewed several tools capable of non-destructive mapping of the cervix at high resolution in a clinical environment including infrared spectroscopy and Raman spectroscopy in terms of clinical performance for diagnosis. Drezek *et al*[54] presented an overview of various optical techniques including optical spectroscopy for the detection of precancerous lesions in the uterine cervix presented at the Second International Conference on Cervical Cancer. This review strong recommends the use of the Littenberg method for assessing new techniques to ensure that better technologies will stand out.

Several studies reported on the quantification of physiological parameters based on measured optical spectra,

which provided insight into the development of cervical dysplasia at various stages. Chang *et al*[55] used an analytical model to estimate the contributions of several optical biomarkers by analyzing spectra from diffuse reflectance spectroscopy and fluorescence spectroscopy measurements. The model was applied to 493 *in vivo* fluorescence measurements of cervical tissue acquired from 292 patients. The results show an increase in epithelial flavin adenine dinucleotide (FAD) fluorescence, a decrease in epithelial keratin fluorescence, an increase in epithelial light scattering, a decrease in stromal collagen fluorescence, and an increase in stromal hemoglobin light absorption in dysplastic tissue compared to normal tissue. These changes likely reflect an increase in the metabolic activity and loss of differentiation of epithelial dysplastic cells, and stromal angiogenesis associated with dysplasia.

Chang *et al*[56] assessed the capability of a diffuse reflectance spectroscopy technique to identify contrasts in optical biomarkers at different grades of cervical intraepithelial neoplasia (CIN) using a numerical model. In a total of 89 sites examined in 38 patients, there were 46 squamous normal sites, 18 CIN 1 sites, and 15 CIN 2(+) sites. Total hemoglobin was statistically higher in CIN 2(+) compared with normal and CIN 1 sites, which was attributed to stromal angiogenesis. Scattering was significantly reduced in CIN 1 and CIN 2(+) compared with normal sites, which was attributed to breakdown of the collagen network in the cervical stroma.

Lung

Typical optical spectroscopy equipment can be readily used for characterization of tissue biopsies from the lung[57-59]. Huang *et al*[59] used a near-infrared (NIR) Raman spectroscopy system at 785 nm excitation to measure bronchial tissue specimens including 12 normal specimens, 10 squamous cell carcinoma (SCC) and 6 adenocarcinoma specimens obtained from 10 patients. They demonstrated that Raman spectra differed significantly between normal and malignant tumor tissue, with tumors showing higher percentage signals for nucleic acid, tryptophan and phenylalanine and lower percentage signals for phospholipids, proline and valine, compared to normal tissue.

Yamazaki *et al*[58] constructed a near-infrared multichannel Raman system with an excitation wavelength at 1064 nm. They collected a total of 210 Raman spectra. The resulting sensitivity of cancer prediction was up to 91% and the specificity was 97% with an error margin of $P < 0.0001$ according to Fisher's exact test.

Aerts *et al*[57] successfully related HIF1a, which is one of the hypoxia-related proteins, to *in vivo* spectroscopic measurements of tumor blood saturation performed during bronchoscopy in 17 tissue samples. There was a significant difference in the spectroscopically determined saturations between the biopsies with negative expression of HIF1a and the biopsies with positive expression of HIF1a ($P < 0.005$).

Optical spectroscopy can also be incorporated into a commercial endoscopy system to perform *in vivo* examinations of the lung. Zeng *et al*[60] developed an integrated endoscopy system for simultaneous imaging and spectroscopy to detect early lung cancers. Zeng *et al*[61] proposed to use autofluorescence imaging and white light reflectance imaging to obtain high diagnostic sensitivity, while at the same time using non-contact point reflectance/fluorescence spectroscopy to reduce false positive biopsies. A pilot clinical study involving 22 lung patients demonstrated that the malignant lung lesions can be differentiated from the benign lesions using this system with a sensitivity and specificity of more than 80%.

Stomach

Numerous studies have reported on the examination of *ex vivo* stomach tissue samples using optical spectroscopy. Kawabata *et al*[62] performed Raman spectroscopy measurements on 251 fresh biopsy specimens obtained from 49 gastric cancer patients. Fresh specimens were measured with an excitation wavelength of 1064 nm. A sensitivity of 66%, a specificity of 73%, and an overall accuracy of 70% were achieved for the differentiation of gastric carcinoma from normal mucosa. Teh *et al*[63] applied near-infrared (NIR) Raman spectroscopy at 785-nm excitation in a total of 73 gastric tissue samples (55 normal, 18 cancer) from 53 patients. The predictive sensitivity and specificity of the independent validation dataset were 88.9% and 92.9%, respectively, for separating cancer from normal samples.

Given the high chemical specificity of Raman spectroscopy, it can be used to find the source of Raman signals contributing to cancer diagnosis. Teh *et al*[64] measured Raman spectra of 88 gastric tissue samples from 56 patients. Significant differences in Raman spectra were observed among normal, *Helicobacter pylori* infection (*Hp*-infection) and intestinal metaplasia (IM) gastric tissue, which were attributed to proteins, lipids and porphyrin. Data analysis yielded diagnostic sensitivities of 91.7%, 80.0%, and 80.0%, and specificities of 80.0%, 100%, and 92.7%, respectively, for the classification of normal, Hp-infection and IM gastric tissues. Raman spectroscopy has also been used in the early diagnosis and typing of intestinal and diffuse adenocarcinoma of the stomach[65], in which predictive accuracies of 88%, 92% and 94% were achieved for normal stomach, and intestinal- and diffuse-type gastric adenocarcinomas, respectively.

Optical spectroscopy has been incorporated into endoscopy systems for *in vivo* measurements of stomach cancer. Mayinger *et al*[66] evaluated light-induced autofluorescence spectroscopy in a commercial endoscopy system for the *in vivo* diagnosis of gastric cancer. A total of 15 patients with pure adenocarcinoma and 16 patients with gastric cancer containing signet-ring cells were recruited into the study. A sensitivity of 84% and a specificity of 87% were obtained for the diagnosis of pure adenocarcinoma of the stomach. The diagnostic performance was found to decrease with increasing numbers of signet-ring cells and tumor grade.

Colon

Some optical spectroscopy techniques such as diffuse reflectance spectroscopy have been incorporated into colonoscopy[67] or flexible sigmoidoscopy[68] to perform *in vivo*

measurements. Dhar *et al*[69] assessed the diagnostic potential of elastic scattering spectroscopy, which is essentially a particular type of diffuse reflectance spectroscopy, in colonoscopy to differentiate abnormal colon tissues *in vivo*. A total of 483 spectra (290 normal, 19 hyperplastic, 69 adenomatous polyps, 74 chronic colitis, and 31 colorectal cancer) were obtained from 138 sites in 45 patients at colonoscopy. The sensitivity and specificity of differentiating adenomas from hyperplastic polyps, cancer from adenomatous polyps, colitis from normal tissue, dysplastic mucosa (from polyps) from colitis were 84% and 84%, 80% and 75%, 77% and 82%, 85% and 88%, respectively.

Zonios *et al*[70] first analyzed diffuse reflectance spectra collected from adenomatous colon polyps and normal colonic mucosa of patients undergoing colonoscopy to estimate the following four parameters: hemoglobin concentration, hemoglobin oxygen saturation, effective scatterer density, and effective scatterer size. It was observed that normal and adenomatous tissue sites exhibited differences in hemoglobin concentration and effective scatterer size, which were in agreement with other studies that employed standard methods. A similar method was used by Wang *et al*[67] to quantify total hemoglobin concentration (THC) and oxygen saturation (StO_2) *in vivo* in 27 patients with colorectal cancer (CRC). Increased hemoglobin concentration and decreased oxygenation were observed from normal sites to premalignant tissues and then to malignant tissues.

Roy *et al*[68] incorporated polarization-gated spectroscopy into flexible sigmoidoscopy to detect an early increase in blood supply (EIBS) in the endoscopically normal rectum (n = 366). The rectal mucosal oxyhemoglobin content in females with advanced proximal neoplasia (n = 10) was significantly higher than that in the control group. It is worth noting that the addition of rectal oxyhemoglobin information dramatically increased the sensitivity to advanced neoplasia compared to flexible sigmoidoscopy alone. The sensitivity and specificity were 100% and 76.8%, respectively.

The research in Raman spectroscopy has been mostly limited to *ex vivo* studies likely due to the technical difficulty in obtaining Raman spectra at a reasonable signal to noise ratio. Stone *et al*[71] carried out Raman measurements for optical diagnostics in various organs including colon using an optimized commercial Raman microspectrometer. Both the sensitivity and the specificity were greater than 90% for all tissues. Widjaja *et al*[72] combined near-infrared (NIR) Raman spectroscopy at 785 nm excitation with support vector machines (SVM) for the classification of different histopathological groups in colon tissues. A total of 105 colonic tissue specimens from 59 patients including 41 normal, 18 hyperplastic polyps and 46 adenocarcinomas were included in this study. The results showed that the maximum overall diagnostic accuracy ranged from 98.4% to 99.9%. Beljebbar *et al*[73] used near-infrared Raman microspectroscopic imaging to investigate the changes in composition from normal colonic tissues to adenocarcinoma *ex vivo*. Multivariate statistical analysis was applied to the Raman spectra to identify the molecular composition and distribution of lipids, proteins, mucus and collagens in normal and malignant tissue. The results matched those of conventional histopathological examination.

Blood plasma has been also used as samples for optical measurements. Fluorescence spectroscopy in blood has been exploited by Lualdi *et al*[74] to diagnose colorectal cancer. The study involved 341 subjects including 169 normal blood donors. Plasma fluorescence spectrum was measured in all subjects. The fluorescence emission peak around 615-635 nm was assigned to endogenous porphyrin. The peak intensity was significantly different between patients bearing colorectal cancer and normal blood donors. The ROC analysis resulted in an area under the curve of 0.72, close to that reported for the carcinoembryonic antigen (CEA) test, which suggests that this method could be a cost effective alternative screening test to CEA.

Dekker *et al*[75] and Wallace *et al*[76] reviewed recent advances in colonic imaging, which included various optical imaging techniques. Many of these optical imaging techniques, such as fluorescence imaging and narrow-band imaging, are essentially the extension of optical spectroscopy techniques, in which only the data at a few discrete wavelengths are acquired at many pixels. Moglia *et al*[77] reviewed another exciting *in vivo* imaging technique, capsule endoscopy, which enables remote diagnostic inspection of the gastrointestinal tract without sedation and with minimal discomfort.

Prostate

Various optical spectroscopy techniques have been explored for the study of *ex vivo* prostatic tissue samples, and these have provided the basis for future *in vivo* studies. Because the prostate is a solid organ and light typically cannot penetrate the whole organ, optical spectroscopy techniques would have to be incorporated into biopsy needles or applied during prostatectomy to be useful. Sharma *et al*[78] reported the development of a needle like, bifurcated, fiber-optic probe for diffuse reflectance spectroscopy measurements in human prostate cancer. The results from 23 prostate specimens demonstrate that the derived hemodynamic parameters and optical properties can serve as good biomarkers to differentiate tumor tissue from normal tissue in the human prostate.

Crow *et al*[79] employed a fiber-optic Raman system to differentiate between benign and malignant bladder and prostate pathologic findings *in vitro*, in which a total of 197 Raman spectra were recorded from 38 snap-frozen prostate samples collected at transurethral resection of the prostate. An overall accuracy of 86% was reported for differentiation of benign prostatic hyperplasia and prostatitis from prostate cancer.

The combination of multiple complementary techniques has been reported to improve prostate cancer detection. Salomon *et al*[80] combined laser-induced autofluorescence, white-light remission, and high-frequency impedance spectroscopy in an *ex vivo* study. Ninety-five frozen tissue samples from 32 patients undergoing radical prostatectomy for clinically localized prostate cancer were thawed for data acquisition. The statistical analysis of laser-induced autofluorescence and white-light remis-

sion data demonstrated a differentiation of benign and malignant prostate tissue with a sensitivity of 87.5% and a specificity of 87.3%. By adding the acquired high-frequency impedance data to the statistical analysis, sensitivity and specificity were increased to 93.8% and 92.4%.

Interstitial photodynamic therapy (PDT) in prostate cancer has been intensively studied. This therapy is particularly suited to the prostate because of its capability of precise delivery of light dosage and minimum damage to surrounding vital organs. Optical spectroscopy techniques have been shown to be valuable in monitoring relevant light and tissue parameters for the optimization of PDT outcome. Zhu *et al*[81] quantified the distribution of light fluence rate, optical properties, drug concentration, and tissue oxygenation for PDT of prostate cancer using diffuse reflectance spectroscopy and fluorescence spectroscopy before and after PDT treatment. This study shows significant inter- and intra-prostatic variations in tissue optical properties and drug distribution, which suggests that a real-time dosimetry measurement and feedback system is needed for monitoring these values during treatment to ensure the outcome.

Yu *et al*[82] reported the development of an optical system, combining diffuse reflectance spectroscopy (DRS) for measurement of tumor blood oxygenation and diffuse correlation spectroscopy (DCS) for measurement of tumor blood flow and its application in real time clinical monitoring during interstitial prostate PDT, which was tested on three patients. Prostrate blood oxygen saturation (StO2) was found to decrease only slightly (approximately 3%) after treatment. Prostate blood flow and total hemoglobin concentration over the course of PDT decreased by 50% and 15%, respectively. Johansson *et al*[23] developed an instrument for interstitial PDT on prostate tissue that combines therapeutic light delivery and monitoring of light transmission. They demonstrated this using a system to obtain data on the light distribution within the target tissue and to provide real time treatment feedback based on a light dose threshold model for PDT.

Fluorescence spectroscopy was used by Zaak *et al*[83] to study the feasibility of 5-aminolevulinic-acid (5-ALA)-induced photodynamic diagnosis (PDD) for margin evaluation during radical prostatectomy (RP) in patients with prostate cancer. Eight out of ten patients demonstrated negative margins and one positive margin in fluorescence measurements, which were confirmed by histology. One positive margin in fluorescence measurements was not confirmed.

A few review articles may help interested readers to learn more about optical spectroscopy in prostate cancer management. Hanchanale *et al*[84] reviewed the use of Raman spectroscopy in urological applications including margin assessment during prostatectomy. Manyak *et al*[85] reviewed the advance of medical imaging for prostate cancer including optical techniques such as hyperspectral spectroscopy.

Skin

Because of easy accessibility, skin cancer has been extensively studied in the past two decades both *ex vivo* and *in vivo*. The papers reviewed next were all *in vivo* studies to highlight the most recent progress. Zonios *et al*[86] developed a method for estimating the absorption spectra of melanin *in vivo* based on diffuse reflectance spectroscopy of human skin. They found that the histologic transition from dysplastic nevi to melanoma *in situ* and then to malignant melanoma was reflected in the melanin absorption spectra.

Marchesini *et al*[87] attempted to determine the role of melanin in the various steps of progression of melanocytic neoplasia using diffuse reflectance spectroscopy. They examined 288 melanomas in different phases of progression, i.e. *in situ*, horizontal and vertical growth phase invasive melanomas, 424 dysplastic nevi, and 957 melanocytic lesions. The absorbance spectra in the different groups showed that melanin level was correlated with the progression from dysplastic nevi to vertical growth phase melanomas. In addition, it was observed that *in vivo* diffuse reflectance spectroscopy can be used to differentiate eumelanin and pheomelanin in lesions.

Sterenborg *et al*[88] examined the feasibility of using *in vivo* autofluorescence at an excitation wavelength of 375 nm for the diagnosis of skin cancer in 1995. They did not observe any significant differences in the shape of fluorescence spectra or spatial distribution of fluorescence intensity between tumors and the corresponding control sites, which was likely due to the choice of the excitation wavelength.

As technology has advanced since then, several groups have reported the effective diagnosis of skin cancer using fluorescence spectroscopy. Brancaleon *et al*[89] examined the autofluorescence of normal skin and nonmelanoma skin cancers (NMSC) *in vivo* excited by UV light in 18 patients. They observed that the endogenous fluorescence due to tryptophan residues in both basal cell carcinomas (BCC) and squamous cell carcinomas (SCC) was stronger than in normal tissue, probably due to epidermal thickening and/or hyperproliferation. In contrast, the fluorescence intensity associated with dermal collagen crosslinks was generally lower in tumors than in the surrounding normal tissue, probably because of degradation or erosion of the connective tissue due to enzymes released by the tumor.

Panjehpour *et al*[90] used laser-induced fluorescence spectroscopy at the visible excitation wavelength of 410 nm to detect NMSC *in vivo*. Two hundred and seventy nine measurements were performed in 49 patients. Patients were classified as having either skin types Ⅰ, Ⅱ, or Ⅲ. Cancers were classified correctly in 93%, 89%, and 78% of patients with skin types Ⅰ, Ⅱ, and Ⅲ, respectively. Normal tissues were classified correctly in 93%, 88%, and 50% of patients with skin types Ⅰ, Ⅱ, and Ⅲ, respectively. Using the same threshold, pre-cancerous spectra were classified correctly in 78% and 100% of patients with skin types Ⅰ and Ⅲ, respectively. Benign lesions were classified correctly in 100%, 46%, and 27% of patients with skin types Ⅰ, Ⅱ, and Ⅲ, respectively.

In contrast to UV or visible excitation in conventional fluorescence spectroscopy, Han *et al*[91] developed an NIR autofluorescence and reflectance imaging system excited at 785 nm aiming to characterize cutaneous melanins *in vivo*. Their preliminary results show that cutane-

ous melanin in pigmented skin disorders emits higher NIR autofluorescence than surrounding normal tissue. Because NIR light penetrates deeper in the skin, this technique is expected to examine a larger volume of the skin tissue, which may be useful for clinical evaluation and diagnosis of pigmented skin lesions.

Raman spectroscopy also appears to be an effective optical technique for skin cancer diagnosis. Lieber *et al*[92] used a portable confocal Raman system to measure Raman spectra from 21 suspected NMSC in 19 patients. A 100% (21/21) sensitivity and 91% (19/21) specificity for abnormality, with a 95% (40/42) overall classification accuracy were achieved.

Zhao *et al*[93] reported the development of a rapid real-time Raman spectrometer system with measurement times of less than 1 s in a preliminary study. In total, 289 skin cancers and benign skin lesions were measured. Skin cancers could be well differentiated from benign skin lesions (sensitivity 91% and specificity 75%) and malignant melanoma from benign pigmented lesions (sensitivity 97% and specificity 78%).

For a review on the application of Raman spectroscopy in skin cancer, please refer to Eikje *et al*[94], which includes a survey of introduced sampling methods for IR and Raman spectroscopy in dermatology, and describes the differences between microscopic, macroscopic and fiber-optic measurements of skin cancer. The authors are optimistic about the potential role of vibrational spectroscopy including Raman spectroscopy as a rapid screening tool in dermatology. Krafft *et al*[95] also reviewed the application of Raman spectroscopy in the recognition of a variety of diseases including skin tumors. Mogensen *et al*[96] reviewed the diagnostic accuracy of nonmelanoma skin cancer diagnostic tests and technologies including optical spectroscopy techniques such as spectroscopy and fluorescence imaging. They pointed out the need for larger scale trials despite the promising diagnostic accuracy using optical techniques.

PRACTICAL CONSIDERATIONS OF APPLYING OPTICAL SPECTROSCOPY IN CLINICAL SETTINGS AND COMMERCIALLY AVAILABLE CLINICAL EQUIPMENT

Limiting factors

Multiple factors can affect the feasibility and acceptance of applying optical spectroscopy techniques in clinical oncology. The following factors are particularly important from the author's point of view.

Speed of data acquisition and analysis: Ideally real time data acquisition and analysis is desired. The time of data acquisition depends on the amount of required data and the signal-to-noise ratio. In diffuse reflectance spectroscopy and fluorescence spectroscopy, the signal-to-noise ratio is typically not an issue, thus, real time or nearly real time measurements could be readily achieved[97,98]. Real time *in vivo* measurements in Raman spectroscopy have been achieved in the skin first[99,100], and recently in the endoscopic setting[101] enabled by the advances in ultra sensitive detectors.

Cost of equipment and maintenance: The equipment for *in vivo* diffuse reflectance spectroscopy is relatively cheap because of the advances in white light sources and compact spectrometers. Fluorescence spectroscopy used to require a large investment in relation to its equipment due to the fact that it needs a strong laser in the UV or visible range to excite fluorescence. This cost has decreased quite significantly due to the emergence of new narrow band light sources such as LEDsβ. However, if a range of excitation wavelengths and high sensitivity are needed, a traditional fluorescence spectrophotometer, which uses monochromators for wavelength selection, would still possess advantages, for which the size and cost could go up quickly. The cost of a Raman system is in general the most expensive of these three techniques because of the strict requirement on the wavelength purity of the excitation light and on the sensitivity of the detection module. The required maintenance of systems is minimal in all three techniques, although the calibrations of wavelength accuracy and system throughput should be performed regularly to ensure the accuracy of measured spectra.

Complexity of operation: The equipment operation is straightforward in those commercial systems for all three techniques. Currently, most data analysis algorithms employ multivariate statistical methods to yield a yes/no answer on whether a given sample contains cancer at a certain stage. This information could reinforce the result of the corresponding standard clinical procedure when they agree with each other or remind physicians to double check the sample when they disagree.

Accuracy: Although most studies in the optical diagnosis of cancer have reported high accuracy, there is a large variation in the exact values of accuracy even for the same type of cancer. The potential contributing factors to this situation include differences in the equipment, laser and detector configuration, data analysis algorithms and measurement protocols in addition to inherent inter-patient variation. For this reason, it is necessary for the scientific community to standardize the measurement protocols and other controllable factors that may affect diagnostic accuracy, which would help yield consistent results in the diagnostic accuracy of optical techniques. Such consensus should greatly facilitate the acceptance of optical spectroscopy techniques by the medical community.

Clinical value added to the current clinical procedure: It is imperative to convince physicians that optical spectroscopy techniques can add extra value to clinical cancer management for them to accept the techniques. This would require comparative clinical studies that directly compare the clinical performance of standard procedures and that of revised procedures in which optical spec-

troscopy techniques are incorporated. Such studies will provide the evidence to demonstrate the clinical value of optical spectroscopy added to standard procedures.

Commercially available equipment for clinical applications of optical spectroscopy

Several clinically approved commercial instruments based on optical spectroscopy are available on the market. A few examples are listed below. Tissue oximeters are commercially available and can measure tissue oxygenation in a tissue volume, which is essentially the average contribution of all capillaries and small blood vessels in the tissue volume right underneath the sensor. Most tissue oximeters employ diffuse reflectance spectroscopy[102,103]. Tissue measurements are feasible only when the suspicious site is easy to access. It should be noted that a tissue oximeter is different from a pulse oximeter in that the former measures tissue oxygenation in a local tissue region while the latter measures arterial oxygen saturation. Tissue oxygenation is an important parameter for the diagnosis of many type of cancers.

Fluorescence spectroscopy and diffuse reflectance spectroscopy have been incorporated into a videoendoscopy system to enhance imaging contrast in gastric cancer[104], in which the number of available spectral bands are much smaller than those in point spectroscopy measurements due to the physical restraints in an endoscope. The disadvantage of a small number of spectral bands can be overcome to some extent by a spectral imaging color enhancement technique[105]. In this technique, more spectral bands are reconstructed using a specialized estimation algorithm from the data measured in three spectral bands available in ordinary endoscopy systems. This technique demonstrated certain advantages under several special situations for image enhancement to help visualize Barrett's esophagus.

A commercial cervical imaging system[106] incorporating both reflectance and fluorescence spectroscopy was approved by the US Food and Drug Administration (FDA) in March 2006. This system can be used as an adjunct tool to improve colposcopic detection of high-grade cervical intraepithelial neoplasia (CIN). In two prospective randomized clinical trials, the addition of this system to colposcopy resulted in a 25% or greater increase in the true positive biopsy rate for patients with atypical squamous cell or low-grade squamous intraepithelial lesions on Pap smear, and only a 4% increase in the false-positive rate, compared to those with colposcopy alone.

TECHNICAL CHALLENGES AND STANDARD ISSUES

Technical challenges

Challenges in consistent optical coupling, speed and data interpretation: Optical measurements are quite sensitive to optical coupling, which could cause inconsistent performance of optical techniques. Several strategies can be used to overcome this problem. For example, a pressure gauge could be used to monitor the pressure of probe-tissue contact. Although it works, this strategy requires extra effort from users and additional cost for an automated feedback mechanism. Alternatively, the shape rather than the absolute intensity of the spectra can be used for diagnosis, which would eliminate the problem of optical coupling at the cost of discarding the diagnostic information that may exist in absolute intensity measurements.

Speed is one significant hurdle that prevents the broad use of those optical techniques requiring a large amount of data. While data acquisition speed can be improved by advances in light sources and detectors, a more effective strategy is to acquire and analyze data at only a few optimal spectral bands rather than the entire spectrum. It turns out that this is possible for the determination of specific biomarkers[107]. For this purpose it is important to understand the mechanism of cancer development because it would help identify most diagnostic biomarkers and find corresponding optimal spectral bands.

Data interpretation is another important issue that deserves significant attention. Currently, most data analysis algorithms in optical spectroscopy yield a definite "yes/no" result for a given tissue sample. This may not be the best solution in an *in vivo* scenario because it excludes the possibility of an intermediate status and could result in artificial errors. A better choice might be to calculate the probability for a given tissue sample to be a cancer. This probability could be determined for all pixels in a small area, in which the spatial context would help clinicians determine the true answer.

Translation to spectral imaging and microscopic imaging: It seems natural for optical spectroscopy to evolve from point measurements to spectral imaging to cover a large field of view. Images also provide a spatial context similar to what physicians typically see in clinical settings. Because of time restraint, spectral imaging often contains much fewer spectral bands, thus, could be less sensitive to malignant changes in tissues compared to the entire spectrum. Therefore, a combination of spectral imaging and point measurements might be most useful, in which spectral imaging data help locate suspicious areas, while point spectroscopy measurements can check identified sites in detail. This approach has been demonstrated to be effective in an endoscopic setup[60]. The challenges in handling a large amount of data, speeding up data acquisition and accommodating complex illumination-collection configurations need to be addressed before spectral imaging could be useful in clinical settings.

Optical spectroscopy using a fiber-optic probe examines a large tissue volume, which could result in low sensitivity in a small target such as a small tumor. This can be serious in Raman spectroscopy, because Raman signals are typically low in tissue samples. Microscopic imaging at a high spatial resolution[108] in an endoscopic setup has been demonstrated, which can overcome the above problem. In the laser scanning mode, excitation light can be focused on a small spot to enhance the sensitivity to the target area and increase emission signals.

Quantitative optical spectroscopy and imaging: Opti-

cal spectroscopy can be used to quantify several biochemical and biophysical parameters in tissues as discussed in this review. Light transport models such as diffusion theory or the Monte Carlo method were used to relate tissue optical properties to optical measurements. Moreover, physical laws such as Beer-Lambert's law and Mie approximation were used to link biochemical and biophysical parameters to tissue optical properties. The resulting parameters, such as hemoglobin concentration and oxygenation, the average size of scatterers *etc*, could be correlated with the physiology of tissues, which provides insight into cancer development. These parameters could also be used for cancer diagnosis, which provides an alternative to pure statistical classification.

Although this approach has achieved great success, several assumptions made in this approach impose limitations on the interpretation of results and its applications. For example, most such models assume a semi-infinite homogeneous tissue model, in which the concentrations of chromophores are distributed uniformly. The Mie approximation assumes perfectly spherical scatterers. Although the models with these assumptions have yielded meaningful results, they definitely do not fully exploit all the diagnostic information present in optical spectroscopy. Several attempts[109,110] have been made to build more realistic tissue models, for example, applying a layered tissue model instead of a homogeneous tissue model or inhomogeneous scattering particles, to further refine the techniques.

Standard issues

Establishment of standards for the evaluation of techniques: It is important to establish standard methods to evaluate new optical techniques in order to be compatible with those established imaging techniques and be accepted by clinical practitioners. Currently each optical technique is evaluated by the group in which it is developed using a somehow unique method. For optical techniques targeting a similar clinical application, it might be helpful for leading groups to establish recommended standards in the protocol of evaluation, for instance, the size of the patient population and distribution of age and gender, the table or plots that demonstrates representative results and the measures of accuracy *etc*. These standards will facilitate the comparison across different techniques from the point of view of clinicians as well as colleagues in the scientific community. Although such principles may have existed in the phase of clinical research, the author believes that it is worth setting up similar standards even at the early stage of technical development for the purpose of evaluation. These are similar to those industrial standards and aim to maintain high quality and good reliability of scientific research, which will help the technique get accepted by the medical community at a later stage.

Compatibility of optical techniques with current procedures: It is quite clear for some optical techniques that they cannot fulfill the requirement of assumed tasks alone. The unique advantage of high optical contrast makes optical techniques complementary to most existing imaging modalities. Once the capability of an optical technique is well understood, it would be helpful to perform clinical studies to decide how the optical technique could fit into the current procedure in cancer management. Since the current procedure typically contains the use of those established techniques, it would be more acceptable if the optical technique could be integrated into the established technique and provide extra valuable information without incurring unjustifiable cost and time commitment. Some pioneering efforts[16,38,111] have been made to investigate the complementary attributes of optical spectroscopy and MRI in breast cancer management.

CONCLUSION

Because of its non-invasiveness and high optical contrast, optical spectroscopy has been intensively studied in cancer diagnosis and has demonstrated great potential in finding its unique role in clinical cancer management. Some commercial instruments based on optical spectroscopy have been approved for clinical use. It is reasonable to anticipate that more optical spectroscopy techniques will find their niches in clinical settings given the dramatic increase in the market and research in the field of biomedical optics. Achieving this goal would require the collaborative efforts of both the scientific community and the medical community worldwide.

REFERENCES

1 **Lau C**, Sćepanović O, Mirkovic J, McGee S, Yu CC, Fulghum S, Wallace M, Tunnell J, Bechtel K, Feld M. Re-evaluation of model-based light-scattering spectroscopy for tissue spectroscopy. *J Biomed Opt* 2009; **14**: 024031

2 **Kim Y**, Liu Y, Backman V. Coherent backscattering spectroscopy: a new technique for tissue diagnosis. *Conf Proc IEEE Eng Med Biol Soc* 2004; **7**: 5285-5288

3 **Bosschaart N**, Aalders MC, Faber DJ, Weda JJ, van Gemert MJ, van Leeuwen TG. Quantitative measurements of absorption spectra in scattering media by low-coherence spectroscopy. *Opt Lett* 2009; **34**: 3746-3748

4 **Arifler D**, MacAulay C, Follen M, Richards-Kortum R. Spatially resolved reflectance spectroscopy for diagnosis of cervical precancer: Monte Carlo modeling and comparison to clinical measurements. *J Biomed Opt* 2006; **11**: 064027

5 **Brown JQ**, Wilke LG, Geradts J, Kennedy SA, Palmer GM, Ramanujam N. Quantitative optical spectroscopy: a robust tool for direct measurement of breast cancer vascular oxygenation and total hemoglobin content in vivo. *Cancer Res* 2009; **69**: 2919-2926

6 **Cerussi A**, Shah N, Hsiang D, Durkin A, Butler J, Tromberg BJ. In vivo absorption, scattering, and physiologic properties of 58 malignant breast tumors determined by broadband diffuse optical spectroscopy. *J Biomed Opt* 2006; **11**: 044005

7 **Mourant JR**, Freyer JP, Hielscher AH, Eick AA, Shen D, Johnson TM. Mechanisms of light scattering from biological cells relevant to noninvasive optical-tissue diagnostics. *Appl Opt* 1998; **37**: 3586-3593

8 **Bigio IJ**, Mourant JR, Boyer J, Johnson T. "Elastic scattering spectroscopy as a diagnostic for tissue pathologies," in Proceedings of 1994 Conference on Lasers and Electro-Optics and The International Electronics Conference CLEO/IQEC, 8-13 May 1994, (Opt. Soc. America, Anaheim, CA, USA, 1994), 1994: 70-71

9 **Bigio IJ**, Mourant JR, Boyer J, Johnson TM. "Elastic scatter-

ing spectroscopy for diagnosis of tissue pathologies," in OSA Trends in Optics and Photonics on Biomedical Optical Spectroscopy and Diagnostics. Vol.3. From the Topical Meeting, 20-22 March 1996, (Opt. Soc. America, Orlando, FL, USA, 1996), 1996: 14-19
10 **Chaiken J**, Goodisman J, Deng B, Bussjager RJ, Shaheen G. Simultaneous, noninvasive observation of elastic scattering, fluorescence and inelastic scattering as a monitor of blood flow and hematocrit in human fingertip capillary beds. *J Biomed Opt* 2009; **14**: 050505
11 **Shafer-Peltier KE**, Haka AS, Motz JT, Fitzmaurice M, Dasari RR, Feld MS. Model-based biological Raman spectral imaging. *J Cell Biochem Suppl* 2002; **39**: 125-137
12 **Skala MC**, Riching KM, Gendron-Fitzpatrick A, Eickhoff J, Eliceiri KW, White JG, Ramanujam N. In vivo multiphoton microscopy of NADH and FAD redox states, fluorescence lifetimes, and cellular morphology in precancerous epithelia. *Proc Natl Acad Sci USA* 2007; **104**: 19494-19499
13 **Gill EM**, Palmer G, Ramanujam N. Steady-state Fluorescence Imaging of Neoplasia. In: Marriott G, editor. *Methods Enzymol* 2003; **361**: 452-81
14 **Ramanujam N**. Fluorescence spectroscopy of neoplastic and non-neoplastic tissues. *Neoplasia* 2000; **2**: 89-117
15 **Utzinger** U, Richards-Kortum RR. Fiber optic probes for biomedical optical spectroscopy. *J Biomed Opt* 2003; **8**: 121-147
16 **Tromberg BJ**, Pogue BW, Paulsen KD, Yodh AG, Boas DA, Cerussi AE. Assessing the future of diffuse optical imaging technologies for breast cancer management. *Med Phys* 2008; **35**: 2443-2451
17 **Blackmore KM**, Knight JA, Jong R, Lilge L. Assessing breast tissue density by transillumination breast spectroscopy (TIBS): an intermediate indicator of cancer risk. *Br J Radiol* 2007; **80**: 545-556
18 **El-Tawil SG**, Adnan R, Muhamed ZN, Othman NH. Comparative study between Pap smear cytology and FTIR spectroscopy: a new tool for screening for cervical cancer. *Pathology* 2008; **40**: 600-603
19 **Parker MF**. Emerging technology in cervical cancer screening: spectroscopy. *Clin Obstet Gynecol* 2005; **48**: 209-217
20 **Kan CW**, Jiang BC, Nieman LT, Sokolov K, Markey MK. Comparison of linear and non-linear classifiers for oral cancer screening by optical spectroscopy. *AMIA Annu Symp Proc* 2007; 1003
21 **Lin WC**, Mahadevan-Jansen A, Johnson MD, Weil RJ, Toms SA. In vivo optical spectroscopy detects radiation damage in brain tissue. *Neurosurgery* 2005; **57**: 518-525; discussion 518-525
22 **Tromberg BJ**, Cerussi A, Shah N, Compton M, Durkin A, Hsiang D, Butler J, Mehta R. Imaging in breast cancer: diffuse optics in breast cancer: detecting tumors in pre-menopausal women and monitoring neoadjuvant chemotherapy. *Breast Cancer Res* 2005; **7**: 279-285
23 **Johansson A**, Axelsson J, Andersson-Engels S, Swartling J. Realtime light dosimetry software tools for interstitial photodynamic therapy of the human prostate. *Med Phys* 2007; **34**: 4309-4321
24 **Weersink RA**, Bogaards A, Gertner M, Davidson SR, Zhang K, Netchev G, Trachtenberg J, Wilson BC. Techniques for delivery and monitoring of TOOKAD (WST09)-mediated photodynamic therapy of the prostate: clinical experience and practicalities. *J Photochem Photobiol B* 2005; **79**: 211-222
25 **Perrey S**. Non-invasive NIR spectroscopy of human brain function during exercise. *Methods* 2008; **45**: 289-299
26 **Jacobs AH**, Kracht LW, Gossmann A, Rüger MA, Thomas AV, Thiel A, Herholz K. Imaging in neurooncology. *NeuroRx* 2005; **2**: 333-347
27 **Gibson A**, Dehghani H. Diffuse optical imaging. *Philos Transact A Math Phys Eng Sci* 2009; **367**: 3055-3072
28 **Huppert TJ**, Diamond SG, Franceschini MA, Boas DA. HomER: a review of time-series analysis methods for near-infrared spectroscopy of the brain. *Appl Opt* 2009; **48**: D280-D298
29 **Toms SA**, Konrad PE, Lin WC, Weil RJ. Neuro-oncological applications of optical spectroscopy. *Technol Cancer Res Treat* 2006; **5**: 231-238
30 **Lin WC**, Toms SA, Johnson M, Jansen ED, Mahadevan-Jansen A. In vivo brain tumor demarcation using optical spectroscopy. *Photochem Photobiol* 2001; **73**: 396-402
31 **Antonsson J**, Eriksson O, Blomstedt P, Bergenheim AT, I Hariz M, Richter J, Zsigmond P, Wårdell K. Diffuse reflectance spectroscopy measurements for tissue-type discrimination during deep brain stimulation. *J Neural Eng* 2008; **5**: 185-190
32 **Lin WC**, Sandberg DI, Bhatia S, Johnson M, Morrison G, Ragheb J. Optical spectroscopy for in-vitro differentiation of pediatric neoplastic and epileptogenic brain lesions. *J Biomed Opt* 2009; **14**: 014028
33 **Krafft** C, Sobottka SB, Schackert G, Salzer R. Near infrared Raman spectroscopic mapping of native brain tissue and intracranial tumors. *Analyst* 2005; **130**: 1070-1077
34 **Pogue BW**, Poplack SP, McBride TO, Wells WA, Osterman KS, Osterberg UL, Paulsen KD. Quantitative hemoglobin tomography with diffuse near-infrared spectroscopy: pilot results in the breast. *Radiology* 2001; **218**: 261-266
35 **Ntziachristos V**, Yodh AG, Schnall MD, Chance B. MRI-guided diffuse optical spectroscopy of malignant and benign breast lesions. *Neoplasia* 2002; **4**: 347-354
36 **Shah N**, Cerussi AE, Jakubowski D, Hsiang D, Butler J, Tromberg BJ. The role of diffuse optical spectroscopy in the clinical management of breast cancer. *Dis Markers* 2003; **19**: 95-105
37 **Hsiang D**, Shah N, Yu H, Su MY, Cerussi A, Butler J, Baick C, Mehta R, Nalcioglu O, Tromberg B. Coregistration of dynamic contrast enhanced MRI and broadband diffuse optical spectroscopy for characterizing breast cancer. *Technol Cancer Res Treat* 2005; **4**: 549-558
38 **Carpenter CM**, Pogue BW, Jiang S, Dehghani H, Wang X, Paulsen KD, Wells WA, Forero J, Kogel C, Weaver JB, Poplack SP, Kaufman PA. Image-guided optical spectroscopy provides molecular-specific information in vivo: MRI-guided spectroscopy of breast cancer hemoglobin, water, and scatterer size. *Opt Lett* 2007; **32**: 933-935
39 **Srinivasan S**, Pogue BW, Jiang S, Dehghani H, Kogel C, Soho S, Gibson JJ, Tosteson TD, Poplack SP, Paulsen KD. In vivo hemoglobin and water concentrations, oxygen saturation, and scattering estimates from near-infrared breast tomography using spectral reconstruction. *Acad Radiol* 2006; **13**: 195-202
40 **Culver JP**, Choe R, Holboke MJ, Zubkov L, Durduran T, Slemp A, Ntziachristos V, Chance B, Yodh AG. Three-dimensional diffuse optical tomography in the parallel plane transmission geometry: evaluation of a hybrid frequency domain/continuous wave clinical system for breast imaging. *Med Phys* 2003; **30**: 235-247
41 **Bigio IJ**, Bown SG, Briggs G, Kelley C, Lakhani S, Pickard D, Ripley PM, Rose IG, Saunders C. Diagnosis of breast cancer using elastic-scattering spectroscopy: preliminary clinical results. *J Biomed Opt* 2000; **5**: 221-228
42 **Haka AS**, Volynskaya Z, Gardecki JA, Nazemi J, Lyons J, Hicks D, Fitzmaurice M, Dasari RR, Crowe JP, Feld MS. In vivo margin assessment during partial mastectomy breast surgery using raman spectroscopy. *Cancer Res* 2006; **66**: 3317-3322
43 **Ramanujam N**, Brown J, Bydlon TM, Kennedy SA, Richards LM, Junker MK, Gallagher J, Barry WT, Wilke LG, Geradts J. Quantitative spectral reflectance imaging device for intraoperative breast tumor margin assessment. *Conf Proc IEEE Eng Med Biol Soc* 2009; **2009**: 6554-6556
44 **Keller MD**, Majumder SK, Kelley MC, Meszoely IM, Boulos FI, Olivares GM, Mahadevan-Jansen A. Autofluorescence and diffuse reflectance spectroscopy and spectral imaging for breast surgical margin analysis. *Lasers Surg Med* 2010; **42**: 15-23

45 **Manoharan R**, Shafer K, Perelman L, Wu J, Chen K, Deinum G, Fitzmaurice M, Myles J, Crowe J, Dasari RR, Feld MS. Raman spectroscopy and fluorescence photon migration for breast cancer diagnosis and imaging. *Photochem Photobiol* 1998; **67**: 15-22

46 **van Veen RL**, Amelink A, Menke-Pluymers M, van der Pol C, Sterenborg HJ. Optical biopsy of breast tissue using differential path-length spectroscopy. *Phys Med Biol* 2005; **50**: 2573-2581

47 **Yu B**, Burnside ES, Sisney GA, Harter JM, Zhu C, Dhalla AH, Ramanujam N. Feasibility of near-infrared diffuse optical spectroscopy on patients undergoing imageguided core-needle biopsy. *Opt Express* 2007; **15**: 7335-7350

48 **Zhu C**, Burnside ES, Sisney GA, Salkowski LR, Harter JM, Yu B, Ramanujam N. Fluorescence spectroscopy: an adjunct diagnostic tool to image-guided core needle biopsy of the breast. *IEEE Trans Biomed Eng* 2009; **56**: 2518-2528

49 **Chidananda SM**, Satyamoorthy K, Rai L, Manjunath AP, Kartha VB. Optical diagnosis of cervical cancer by fluorescence spectroscopy technique. *Int J Cancer* 2006; **119**: 139-145

50 **Mitchell MF**, Cantor SB, Ramanujam N, Tortolero-Luna G, Richards-Kortum R. Fluorescence spectroscopy for diagnosis of squamous intraepithelial lesions of the cervix. *Obstet Gynecol* 1999; **93**: 462-470

51 **Murali Krishna C**, Sockalingum GD, Vidyasagar MS, Manfait M, Fernanades DJ, Vadhiraja BM, Maheedhar K. An overview on applications of optical spectroscopy in cervical cancers. *J Cancer Res Ther* 2008; **4**: 26-36

52 **Cardenas-Turanzas M**, Freeberg JA, Benedet JL, Atkinson EN, Cox DD, Richards-Kortum R, MacAulay C, Follen M, Cantor SB. The clinical effectiveness of optical spectroscopy for the in vivo diagnosis of cervical intraepithelial neoplasia: where are we? *Gynecol Oncol* 2007; **107**: S138-S146

53 **Bazant-Hegemark F**, Edey K, Swingler GR, Read MD, Stone N. Review: optical micrometer resolution scanning for non-invasive grading of precancer in the human uterine cervix. *Technol Cancer Res Treat* 2008; **7**: 483-496

54 **Drezek RA**, Richards-Kortum R, Brewer MA, Feld MS, Pitris C, Ferenczy A, Faupel ML, Follen M. Optical imaging of the cervix. *Cancer* 2003; **98**: 2015-2027

55 **Chang SK**, Marin N, Follen M, Richards-Kortum R. Model-based analysis of clinical fluorescence spectroscopy for in vivo detection of cervical intraepithelial dysplasia. *J Biomed Opt* 2006; **11**: 024008

56 **Chang VT**, Cartwright PS, Bean SM, Palmer GM, Bentley RC, Ramanujam N. Quantitative physiology of the precancerous cervix in vivo through optical spectroscopy. *Neoplasia* 2009; **11**: 325-332

57 **Aerts JG**, Amelink A, van der Leest C, Hegmans JP, Hemmes A, den Hamer B, Sterenborg HC, Hoogsteden HC, Lambrecht BN. HIF1a expression in bronchial biopsies correlates with tumor microvascular saturation determined using optical spectroscopy. *Lung Cancer* 2007; **57**: 317-321

58 **Yamazaki H**, Kaminaka S, Kohda E, Mukai M, Hamaguchi HO. The diagnosis of lung cancer using 1064-nm excited near-infrared multichannel Raman spectroscopy. *Radiat Med* 2003; **21**: 1-6

59 **Huang Z**, McWilliams A, Lui H, McLean DI, Lam S, Zeng H. Near-infrared Raman spectroscopy for optical diagnosis of lung cancer. *Int J Cancer* 2003; **107**: 1047-1052

60 **Zeng H**, Petek M, Zorman MT, McWilliams A, Palcic B, Lam S. Integrated endoscopy system for simultaneous imaging and spectroscopy for early lung cancer detection. *Opt Lett* 2004; **29**: 587-589

61 **Zeng H**, Fawzy YS, Short MA, Tercelj M, McWilliams A, Petek M, Palcic B, Zhao J, Lui H, Lam S. Combining field imaging endoscopy with point analysis spectroscopy for improving early lung cancer detection. *Conf Proc IEEE Eng Med Biol Soc* 2008; **2008**: 1849-1850

62 **Kawabata T**, Mizuno T, Okazaki S, Hiramatsu M, Setoguchi T, Kikuchi H, Yamamoto M, Hiramatsu Y, Kondo K, Baba M, Ohta M, Kamiya K, Tanaka T, Suzuki S, Konno H. Optical diagnosis of gastric cancer using near-infrared multichannel Raman spectroscopy with a 1064-nm excitation wavelength. *J Gastroenterol* 2008; **43**: 283-290

63 **Teh SK**, Zheng W, Ho KY, Teh M, Yeoh KG, Huang Z. Diagnosis of gastric cancer using near-infrared Raman spectroscopy and classification and regression tree techniques. *J Biomed Opt* 2008; **13**: 034013

64 **Teh SK**, Zheng W, Ho KY, Teh M, Yeoh KG, Huang Z. Near-infrared Raman spectroscopy for optical diagnosis in the stomach: identification of Helicobacter-pylori infection and intestinal metaplasia. *Int J Cancer* 2010; **126**: 1920-1927

65 **Teh SK**, Zheng W, Ho KY, Teh M, Yeoh KG, Huang Z. Near-infrared Raman spectroscopy for early diagnosis and typing of adenocarcinoma in the stomach. *Br J Surg* 2010; **97**: 550-557

66 **Mayinger B**, Jordan M, Horbach T, Horner P, Gerlach C, Mueller S, Hohenberger W, Hahn EG. Evaluation of in vivo endoscopic autofluorescence spectroscopy in gastric cancer. *Gastrointest Endosc* 2004; **59**: 191-198

67 **Wang HW**, Jiang JK, Lin CH, Lin JK, Huang GJ, Yu JS. Diffuse reflectance spectroscopy detects increased hemoglobin concentration and decreased oxygenation during colon carcinogenesis from normal to malignant tumors. *Opt Express* 2009; **17**: 2805-2817

68 **Roy HK**, Gomes AJ, Ruderman S, Bianchi LK, Goldberg MJ, Stoyneva V, Rogers JD, Turzhitsky V, Kim Y, Yen E, Jameel M, Bogojevic A, Backman V. Optical measurement of rectal microvasculature as an adjunct to flexible sigmoidosocopy: gender-specific implications. *Cancer Prev Res* (Phila) 2010; **3**: 844-851

69 **Dhar A**, Johnson KS, Novelli MR, Bown SG, Bigio IJ, Lovat LB, Bloom SL. Elastic scattering spectroscopy for the diagnosis of colonic lesions: initial results of a novel optical biopsy technique. *Gastrointest Endosc* 2006; **63**: 257-261

70 **Zonios G**, Perelman LT, Backman V, Manoharan R, Fitzmaurice M, Van Dam J, Feld MS. Diffuse reflectance spectroscopy of human adenomatous colon polyps in vivo. *Appl Opt* 1999; **38**: 6628-6637

71 **Stone N**, Kendall C, Smith J, Crow P, Barr H. Raman spectroscopy for identification of epithelial cancers. *Faraday Discuss* 2004; **126**: 141-157; discussion 169-183

72 **Widjaja E**, Zheng W, Huang Z. Classification of colonic tissues using near-infrared Raman spectroscopy and support vector machines. *Int J Oncol* 2008; **32**: 653-662

73 **Beljebbar A**, Bouché O, Diébold MD, Guillou PJ, Palot JP, Eudes D, Manfait M. Identification of Raman spectroscopic markers for the characterization of normal and adenocarcinomatous colonic tissues. *Crit Rev Oncol Hematol* 2009; **72**: 255-264

74 **Lualdi M**, Colombo A, Leo E, Morelli D, Vannelli A, Battaglia L, Poiasina E, Marchesini R. Natural fluorescence spectroscopy of human blood plasma in the diagnosis of colorectal cancer: feasibility study and preliminary results. *Tumori* 2007; **93**: 567-571

75 **Dekker E**, Fockens P. Advances in colonic imaging: new endoscopic imaging methods. *Eur J Gastroenterol Hepatol* 2005; **17**: 803-808

76 **Wallace MB**, Kiesslich R. Advances in endoscopic imaging of colorectal neoplasia. *Gastroenterology* 2010; **138**: 2140-2150

77 **Moglia A**, Menciassi A, Dario P, Cuschieri A. Capsule endoscopy: progress update and challenges ahead. *Nat Rev Gastroenterol Hepatol* 2009; **6**: 353-362

78 **Sharma V**, Kashyap D, Mathker A, Narvenkar S, Bensalah K, Kabbani W, Tuncel A, Cadeddu JA, Liu H. Optical reflectance spectroscopy for detection of human prostate cancer. *Conf Proc IEEE Eng Med Biol Soc* 2009; **2009**: 118-121

79 **Crow P**, Molckovsky A, Stone N, Uff J, Wilson B, Wong-KeeSong LM. Assessment of fiberoptic near-infrared raman spectroscopy for diagnosis of bladder and prostate cancer. *Urology* 2005; **65**: 1126-1130

80 **Salomon G**, Hess T, Erbersdobler A, Eichelberg C, Greschner

S, Sobchuk AN, Korolik AK, Nemkovich NA, Schreiber J, Herms M, Graefen M, Huland H. The feasibility of prostate cancer detection by triple spectroscopy. *Eur Urol* 2009; **55**: 376-383
81 **Zhu TC**, Finlay JC, Hahn SM. Determination of the distribution of light, optical properties, drug concentration, and tissue oxygenation in-vivo in human prostate during motexafin lutetium-mediated photodynamic therapy. *J Photochem Photobiol B* 2005; **79**: 231-241
82 **Yu G**, Durduran T, Zhou C, Zhu TC, Finlay JC, Busch TM, Malkowicz SB, Hahn SM, Yodh AG. Real-time in situ monitoring of human prostate photodynamic therapy with diffuse light. *Photochem Photobiol* 2006; **82**: 1279-1284
83 **Zaak D**, Sroka R, Khoder W, Adam C, Tritschler S, Karl A, Reich O, Knuechel R, Baumgartner R, Tilki D, Popken G, Hofstetter A, Stief CG. Photodynamic diagnosis of prostate cancer using 5-aminolevulinic acid--first clinical experiences. *Urology* 2008; **72**: 345-348
84 **Hanchanale VS**, Rao AR, Das S. Raman spectroscopy and its urological applications. *Indian J Urol* 2008; **24**: 444-450
85 **Manyak MJ**, Javitt M, Kang PS, Kreuger WR, Storm ES. The evolution of imaging in advanced prostate cancer. *Urol Clin North Am* 2006; **33**: 133-146, v
86 **Zonios G**, Dimou A, Bassukas I, Galaris D, Tsolakidis A, Kaxiras E. Melanin absorption spectroscopy: new method for noninvasive skin investigation and melanoma detection. *J Biomed Opt* 2008; **13**: 014017
87 **Marchesini R**, Bono A, Carrara M. In vivo characterization of melanin in melanocytic lesions: spectroscopic study on 1671 pigmented skin lesions. *J Biomed Opt* 2009; **14**: 014027
88 **Sterenborg H**, Motamedi M, Wagner RF, Duvic M, Thomsen S, Jacques SL. In vivo fluorescence spectroscopy and imaging of human skin tumors. *Lasers Med Sci* 1994; **9**: 191-201
89 **Brancaleon L**, Durkin AJ, Tu JH, Menaker G, Fallon JD, Kollias N. In vivo fluorescence spectroscopy of nonmelanoma skin cancer. *Photochem Photobiol* 2001; **73**: 178-183
90 **Panjehpour M**, Julius CE, Phan MN, Vo-Dinh T, Overholt S. Laser-induced fluorescence spectroscopy for in vivo diagnosis of non-melanoma skin cancers. *Lasers Surg Med* 2002; **31**: 367-373
91 **Han X**, Lui H, McLean DI, Zeng H. Near-infrared autofluorescence imaging of cutaneous melanins and human skin in vivo. *J Biomed Opt* 2009; **14**: 024017
92 **Lieber CA**, Majumder SK, Ellis DL, Billheimer DD, Mahadevan-Jansen A. In vivo nonmelanoma skin cancer diagnosis using Raman microspectroscopy. *Lasers Surg Med* 2008; **40**: 461-467
93 **Zhao J**, Lui H, McLean DI, Zeng H. Real-time Raman spectroscopy for non-invasive skin cancer detection - preliminary results. *Conf Proc IEEE Eng Med Biol Soc* 2008; **2008**: 3107-3109
94 **Eikje NS**, Aizawa K, Ozaki Y. Vibrational spectroscopy for molecular characterisation and diagnosis of benign, premalignant and malignant skin tumours. *Biotechnol Annu Rev* 2005; **11**: 191-225
95 **Krafft C**, Steiner G, Beleites C, Salzer R. Disease recognition by infrared and Raman spectroscopy. *J Biophotonics* 2009; **2**: 13-28
96 **Mogensen M**, Jemec GB. Diagnosis of nonmelanoma skin cancer/keratinocyte carcinoma: a review of diagnostic accuracy of nonmelanoma skin cancer diagnostic tests and technologies. *Dermatol Surg* 2007; **33**: 1158-1174
97 **Zonios G**, Bykowski J, Kollias N. Skin melanin, hemoglobin, and light scattering properties can be quantitatively assessed in vivo using diffuse reflectance spectroscopy. *J Invest Dermatol* 2001; **117**: 1452-1457
98 **Sokolov K**, Follen M, Richards-Kortum R. Optical spectroscopy for detection of neoplasia. *Curr Opin Chem Biol* 2002; **6**: 651-658
99 **Zhao J**, Lui H, McLean DI, Zeng H. Integrated real-time Raman system for clinical in vivo skin analysis. *Skin Res Technol* 2008; **14**: 484-492
100 **Huang Z**, Zeng H, Hamzavi I, McLean DI, Lui H. Rapid near-infrared Raman spectroscopy system for real-time in vivo skin measurements. *Opt Lett* 2001; **26**: 1782-1784
101 **Huang Z**, Teh SK, Zheng W, Mo J, Lin K, Shao X, Ho KY, Teh M, Yeoh KG. Integrated Raman spectroscopy and trimodal wide-field imaging techniques for real-time in vivo tissue Raman measurements at endoscopy. *Opt Lett* 2009; **34**: 758-760
102 **Benaron DA**, Parachikov IH, Cheong WF, Friedland S, Rubinsky BE, Otten DM, Liu FW, Levinson CJ, Murphy AL, Price JW, Talmi Y, Weersing JP, Duckworth JL, Hörchner UB, Kermit EL. Design of a visible-light spectroscopy clinical tissue oximeter. *J Biomed Opt* 2005; **10**: 44005
103 **ViOptix I**. ODISsey™ Tissue Oximeter. 2010. Available from: URL: http://www.vioptix.com/docs/technology/product.asp
104 **Uedo N**, Iishi H, Tatsuta M, Yamada T, Ogiyama H, Imanaka K, Sugimoto N, Higashino K, Ishihara R, Narahara H, Ishiguro S. A novel videoendoscopy system by using autofluorescence and reflectance imaging for diagnosis of esophagogastric cancers. *Gastrointest Endosc* 2005; **62**: 521-528
105 **Osawa H**, Yamamoto H, Yamada N, Yoshizawa M, Sunada K, Kita H, Ajibe H, Satoh K, Sugano K. Diagnosis of endoscopic Barrett's esophagus by transnasal flexible spectral imaging color enhancement. *J Gastroenterol* 2009; **44**: 1125-1132
106 **Kendrick JE**, Huh WK, Alvarez RD. LUMA cervical imaging system. *Expert Rev Med Devices* 2007; **4**: 121-129
107 **Liu Q**, Vo-Dinh T. Spectral filtering modulation method for estimation of hemoglobin concentration and oxygenation based on a single fluorescence emission spectrum in tissue phantoms. *Med Phys* 2009; **36**: 4819-4829
108 **Nakao M**, Yoshida S, Tanaka S, Takemura Y, Oka S, Yoshihara M, Chayama K. Optical biopsy of early gastroesophageal cancer by catheter-based reflectance-type laser-scanning confocal microscopy. *J Biomed Opt* 2008; **13**: 054043
109 **Seo I**, You JS, Hayakawa CK, Venugopalan V. Perturbation and differential Monte Carlo methods for measurement of optical properties in a layered epithelial tissue model. *J Biomed Opt* 2007; **12**: 014030
110 **Li X**, Chen Z, Taflove A, Backman V. Equiphase-sphere approximation for light scattering by stochastically inhomogeneous microparticles. *Phys Rev E Stat Nonlin Soft Matter Phys* 2004; **70**: 056610
111 **Shah N**, Gibbs J, Wolverton D, Cerussi A, Hylton N, Tromberg BJ. Combined diffuse optical spectroscopy and contrast-enhanced magnetic resonance imaging for monitoring breast cancer neoadjuvant chemotherapy: a case study. *J Biomed Opt* 2005; **10**: 051503

S- Editor Cheng JX **L- Editor** Webster JR **E- Editor** Ma WH

World Journal of Clinical Oncology

Online Submissions: http://www.wjgnet.com/2218-4333office
wjco@wjgnet.com
doi:10.5306/wjco.v2.i1.64

World J Clin Oncol 2011 January 10; 2(1): 64-72
ISSN 2218-4333 (online)

TOPIC HIGHLIGHT

E YK Ng, PhD, PGDTHE, Associate Professor, *Series Editor*

Optical mammography: Diffuse optical imaging of breast cancer

Kijoon Lee

Kijoon Lee, Division of Bioengineering, School of Chemical and Biomedical Engineering, Nanyang Technological University, Singapore 637457, Singapore
Author contributions: Lee K is the sole author of this review paper.
Correspondence to: Dr. Kijoon Lee, PhD, Division of Bioengineering, School of Chemical and Biomedical Engineering, Nanyang Technological University, 70 Nanyang, Singapore 637457, Singapore. kjlee@ntu.edu.sg
Telephone: + 65-63162894 Fax: + 65-67911761
Received: August 10, 2010 Revised: November 1, 2010
Accepted: November 8, 2010
Published online: January 10, 2011

Abstract

Existing imaging modalities for breast cancer screening, diagnosis and therapy monitoring, namely X-ray mammography and magnetic resonance imaging, have been proven to have limitations. Diffuse optical imaging is a set of non-invasive imaging modalities that use near-infrared light, which can be an alternative, if not replacement, to those existing modalities. This review covers the background knowledge, recent clinical outcome, and future outlook of this newly emerging medical imaging modality.

Key words: Diffuse optical imaging; Diffuse optical spectroscopy; Breast cancer; Optical mammography; Therapy monitoring

Peer reviewer: Yun Gong, MD, Associate Professor, Department of Pathology, Unit 53, The University of Texas, M D Anderson Cancer Center, 1515 Holcombe Blvd, Houston, TX 77030, United States

Lee K. Optical mammography: Diffuse optical imaging of breast cancer. *World J Clin Oncol* 2011; 2(1): 64-72 Available from: URL: http://www.wjgnet.com/2218-4333/full/v2/i1/64.htm DOI: http://dx.doi.org/10.5306/wjco.v2.i1.64

INTRODUCTION

All women who reach a certain age are recommended to undergo annual breast cancer screening, although policies vary according to the country. The modality of choice for screening is mostly X-ray mammography. However, many clinical studies have cast doubt on its use. For women under 40 years of age, X-ray mammography is known to be ineffective because of the high radiographic density of young breasts[1,2]. Also, the dose of radioactivity that the patient receives every year for screening could cause cancer, which defeats the purpose of screening. There are other imaging modalities such as ultrasound or magnetic resonance imaging (MRI) that can be used in addition to X-ray mammography, but each of them has its own drawback[3]. Ultrasound has low sensitivity, especially before the tumor becomes hardened, whereas MRI has limited specificity and high cost of operation[4]. Other breast-specific imaging modalities are also being developed, such as breast computed tomography (bCT)[5,6] and breast positron emission tomography (bPET)[7,8], but their high cost and instrumental complexity are a hindrance to general use.

Diffuse optical imaging (DOI) is being studied extensively worldwide as a possible alternative to the breast imaging modalities mentioned above. DOI uses a set of optical transmission measurements on various positions on the sample surface, by which one can reconstruct a 3D map of the inner optical properties of the sample, namely absorption and scattering coefficients. Multispectral measurement using multiple wavelengths in the 650-900-nm range makes it possible to convert the optical property maps into the concentration maps of intrinsic absorbers, such as oxyhemoglobin (HbO_2), deoxy-hemoglobin (Hb), water, and

lipid. Such 3D maps of hemodynamic parameters serve as indicators of malignant tumors, as it is known that tumor position is strongly correlated with total hemoglobin concentration *via* angiogenesis.

In this review, the concept of DOI is introduced, current clinical applications are explained, and its future outlook is presented. A detailed theory of how to model the propagation of photons in highly scattering media and how to reconstruct 3D images out of a finite number of surface measurements is out of the scope of this paper, although a few basic equations and remarks are given in the next section. For a more comprehensive review on DOI with detailed theory, including diffuse correlation spectroscopy (DCS) that measures deep tissue blood flow, see the excellent earlier reviews by Choe *et al*[9] (breast application only) or Durduran *et al*[10] (breast, brain and other applications).

RATIONALE

Background theory

The name DOI comes from the fact that photons propagate through highly scattering media in a diffusive manner, and that we are using the diffusion model for deep tissue imaging. There are many variants in naming conventions: diffuse optical spectroscopy (DOS) or near-infrared spectroscopy (NIRS) is used for a low number of source-detector pairs, and diffuse optical tomography (DOT) is used when actual 3D imaging is attempted and final images are shown in tomographic slices. In this paper, we stick to the general term DOI to represent many variants in the literature.

The photon propagation best resembles diffusion when absorption is much smaller than scattering ($\mu_a << \mu_s'$), and when source-detector separation is not too close. We can regard the diffusion model for photon propagation as a simplification of a more general radiative transfer equation in a limiting condition[11,12].

The photon diffusion equation, which is the starting point of DOI, is described below:

$$\nabla \cdot \left(D \nabla \Phi\left(\vec{r},t\right)\right) - \nu \mu_a \Phi\left(\vec{r},t\right) + \nu S\left(\vec{r},t\right) = \frac{\partial \Phi\left(\vec{r},t\right)}{\partial t}$$

Here D is the photon diffusion coefficient, μ_a is the absorption coefficient, Φ is the photon fluence rate, ν is the speed of light in the medium, and S is the source term. This equation is identical to the classical diffusion equation except for the presence of an absorption term. Therefore, given the spatial distribution of D and μ_a, one can calculate the fluence rate at all positions with arbitrary precision, given the source and boundary condition. The diffusion coefficient D is related to the reduced scattering coefficient μ_s' by $D = \nu/3\ (\mu_a + \mu_s')$, which results in $D \approx \nu/3\mu_s'$ when absorption is negligible compared to scattering. Note that the reduced scattering coefficient (μ_s', reciprocal of transport length) is different from the scattering coefficient (μ_s, reciprocal of scattering length), but still represents the magnitude of scattering.

When absorption (μ_a) and scattering (μ_s') is distributed homogeneously, the above equation can be solved analytically for such simple geometries as bulk, half-space, slab, cylinder or even sphere[13]. The half-space solution is especially important because many practical DOI probes are accessing the sample from one side, either by a pair of optical fibers or by free-space coupling. When half-space geometry is assumed, the sensitivity volume inside the sample can be calculated by multiplying light fluence rate distribution from the source fiber with the probability distribution of a photon's original position that reaches the detector fiber (Figure 1). The sensitivity volume has a banana-shape pattern, and we can take note of several important features of DOI from this: (1) in half-space geometry, the probing depth of a source-detector pair is roughly one half of the source-detector distance; (2) the sensitivity always peaks right beneath the source and detector fiber; (3) there is a dead volume above the banana shape to which the diffuse optical probe is not sensitive; and (4) measurement from a single source-detector pair can detect the overall change of optical property within the sensitivity volume, but it does not tell us where the change has occurred within that volume. One would need many source-detector pairs whose sensitivity volumes partially overlap within the diffuse medium, in order to attempt finer localization of the optical property change. It suggests there has to be many source-detector pairs to increase the resolving power of DOI.

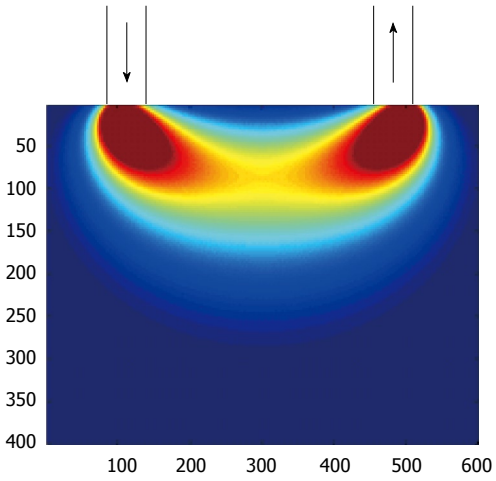

Figure 1 Sensitivity function of a single source-detector pair, calculated by analytical half-space Green's function of photon diffusion equation. The most sensitive position appears to be the region directly below the source and detector.

Instrumentation

Although all diffuse optical instruments share a similar look in terms of probe geometry, there are three different categories in which an instrument works, namely continuous wave (CW), frequency domain (FD) and time domain (TD). The types of light source and detector are vastly different across the category. In terms of light source, CW uses continuous wave or low-frequency modulated laser diode or light-emitting diodes, FD uses RF-modulated laser diodes, and TD uses short-duration pulsed laser. Detectors need to be different accordingly, because FD requires either in-phase quadrature (IQ) demodulation or a frequen-

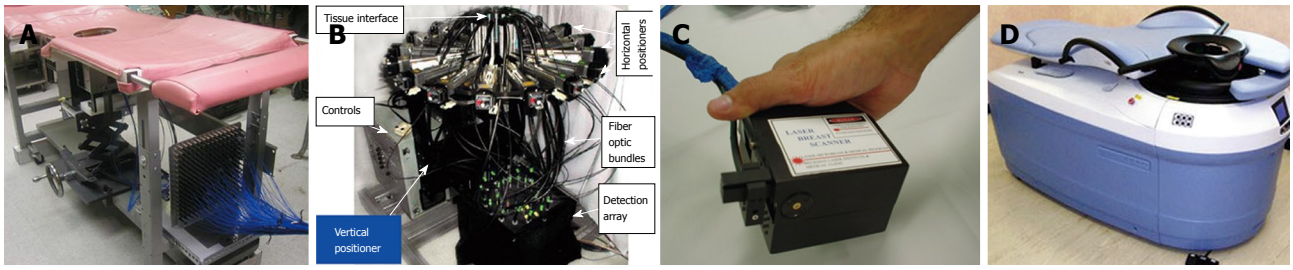

Figure 2 Various types of diffuse optical imaging instruments. A: Parallel plate frequency-domain instrument from University of Pennsylvania; B: Ring-type frequency-domain system from Dartmouth; C: Hand-held scanning system from University of California at Irvine; D: Time-domain multispectral transmission type from ART, Canada.

cy-lowering technique (homodyne/heterodyne) for phase-sensitive measurement, and TD requires photon-counting detectors to obtain time-point-spread-function (TPSF). The complexity of instruments increases towards the TD type, but the level of information per source-detector pair also increases accordingly. Therefore, users have to decide on which type of DOI best suits their application.

Some examples of different breast DOI instruments are given in Figure 2. The Yodh group in the University of Pennsylvania has built a series of parallel plate transmission geometry CW + FD instruments that acquire a lot of data using fast CCD[14,15]; the Pogue group from Dartmouth College has developed a three-tier, ring-type, fiber-based FD instrument[16,17], whereas the Tromberg group from University of California, Irvine has developed a hand-held scanning FD DOI device to be used with supine position breasts[18,19]. A Canadian company, ART, has also developed a time-domain transmission DOI device based on scanning fibers and photomultiplier tubes, and clinical trials are underway[20].

Image reconstruction and artifact issues

The way visual images are reconstructed from raw optical transmission data in DOI is very different from that of MRI or X-ray CT. As opposed to those established medical imaging modalities where an exact mathematical relationship exists, by which one can transform the measured data into images for visualization, there has been no consensus in the DOI community as to how we should reconstruct diffuse optical images. This is partly because there is no standard instrument specification shared across institutions, but mostly because of the fact that diffuse optical image reconstruction is an optimization problem solving process of an ill-posed and usually under-determined system. In more specific terms, DOI image reconstruction is equivalent to finding out a spatial distribution of variables that minimizes the discrepancy between experimental measurement and calculated fluence rates. The discrepancy can be defined as an objective function written below:

$$\chi^2 = \sum_{s,d} \left[\Phi_M - \Phi_C(\mu_a(\vec{r}), \mu_s'(\vec{r})) \right]^2$$

Where subscripts *M* and *C* refer to measurement and calculation, respectively, and summation is done over all available source-detector pairs. Detailed forms of the objective function can vary depending on the types of regularization used, the types of weighting used, and also on whether multispectral measurement is used. In order to minimize this objective function, one normally uses iterative methods to update μ_a and μ_s' distributions towards the global minimum. Some examples of the reconstructed images are shown in Figure 3, where 3D distribution of absorption coefficients at a single wavelength is reconstructed from a breast-mimicking phantom and a real patient breast with a malignant tumor[21]. The absorption contrasts hidden in a diffuse medium is clearly seen in both cases.

Much effort has been put into developing fast, accurate, and stable optimization algorithms with given constraints from various DOI instruments[22,23], and hence resulted in a plethora of DOI image reconstruction algorithms: linear and non-linear methods, analytical and numerical methods, and line search and trust region methods. One recent development by Konecky *et al*[24] in linear analytical reconstruction is noteworthy, because it presents a way to solve a large data problem in a fast and memory-efficient way. When the boundary geometry of the diffuse medium has translational or rotational symmetry (infinite slab or cylinder, respectively), one can find a (spatial) Fourier domain representation of the solution of the photon diffusion equation, and linear inversion is very efficiently carried out. A high-resolution diffuse optical image is obtained using this algorithm from a large data set from consecutive transmission measurements from source-detector positions on a very fine grid, and it shows even sub-centimeter structures of complex-shaped target phantoms. Although this algorithm has limitations of being a linear reconstruction and has limited applicable boundary geometry, it provides a way to reconstruct systematically an image with relatively few arbitrary factors to tweak, and its application in actual breast cancer imaging is highly anticipated.

The lack of standard procedure in diffuse optical image reconstruction makes it challenging for the beginners to read and compare diffuse optical images correctly. No two research groups have used the same algorithm and protocol, until recent endeavor among the DOI community to standardize various algorithms into sharable packages such as NIRFAST[25,26], TOAST[22,27], and PMI toolbox[28]. To date, all the above software packages are available in MatLab, so that even beginners in programming can use them.

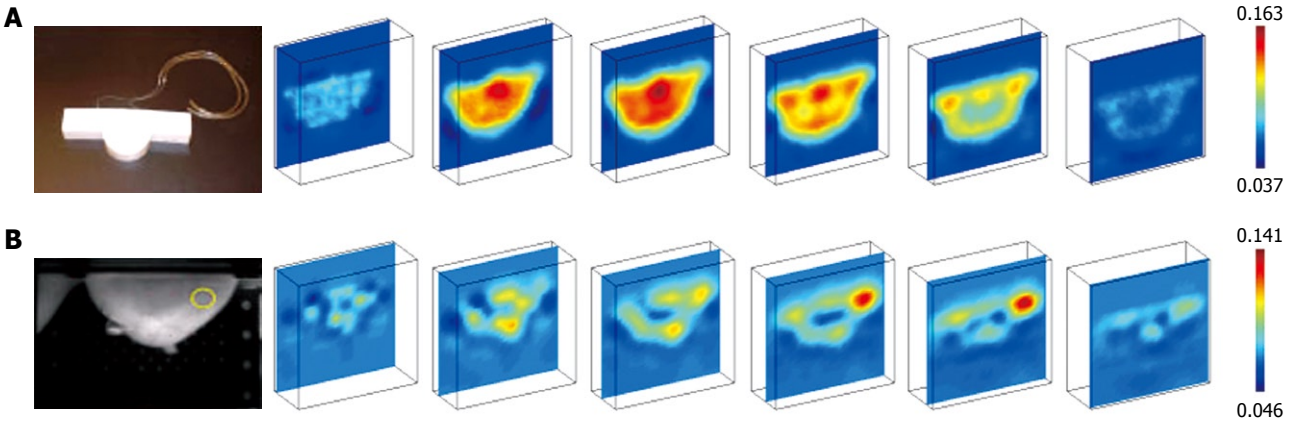

Figure 3 Example of 3D diffuse optical imaging images. A: Silicone phantom that mimics human breast; B: Actual human breast with a malignant tumor in the upper right region (from Lee *et al*[21]).

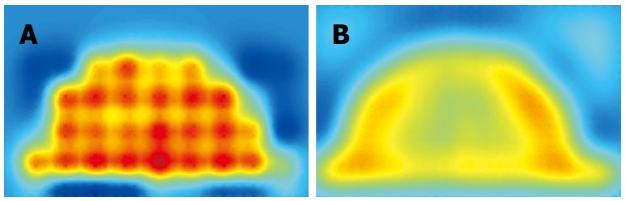

Figure 4 Example of diffuse optical imaging artifacts related to source positions. The images are single slices of 3D diffuse optical imaging (DOI) reconstruction that is parallel and close to 9 × 5 source grid positions, (A) before and (B) after applying the spatially dependent regularization. The target is a breast mimicking phantom made of silicone.

No matter what package you use for diffuse optical image reconstruction, there is an important issue that users of such images should bear in mind. It is about the possible image artifact that is specific to DOI, and also about the method of suppressing such artifacts. For example, the first image in Figure 4 shows many highly absorbing points that appear as a grid pattern. This happens because this reconstructed slice is very close to a plate that holds 9 × 5 source optical fibers. As explained earlier, positions right beneath the source and detector fibers have the highest sensitivity, and those volumes are updated preferentially in the iterative optimization process. When initial values in iterative reconstruction are set to a lower value than the real average absorption coefficient, all the positions in non-sensitive regions stay at the initial values, and only the points within an appreciable sensitivity volume keep increasing, which results in a grid-like pattern in Figure 4A.

Inverse problem solving generally has issues of unwanted high-frequency noise that starts to appear with many iterations, and researchers use regularization methods to suppress the image noise. One way to suppress source and detector position-specific noise, as shown in Figure 4A, is to use spatially dependent regularization in such a way that high-frequency noise close to the source and detector plane are penalized more than those points deep inside the volume. Figure 4B shows a reconstructed image of the same slice after the regularization treatment[29]. Another way to suppress source and detector artifacts is to let the coupling coefficient values float during reconstruction, so that the algorithm finds the best source and detector coupling coefficients on its own[30]. It is usually difficult to know exactly the coupling coefficient due to optical probe contact problems (for probes in contact) and surface irregularity of *in vivo* samples (for non-contact probes), therefore, it makes sense to leave them as unknowns and use optimization algorithms to find them.

CLINICAL OUTCOMES

Assessing normal breast tissue properties

DOI is used in breast cancer imaging under the assumption that there is an optical property contrast between the cancerous and normal tissue. Therefore, early studies were focused on determining optical properties of normal breasts to serve as a baseline[31-38]. However, the optical properties of normal breast tissue vary significantly depending on age, body-mass index (BMI), breast size, and hormonal status. Therefore, one needs to understand the relationship between optical properties and those surrogate markers listed above, to apply DOI properly in cancer imaging. The most noticeable dependency is found between total hemoglobin concentration (THC) and BMI[31,35,39]. They are inversely related because high BMI generally means more adipose tissue, which has less blood supply than glandular tissue. It should be mentioned that we still need more systematic DOI studies on normal breast tissue, because most of the studies listed above are limited to Europe and North America, and the instrument and measurement protocols are not standardized.

Detection and characterization of breast tumors

The optical property contrast from endogenous chromophores (Hb, HbO_2, water, and lipid) has been shown to be significant enough to distinguish cancerous from normal tissue. The most prominent indicator for cancerous tissue is high THC, as reported by most of the DOI research groups[32,40-42]. The physiology behind this has to do with angiogenesis that accompanies malignant tumor growth, and some groups have actually measured microvessel den-

sities to prove it more directly[40,43]. Also, increase in scattering coefficient has been observed in cancerous tissue, which can be explained by rapid cell proliferation and an increase in the number of cell organelles[43-46].

Another important marker for cancer detection is tissue oxygenation (StO_2), because malignant tumor normally elevates the level of oxygen metabolic rate. However, the DOI literature has contrasting reports on StO_2 in cancerous tissue. A decrease of StO_2 has been reported by some groups[47-49], whereas no statistically significant changes have been reported by others[19,20,42,45,50]. This discrepancy could be attributable to the fact that tissue oxygenation differs depending on cancer stage and type.

Multiple physiological parameters show contrast between tumor and normal tissue, therefore, some groups have proposed the use of a customized optical index to maximize the contrast. Choe *et al*[46] have proposed an optical index defined as $rTHC \times r\mu_s'/rStO_2$, where *r* stands for relative value. They have seen an average twofold increase in optical index in 41 malignant tumor cases. It is hard to apply this optical index to general DOI data, because that clinical result was based on a unique parallel-plate CW/RF hybrid DOI instrument[51] with a fine-tuned, non-linear image reconstruction algorithm that incorporated a spatially variant[52] and envelope-guided[53] regularization scheme. However, it was still a meaningful attempt to devise an optical index that not only increases the tumor-to-normal contrast, but also has a physiological foundation.

If patients do not mind receiving an injection, an exogenous chromophore or fluorophore can be injected to improve tumor contrast. Indocyanine green (ICG) is an FDA-approved blood-pooling agent that is popular in the DOI community, and it has been shown to enhance tumor contrast significantly *via* enhanced absorption[54-56]. The fluorescence signal from ICG can also be used to enhance the accuracy of DOI, as shown by the Sevick-Muraca group in breast phantom and canine mammary tumors[57,58] and by the Yodh group in human breast[59].

Sensitivity, specificity, and receiver operating characteristic curve

When a new diagnostic tool is developed, one normally asks about its sensitivity and specificity. However, such quantities can only be defined in dichotomous tests where the output is either true or false (positive or negative) as shown in Table 1[60]. The physiological parameters that DOI provides are continuous variables (THC and StO_2, for example), and thus, one cannot define sensitivity or specificity until a cut-off value is determined. That is why many DOI studies have displayed their results in receiver operating characteristic (ROC) curves rather than showing a single pair of sensitivity and specificity values[47]. The ROC curve is a 2D plot in which the sensitivity (or true positive rate), is plotted against 1-specificity (or false positive rate). The ROC curve shows the overall behavior of sensitivity and specificity for all possible threshold values, and its area under the curve (AUC) serves as an indicator of how effective the imaging modality is, in terms of differentiating malignant from benign lesions. The maximum possible value of AUC is 1, where disease group is totally separated from healthy group, whereas the minimum possible value of AUC is 0.5, where two groups completely overlap.

Table 1 Results of a dichotomous test in a 2 × 2 table

	Gold standard	
	Positive (disease)	Negative (no disease)
Test		
Positive	TP	FP
Negative	FN	TN

Sensitivity = TP/(TP + FN); specificity = TN/(TN + FP). TP: True-positive; FP: False-positive; FN: False-negative; TN: True-negative.

As an example, Choe *et al*[46] have shown an AUC of 0.98 from the contrast of THC and 0.57 from the contrast of StO_2 between malignant and benign lesions. This shows that THC is a more useful marker for malignancy assessment than StO_2. In the ROC curve of THC, a threshold value of $rTHC = 1.06$ gives a sensitivity of 98% and a specificity of 90%.

Therapy monitoring

Neoadjuvant chemotherapy (NAC) has become an established form of breast cancer treatment[61]. Normally, it is prescribed for patients with locally advanced breast cancer to downstage the disease to make it operable, but now it is also used for operable cases to achieve better cosmesis. Two of the landmark trials were the National Surgical Adjuvant Breast and Bowel Project (NSABP) B-18[61] and European Organization for Research and Treatment of Cancer study 10902[62], which have demonstrated that NAC allows more patients to undergo breast-preserving surgery. NAC also allows us to acquire early information on the physiological response and mechanism of a disease. Therefore, it is crucial to develop a convenient non-invasive imaging method to monitor NAC, which will enable oncologists to optimize the treatment protocol.

Many different imaging modalities have been used to assess the tumor response during NAC, including X-ray mammography, ultrasound, MRI, and FDG-PET[63]. However, each modality has significant limitations to be used successfully as an NAC monitoring instrument. DOI, in contrast, is based on low-power, near-infrared light and is particularly suitable for this purpose. It is non-invasive, portable, and relatively cost-effective. DOI also allows frequent measurements with few space constraints, which enables doctors to obtain an immediate feedback that is useful for tailoring the treatment protocols to fit individual patients. Especially for such drugs as anti-angiogenic agents, frequent DOI monitoring can be a great help in strategizing the timing of treatment.

Many DOI research groups have performed NAC monitoring studies successfully. Since its first report by the Tromberg group in University of California, Irvine[32], the Yodh group in University of Pennsylvania[42] (Figure 5) and the Pogue group in Dartmouth[64] have used their own in-

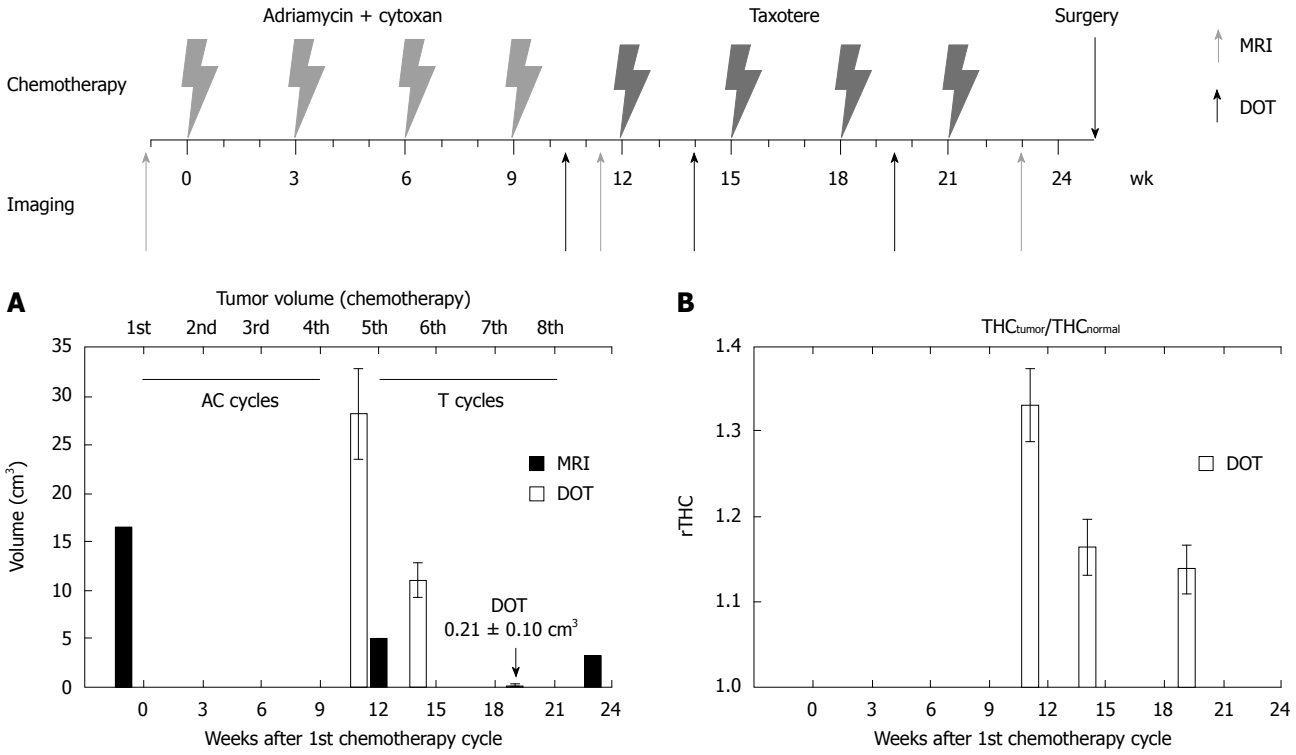

Figure 5 (Upper) Neoadjuvant chemotherapy timing diagram. Four cycles of adriamycin + cytoxan are followed by four cycles of taxotere. Time points for magnetic resonance imaging (MRI) and diffuse optical tomography (DOT) measurement are indicated. (Lower) A: Decrease in tumor volume; B: Change in total hemoglobin concentration (THC) (from Choe *et al*[42], copyright, 2005, American Association of Physicists in Medicine).

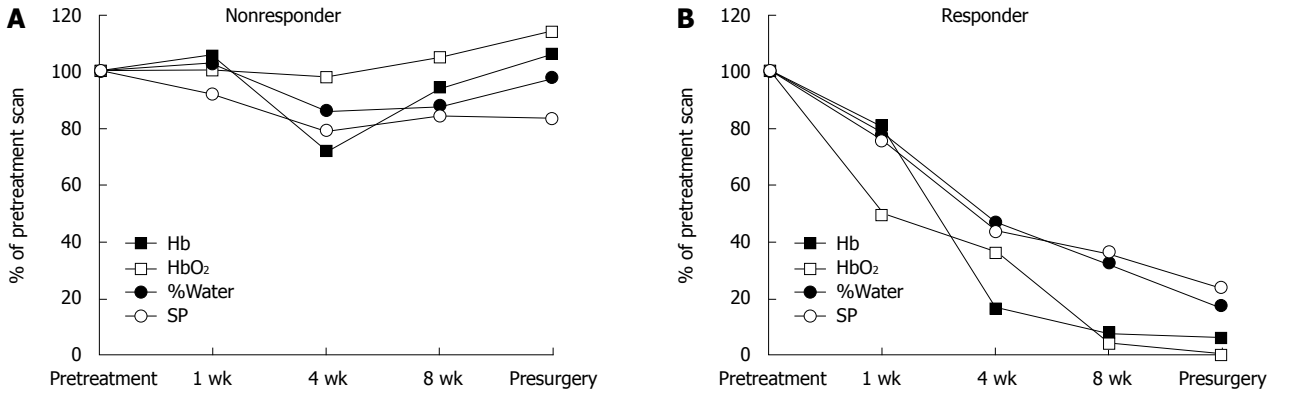

Figure 6 Non-responders (A) *vs* responders (B) to neoadjuvant chemotherapy for each of the optical parameters as measured by diffuse optical imaging in breast tumors (from Soliman *et al*, copyright, 2010, American Association for Cancer Research). SP: Scattering power.

house DOI instruments. Although most of these studies have used only a small number of patients, they have shown consistently that valuable information on treatment efficacy can be obtained by DOI within days or weeks of the onset of chemotherapy. Most recently, Soliman *et al*[65], by using a commercial DOI instrument (Softscan, ART Canada), have reported large decreases in Hb, HbO_2, percent water, and scatter power, from the NAC responder group. From 10 patients with aggressive diseases who received a variety of NAC regimens, they observed that the Hb concentration decreased more (67.6%, std 20.8%) for responders, than non-responders (17.7%, std 9.8%), after 4 wk of NAC. This shows that separation of pathological responders from non-responders is possible early in treatment (Figure 6).

Multimodal assessment of breast cancer

Although stand-alone DOI instruments are being successfully used in breast cancer imaging, many research groups have noticed that combining DOI with other imaging modalities can give us much more accurate reconstruction of breast lesions. When combined with structural imaging modalities such as MRI[54,66], ultrasound[67], and X-ray mammography[68], the structural information (boundary shape as well as inner structure) can be used as a priori information that constrains DOI image reconstruction. DOI alone cannot produce a crisp image due to ill-posed nature of the inverse problem, therefore, incorporation of such structural information can dramatically improve image accuracy *via* reducing the number of variables.

Multimodal measurement can be performed concurrently (at nearly the same time in the same setting), or non-concurrently (at two different time points in a different setting). Concurrent multimodal measurement may be more desirable in terms of image registration, but there are many instrument-related constraints that might render it impractical. For example, in order incorporate DOI into MRI, one needs to replace all components with non-magnetic material and also use very long optical fibers that connect to the control module located outside the MRI room. Therefore, some researchers are studying non-concurrent multimodal measurement, although it is challenging to register between two breast images with different deformation[69]. Promising results using the non-concurrent image registration have been reported between bPET and DOI[70].

CONCLUSION

DOI has tremendous potential in terms of clinical application. Although this review focuses on its use in breast cancer imaging, many other applications have been reported in brain functional imaging[71,72], muscle studies[73], head and neck cancer therapy monitoring[74], and photodynamic therapy monitoring[75,76]. DOI in breast, along with the emerging DCS that measures relative blood flow, will completely change our method of breast cancer screening and therapy monitoring in the future. Although X-ray mammography will remain as a method of choice for some time, the advantages of optical mammography will eventually be recognized in the clinical community. There are many challenges to overcome, such as improving spatial resolution, increasing tumor specificity, and proper artifact removal. However, the most important aspect is the standardization of instruments and software. Several big research groups are using their own custom-made instruments and reconstruction software, and the way in which they are collaborating with hospitals is also different. It is encouraging that the DOI community has realized this issue and is making efforts towards standardization *via* forming a multi-institutional network[77]. In summary, DOI is a promising non-invasive, deep tissue functional imaging modality that is especially suitable for breast cancer diagnosis and treatment monitoring, and it will find increasing applications in clinics.

REFERENCES

1 **Birdwell RL**, Ikeda DM, O'Shaughnessy KF, Sickles EA. Mammographic characteristics of 115 missed cancers later detected with screening mammography and the potential utility of computer-aided detection. *Radiology* 2001; **219**: 192-202
2 **Wazer DE**, Gage I, Homer MJ, Krosnick SH, Schmid C. Age-related differences in patients with nonpalpable breast carcinomas. *Cancer* 1996; **78**: 1432-1437
3 **Karellas A**, Vedantham S. Breast cancer imaging: a perspective for the next decade. *Med Phys* 2008; **35**: 4878-4897
4 **Price J**, Chen SW. Screening for breast cancer with MRI: recent experience from the Australian Capital Territory. *J Med Imaging Radiat Oncol* 2009; **53**: 69-80
5 **Yang K**, Huang SY, Packard NJ, Boone JM. Noise variance analysis using a flat panel x-ray detector: a method for additive noise assessment with application to breast CT applications. *Med Phys* 2010; **37**: 3527-3537
6 **Glick SJ**. Breast CT. *Annu Rev Biomed Eng* 2007; **9**: 501-526
7 **Peng H**, Levin CS. Design study of a high-resolution breast-dedicated PET system built from cadmium zinc telluride detectors. *Phys Med Biol* 2010; **55**: 2761-2788
8 **Freifelder R**, Karp JS. Dedicated PET scanners for breast imaging. *Phys Med Biol* 1997; **42**: 2463-2480
9 **Choe R**, Yodh AG. Diffuse optical tomography of the breast. In: Suri J, Rangayyan RM, Laxminarayan S, editors. Emerging technologies in breast imaging and mammography. Stevenson Ranch, CA: American Scientific Publishers, 2008: 317-342
10 **Durduran T**, Choe R, Baker WB, Yodh AG. Diffuse optics for tissue monitoring and tomography. *Rep Prog Phys* 2010; 73: 076701
11 **Farrell TJ**, Patterson MS, Wilson B. A diffusion theory model of spatially resolved, steady-state diffuse reflectance for the noninvasive determination of tissue optical properties in vivo. *Med Phys* 1992; **19**: 879-888
12 **Ishimaru A**. Wave Propagation and scattering in random media. San Diego, CA: Academic, 1978
13 **Markel VA**, Schotland JC. Inverse problem in optical diffusion tomography. II. Role of boundary conditions. *J Opt Soc Am A Opt Image Sci Vis* 2002; **19**: 558-566
14 **Culver JP**, Choe R, Holboke MJ, Zubkov L, Durduran T, Slemp A, Ntziachristos V, Chance B, Yodh AG. Three-dimensional diffuse optical tomography in the parallel plane transmission geometry: evaluation of a hybrid frequency domain/continuous wave clinical system for breast imaging. *Med Phys* 2003; **30**: 235-247
15 **Lee K**, Konecky SD, Choe R, Ban HY, Corlu A, Durduran T, Yodh AG. Transmission RF diffuse optical tomography instrument for human breast imaging. Munich, Germany: Proceeding of European Conference on Biomedical Optics, 2007: 6629-6663
16 **Dehghani H**, Doyley MM, Pogue BW, Jiang S, Geng J, Paulsen KD. Breast deformation modelling for image reconstruction in near infrared optical tomography. *Phys Med Biol* 2004; **49**: 1131-1145
17 **McBride TO**, Pogue BW, Poplack S, Soho S, Wells WA, Jiang S, Osterberg UL, Paulsen KD. Multispectral near-infrared tomography: a case study in compensating for water and lipid content in hemoglobin imaging of the breast. *J Biomed Opt* 2002; **7**: 72-79
18 **Srinivasan S**, Pogue BW, Jiang SD, Dehghani H, Paulsen KD. Spectrally constrained NIR tomography for breast imaging: Simulations and clinical results. In: Chance B, Alfano RR, Tromberg BJ, SevickMuraca EM, editors. Optical Tomography and Spectroscopy of Tissue VI. Volume 5693. Bellingham: Spie-Int Soc Optical Engineering, 2005: 293-300
19 **Cerussi A**, Shah N, Hsiang D, Durkin A, Butler J, Tromberg BJ. In vivo absorption, scattering, and physiologic properties of 58 malignant breast tumors determined by broadband diffuse optical spectroscopy. *J Biomed Opt* 2006; **11**: 044005
20 **Intes X**. Time-domain optical mammography SoftScan: initial results. *Acad Radiol* 2005; **12**: 934-947
21 **Lee K**, Choe R, Corlu A, Konecky SD, Durduran T, Yodh AG. Artifact Reduction in CW Transmission Diffuse Optical Tomography. Miami Beach, FL: OSA Biomedical Optics Topical Meeting, 2004: WB2
22 **Arridge SR**. Optical tomography in medical imaging. *Inverse Probl* 1999; **15**: R41-R93
23 **Dehghani H**, Srinivasan S, Pogue BW, Gibson A. Numerical modelling and image reconstruction in diffuse optical tomography. *Philos Transact A Math Phys Eng Sci* 2009; **367**: 3073-3093
24 **Konecky SD**, Panasyuk GY, Lee K, Markel V, Yodh AG, Schotland JC. Imaging complex structures with diffuse light. *Opt Express* 2008; **16**: 5048-5060
25 **Dehghani H**, Eames ME, Yalavarthy PK, Davis SC, Srinivasan S, Carpenter CM, Pogue BW, Paulsen KD. Near infrared

optical tomography using NIRFAST: Algorithm for numerical model and image reconstruction. *Commun Numer Methods Eng* 2008; **25**: 711-732
26 **NIRFAST**. Available from: URL: http://www.dartmouth.edu/~nir/nirfast/
27 **TOAST**. Available from: URL: http://www.medphys.ucl.ac.uk/~martins/toast/dot.html
28 **PMItoolbox**. Available from: URL: http://www.nmr.mgh.harvard.edu/~jstott/PMI/
29 **Lee K**, Choe R, Corlu A, Konecky SD, Durduran T, Yodh AG. Diffuse Light Propagation in a Parallel Plate CW DOT Instrument with Non-Contact Detectors. Fort Lauderdale, FL: OSA Biomedical Optics Topical Meeting, 2006: SH59
30 **Schweiger M**, Nissilä I, Boas DA, Arridge SR. Image reconstruction in optical tomography in the presence of coupling errors. *Appl Opt* 2007; **46**: 2743-2756
31 **Durduran T**, Choe R, Culver JP, Zubkov L, Holboke MJ, Giammarco J, Chance B, Yodh AG. Bulk optical properties of healthy female breast tissue. *Phys Med Biol* 2002; **47**: 2847-2861
32 **Jakubowski DB**, Cerussi AE, Bevilacqua F, Shah N, Hsiang D, Butler J, Tromberg BJ. Monitoring neoadjuvant chemotherapy in breast cancer using quantitative diffuse optical spectroscopy: a case study. *J Biomed Opt* 2004; **9**: 230-238
33 **Thomsen S**, Tatman D. Physiological and pathological factors of human breast disease that can influence optical diagnosis. *Ann N Y Acad Sci* 1998; **838**: 171-193
34 **Jiang S**, Pogue BW, Paulsen KD, Kogel C, Poplack SP. In vivo near-infrared spectral detection of pressure-induced changes in breast tissue. *Opt Lett* 2003; **28**: 1212-1214
35 **Srinivasan S**, Pogue BW, Jiang S, Dehghani H, Kogel C, Soho S, Gibson JJ, Tosteson TD, Poplack SP, Paulsen KD. Interpreting hemoglobin and water concentration, oxygen saturation, and scattering measured in vivo by near-infrared breast tomography. *Proc Natl Acad Sci USA* 2003; **100**: 12349-12354
36 **Tromberg BJ**, Shah N, Lanning R, Cerussi A, Espinoza J, Pham T, Svaasand L, Butler J. Non-invasive in vivo characterization of breast tumors using photon migration spectroscopy. *Neoplasia* 2000; **2**: 26-40
37 **Chance B**. Near-infrared images using continuous, phase-modulated, and pulsed light with quantitation of blood and blood oxygenation. *Ann N Y Acad Sci* 1998; **838**: 29-45
38 Suzuki K, Yamashita Y, Ohta K, Kaneko M, Yoshida M, Chance B. Quantitative measurement of optical parameters in normal breasts using time-resolved spectroscopy: in vivo results of 30 Japanese women. *J Biomed Opt* 1996; **1**: 330
39 **Spinelli L**, Torricelli A, Pifferi A, Taroni P, Danesini GM, Cubeddu R. Bulk optical properties and tissue components in the female breast from multiwavelength time-resolved optical mammography. *J Biomed Opt* 2004; **9**: 1137-1142
40 **Pogue BW**, Poplack SP, McBride TO, Wells WA, Osterman KS, Osterberg UL, Paulsen KD. Quantitative hemoglobin tomography with diffuse near-infrared spectroscopy: pilot results in the breast. *Radiology* 2001; **218**: 261-266
41 **Jiang H**, Xu Y, Iftimia N, Eggert J, Klove K, Baron L, Fajardo L. Three-dimensional optical tomographic imaging of breast in a human subject. *IEEE Trans Med Imaging* 2001; **20**: 1334-1340
42 **Choe R**, Corlu A, Lee K, Durduran T, Konecky SD, Grosicka-Koptyra M, Arridge SR, Czerniecki BJ, Fraker DL, DeMichele A, Chance B, Rosen MA, Yodh AG. Diffuse optical tomography of breast cancer during neoadjuvant chemotherapy: a case study with comparison to MRI. *Med Phys* 2005; **32**: 1128-1139
43 **Srinivasan S**, Pogue BW, Brooksby B, Jiang S, Dehghani H, Kogel C, Wells WA, Poplack SP, Paulsen KD. Near-infrared characterization of breast tumors in vivo using spectrally-constrained reconstruction. *Technol Cancer Res Treat* 2005; **4**: 513-526
44 **Li C**, Grobmyer SR, Massol N, Liang X, Zhang Q, Chen L, Fajardo LL, Jiang H. Noninvasive in vivo tomographic optical imaging of cellular morphology in the breast: possible convergence of microscopic pathology and macroscopic radiology. *Med Phys* 2008; **35**: 2493-2501
45 **Grosenick D**, Wabnitz H, Moesta KT, Mucke J, Schlag PM, Rinneberg H. Time-domain scanning optical mammography: II. Optical properties and tissue parameters of 87 carcinomas. *Phys Med Biol* 2005; **50**: 2451-2468
46 **Choe R**, Konecky SD, Corlu A, Lee K, Durduran T, Busch DR, Pathak S, Czerniecki BJ, Tchou J, Fraker DL, Demichele A, Chance B, Arridge SR, Schweiger M, Culver JP, Schnall MD, Putt ME, Rosen MA, Yodh AG. Differentiation of benign and malignant breast tumors by in-vivo three-dimensional parallel-plate diffuse optical tomography. *J Biomed Opt* 2009; **14**: 024020
47 **Chance B**, Nioka S, Zhang J, Conant EF, Hwang E, Briest S, Orel SG, Schnall MD, Czerniecki BJ. Breast cancer detection based on incremental biochemical and physiological properties of breast cancers: a six-year, two-site study. *Acad Radiol* 2005; **12**: 925-933
48 **Enfield LC**, Gibson AP, Everdell NL, Delpy DT, Schweiger M, Arridge SR, Richardson C, Keshtgar M, Douek M, Hebden JC. Three-dimensional time-resolved optical mammography of the uncompressed breast. *Appl Opt* 2007; **46**: 3628-3638
49 **Srinivasan S**, Pogue BW, Carpenter C, Jiang S, Wells WA, Poplack SP, Kaufman PA, Paulsen KD. Developments in quantitative oxygen-saturation imaging of breast tissue in vivo using multispectral near-infrared tomography. *Antioxid Redox Signal* 2007; **9**: 1143-1156
50 **Spinelli L**, Torricelli A, Pifferi A, Taroni P, Danesini G, Cubeddu R. Characterization of female breast lesions from multi-wavelength time-resolved optical mammography. *Phys Med Biol* 2005; **50**: 2489-2502
51 **Culver JP**, Choe R, Holboke MJ, Zubkov L, Durduran T, Slemp A, Ntziachristos V, Chance B, Yodh AG. Three-dimensional diffuse optical tomography in the parallel plane transmission geometry: evaluation of a hybrid frequency domain/continuous wave clinical system for breast imaging. *Med Phys* 2003; **30**: 235-247
52 **Pogue BW**, McBride TO, Prewitt J, Osterberg UL, Paulsen KD. Spatially variant regularization improves diffuse optical tomography. *Appl Opt* 1999; **38**: 2950-2961
53 **Kaufman L**, Neumaier A. PET regularization by envelope guided conjugate gradients. *IEEE Trans Med Imaging* 1996; **15**: 385-389
54 **Ntziachristos V**, Yodh AG, Schnall M, Chance B. Concurrent MRI and diffuse optical tomography of breast after indocyanine green enhancement. *Proc Natl Acad Sci USA* 2000; **97**: 2767-2772
55 **Ntziachristos V**, Yodh AG, Schnall MD, Chance B. MRI-guided diffuse optical spectroscopy of malignant and benign breast lesions. *Neoplasia* 2002; **4**: 347-354
56 **Intes X**, Ripoll J, Chen Y, Nioka S, Yodh AG, Chance B. In vivo continuous-wave optical breast imaging enhanced with Indocyanine Green. *Med Phys* 2003; **30**: 1039-1047
57 **Godavarty A**, Eppstein MJ, Zhang C, Theru S, Thompson AB, Gurfinkel M, Sevick-Muraca EM. Fluorescence-enhanced optical imaging in large tissue volumes using a gain-modulated ICCD camera. *Phys Med Biol* 2003; **48**: 1701-1720
58 **Reynolds JS**, Troy TL, Mayer RH, Thompson AB, Waters DJ, Cornell KK, Snyder PW, Sevick-Muraca EM. Imaging of spontaneous canine mammary tumors using fluorescent contrast agents. *Photochem Photobiol* 1999; **70**: 87-94
59 **Corlu A**, Choe R, Durduran T, Rosen MA, Schweiger M, Arridge SR, Schnall MD, Yodh AG. Three-dimensional in vivo fluorescence diffuse optical tomography of breast cancer in humans. *Opt Express* 2007; **15**: 6696-6716
60 **Hulley SB**, Cummings SR, Browner WS, Grady DG, Newman TB. Designing Clinical Research. 3rd ed. Philadelphia: Lippincott Williams & Wilkins, 2007
61 **Fisher B**, Bryant J, Wolmark N, Mamounas E, Brown A,

Fisher ER, Wickerham DL, Begovic M, DeCillis A, Robidoux A, Margolese RG, Cruz AB Jr, Hoehn JL, Lees AW, Dimitrov NV, Bear HD. Effect of preoperative chemotherapy on the outcome of women with operable breast cancer. *J Clin Oncol* 1998; **16**: 2672-2685

62 **van der Hage JA**, van de Velde CJ, Julien JP, Tubiana-Hulin M, Vandervelden C, Duchateau L. Preoperative chemotherapy in primary operable breast cancer: results from the European Organization for Research and Treatment of Cancer trial 10902. *J Clin Oncol* 2001; **19**: 4224-4237

63 **Dose-Schwarz J**, Tiling R, Avril-Sassen S, Mahner S, Lebeau A, Weber C, Schwaiger M, Jänicke F, Untch M, Avril N. Assessment of residual tumour by FDG-PET: conventional imaging and clinical examination following primary chemotherapy of large and locally advanced breast cancer. *Br J Cancer* 2010; **102**: 35-41

64 **Jiang S**, Pogue BW, Carpenter CM, Poplack SP, Wells WA, Kogel CA, Forero JA, Muffly LS, Schwartz GN, Paulsen KD, Kaufman PA. Evaluation of breast tumor response to neoadjuvant chemotherapy with tomographic diffuse optical spectroscopy: case studies of tumor region-of-interest changes. *Radiology* 2009; **252**: 551-560

65 **Soliman H**, Gunasekara A, Rycroft M, Zubovits J, Dent R, Spayne J, Yaffe MJ, Czarnota GJ. Functional imaging using diffuse optical spectroscopy of neoadjuvant chemotherapy response in women with locally advanced breast cancer. *Clin Cancer Res* 2010; **16**: 2605-2614

66 **Brooksby B**, Jiang SD, Dehghani H, Pogue BW, Paulsen KD, Kogel C, Doyley M, Weaver JB, Poplack SP. Magnetic resonance-guided near-infrared tomography of the breast. *Rev Sci Instrum* 2004; **75**: 5262-5270

67 **Chen NG**, Guo P, Yan S, Piao D, Zhu Q. Simultaneous near-infrared diffusive light and ultrasound imaging. *Appl Opt* 2001; **40**: 6367-6380

68 **Zhang Q**, Brukilacchio TJ, Li A, Stott JJ, Chaves T, Hillman E, Wu T, Chorlton M, Rafferty E, Moore RH, Kopans DB, Boas DA. Coregistered tomographic x-ray and optical breast imaging: initial results. *J Biomed Opt* 2005; **10**: 024033

69 **Azar FS**, Lee K, Khamene A, Choe R, Corlu A, Konecky SD, Sauer F, Yodh AG. Standardized platform for coregistration of nonconcurrent diffuse optical and magnetic resonance breast images obtained in different geometries. *J Biomed Opt* 2007; **12**: 051902

70 **Konecky SD**, Choe R, Corlu A, Lee K, Wiener R, Srinivas SM, Saffer JR, Freifelder R, Karp JS, Hajjioui N, Azar F, Yodh AG. Comparison of diffuse optical tomography of human breast with whole-body and breast-only positron emission tomography. *Med Phys* 2008; **35**: 446-455

71 **Durduran T**, Zhou C, Edlow BL, Yu G, Choe R, Kim MN, Cucchiara BL, Putt ME, Shah Q, Kasner SE, Greenberg JH, Yodh AG, Detre JA. Transcranial optical monitoring of cerebrovascular hemodynamics in acute stroke patients. *Opt Express* 2009; **17**: 3884-3902

72 **Zhou C**, Eucker SA, Durduran T, Yu G, Ralston J, Friess SH, Ichord RN, Margulies SS, Yodh AG. Diffuse optical monitoring of hemodynamic changes in piglet brain with closed head injury. *J Biomed Opt* 2009; **14**: 034015

73 **Yu G**, Durduran T, Lech G, Zhou C, Chance B, Mohler ER 3rd, Yodh AG. Time-dependent blood flow and oxygenation in human skeletal muscles measured with noninvasive near-infrared diffuse optical spectroscopies. *J Biomed Opt* 2005; **10**: 024027

74 **Sunar U**, Makonnen S, Zhou C, Durduran T, Yu G, Wang HW, Lee WM, Yodh AG. Hemodynamic responses to antivascular therapy and ionizing radiation assessed by diffuse optical spectroscopies. *Opt Express* 2007; **15**: 15507-15516

75 **Yu G**, Durduran T, Zhou C, Zhu TC, Finlay JC, Busch TM, Malkowicz SB, Hahn SM, Yodh AG. Real-time in situ monitoring of human prostate photodynamic therapy with diffuse light. *Photochem Photobiol* 2006; **82**: 1279-1284

76 **Wang HW**, Finlay JC, Lee K, Zhu TC, Putt ME, Glatstein E, Koch CJ, Evans SM, Hahn SM, Busch TM, Yodh AG. Quantitative comparison of tissue oxygen and motexafin lutetium uptake by ex vivo and noninvasive in vivo techniques in patients with intraperitoneal carcinomatosis. *J Biomed Opt* 2007; **12**: 034023

77 **Tromberg BJ**, Pogue BW, Paulsen KD, Yodh AG, Boas DA, Cerussi AE. Assessing the future of diffuse optical imaging technologies for breast cancer management. *Med Phys* 2008; **35**: 2443-2451

S- Editor Cheng JX **L- Editor** Kerr C **E- Editor** Ma WH

World Journal of Clinical Oncology

Online Submissions: http://www.wjgnet.com/2218-4333office
wjco@wjgnet.com
www.wjgnet.com

World J Clin Oncol 2011 January 10; 2(1): I
ISSN 2218-4333 (online)

Acknowledgments to reviewers of *World Journal of Clinical Oncology*

Many reviewers have contributed their expertise and time to the peer review, a critical process to ensure the quality of *World Journal of Clinical Oncology*. The editors and authors of the articles submitted to the journal are grateful to the following reviewers for evaluating the articles (including those published in this issue and those rejected for this issue) during the last editing time period.

Ali Syed Arbab, MD, PhD, Associate Scientist and Director, Cellular and Molecular Imaging Laboratory, Department of Radiology, Henry Ford Hospital, 1 Ford Place, 2F, Box 82, Detroit, MI 48202, United States

Hengmi Cui, PhD, Assistant Professor, Center for Epigenetics and Division of Molecular Medicine, Johns Hopkins University School of Medicine, 855 N Wolfe Street/572 Rangos Building, Baltimore, MD 21205, United States

Yun Gong, MD, Associate Professor, Department of Pathology, Unit 53, The University of Texas, M D Anderson Cancer Center, 1515 Holcombe Blvd, Houston, TX 77030, United States

Nathalie Lassau, MD, PhD, Imaging Department, Institut Gustave Roussy, 39 Rue Camille Desmoulins, 94800 Villejuif, France

Murielle Mimeault, PhD, Department of Biochemistry and Molecular Biology, College of Medicine, Eppley Cancer Institute, 7052 DRC, University of Nebraska Medical Center, 985870 Nebraska Medical Center, Omaha, NE 68198-5870, United States

Ravi Murthy, MD, Interventional Radiology, UT MD Anderson Cancer Center, 1400 Pressler Street, Unit 1471, Houston, TX 77042, United States

Ravi Murthy, MD, Interventional Radiology, UT MD Anderson Cancer Center, 1400 Pressler Street, Unit 1471, Houston, TX 77042, United States

Domenico Rubello, MD, Professor, Director of the Department of Nuclear Medicine, PET/CT Centre, Radiology, Medical Physics, Santa Maria della Misericordia Hospital; Via Tre Martiri 140, ZIP 45100, Rovigo, Italy

Harun M Said, Assistant Professor, Department of Radiation Oncology, University of Wuerzburg, Josef Schneider Str.11, D-97080 Wuerzburg, Germany

Sherven Sharma, Gene Medicine Laboratory, VA Greater Los Angeles Health Care System,11301 Wilshire Blvd., Bldg. 114, Rm. 103, Los Angeles, CA 90073-1003, United States

Ronald Xiaorong Xu, PhD, Assistant Professor, Biomedical Engineering Department, The Ohio State University, 270 Bevis Hall, 1080 Carmack Rd., Columbus, OH 43210, United States

Tzu-Chen Yen, MD, PhD, Professor and Chairperson, Department of Nuclear Medicine and Molecular Imaging Center, Chang Gung Memorial Hospital and University, Taoyuan, Taiwan, China

William Andrew Yeudall, BDS, PhD, Associate Professor, VCU Philips Institute of Oral and Craniofacial Molecular Biology, Virginia Commonwealth University School of Dentistry, 521 N 11th St, Richmond, VA 23298-0566, United States

World Journal of Clinical Oncology

Online Submissions: http://www.wjgnet.com/2218-4333office
wjco@wjgnet.com
www.wjgnet.com

World J Clin Oncol 2011 January 10; 2(1): I
ISSN 2218-4333 (online)

Meetings

Events Calendar 2011

January 20-22, 2011
2011 Gastrointestinal Cancers Symposium,The Moscone West Building, San Francisco, CA, United States

World Journal of Clinical Oncology

Online Submissions: http://www.wjgnet.com/2218-4333office
wjco@wjgnet.com
www.wjgnet.com

World J Clin Oncol 2011 January 10; 2(1): I-V
ISSN 2218-4333 (online)

Instructions to authors

GENERAL INFORMATION

World Journal of Clinical Oncology (*World J Clin Oncol*, *WJCO*, online ISSN 2218-4333, DOI: 10.5306) is a monthly peer-reviewed, online, open-access (OA), journal supported by an editorial board consisting of 315 experts in oncology from 33 countries.

The biggest advantage of the OA model is that it provides free, full-text articles in PDF and other formats for experts and the public without registration, which eliminates the obstacle that traditional journals possess and usually delays the speed of the propagation and communication of scientific research results. The open access model has been proven to be a true approach that may achieve the ultimate goal of the journals, i.e. the maximization of the value to the readers, authors and society.

Maximization of personal benefits

The role of academic journals is to exhibit the scientific levels of a country, a university, a center, a department, and even a scientist, and build an important bridge for communication between scientists and the public. As we all know, the significance of the publication of scientific articles lies not only in disseminating and communicating innovative scientific achievements and academic views, as well as promoting the application of scientific achievements, but also in formally recognizing the "priority" and "copyright" of innovative achievements published, as well as evaluating research performance and academic levels. So, to realize these desired attributes of *WJCO* and create a well-recognized journal, the following four types of personal benefits should be maximized. The maximization of personal benefits refers to the pursuit of the maximum personal benefits in a well-considered optimal manner without violation of the laws, ethical rules and the benefits of others. (1) Maximization of the benefits of editorial board members: The primary task of editorial board members is to give a peer review of an unpublished scientific article *via* online office system to evaluate its innovativeness, scientific and practical values and determine whether it should be published or not. During peer review, editorial board members can also obtain cutting-edge information in that field at first hand. As leaders in their field, they have priority to be invited to write articles and publish commentary articles. We will put peer reviewers' names and affiliations along with the article they reviewed in the journal to acknowledge their contribution; (2) Maximization of the benefits of authors: Since *WJCO* is an open-access journal, readers around the world can immediately download and read, free of charge, high-quality, peer-reviewed articles from *WJCO* official website, thereby realizing the goals and significance of the communication between authors and peers as well as public reading; (3) Maximization of the benefits of readers: Readers can read or use, free of charge, high-quality peer-reviewed articles without any limits, and cite the arguments, viewpoints, concepts, theories, methods, results, conclusion or facts and data of pertinent literature so as to validate the innovativeness, scientific and practical values of their own research achievements, thus ensuring that their articles have novel arguments or viewpoints, solid evidence and correct conclusion; and (4) Maximization of the benefits of employees: It is an iron law that a first-class journal is unable to exist without first-class editors, and only first-class editors can create a first-class academic journal. We insist on strengthening our team cultivation and construction so that every employee, in an open, fair and transparent environment, could contribute their wisdom to edit and publish high-quality articles, thereby realizing the maximization of the personal benefits of editorial board members, authors and readers, and yielding the greatest social and economic benefits.

Aims and scope

The aim of *WJCO* is to report rapidly new theories, methods and techniques for prevention, diagnosis, treatment, rehabilitation and nursing in the field of oncology. *WJCO* covers etiology, epidemiology, evidence-based medicine, informatics, diagnostic imaging, endoscopy, tumor recurrence and metastasis, tumor stem cells, radiotherapy, chemotherapy, interventional radiology, palliative therapy, clinical chemotherapy, biological therapy, minimally invasive therapy, physiotherapy, psycho-oncology, comprehensive therapy, oncology-related traditional medicine, integrated Chinese and Western medicine, and nursing. *WJCO* covers tumors in various organs/tissues, including the female reproductive system, bone and soft tissue, respiratory system, urinary system, endocrine system, skin, breast, nervous system, head and neck, digestive system, and hematologic and lymphatic system. The journal also publishes original articles and reviews that report the results of applied and basic research in fields related to oncology, such as immunology, physiopathology, cell biology, pharmacology, medical genetics, and pharmacology of Chinese herbs.

Columns

The columns in the issues of *WJCO* will include: (1) Editorial: To introduce and comment on major advances and developments in the field; (2) Frontier: To review representative achievements, comment on the state of current research, and propose directions for future research; (3) Topic Highlight: This column consists of three formats, including (A) 10 invited review articles on a hot topic, (B) a commentary on common issues of this hot topic, and (C) a commentary on the 10 individual articles; (4) Observation: To update the development of old and new questions, highlight unsolved problems, and provide strategies on how to solve the questions; (5) Guidelines for Basic Research: To provide Guidelines for basic research; (6) Guidelines for Clinical Practice: To provide guidelines for clinical diagnosis and treatment; (7) Review: To review systemically progress and unresolved problems in the field, comment on the state of current research, and make suggestions for future work; (8) Original Articles: To report innovative and original findings in oncology; (9) Brief Articles: To briefly report the novel and innovative findings in oncology; (10) Case Report: To report a rare or typical case; (11) Letters to the Editor: To discuss and make reply to the contributions published in *WJCO*, or to introduce and comment on a controversial issue of general interest; (12) Book Reviews: To introduce and comment on quality monographs of oncology; and (13) Guidelines: To introduce consensuses and guidelines reached by international and national academic authorities worldwide on the research oncology.

Name of journal

World Journal of Clinical Oncology

CSSN

ISSN 2218-4333 (online)

Published by

Baishideng Publishing Group Co., Limited

SPECIAL STATEMENT

All articles published in this journal represent the viewpoints of the authors except where indicated otherwise.

Biostatistical editing

Statisital review is performed after peer review. We invite an expert in Biomedical Statistics from to evaluate the statistical method used in the paper, including *t*-test (group or paired comparisons), chi-squared test, Ridit, probit, logit, regression (linear, curvilinear, or stepwise), correlation, analysis of variance, analysis of covariance, *etc*. The reviewing points include: (1) Statistical methods should be described when they are used to verify the results; (2) Whether the statistical techniques are suitable or correct; (3) Only homogeneous data can be averaged. Standard deviations are preferred to standard errors. Give the number of observations and subjects (*n*). Losses in observations, such as drop-outs from the study should be reported; (4) Values such as ED50, LD50, IC50 should have their 95% confidence limits calculated and compared by weighted probit analysis (Bliss and Finney); and (5) The word 'significantly' should be replaced by its synonyms (if it indicates extent) or the *P* value (if it indicates statistical significance).

Conflict-of-interest statement

In the interests of transparency and to help reviewers assess any potential bias, *WJCO* requires authors of all papers to declare any competing commercial, personal, political, intellectual, or religious interests in relation to the submitted work. Referees are also asked to indicate any potential conflict they might have reviewing a particular paper. Before submitting, authors are suggested to read "Uniform Requirements for Manuscripts Submitted to Biomedical Journals: Ethical Considerations in the Conduct and Reporting of Research: Conflicts of Interest" from International Committee of Medical Journal Editors (ICMJE), which is available at: http://www.icmje.org/ethical_4conflicts.html.

Sample wording: [Name of individual] has received fees for serving as a speaker, a consultant and an advisory board member for [names of organizations], and has received research funding from [names of organization]. [Name of individual] is an employee of [name of organization]. [Name of individual] owns stocks and shares in [name of organization]. [Name of individual] owns patent [patent identification and brief description].

Statement of informed consent

Manuscripts should contain a statement to the effect that all human studies have been reviewed by the appropriate ethics committee or it should be stated clearly in the text that all persons gave their informed consent prior to their inclusion in the study. Details that might disclose the identity of the subjects under study should be omitted. Authors should also draw attention to the Code of Ethics of the World Medical Association (Declaration of Helsinki, 1964, as revised in 2004).

Statement of human and animal rights

When reporting the results from experiments, authors should follow the highest standards and the trial should conform to Good Clinical Practice (for example, US Food and Drug Administration Good Clinical Practice in FDA-Regulated Clinical Trials; UK Medicines Research Council Guidelines for Good Clinical Practice in Clinical Trials) and/or the World Medical Association Declaration of Helsinki. Generally, we suggest authors follow the lead investigator's national standard. If doubt exists whether the research was conducted in accordance with the above standards, the authors must explain the rationale for their approach and demonstrate that the institutional review body explicitly approved the doubtful aspects of the study.

Before submitting, authors should make their study approved by the relevant research ethics committee or institutional review board. If human participants were involved, manuscripts must be accompanied by a statement that the experiments were undertaken with the understanding and appropriate informed consent of each. Any personal item or information will not be published without explicit consents from the involved patients. If experimental animals were used, the materials and methods (experimental procedures) section must clearly indicate that appropriate measures were taken to minimize pain or discomfort, and details of animal care should be provided.

SUBMISSION OF MANUSCRIPTS

Manuscripts should be typed in 1.5 line spacing and 12 pt. Book Antiqua with ample margins. Number all pages consecutively, and start each of the following sections on a new page: Title Page, Abstract, Introduction, Materials and Methods, Results, Discussion, Acknowledgements, References, Tables, Figures, and Figure Legends. Neither the editors nor the publisher are responsible for the opinions expressed by contributors. Manuscripts formally accepted for publication become the permanent property of Baishideng Publishing Group Co., Limited, and may not be reproduced by any means, in whole or in part, without the written permission of both the authors and the publisher. We reserve the right to copy-edit and put onto our website accepted manuscripts. Authors should follow the relevant guidelines for the care and use of laboratory animals of their institution or national animal welfare committee. For the sake of transparency in regard to the performance and reporting of clinical trials, we endorse the policy of the ICMJE to refuse to publish papers on clinical trial results if the trial was not recorded in a publicly-accessible registry at its outset. The only register now available, to our knowledge, is http://www.clinicaltrials.gov sponsored by the United States National Library of Medicine and we encourage all potential contributors to register with it. However, in the case that other registers become available you will be duly notified. A letter of recommendation from each author's organization should be provided with the contributed article to ensure the privacy and secrecy of research is protected.

Authors should retain one copy of the text, tables, photographs and illustrations because rejected manuscripts will not be returned to the author(s) and the editors will not be responsible for loss or damage to photographs and illustrations sustained during mailing.

Online submissions

Manuscripts should be submitted through the Online Submission System at: http://www.wjgnet.com/2218-4333office. Authors are highly recommended to consult the ONLINE INSTRUCTIONS TO AUTHORS (http://www.wjgnet.com/2218-4333/g_info_20100722172206.htm) before attempting to submit online. For assistance, authors encountering problems with the Online Submission System may send an email describing the problem to wjco@wjgnet.com, or by telephone: +86-10-85381892. If you submit your manuscript online, do not make a postal contribution. Repeated online submission for the same manuscript is strictly prohibited.

MANUSCRIPT PREPARATION

All contributions should be written in English. All articles must be submitted using word-processing software. All submissions must be typed in 1.5 line spacing and 12 pt. Book Antiqua with ample margins. Style should conform to our house format. Required information for each of the manuscript sections is as follows:

Title page

Title: Title should be less than 12 words.

Running title: A short running title of less than 6 words should be provided.

Authorship: Authorship credit should be in accordance with the standard proposed by International Committee of Medical Journal Editors, based on (1) substantial contributions to conception and design, acquisition of data, or analysis and interpretation of data; (2) drafting the article or revising it critically for important intellectual content; and (3) final approval of the version to be published. Authors should meet conditions 1, 2, and 3.

Institution: Author names should be given first, then the complete name of institution, city, province and postcode. For example, Xu-Chen Zhang, Li-Xin Mei, Department of Pathology, Chengde Medical College, Chengde 067000, Hebei Province, China. One author may be represented from two institutions, for example, George

Sgourakis, Department of General, Visceral, and Transplantation Surgery, Essen 45122, Germany; George Sgourakis, 2nd Surgical Department, Korgialenio-Benakio Red Cross Hospital, Athens 15451, Greece

Author contributions: The format of this section should be: Author contributions: Wang CL and Liang L contributed equally to this work; Wang CL, Liang L, Fu JF, Zou CC, Hong F and Wu XM designed the research; Wang CL, Zou CC, Hong F and Wu XM performed the research; Xue JZ and Lu JR contributed new reagents/analytic tools; Wang CL, Liang L and Fu JF analyzed the data; and Wang CL, Liang L and Fu JF wrote the paper.

Supportive foundations: The complete name and number of supportive foundations should be provided, e.g. Supported by National Natural Science Foundation of China, No. 30224801

Correspondence to: Only one corresponding address should be provided. Author names should be given first, then author title, affiliation, the complete name of institution, city, postcode, province, country, and email. All the letters in the email should be in lower case. A space interval should be inserted between country name and email address. For example, Montgomery Bissell, MD, Professor of Medicine, Chief, Liver Center, Gastroenterology Division, University of California, Box 0538, San Francisco, CA 94143, United States. montgomery.bissell@ucsf.edu

Telephone and fax: Telephone and fax should consist of +, country number, district number and telephone or fax number, e.g. Telephone: +86-10-59080039 Fax: +86-10-85381893

Peer reviewers: All articles received are subject to peer review. Normally, three experts are invited for each article. Decision for acceptance is made only when at least two experts recommend an article for publication. Reviewers for accepted manuscripts are acknowledged in each manuscript, and reviewers of articles which were not accepted will be acknowledged at the end of each issue. To ensure the quality of the articles published in *WJCO*, reviewers of accepted manuscripts will be announced by publishing the name, title/position and institution of the reviewer in the footnote accompanying the printed article. For example, reviewers: Professor Jing-Yuan Fang, Shanghai Institute of Digestive Disease, Shanghai, Affiliated Renji Hospital, Medical Faculty, Shanghai Jiaotong University, Shanghai, China; Professor Xin-Wei Han, Department of Radiology, The First Affiliated Hospital, Zhengzhou University, Zhengzhou, Henan Province, China; and Professor Anren Kuang, Department of Nuclear Medicine, Huaxi Hospital, Sichuan University, Chengdu, Sichuan Province, China.

Abstract

There are unstructured abstracts (no more than 256 words) and structured abstracts (no more than 480). The specific requirements for structured abstracts are as follows:

An informative, structured abstracts of no more than 480 words should accompany each manuscript. Abstracts for original contributions should be structured into the following sections. AIM (no more than 20 words): Only the purpose should be included. Please write the aim as the form of "To investigate/study/…; MATERIALS AND METHODS (no more than 140 words); RESULTS (no more than 294 words): You should present *P* values where appropriate and must provide relevant data to illustrate how they were obtained, e.g. 6.92 ± 3.86 *vs* 3.61 ± 1.67, $P < 0.001$; CONCLUSION (no more than 26 words).

Key words

Please list 5-10 key words, selected mainly from *Index Medicus*, which reflect the content of the study.

Text

For articles of these sections, original articles and brief articles, the main text should be structured into the following sections: INTRODUCTION, MATERIALS AND METHODS, RESULTS and DISCUSSION, and should include appropriate Figures and Tables. Data should be presented in the main text or in Figures and Tables, but not in both. The main text format of these sections, editorial, topic highlight, case report, letters to the editors, can be found at: http://www.wjgnet.com/2218-4333/g_info_list.htm.

Illustrations

Figures should be numbered as 1, 2, 3, *etc.*, and mentioned clearly in the main text. Provide a brief title for each figure on a separate page. Detailed legends should not be provided under the figures. This part should be added into the text where the figures are applicable. Figures should be either Photoshop or Illustrator files (in tiff, eps, jpeg formats) at high-resolution. Examples can be found at: http://www.wjgnet.com/1007-9327/13/4520.pdf; http://www.wjgnet.com/1007-9327/13/4554.pdf; http://www.wjgnet.com/1007-9327/13/4891.pdf; http://www.wjgnet.com/1007-9327/13/4986.pdf; http://www.wjgnet.com/1007-9327/13/4498.pdf. Keeping all elements compiled is necessary in line-art image. Scale bars should be used rather than magnification factors, with the length of the bar defined in the legend rather than on the bar itself. File names should identify the figure and panel. Avoid layering type directly over shaded or textured areas. Please use uniform legends for the same subjects. For example: Figure 1 Pathological changes in atrophic gastritis after treatment. A: ...; B: ...; C: ...; D: ...; E: ...; F: ...; G: …*etc.* It is our principle to publish high resolution-figures for the printed and E-versions.

Tables

Three-line tables should be numbered 1, 2, 3, *etc.*, and mentioned clearly in the main text. Provide a brief title for each table. Detailed legends should not be included under tables, but rather added into the text where applicable. The information should complement, but not duplicate the text. Use one horizontal line under the title, a second under column heads, and a third below the Table, above any footnotes. Vertical and italic lines should be omitted.

Notes in tables and illustrations

Data that are not statistically significant should not be noted. $^{a}P < 0.05$, $^{b}P < 0.01$ should be noted ($P > 0.05$ should not be noted). If there are other series of *P* values, $^{c}P < 0.05$ and $^{d}P < 0.01$ are used. A third series of *P* values can be expressed as $^{e}P < 0.05$ and $^{f}P < 0.01$. Other notes in tables or under illustrations should be expressed as ^{1}F, ^{2}F, ^{3}F; or sometimes as other symbols with a superscript (Arabic numerals) in the upper left corner. In a multi-curve illustration, each curve should be labeled with ●, ○, ■, □, ▲, △, *etc.*, in a certain sequence.

Acknowledgments

Brief acknowledgments of persons who have made genuine contributions to the manuscript and who endorse the data and conclusions should be included. Authors are responsible for obtaining written permission to use any copyrighted text and/or illustrations.

REFERENCES

Coding system

The author should number the references in Arabic numerals according to the citation order in the text. Put reference numbers in square brackets in superscript at the end of citation content or after the cited author's name. For citation content which is part of the narration, the coding number and square brackets should be typeset normally. For example, "Crohn's disease (CD) is associated with increased intestinal permeability[1,2]". If references are cited directly in the text, they should be put together within the text, for example, "From references[19,22-24], we know that..."

When the authors write the references, please ensure that the order in text is the same as in the references section, and also ensure the spelling accuracy of the first author's name. Do not list the same citation twice.

PMID and DOI

Pleased provide PubMed citation numbers to the reference list, e.g. PMID and DOI, which can be found at http://www.ncbi.nlm.nih.gov/sites/entrez?db=pubmed and http://www.crossref.org/SimpleTextQuery/, respectively. The numbers will be used in E-version of this journal.

Style for journal references

Authors: the name of the first author should be typed in bold-faced letters. The family name of all authors should be typed with the initial letter capitalized, followed by their abbreviated first and middle initials. (For example, Lian-Sheng Ma is abbreviated as Ma LS, Bo-Rong Pan as Pan BR). The title of the cited article and italicized journal title (journal title should be in its abbreviated form as shown in PubMed), publication date, volume number (in black), start page, and end page [PMID: 11819634 DOI: 10.3748/wjg.13.5396].

Style for book references

Authors: the name of the first author should be typed in bold-faced letters. The surname of all authors should be typed with the initial letter capitalized, followed by their abbreviated middle and first initials. (For example, Lian-Sheng Ma is abbreviated as Ma LS, Bo-Rong Pan as Pan BR) Book title. Publication number. Publication place: Publication press, Year: start page and end page.

Format

Journals

English journal article (list all authors and include the PMID where applicable)

1 **Jung EM**, Clevert DA, Schreyer AG, Schmitt S, Rennert J, Kubale R, Feuerbach S, Jung F. Evaluation of quantitative contrast harmonic imaging to assess malignancy of liver tumors: A prospective controlled two-center study. *World J Gastroenterol* 2007; **13**: 6356-6364 [PMID: 18081224 DOI: 10.3748/wjg.13.6356]

Chinese journal article (list all authors and include the PMID where applicable)

2 **Lin GZ**, Wang XZ, Wang P, Lin J, Yang FD. Immunologic effect of Jianpi Yishen decoction in treatment of Pixu-diarrhoea. *Shijie Huaren Xiaohua Zazhi* 1999; **7**: 285-287

In press

3 **Tian D**, Araki H, Stahl E, Bergelson J, Kreitman M. Signature of balancing selection in Arabidopsis. *Proc Natl Acad Sci USA* 2006; In press

Organization as author

4 **Diabetes Prevention Program Research Group**. Hypertension, insulin, and proinsulin in participants with impaired glucose tolerance. *Hypertension* 2002; **40**: 679-686 [PMID: 12411462 PMCID:2516377 DOI:10.1161/01.HYP.0000035706.28494.09]

Both personal authors and an organization as author

5 **Vallancien G**, Emberton M, Harving N, van Moorselaar RJ; Alf-One Study Group. Sexual dysfunction in 1, 274 European men suffering from lower urinary tract symptoms. *J Urol* 2003; **169**: 2257-2261 [PMID: 12771764 DOI:10.1097/01.ju.0000067940.76090.73]

No author given

6 21st century heart solution may have a sting in the tail. *BMJ* 2002; **325**: 184 [PMID: 12142303 DOI:10.1136/bmj.325.7357.184]

Volume with supplement

7 **Geraud G**, Spierings EL, Keywood C. Tolerability and safety of frovatriptan with short- and long-term use for treatment of migraine and in comparison with sumatriptan. *Headache* 2002; **42** Suppl 2: S93-99 [PMID: 12028325 DOI:10.1046/j.1526-4610.42.s2.7.x]

Issue with no volume

8 **Banit DM**, Kaufer H, Hartford JM. Intraoperative frozen section analysis in revision total joint arthroplasty. *Clin Orthop Relat Res* 2002; (**401**): 230-238 [PMID: 12151900 DOI:10.1097/00003086-200208000-00026]

No volume or issue

9 Outreach: Bringing HIV-positive individuals into care. *HRSA Careaction* 2002; 1-6 [PMID: 12154804]

Books

Personal author(s)

10 **Sherlock S**, Dooley J. Diseases of the liver and billiary system. 9th ed. Oxford: Blackwell Sci Pub, 1993: 258-296

Chapter in a book (list all authors)

11 **Lam SK**. Academic investigator's perspectives of medical treatment for peptic ulcer. In: Swabb EA, Azabo S. Ulcer disease: investigation and basis for therapy. New York: Marcel Dekker, 1991: 431-450

Author(s) and editor(s)

12 **Breedlove GK**, Schorfheide AM. Adolescent pregnancy. 2nd ed. Wieczorek RR, editor. White Plains (NY): March of Dimes Education Services, 2001: 20-34

Conference proceedings

13 **Harnden P**, Joffe JK, Jones WG, editors. Germ cell tumours V. Proceedings of the 5th Germ cell tumours Conference; 2001 Sep 13-15; Leeds, UK. New York: Springer, 2002: 30-56

Conference paper

14 **Christensen S**, Oppacher F. An analysis of Koza's computational effort statistic for genetic programming. In: Foster JA, Lutton E, Miller J, Ryan C, Tettamanzi AG, editors. Genetic programming. EuroGP 2002: Proceedings of the 5th European Conference on Genetic Programming; 2002 Apr 3-5; Kinsdale, Ireland. Berlin: Springer, 2002: 182-191

Electronic journal (list all authors)

15 Morse SS. Factors in the emergence of infectious diseases. Emerg Infect Dis serial online, 1995-01-03, cited 1996-06-05; 1(1): 24 screens. Available from: URL: http://www.cdc.gov/ncidod/eid/index.htm

Patent (list all authors)

16 **Pagedas AC**, inventor; Ancel Surgical R&D Inc., assignee. Flexible endoscopic grasping and cutting device and positioning tool assembly. United States patent US 20020103498. 2002 Aug 1

Statistical data

Write as mean ± SD or mean ± SE.

Statistical expression

Express *t* test as *t* (in italics), *F* test as *F* (in italics), chi square test as χ^2 (in Greek), related coefficient as *r* (in italics), degree of freedom as υ (in Greek), sample number as *n* (in italics), and probability as *P* (in italics).

Units

Use SI units. For example: body mass, m (B) = 78 kg; blood pressure, p (B) = 16.2/12.3 kPa; incubation time, t (incubation) = 96 h, blood glucose concentration, c (glucose) 6.4 ± 2.1 mmol/L; blood CEA mass concentration, p (CEA) = 8.6 24.5 μg/L; CO_2 volume fraction, 50 mL/L CO_2, not 5% CO_2; likewise for 40 g/L formaldehyde, not 10% formalin; and mass fraction, 8 ng/g, *etc.* Arabic numerals such as 23, 243, 641 should be read 23 243 641.

The format for how to accurately write common units and quantums can be found at: http://www.wjgnet.com/2218-4333/g_info_20100723153305.htm.

Abbreviations

Standard abbreviations should be defined in the abstract and on first mention in the text. In general, terms should not be abbreviated unless they are used repeatedly and the abbreviation is helpful to the reader. Permissible abbreviations are listed in Units, Symbols and Abbreviations: A Guide for Biological and Medical Editors and Authors (Ed. Baron DN, 1988) published by The Royal Society of Medicine, London. Certain commonly used abbreviations, such as DNA, RNA, HIV, LD50, PCR, HBV, ECG, WBC, RBC, CT, ESR, CSF, IgG, ELISA, PBS, ATP, EDTA, mAb, can be used directly without further explanation.

Italics
Quantities: *t* time or temperature, *c* concentration, *A* area, *l* length, *m* mass, *V* volume.
Genotypes: *gyrA*, *arg* 1, *c myc*, *c fos*, *etc.*
Restriction enzymes: *Eco*RI, *Hin*dI, *Bam*HI, *Kbo* I, *Kpn* I, *etc.*
Biology: *H. pylori*, *E coli*, *etc.*

Examples for paper writing
Editorial: http://www.wjgnet.com/2218-4333/g_info_20100723140942.htm

Frontier: http://www.wjgnet.com/2218-4333/g_info_20100723141035.htm

Topic highlight: http://www.wjgnet.com/2218-4333/g_info_20100723141239.htm

Observation: http://www.wjgnet.com/2218-4333/g_info_20100723141532.htm

Guidelines for basic research: http://www.wjgnet.com/2218-4333/g_info_20100723142040.htm

Guidelines for clinical practice: http://www.wjgnet.com/2218-5836/g_info_20100723142248.htm

Review: http://www.wjgnet.com/2218-4333/g_info_20100723145519.htm

Original articles: http://www.wjgnet.com/2218-4333/g_info_20100723145856.htm

Brief articles: http://www.wjgnet.com/2218-4333/g_info_20100723150253.htm

Case report: http://www.wjgnet.com/2218-4333/g_info_20100723150420.htm

Letters to the editor: http://www.wjgnet.com/2218-4333/g_info_20100723150642.htm

Book reviews: http://www.wjgnet.com/2218-4333/g_info_20100723150839.htm

Guidelines: http://www.wjgnet.com/2218-4333/g_info_20100723150924.htm

SUBMISSION OF THE REVISED MANUSCRIPTS AFTER ACCEPTED

Please revise your article according to the revision policies of *WJCO*. The revised version including manuscript and high-resolution image figures (if any) should be copied on a floppy or compact disk. The author should send the revised manuscript, along with printed high-resolution color or black and white photos, copyright transfer letter, and responses to the reviewers by courier (such as EMS/DHL).

Editorial Office

World Journal of Clinical Oncology
Editorial Department: Room 903, Building D,
Ocean International Center,
No. 62 Dongsihuan Zhonglu,
Chaoyang District, Beijing 100025, China
E-mail: wjco@wjgnet.com
http://www.wjgnet.com
Telephone: +86-10-85381892
Fax: +86-10-85381893

Language evaluation
The language of a manuscript will be graded before it is sent for revision. (1) Grade A: priority publishing; (2) Grade B: minor language polishing; (3) Grade C: a great deal of language polishing needed; and (4) Grade D: rejected. Revised articles should reach Grade A or B.

Copyright assignment form
Please download a Copyright assignment form from http://www.wjgnet.com/2218-4333/g_info_20100723153117.htm.

Responses to reviewers
Please revise your article according to the comments/suggestions provided by the reviewers. The format for responses to the reviewers' comments can be found at: http://www.wjgnet.com/2218-4333/g_info_20100723152755.htm.

Proof of financial support
For paper supported by a foundation, authors should provide a copy of the document and serial number of the foundation.

Links to documents related to the manuscript
WJCO will be initiating a platform to promote dynamic interactions between the editors, peer reviewers, readers and authors. After a manuscript is published online, links to the PDF version of the submitted manuscript, the peer-reviewers' report and the revised manuscript will be put on-line. Readers can make comments on the peer reviewer's report, authors' responses to peer reviewers, and the revised manuscript. We hope that authors will benefit from this feedback and be able to revise the manuscript accordingly in a timely manner.

Science news releases
Authors of accepted manuscripts are suggested to write a science news item to promote their articles. The news will be released rapidly at EurekAlert/AAAS (http://www.eurekalert.org). The title for news items should be less than 90 characters; the summary should be less than 75 words; and main body less than 500 words. Science news items should be lawful, ethical, and strictly based on your original content with an attractive title and interesting pictures.

Publication fee
Authors of accepted articles must pay a publication fee.
EDITORIAL, TOPIC HIGHLIGHTS, BOOK REVIEWS and LETTERS TO THE EDITOR are published free of charge.